

**Estimation of Emission Rates and Lung Dose from Various
Simulated Indoor Workplace Related Aerosol Sources**

Doctoral Dissertation by

Norbert Serfozo



**School of Environmental Engineering
Technical University of Crete**

May 2017

Chania, Greece

“An investigator starts research in a new field with faith, a foggy idea, and a few wild experiments. Eventually the interplay of negative and positive results guides the work. By the time the research is completed, he or she knows how it should have been started and conducted.”

Donald J. Cram
Nobel Laureate in Chemistry, 1987

PhD. Dissertation Committee

- Dr. Mihalis Lazaridis (supervisor), School of Environmental Engineering, Technical University of Crete (Chania, Greece)
- Dr. Nikolaos Kalogerakis, School of Environmental Engineering, Technical University of Crete (Chania, Greece)
- Dr. Konstantinos Eleftheriadis, Institute of Nuclear Technology & Radiation Protection, National Center for Scientific Research—NCSR "Demokritos" (Athens, Greece)
- Dr. Jakub Ondráček (co-supervisor), Institute of Chemical Process Fundamentals, Academy of Sciences of the Czech Republic (Prague, Czech Republic)
- Dr. Dionysia Kolokotsa, School of Environmental Engineering, Technical University of Crete (Chania, Greece)
- Dr. Theodoros Glytsos, School of Environmental Engineering, Technical University of Crete (Chania, Greece)
- Dr. Vladimír Ždímal, Institute of Chemical Process Fundamentals, Academy of Sciences of the Czech Republic (Prague, Czech Republic)

The presented doctoral dissertation was submitted within the postgraduate study program “Environmental Engineering” and was carried out in the Atmospheric Aerosol Laboratory of the School of Environmental Engineering at the Technical University of Crete (Chania, Greece) under the supervision of Dr. Mihalis Lazaridis and co-supervision of Dr. Jakub Ondráček. The research was supported by the European Union 7th framework program HEXACOMM FP7/2007-2013 under grant agreement N° 315760.

ACKNOWLEDGMENTS

First off, I would like to say that it has been a priceless experience to be a PhD. researcher. This period of my life has been definitely of great importance. The ups and downs of these last years I spent in Chania taught me and gave me a lot; foremost, a chance for self-improvement and development from both professional and personal perspectives.

Therefore, I would like to thank Dr. Mihalis Lazaridis, the initiator and coordinator of HEXACOMM project, which I was involved in for the greater part of my PhD. research. Mihalis was also supervisor of this thesis and I greatly appreciate his support, patience, given opportunity and the trust he put in me in the realization of this dissertation even though I came up from slightly different research field. Next I want to extend my sincere gratefulness to my colleague and friend Dr. Thodoros Glytsos for he supported me, encouraged me and helped me in countless research and personal matters over the past years. I would like to thank Dr. Sofia Eirini Chatoutsidou for her vital cooperation and assistance in several important research works in the course of our PhD. studies. I also acknowledge other colleagues from our laboratory, Elena Mammi-Galani, Dr. Eleftheria Chalvatzaki and Dr. Ilias Kopanakis, for their assistance whenever needed. I am also thankful to Dr. Konstantinos Eleftheriadis of NCSR Demokritos for hosting me for a short visit in his laboratory. Kostas introduced me to new methods of aerosol measurements, which has been crucial and valuable knowledge for my further research.

My deep gratitude goes to a colleague, friend and co-supervisor of this dissertation, Dr. Jakub Ondráček of ICPF CAS in Prague. Jakub's invaluable professional help, resourcefulness, attention to details and fruitful discussions even in late night hours were of utmost benefit in forming of my research progress. I greatly appreciate the host of my secondment at ICPF, Dr. Vladimír Ždímal, who made me feel welcomed and offered me indispensable professional and administrative assistance. I am grateful for his willingness, encouragement, reasonable suggestions and insightful remarks not only on research related topics even after the end of my secondment, not mentioning the instant e-mail replies.

Last, but not least, I would like to express my heartfelt gratitude to my family, especially to my parents and my brother David. For they supported me, believed in me, and encouraged me throughout the years to follow my own dreams. Achieving this important milestone in my professional career would not be possible without their help, solicitude and moral values that they embedded in me in the course of my life.

ABSTRACT

The presented doctoral dissertation deals with the estimation of emission rates from various aerosol sources, which may occur in a wide range of indoor workplace environments. Moreover, substantial increase in particle number and mass concentration may lead to high exposure levels of possibly harmful airborne contaminants. Thus, respiratory protection and human dose are also essential parts of this research.

In the first part of Chapter 4, particle number concentration and size distribution along with PM and TVOC were measured during emissions from painting materials (turpentine oils) inside an indoor microenvironment (laboratory room of 54 m³). New particle formation events were observed in all 10 experiments. The nucleation events lasted on average less than one hour with an average growth rate 33.9 ±9.1 nm/h and average formation rate 21.1 ±8.7 cm⁻³s⁻¹. After the end of the nucleation event, a condensational growth of indoor particles followed with average growth rate 11.6 ±2.8 nm/h and duration between 1.4 and 4.1 h. High concentrations up to 3.24 ppm were measured for the indoor TVOC concentrations during the experiments. High nucleation rates indoors were observed in conjunction with high TVOC concentrations originating from painting materials which resulted to high exposure concentration levels of particle number concentration.

The next part of this study evaluates the nanoparticle emissions from laser printers in a print room (PR) and an office. Printing was identified as the most significant indoor source of nanoparticles (< 100 nm) resulting in a substantial increase of indoor PN concentration in the PR during the workdays. Average particle concentration during opened hours was measured to be 5.4 × 10³ #/cm³ and similarly, as it was observed in the chamber study, printers' startup on any given day was characterized by a sharp increase in particle concentrations (on average 4.4 × 10⁴ #/cm³). Printer from the PR examined in a chamber (7.6 m³) was generating nanoparticles (vast majority < 50 nm with mode on ~15 nm) primarily during cold startup (1.9 × 10⁴ to 1.6 × 10⁵ #/cm³).

Dust reuspension may significantly contribute to increased mass concentration in an indoor environment. Therefore, PM₁₀ and number concentration were measured during walking experiments inside a laboratory. The different dust loadings were used (25, 15, 5, 1 g/m²) in order to evaluate the impact of surface loading on the indoor PM₁₀ mass concentration and on the resuspension rate. Moreover, the experiments involved two different walking patterns (rectangular and line). The average resuspension rate was

calculated to be equal to $10^{-2} - 10^{-3} \text{ h}^{-1}$. No impact on resuspension rate was observed for different walking patterns or walking speed. On the other hand, the measured mass concentration inside the room was increased when using higher dust loading on the floor.

The objective of the last part of Chapter 4 was to determine the emission rates from two arc welding processes (SMAW and TIG) and cutting processes in a simulated confined workspace of experimental chamber. All 3 investigated processes generated high particle number concentrations ranging from 2.4 to $3.6 \times 10^6 \text{ \#/cm}^3$ and were the highest during TIG welding. Among all 3 processes, PM_{10} from cutting reached the highest mass concentrations (11 and 22 mg/m^3), while SMAW had the highest contribution of fine particles ($\sim 4.1 \text{ mg/m}^3$), consisting mostly of $\text{PM}_{1-2.5}$.

Chapter 5 deals with penetrations and the most penetrating particle size (MPPS) of 47 mm filters from CE-marked filtering facepiece respirators (FFRs) These were then compared to identical FFR models tested in manikin-based chamber tests. These two experimental methods were in good agreement ($R^2=0.91$). Penetrations were evaluated size-selectively using 9 sizes of charge-neutralized monodisperse aerosol (20-400 nm CMD). Comparison of the penetrations at MPPS from all the examined filters and FFRs showed within-respirator variations in all three filtering classes. The MPPS in this study was found to be in the range of 25-65 nm (CMD) in all measurements. It is concluded that the EN 149 method underestimates particle penetration (especially for particles $<100 \text{ nm}$) due to the inadequate penetration test method for respirator certification.

Human dose from aforementioned aerosol sources was assessed in ExDoM2 model and the results are presented in Chapter 6. During emissions from painting materials, the average increase of total dose represented 4.6 and 1.3-fold at emission and post-emission period, respectively, compared to the exposure dose from BC. Increase of total dose in the PR represented 13.4 and 1.2-fold at printers' startup and printing, respectively. Cumulative deposited and retained dose were also estimated for 4 different scenarios for resuspended dust, and arc welding. Results revealed that: (1) In both emission cases, the first scenario—staying in the polluted workspace for the entire time period without a use of FFR, was the 'worst case' scenario; and that (2) It would be more beneficial in respect to total deposited dose if the exposed simulated subject not wearing FFR at the duration of emission, would leave the polluted workspace immediately after the end of emission. Due to very small contribution of fine particles in the resuspended dust, only $\sim 4\%$ of total dose were deposited in the thoracic region. On the contrary, retained dose in the thoracic region was the highest for arc welding processes ($\sim 20\%$).

TABLE OF CONTENTS

1. Introduction to Aerosol Characterization

| | |
|---|----|
| 1.1. Introduction | 1 |
| 1.2. Particle Size and Equivalent Diameter | 2 |
| 1.3. Particle Concentration and Size Distribution | 4 |
| 1.4. Indoor Particle Dynamics | 7 |
| 1.5. Aerosol Filtration Mechanisms | 9 |
| 1.6. Aerosol Deposition Models | 12 |

2. Dissertation Outline and Objectives

13

| | |
|---|----|
| 2.1. Estimation of Emission Rates | 13 |
| 2.2. Size-Resolved Penetration of Filtering Facepiece Respirators | 15 |
| 2.3. Calculation of Human Dose | 15 |

3. Instrumentation and Experimental Chamber

| | |
|---|----|
| 3.1. Particle Counters and Sizers | 16 |
| 3.2. Aerosol Monitors and Sizers | 17 |
| 3.3. Experimental Chamber | 17 |

4. Estimation of Emission Rates

19

| | |
|--|----|
| 4.1. New Particle Formation Events from Painting Materials | |
| 4.1.1. Introduction..... | 20 |
| 4.1.2. Experimental Setup..... | 22 |
| 4.1.3. Measurement Protocol..... | 23 |
| 4.1.4. Calculation of Growth and Formation Rates | 24 |
| 4.1.5. Estimation of Deposition Losses | 25 |
| 4.1.6. Indoor Particle Number and Mass Concentrations..... | 26 |
| 4.1.7. Particle Size Distribution | 29 |
| 4.1.8. Characterization of New Particle Formation Events | 32 |
| 4.1.9. PSD during Different Stages of the Experiment..... | 36 |
| 4.1.10. Conclusions | 41 |
| 4.2. Evaluation of Nanoparticle Emissions from Laser Printers | |
| 4.2.1. Introduction..... | 42 |
| 4.2.2. Sampling Site and Experimental Chamber | 45 |
| 4.2.3. Methods and Instrumentation | 47 |

| | |
|--|-----|
| 4.2.4. Two-Compartment Indoor Mass Balance Model | 49 |
| 4.2.5. PN Concentrations in the Print Room | 51 |
| 4.2.6. Contribution of Printer Emissions in the Print Room | 54 |
| 4.2.7. PM Concentrations and I/O Ratio during the Field Study | 58 |
| 4.2.8. Effect of Printer's Startup on PN Concentration in the Chamber | 62 |
| 4.2.9. Effect of Printing and Idling on PN Concentration in the Chamber..... | 64 |
| 4.2.10. Effect of Printer Startup and Printing on PSD in the Chamber | 67 |
| 4.2.11. Effect of Printing on Mass and TVOC in the Chamber | 69 |
| 4.2.12. Conclusions | 71 |
| 4.3. Particle Resuspension during Walking in an Indoor Microenvironment | |
| 4.3.1. Introduction..... | 73 |
| 4.3.2. Experimental setup | 75 |
| 4.3.3. Instrumentation and Measurement Protocol | 76 |
| 4.3.4. Dust analysis | 79 |
| 4.3.5. Model Description | 80 |
| 4.3.6. Indoor Particle Concentration | 84 |
| 4.3.7. Indoor PM ₁₀ Concentration at Different Dust Loadings..... | 87 |
| 4.3.8. Estimation of Infiltration Rate | 89 |
| 4.3.9. Dust Loading | 91 |
| 4.3.10. Resuspension Rate | 93 |
| 4.3.11. Conclusions | 97 |
| 4.4. Estimation of Emission Rates from Arc Welding and Cutting | |
| 4.4.1. Introduction..... | 98 |
| 4.4.2. Experimental Setup | 101 |
| 4.4.3. Calculation of Deposition Losses inside the Chamber Volume | 103 |
| 4.4.4. Effect of Welding and Cutting on Particle Number Concentration..... | 104 |
| 4.4.5. Effect of Welding and Cutting on Particulate Mass | 107 |
| 4.4.6. Deposition Loss Rate in the Chamber Volume | 108 |
| 4.4.7. Effect of Welding and Cutting on TVOC concentration levels..... | 109 |
| 4.4.8. Conclusions | 110 |

5. Size-Resolved Penetration of Filtering Facepiece Respirators

| | |
|-----------------------------------|-----|
| 5.1. Introduction..... | 111 |
| 5.2. Materials and Methods | |
| 5.2.1. Filtering Facepieces | 117 |

| | |
|---|-----|
| 5.2.2. Experimental Setup..... | 118 |
| 5.2.3. Data Analysis..... | 122 |
| 5.2.4. Evaluation of the System with Standard Filter Medium | 125 |
| 5.3. Results | |
| 5.3.1. Filter Penetrations..... | 126 |
| 5.3.2. Comparison of Within-Respirator Penetration and MPPS | 127 |
| 5.3.3. FFP Penetrations and Comparison to Filter Measurements | 131 |
| 5.3.4. Comparison of Within-Respirator Penetration | 133 |
| 5.3.5. FFR Leakage Test | 135 |
| 5.4. Discussion | 136 |
| 5.5. Conclusions..... | 142 |

6. Calculation of Human Dose

| | |
|---|-----|
| 6.1. Introduction..... | 143 |
| 6.2. Exposure Dose Model..... | 144 |
| 6.2.1. Human Dose Calculation | 145 |
| 6.2.2. Clearance and Retention Calculation..... | 146 |
| 6.3. Methodology..... | 147 |
| 6.4. Calculation of Deposited Dose (#) from Number Concentration | |
| 6.4.1. Human Dose from Painting Material Emissions | 149 |
| 6.4.2. Human Dose from Laser Printer Emissions | 152 |
| 6.5. Cumulative Deposited and Retained Dose (μg) from Mass Concentration | |
| 6.5.1. Human Dose from Dust Resuspended during Walking..... | 157 |
| 6.5.2. Human Dose from Arc Welding and Cutting of Stainless Steel | 161 |
| 6.6. Study Limitations and Recommendations | 166 |
| 6.7. Conclusions..... | 168 |

7. Conclusions and Recommendations

| | |
|--------------------------------|-----|
| 7.1. General Conclusions | 170 |
| 7.2. Recommendations..... | 172 |

References

Appendix

| | |
|--|-----|
| A.1. Publications in International Peer Reviewed Scientific Journals | 198 |
| A.2. International Scientific Conferences | 199 |

ABBREVIATIONS

| | |
|---------|--|
| AI | Alveolar-Interstitial |
| BC | Background Concentration |
| CE | ‘Conformité Européen’ |
| CMD | Count Median Diameter |
| CPC | Condensation Particle Counter |
| DMA | Differential Mobility Analyzer |
| EN | European Norm |
| ET | Extrathoracic |
| FFP | Filtering Facepiece Protection |
| FFR | Filtering Facepiece Respirator |
| GI | Gastrointestinal |
| GR | Growth Rate |
| HEPA | High Efficiency Particulate Air |
| IAQ | Indoor Air Quality |
| MMD | Mass Median Diameter |
| MPPS | Most Penetrating Particle Size |
| NIOSH | National Institute of Occupational Safety and Health |
| NPFE | New Particle Formation Event |
| OPS | Optical Particle Sizer |
| PM | Particulate Matter (refers to mass concentration) |
| PN | Particle Number (refers to number concentration) |
| PR | Print Room |
| PSD | Particle Size Distribution |
| RT | Respiratory Tract |
| SMAW | Shielded Metal Arc Welding |
| SMPS | Scanning Mobility Particle Sizer |
| SOA | Secondary Organic Aerosol |
| SS | Stainless Steel |
| TIG | Tungsten Inert Gas |
| TIL | Total Inward Leakage |
| UFP | Ultrafine Particle |
| (T) VOC | (Total) Volatile Organic Compound |

1. Introduction to Aerosol Characterization

1.1. Introduction

Aerosols are quite ubiquitous; airborne particles from resuspended soil, atmospheric cloud droplets, welding fumes, smoke from power generation, airborne particles from volcanic eruptions, cigarette smoke, and salt particles formed from ocean spray are all examples of aerosols. Many commonly known phenomena such as dust, suspended particulate matter, fume, smoke, mist, fog, haze, clouds, or smog can be described as aerosols. In its simplest form, term aerosol stands for solid or liquid particles suspended in a gas. In homogenous aerosol, all particles are chemically identical, whereas monodisperse aerosols have particles that have similar size. However, most aerosols are polydisperse with a wide range of particle sizes (Hinds, 1999).

Aerosol sources are both natural and anthropogenic. Anthropogenic sources of aerosols include fossil fuel and biofuel burning for energy production, or industrial activities (Austin et al., 2002). On the other hand, natural aerosol sources, such as sea salt, dust, marine organic aerosol, primary biogenic particles (spores, viruses, microbes) or volcanic eruptions can also be a source of air pollution. Anthropogenic and natural aerosol can be introduced to the atmosphere directly as primary aerosol, or as secondary aerosol which has particles that are formed in the atmosphere by chemical reactions of gaseous components. Atmospheric aerosols range in size from a few nanometers (nm) to tens of micrometers (μm) in diameter (Figure 1.1). Once airborne, particles evolve in size and composition through condensation of vapor species or by evaporation, by coagulating with other particles, by chemical reaction, or by activation in the presence of supersaturated water vapor (Seinfeld and Pandis, 2006).

The World Health Organization (WHO) guidelines for air quality are based on a systematic review of the scientific evidence on the association between ambient levels and health outcomes in large populations. However, the last decade many studies focused on the determination of indoor sources and its impact on indoor air quality. Since, people spend most of their time indoors (Robinson and Nelson, 1995), it is of significant importance to recognize and isolate the most common pollutant human activities, as well as to characterize indoor particulate matter and its contribution to indoor air.

1. Introduction to Aerosol Characterization

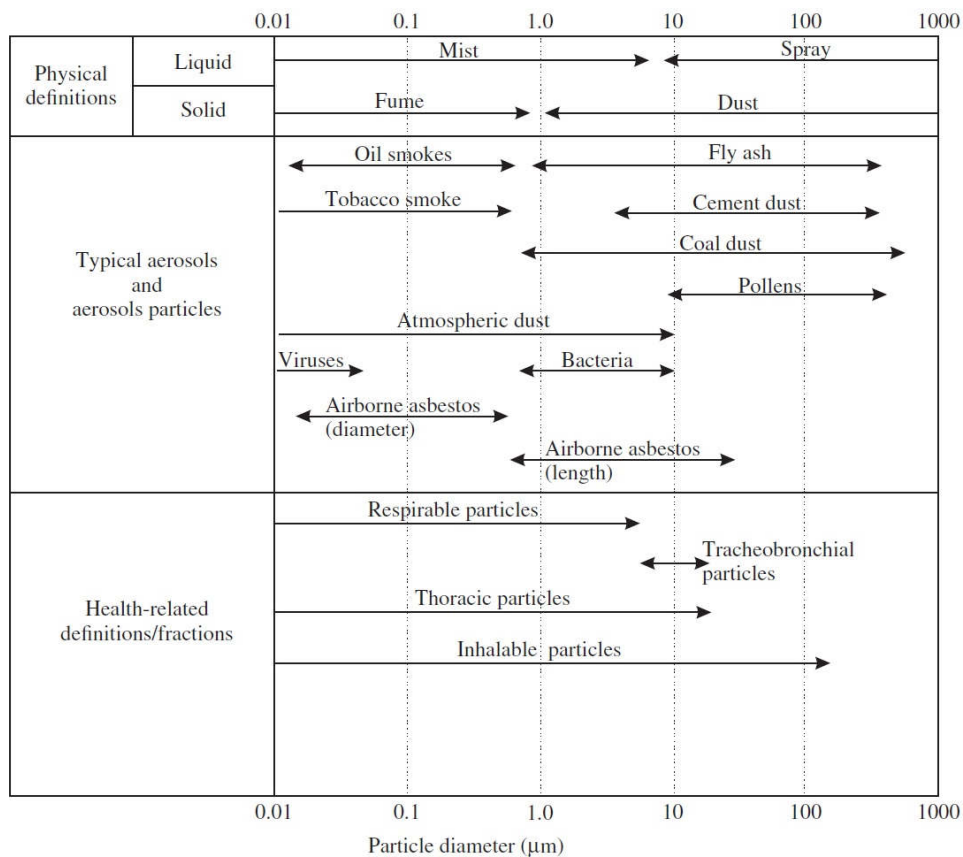


Figure 1.1. Particle size ranges and definitions (adapted from Lazaridis and Colbeck, 2013).

1.2. Particle Size and Equivalent Diameter

Particle size vary widely for different types of aerosol, which in most of the cases is polydisperse rather than monodisperse. Particle size is perhaps the most important property that determines its behavior in a gas, and particles of different sizes behave differently and can be governed by different physical laws (Hinds, 1999). Based on their size, aerosol particles may be classified according to their observed modal distribution, the 50% cut-off diameter, or dosimetric variables related to human exposure (Morawska and Salthammer, 2003):

- Nucleation mode: $d_p < 10 \text{ nm}$
- Aitken mode: particles with diameter $10 \text{ nm} < d_p < 100 \text{ nm}$
- Accumulation mode: $0.1 \text{ } \mu\text{m} < d_p < 1 \text{ } \mu\text{m}$

1. Introduction to Aerosol Characterization

- Ultrafine particles: particles in the Aitkin and nucleation modes
- Fine particles: includes the nucleation, Aitkin and accumulation modes
- Coarse particles: $2 \mu\text{m} < d_p < 10 \mu\text{m}$

Classification according to the site of deposition in the lungs includes several fractions:

- Inhalable: mass fraction of total airborne particles that is inhaled
- Thoracic: mass fraction of inhaled particles that penetrates beyond the larynx
- Extrathoracic: mass fraction of total inhalable particles that fails to penetrate beyond the larynx
- Respirable: mass fraction of total inhaled particles that infiltrates up to the alveolar region.

Particles (or Particulate Matter—PM) significantly vary also in shape. Most airborne aerosol particles have irregular shape, only a very small fraction of particles has spherical shape. Therefore, an approach characterizing the irregular particle shapes is known as the particle equivalent diameter. An equivalent diameter is reported as the diameter of a sphere having the same value of a specific physical property as the particle under consideration. Most theories describing aerosol behavior assume that the particles are spherical. Use of equivalent diameters and other correction factors allows application of these theories to non-spherical particles. Commonly used equivalent diameter are aerodynamic, mobility, and volume equivalent diameter (Kulkarni et al., 2011).

Aerodynamic equivalent diameter is the diameter of a spherical particle with standard density ($\rho_0 = 1000 \text{ kg/m}^3$) having the same terminal velocity when settling under gravity as the particle under consideration. The aerodynamic diameter is useful for describing the behavior of particles typically larger than $0.5 \mu\text{m}$, and is the key parameter for characterizing the deposition in the respiratory tract and in engineered devices such as filters, cyclones, or impactors, where inertial behavior dominates. The volume equivalent diameter is defined as the diameter of a spherical particle of the same volume as the particle under consideration and can be thought of as irregular particle melted to form a droplet with the diameter of a sphere. Stokes diameter (d_s) equals to aerodynamic (d_a) and volume equivalent (d_e) diameter if corrected with dynamic shape factor (χ) for

irregular particles (Eq. 1.1). Stokes diameter has the same density and settling velocity as the particle (ρ_p), and is usually defined in terms of the bulk material density (ρ_b), which avoids the problem of defining the true particle density (Hinds, 1999).

$$d_a = d_e \left(\frac{\rho_p}{\rho_0 \chi} \right)^{\frac{1}{2}} = d_s \left(\frac{\rho_b}{\rho_0} \right)^{\frac{1}{2}} \quad (\text{Eq. 1.1})$$

For extremely small particles (few nanometers), which are dominated by Brownian motion instead of inertia, a mobility equivalent (or diffusive) diameter is used. Mobility equivalent diameter is the diameter of a spherical particle with the same mobility as the particle in question where mobility is defined as the particle velocity produced by a unit external force. Most commonly used mobility diameter is electrical mobility diameter, which is the diameter of a spherical particle with the same electrical mobility as that of particle in question. Additionally, an optical diameter is defined as the diameter of a particle having the same response in an instrument that detects particles by their refraction index.

1.3. Particle Concentration and Size Distribution

Over the last few decades in various fields, such as air pollution, public health, atmospheric science, or manufacturing, the need to measure aerosols has increased significantly. Particle concentration is used to describe spatial distribution of a particular aerosol property and is defined as the specific property of the particle suspension per unit volume of gas (Kulkarni et al., 2011). Particle number, mass, surface area, and volume concentration are the most commonly used types of particle concentration. Particle number concentration is defined as the number of particles per unit volume of gas (most often denoted unit is cm^{-3} or $\#/\text{cm}^3$). Particle number concentration can easily reach $10^7 \#/\text{cm}^3$ or even higher in many industrial environments. Particle mass concentration, on the other hand, is usually determined as the collected particles' weight over a known filtered volume of gas in time. The most common unit of mass concentration is mg/m^3 or

1. Introduction to Aerosol Characterization

$\mu\text{g}/\text{m}^3$ and is used in conjunction with PM_{10} and $\text{PM}_{2.5}$ fractions. $\text{PM}_{2.5}$ (or fine particles) is the mass concentration of particles with aerodynamic diameter smaller than $2.5 \mu\text{m}$, while PM_{10} (coarse particles) is the mass concentration of particles with aerodynamic diameter smaller than $10 \mu\text{m}$, specified by the inlet cut-offs with 50% efficiency.

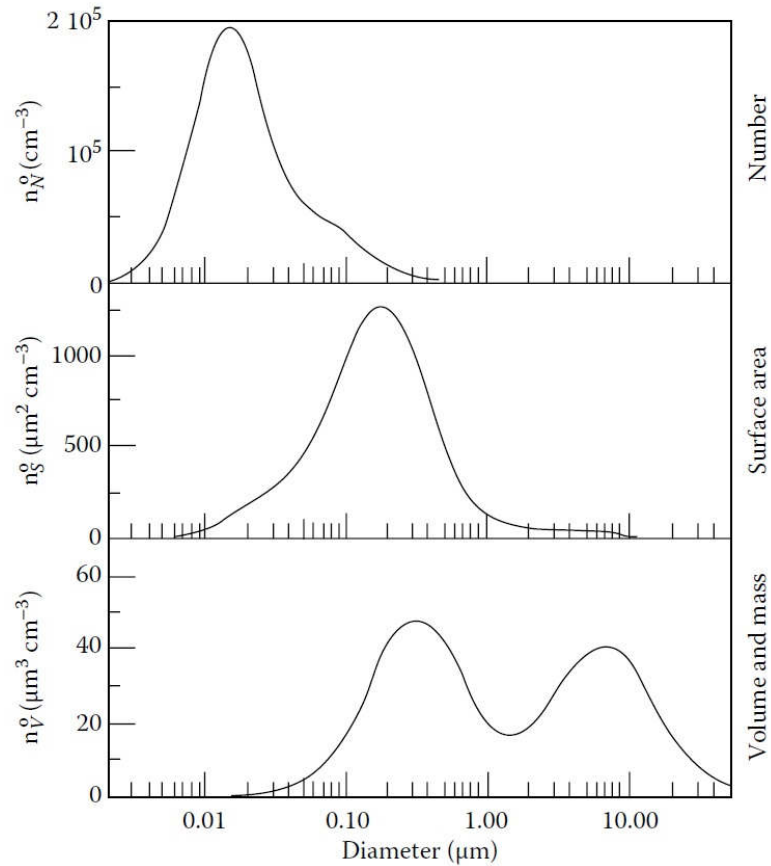


Figure 1.2. Three descriptions of the size distribution of “typical” urban airborne particles (Seinfeld and Pandis, 2006).

Particle size distribution is one of the most of essential characteristics of polydisperse aerosol, i.e. conventionally, a spread of more than about 10–20% (with a geometric standard deviation of 1.1–1.2). It corresponds to the distribution of a specific aerosol property over the investigated particle size range (Figure 1.2). To construct a particle size distribution, the particle size is weighted by either number, mass, surface area, volume, or other aerosol property. The symmetrical normal (or Gaussian)

1. Introduction to Aerosol Characterization

distribution is ideal for describing measurement uncertainties that are distributed symmetrically about a central value, and the uncertainties can take positive or negative values. If the measurement contains no systematic errors, then the distribution of the measurements will be a symmetric bell-shaped curve around the centered value. The mathematical function that describes this curve is called the normal distribution or the Gaussian distribution.

Size distributions more common than normal distributions in aerosol science and technology are lognormal particle size distributions. The lognormal distribution is used extensively in situations where the ratio of the largest to the smallest value is greater than 10 (Figure 1.2). It is used widely for aerosol size distribution due to its convenient form of dealing with the momentum distributions and momentum averages. Lognormal distributions of concentrations are typical of indoor and workplace environments. The lognormal function is simply obtained from the normal function by using logarithmic variables. Aerosol size distributions from many different sources have been found to fit the lognormal distribution. The lognormal number distribution described in John (2011) is given in Eq. (1.2):

$$dN = \frac{N}{\sqrt{2\pi} \ln \sigma_g} \exp \left[-\frac{(\ln d_p - \ln CMD)^2}{2 (\ln \sigma_g)^2} \right] \quad (\text{Eq. 1.2})$$

$$\sigma_g = \left(\frac{d_{84\%}}{d_{16\%}} \right)^{\frac{1}{2}} \quad (\text{Eq. 1.3})$$

where N is the total number of particles, CMD is the count (number) median diameter and σ_g is the geometric standard deviation (GSD) given by Eq. (1.3). GSD is a measure of the width of the peak—if $d_{84\%}$ and $d_{16\%}$ are the diameters that include 84% and 16% of all the particles with diameters from zero to the diameter in question. For a lognormal distribution, CMD is equal to geometric mean diameter (d_g). If the particle number distribution is lognormal, then the surface and volume distributions are also lognormal.

1.4. Indoor Particle Dynamics

Airborne particles undergo a range of physical and chemical processes, which may affect their chemical composition, physical characteristics, and concentration in the air. Emissions from combustion are highly dynamic mixtures of hot gases and particles, undergoing rapid changes, while others, such as mechanically formed dust, are less dynamic. As shown in Figure 1.3, the most significant processes affecting indoor particle concentration levels and other characteristics, include penetration of outdoor particles indoors, deposition of particles originating from both indoor and outdoor sources on indoor surfaces, resuspension of particles deposited on surfaces, coagulation and changes by evaporation or condensation, removal of particles from the indoor environment by ventilation and exfiltration, chemical reactions involving vapors and gases leading to particle generation, and indoor aerosol sources.

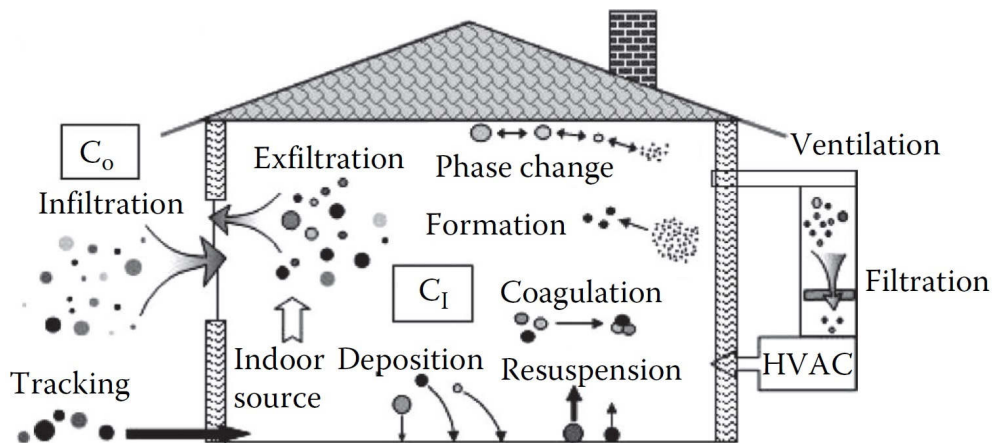


Figure 1.3. Processes affecting indoor aerosol concentrations. C_o and C_i represent the outdoor and indoor concentrations, respectively (adapted from Thatcher et al., 2003).

Outdoor particles can penetrate into indoor air either through opened windows, doors, or through the building envelope leaks, such as cracks or gaps. Penetration of the building envelope, regardless of particle size, becomes insignificant if the windows or doors are opened, which is also characterized by high air exchange rate. On the contrary, penetration through the building envelope is size-dependent. However, ultrafine particles

1. Introduction to Aerosol Characterization

governed by Brownian motion and larger coarse particles do not penetrate the building envelope easily. The size range of particles that penetrates most efficiently is in the accumulation mode, 0.1 to 1 μm (Abt et al., 2000).

Deposition of particles on indoor surfaces is influenced by several factors, such as particle size, airflow currents, available surface area and surface charge, or temperature gradient. Particle diffusion towards the surfaces is significant for very small particles, while gravitational sedimentation is significant for large particles. Particle loss due to deposition is characterized by the deposition loss rate coefficient, which is defined as the number of particles depositing per unit surface area per unit time (Morawska and Salthammer, 2003).

Particles deposited on indoor surfaces may become airborne by resuspension from the surfaces. Detachment of particles require certain forces to be applied. Force required to detach a particle from surface by resuspension may occur as a result of air jets, mechanical forces, or electrostatic forces, and it may involve rolling or sliding of the particle before it becomes airborne (Hinds, 1999). Although particle resuspension from indoor surfaces depends on particle size (Wang et al., 2012a), particles larger than 2.5 μm detach more easily from the surface.

Airborne particles in the indoor environment will bump into each other at a rate that is proportional to the square of their number concentration. The number concentration will decrease rapidly as the particles agglomerate, thus directly changing the size distributions (Nazaroff, 2004), while their mass concentration will remain the same. This process is called coagulation and may be the result of Brownian motion (thermal coagulation), or caused by external forces (kinematic coagulation). Coagulation is very complex, but important particle removal mechanism, which becomes significant for particle number concentrations higher than 10^4 \#/cm^3 (Hussein et al., 2009).

Nucleated condensation (heterogeneous nucleation) occurs at supersaturation ratios lower than 1, and relies on existing submicron particles known as condensation nuclei (soluble or insoluble) or ions, which provide some initial surface area for adsorption of gas-phase molecules. Condensational growth for particles larger than the gas mean free path depends on the rate of diffusion of molecules to the droplet surface. For example, secondary organic aerosol (SOA) forms when concentrations of oxidized

products of the gas-phase reactions of unsaturated hydrocarbons with atmospheric oxidants reach supersaturation and condense onto existing particles. Pressure difference between the ambient vapor pressure and the vapor pressure on the surface of the particle determines the direction of the net vapor flux (Lazaridis and Drossinos, 2013). The process opposite to condensational growth is evaporation. The shrinkage of particles due to evaporation happens when the ambient partial pressure of vapor is less than the pressure of the saturated vapor.

Numerous studies can be found in literature dealing with the characterization of indoor sources and particulate matter emissions (He et al., 2004; Hussein et al., 2006; Géhin et al., 2008; Slezakova et al., 2009; Semple et al., 2012). These studies focus on the most common indoor sources provoked by human activities and its contribution on indoor number and mass concentration. Indoor sources are related with any kind of human activities that take place in different environments such as schools, hospitals, offices, houses. The generated particulate matter influence both the indoor concentration and particle size distribution. Emissions from indoor sources arise from common human activities such as vacuuming, cleaning, cooking, smoking, burning candles, burning wood or simply by walking (Ott et al., 2006, Pagels et al., 2009, Glytsos et al., 2010, Torkmahalleh et al., 2012, Zhang et al., 2012). Although, these activities emit particles with different characteristics, different types of indoor sources are associated with enrichment of indoor air concentration with ultrafine particulate matter.

1.5. Aerosol Filtration Mechanisms

Aerosol filtration is used in various applications, such as respiratory protection, air cleaning hazardous materials processing, or clean rooms. Filters are also used to remove particles from air to promote cleanliness and protect health. Ventilation systems in offices and homes use filters not only to remove nuisance dust, but also to remove pollens, spores, and other organisms that cause disease. Filters used for sampling are characterized by their collection efficiency (E), i.e. the fraction of entering particles retained by the filter. On the other hand, air-cleaning filters are usually characterized in terms of penetration (P)—the fraction of entering particles that penetrates the filter.

1. Introduction to Aerosol Characterization

Single-Fiber Efficiency is an approach considering a single fiber positioned with its axis perpendicular to the airflow in the middle of the filter, and analyzing several mechanisms by which particles can be collected on that filter (Figure 1.4), assuming that the particle remains deposited on the fiber and is permanently removed from the aerosol stream. As described in Raynor et al. (2011), important mechanisms causing particle deposition include (1) diffusion, E_D , (2) interception, E_R , and (3) inertial impaction, E_I . Other mechanisms such as (4) electrostatic attraction, E_{DR} , and (5) gravitational settling, E_G , can also contribute to total efficiency. The single-fiber efficiency (E_F) can be composed of the arithmetic sum of the individual efficiencies.

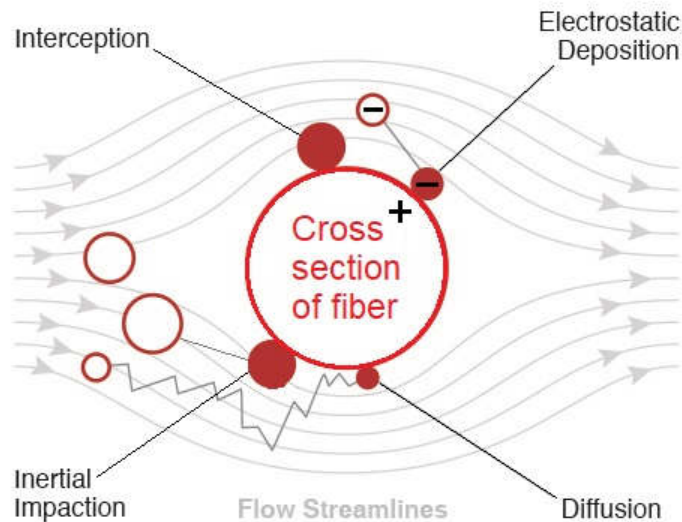


Figure 1.4. Basic particle deposition mechanism (adapted from <http://www.kjfiltration.com/monolith-triboelectric-electrostatic-air-filter-media.html>).

Interception occurs when a particle follows a gas streamline that happens to come within one particle radius of the surface of a fiber. It is assumed that the particles have negligible inertia, settling, and Brownian motion. Interception is the only mechanism that is not a result of a particle departing from its original gas streamline, and which does not depend on flow velocity U_0 . Interception is an important collection mechanism in the particle size range of minimum efficiency.

1. Introduction to Aerosol Characterization

Diffusion occurs when aerosol particles undergo Brownian motion. Particles, especially small ones, do not follow the streamlines but continuously diffuse from one to another. Once a particle is collected on a fiber, it will generally adhere to it due to van der Waals' force. The single-fiber efficiency due to diffusion is the only deposition mechanism that increases with decreasing particle size.

Inertial impaction of particle on a fiber occurs when the particle due to its inertia is unable to adjust quickly enough to the abruptly changing streamlines near the fiber and crosses those streamlines to hit the fiber. Gravitational settling causes the particles with a finite velocity to settle in a gravitational field. Under downward filtration conditions, this mechanism would cause increased collection due to gravity. Gravitational settling contributes significantly only for large particles at low filtration velocities.

Electrostatically enhanced filters are created by the use of multiple materials that produce charge by corona charging, or by induction charging as fibers are produced. The reason for intentionally using electrostatically enhanced filters is that they offer the opportunity to increase filtration efficiency without increasing the pressure drop for the flow through the filter. The combination of particle and filter charging leads to particle collection mainly because permanent charges on filter fibers interact with charges on particles to enhance filtration efficiency via Coulombic forces (Martin and Moyer, 2000).

An increase in particle size causes increased filtration by interception and inertial impaction mechanisms, whereas a decrease in particle size enhances collection by Brownian diffusion. As a consequence, there is an intermediate particle size region where two or more mechanisms are simultaneously operating, yet none is dominant. The particle diameter at which the minimum efficiency occurs is termed the most penetrating particle size (MPPS). MPPS is characterized as the size of a particle with the highest relative particle number concentration passing through a specific filtering material and is also dependent on the detection method and operational conditions. This means that every particle size on the left and right of the MPPS on the penetration curve will have lower penetration values. Although MPPS vary with the type of filter and the filtration velocity, numerous studies in the last years reported the MPPS for filtering facepiece respirator between 30-60 nm (Huang et al., 2007; Rengasamy et al., 2009; Plebani et al., 2012; Ciotti et al., 2012; Penconek et al., 2013).

1.6. Aerosol Deposition Models

Based on the approach, most aerosol deposition models can be identified as empirical, deterministic, or stochastic in nature (Isaacs et al., 2013). In empirical deposition models, regional or total aerosol deposition is described by equations derived by fitting algebraic relationships to experimental data. The empirical ICRP respiratory tract dosimetry model (ICRP, 2012) was developed by the International Commission on Radiological Protection. This model can be used to estimate regional deposition in the lungs as a function of particle characteristics and ventilatory conditions. Other models have been developed for different parts of respiratory tract (Asgharian et al., 1995; Kim and Hu, 2006) or combined with pharmacokinetic model (Carpenter and Kimmel, 1999). Although empirical models do not include information about particle motion or the anatomy of the respiratory system, they may be useful in conjunction with experimental data if parameters of aerosol and ventilatory conditions are known.

Deterministic models are developed using an engineering approach and simplified assumptions about airway geometries and airflow conditions (Martonen, 1993). In deterministic models, the simulated particle deposition patterns are determined solely by the input parameters to the model. Therefore, for any set of model input parameters, the same deposition pattern is found. Many deterministic models are able to model deposition in different respiratory system regions (extrathoracic, tracheobronchial or pulmonary), in individual lung airway generations.

If the morphological lung description is considered to vary within prescribed limits randomly, models of particle deposition are categorized as stochastic (Koblinger, 1985). Since stochastic models do not consider surface features, they may represent less realistic model. However, they have the important advantage of being able to model the realistic biological variability that is present among each lung pathway in a single subject and between individual subjects (Hoffman, 1996). Computational fluid-particle dynamics (CFPD) refers to aerosol deposition model based on CFD simulations. It can be used to predict deposition in complex anatomical geometries where the assumption of a smooth-walled cylinder should not be made, for example, in the larynx, mouth, or nasal passages (Comer et al., 2001; Martonen and Guan, 2001).

2. Dissertation Outline and Objectives

This doctoral research was initiated as a part of the HEXACOMM project (Human Exposure to Aerosol Contaminants in Modern Microenvironments). Hence, following the context of this project, an effort has been made to incorporate the current knowledge and available tools in the field of aerosol science and technology in the dissertation presented herein. That is, to better understand the indoor aerosol emission processes and to investigate how these may influence the human exposure in an indoor workplace microenvironment. Emphasis has been on the estimation of emission rates and characterization of processes, which lead to increase in particle number and mass concentration indoors, particularly in the respirable particle size range. The research presented in this doctoral thesis is mainly of experimental character and an essential part of it was designing and construction of a small environmental experimental chamber. As depicted in Figure 2.1, from broader perspective the presented dissertation has 3 main parts and deals with several questions.

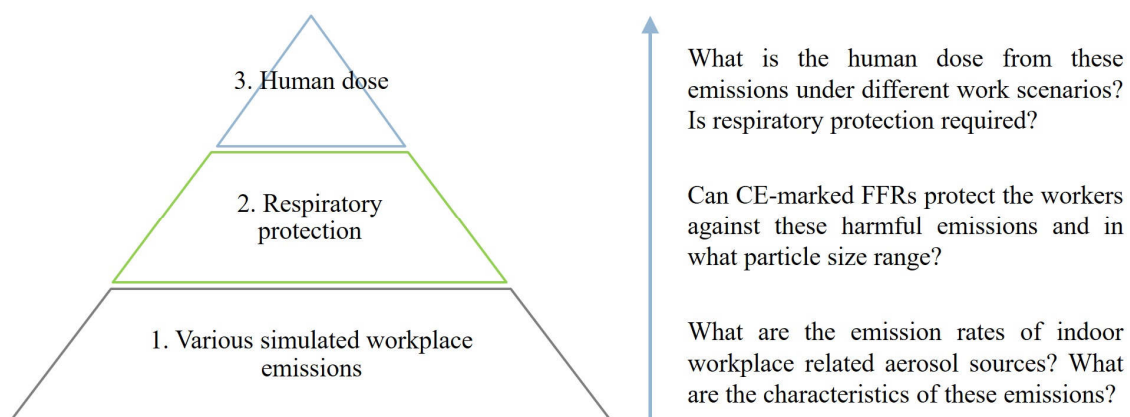


Figure 2.1. Schematics of presented dissertation's outline.

2.1. Estimation of Emission Rates

Four different aerosol sources were investigated in accordance to their prevailing emission characteristics (Chapter 4), i.e. emitting high particle number or mass concentrations. For this purpose, two aerosol emission sources of each were chosen

2. Dissertation Outline and Objectives

(Figure 2.2). The experiments in this research were conducted in the environment of an experimental chamber and laboratory under controlled conditions. Emissions from painting materials, such as turpentine oils, may occur in work environment of art painters or art conservators, where use of ventilation is most of the time not feasible. In the framework of this study, the particle growth and formation rates were determined as well as the impact of turpentine oils on the particle number concentration. Second and more common source of ultrafine particle emissions are printers, which became an inseparable part of many office workplaces. In this case, the effect of printer's startup, printing, and number of printed pages on particle number concentration were investigated in the experimental chamber. Since there is a lack of chamber studies combined with a field study, measurements were conducted also in an actual print room in a detailed field study.

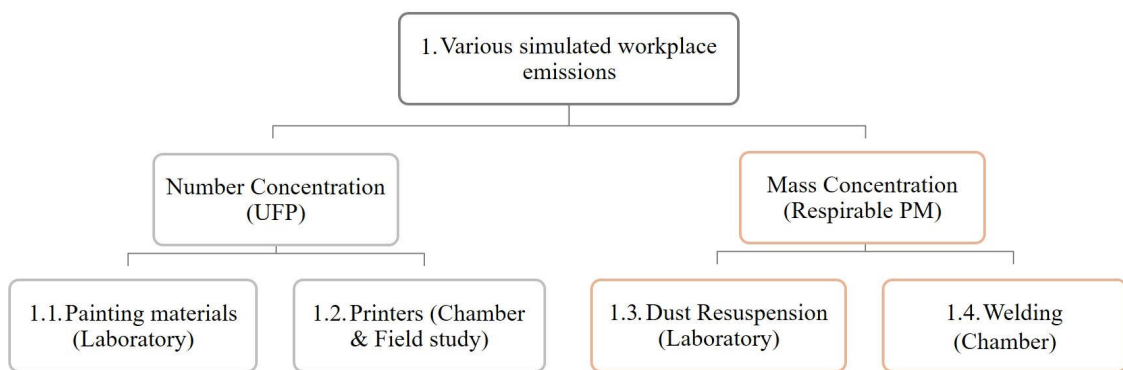


Figure 2.2. Schematics of the different aerosol sources investigated in this research.

From aerosol sources that may generate high mass concentrations, dust resuspension and arc welding processes were examined. Both of these emission sources occur in a wide range of mainly industrial workplace environments (shipbuilding, ironworkers, construction, etc.). In many of these occupational settings ventilation is not a feasible option and working in confined workspaces may be required. The resuspension rate and the effect of different floor dust loading and walking pattern were examined, and their impact on the indoor mass concentration was studied as well. Finally, particle number and mass concentrations were measured in a simulated confined workspace during two arc welding processes.

2.2. Size-Resolved Penetration of Filtering Facepiece Respirators

Personal respiratory protection should be used to prevent the overexposure to harmful aerosol emissions. The motivation to conduct this study was a fact that (1) there is lack of studies on filtering facepiece respirators (FFRs) certified in Europe ('CE-marked') throughout all three respiratory protection classes; and that (2) European Norm uses inadequate certification method to test the filter penetration, which does not give an information about penetration of different particle sizes. Therefore, aim of this study was to challenge CE-marked FFRs with a size-resolved test method using a homemade filter tester with a filter holder, and an experimental chamber with a manikin (Chapter 5).

2.3. Calculation of Human Dose

In the last part of this doctoral thesis (Chapter 6) the human dose was calculated in an empirical aerosol dose model. Different work scenarios including use of respiratory protection were considered. The total deposited particle human dose (#) was assessed for emissions from turpentine oils and laser printers. Furthermore, cumulative deposited and retained dose (μg) in the respiratory tract was assessed for the extrathoracic and the thoracic region for the aerosol emissions from resuspended dust and arc welding.

Detailed study of different workplace aerosols and estimation of emission rates is necessary to understand the indoor particle dynamics. The necessity of size-resolved penetration tests of FFRs in the context of this research is apparent. It is fundamental to know the filtration efficiency of FFRs for different particle sizes. Finally, an accurate estimation of exposure dose should be a compulsory part of IAQ assessment for specific workplaces in order to establish the proper respiratory protection measures. In overall, the novelty of this research inheres in its comprehensive approach. The general concept along with toxicological research could be applied and used as an indicator of personal exposure to aerosol of known composition (particularly for confined workspaces); and for establishing required respiratory protection and new threshold limit values for specific workplace environments, if certain limitations are evaded.

3. Instrumentation and Experimental Chamber

3.1. Particle Counters and Sizers

Throughout this research, a number of online measurement instruments were employed to measure particle number concentration. The Scanning Mobility Particle Sizer—SMPS (CPC Model 5.403 coupled with Vienna type M-DMA, Grimm) measures particle number concentration up to 10^7 #/cm³ in size range 5-350 nm divided into 44 size bins at sample air flow rate 0.3 L/min and a sheath air flow rate 3.0 L/min taking sample every 3 minutes and 50 seconds. It is using bipolar Am²⁴¹ neutralizer to impair Boltzmann charge equilibrium on sampled aerosol. The aerosol is then sized in the Differential Mobility Analyzer (DMA), where only negatively charged aerosol particles of the same size are selected. The number of particles in each size bin is afterwards counted in Condensation Particle Counter (CPC), where the butanol condenses on particles to grow them to detectable size. The particle counting is based on 90° light scattering.

Unlike the previous, the portable NanoScan SMPS (3910, TSI) is based on unipolar charging of the particles where the particles are positively charged in a mixing chamber and sent to radial DMA (RDMA) for size classification and then are counted in isopropanol-based CPC. It measures particle concentrations from 10^2 to 10^6 #/cm³ in the size range of approximately 10–350 nm (13 pre-set channels) under flowrate of 1.0 L/min at a scan time of 60 seconds.

CPC (3775, TSI) was employed to measure the total particle number concentration. The particles pass through a butanol vapor in the saturator chamber (39°C), cool down in the condensation unit (14°C) to grow the particles for easier counting and afterwards they are detected by 90° light scattering. CPC 3775 detects particles up to ~3 μm and its concentration ranges up to 5×10^4 #/cm³ in single particle counting mode, and from 5×10^4 to 10^7 #/cm³ in photometric mode. CPC can sample in high-flow mode (1.5 L/min), or coupled with DMA at low-flow mode (0.3 L/min).

The P-Trak (8525, TSI) uses high-purity isopropyl alcohol to grow microscopic particles for easier detection and counting in the optical chamber. Its concentration range is up to 5×10^5 #/cm³ and it is able to measure particle concentration in the size range between 0.02 and 1 μm at a sample air flow rate of 0.1 L/min.

3.2. Aerosol Monitors and Sizers

Several online aerosol monitors were also used to measure the particle mass concentrations. DustTrak (8520, TSI), DustTrak II (Desktop 8530 and Handheld 8532, TSI) and DustTrak DRX (8534, TSI) are based on a 90° light scattering and can detect particle sizes up to 10 µm. Based on the used inlet nozzle, mass concentration of different particle size fractions (PM₁, PM_{2.5}, PM₄ or PM₁₀) can be measured. DustTrak have concentration range up to 100 mg/m³ at 1.7 L/min flow rate. DustTrak II 8532 (Handheld model) and DustTrak DRX work with flow rate of 3 L/min and are able to measure concentrations up to 150 mg/m³ of particle sizes ranging up to 10 µm and 15 µm for DustTrak II and DRX, respectively. DustTrak II 8530 (Desktop model), on the other hand, detects particle mass concentrations up to 400 mg/m³ under flow rate of 3 L/min.

The Optical Particle Sizer (OPS 3330, TSI) is based on 120° light scatter and filter sampling. It is able to count mass concentrations up to 275 mg/m³ at particle concentrations up to 3000 #/cm³ in the size range 0.3-10 µm. It operates with up to 16 user-adjustable channels at a sample air flow rate of 1 L/min.

In addition, the total volatile organic compound (TVOC) was measured in several measurement campaigns with a PhoCheck Tiger (ION Science). This handheld instrument uses a photoionisation detection (PID) having a resolution from 1 ppb to 20,000 ppm (calibrated to isobutylene at 20 °C at RH equal to 90% with concentration up to 3000 ppm) at flowrate of ~0.3 L/min.

3.3. Experimental Chamber

An essential part of this doctoral research was design and construction of a small environmental stainless steel chamber (Figure 3.1). Its interior dimensions are 2.50×2.39×1.27 m (H×L×W), thus has a volume of 7.56 m³. Chamber is built from two layers of drywall with aluminum skeleton in between (total wall thickness of 75 mm) and its interior surface is covered with 1.5 mm thick stainless steel sheets sealed with high quality industrial silicon glue. Outdoor air entering the chamber is purged through fitted industrial HEPA filter (H14; 610×305×69 mm; 99.995% at 0.3 µm; 0.45 m/s and 110 Pa).

3. Instrumentation and Experimental Chamber

This HEPA can be removed or blocked in order to achieve complete airtightness of the chamber if needed. Small HEPA capsules (flow rate up to 5 L/min) can be used as well with combination of valves to adjust the required flow rate.

Chamber also features fixed window (510×410 mm), glass door (2110×805 mm), and two openings for inlet/outlet. Special sealed tube opening was designed for a glove (PVC Gauntlet, 60 cm long) to enable operating inside the chamber without entering it. For purposes of usage of electrical appliances in emission experiments, classical 230 V socket with cap was placed on the inner wall of the chamber. Chamber and the sampling tubes were tested for leaks prior to the beginning of each measurement and the particle number and mass concentration were monitored constantly. In order to maintain desired environmental conditions throughout the experiments, temperature was controlled with an A/C installed outside the chamber. Uniform particle concentration was ensured by customized fan with adjustable rate installed on the chamber's ceiling as well as a simple G9 LED light (230 V, 42 W). Additionally, vacuum pump (flow up to ~80 L/min) placed outside the chamber allows for chamber cleaning from airborne particles, and can be used in combination with fan to enhance the particle deposition on the chamber's internal surfaces. Walls in the chamber were also cleaned with isopropanol after each experiment.

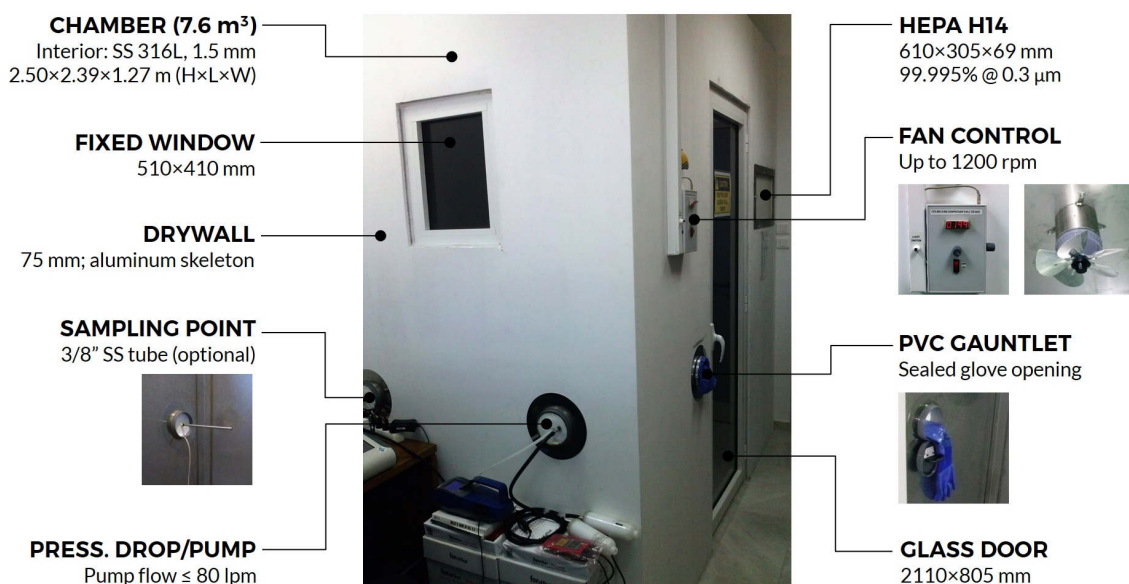


Figure 3.1. Small experimental chamber constructed for the purposes of this research.

4. Estimation of Emission Rates

Almost every human activity generates particles in the indoor air. Usual indoor sources due to human activities is combustion, cooking, cleaning, smoking, printing and walking (Ferro et al., 2004; He et al., 2004; Wallace, 2006; Géhin et al., 2008; Glytsos et al., 2010; Wang et al., 2012a; Semple et al., 2012). Moreover, UFP formation was also observed in a study of emissions from natural paint in presence of ozone underlying that the paint may play a significant role in generation of new particle in indoor environments (Lamorena et al., 2007). Wide use of copy machines and printers in homes and offices may have become a health concern. Numerous studies have shown that these office machines, beside volatile organic compound (VOC) and ozone, also emit nanoparticles (< 100 nm) (He et al., 2007; Destailats et al., 2008; Koivisto et al., 2010). The health impact increases in the offices where the combination of printers' emissions and poor ventilation could be a serious health threat.

However, particles in the indoor air are not only the result of newly formed particles, but arising also from the resuspension of the already existing particles, such as settled dust on indoor surfaces. Any kind of human activity in indoor microenvironments can result in particle resuspension (Spilak et al., 2014). The most common activities that resuspend particles indoors are vacuuming and walking (Corsi et al., 2008; Rosati et al., 2008; Shaughnessy and Vu, 2012). On the other hand, process that may considerably contribute to increase in indoor particle mass concentration is welding. Welders may be exposed to ultrafine particles (UFP; ≤ 100 nm) (Debia et al., 2014; Graczyk et al., 2015) and a variety of toxic airborne contaminants including manganese (Mn) and hexavalent chromium (Cr^{VI}) (Hobson et al., 2011). In particular, full-time welders and other professions that frequently perform welding related operations (boilermakers, pipefitters, construction workers, shipbuilders, automotive workers) are in risk of overexposure to hazardous levels of airborne contaminants.

This chapter presents the results from investigation of aforementioned processes and their impact on increase in particle number and mass concentration in an indoor microenvironment. Emission rates were estimated from experimental data obtained from measurements under controlled conditions in an experimental chamber and laboratory.

4.1. New Particle Formation Events from Painting Materials

4.1.1. Introduction

New particle formation events and condensational growth of particles in the outdoor air were investigated extensively the last decades (Kulmala et al., 2004; Holmes, 2007). Nucleation events were observed in many different sites in the atmospheric air including the free troposphere, lower stratosphere, in arctic, in forest, in coastal areas and in cities (Kulmala et al., 2004; Curtius, 2006; Holmes, 2007). Several mechanisms are proposed for the occurrence of new particle formation, such as the binary homogenous nucleation of sulphuric acid-water system, the ternary homogenous nucleation of sulphuric acid-water-ammonia system, the heterogeneous nucleation on pre-existing particles and the heterogeneous ion-induced nucleation (Kulmala et al., 1991; Lazaridis, 2001; Housiadas et al., 2004; Seinfeld and Pandis, 2006).

A nucleation event provokes the generation of new particles at low particle sizes, usually of few nanometers. Particles in the nucleation mode ($< 0.1 \mu\text{m}$) are the most harmful to human health due to their ability to penetrate very easily through the human respiratory tract. Several health effects (cardiovascular, respiratory, lung cancer) are connected with the presence of ultrafine particles to the ambient air (Pope and Dockery, 2006). However, ultrafine particles emitted to the indoor air originate from primary sources as well. High emission rates or concentrations are reported in the previous studies with substantial increase of indoor ultrafine particles during indoor activities (Géhin et al., 2008; Glytsos et al., 2010; Wang et al., 2012a; Semple et al., 2012).

On the other hand, indoor emissions of chemical substances from building materials, household products and furnishings may lead to secondary organic aerosol formation (Weschler, 2001; Singer et al., 2006; Aoki and Tanabe, 2007; Uhde and Salthammer, 2007; Weschler, 2009). Semivolatile compounds found in indoor environments are provoked by several sources (Weschler and Nazaroff, 2008). In particular, painting materials are a very common source and it involves a wide range of volatile organic compounds (VOC) (Guo et al., 1998; Weschler, 2009). Emissions from wet materials like paints are dominated by evaporation at the beginning and by internal diffusion afterwards (Yang et al., 2001; Zhang and Niu, 2003). A previous study reported

4.1. New Particle Formation Events from Painting Materials

formation of ultrafine particles during the reaction of VOCs and ozone (Fan et al., 2005), suggesting that VOCs may behave as precursor material.

New particle formation events indoors, associated with the presence of VOCs and ozone, conducted in real environments are already reported in the scientific literature (Vartiainen et al., 2006; Betha et al., 2011; Hovorka and Braniš, 2011; Quang et al., 2013). In the work by Quang et al. (2013) nucleation events observed inside a big office building. However, the observed nucleation was the result of outdoor particles transported indoors due to high air exchange rate of the building with the outdoor air. Vartiainen et al. (2006) investigated the formation of indoor particles as a result of d-limonene oxidation. Betha et al. (2011) suggested that the formation of ultrafine particles caused possibly by the ozone-induced oxidation of VOCs, whereas Hovorka and Braniš (2011) associated the nucleation events into a constructing hall with emissions from the paint spraying.

VOC emitted from the paint were more likely to cause ultrafine particle formation event rather than the penetration from outdoors due to low air exchange rate and high residence time of the ultrafine particles inside the hall, as suggested by the authors. This chapter presents an analysis of new particle formation events from painting materials that took place in a laboratory room. The objectives were to measure particle number (PN) and mass (PM) concentrations emitted from painting materials, to investigate the aerosol particle size distribution (PSD) during the emission process and further to examine the formation rates and condensational growth of the particles during the new particle formation events.

4.1.2. Experimental Setup

The measurements were conducted in period of September 2013 to January 2014 in the Atmospheric Aerosol Laboratory at the Technical University of Crete. The area of the laboratory is 19 m² of rectangle shape and its volume is 54 m³ with one door and one window placed at the opposite side. The window and the door were closed at all times. Indoor temperature and humidity were continuously recorded in a nearby laboratory

4.1. New Particle Formation Events from Painting Materials

room (of the same dimensions) using the indoor sensors of Vantage PRO 2 (Davis Instruments, US) meteorological station.

Previous comparative measurements in the two laboratory rooms showed that there were no significant differences in the indoor conditions, and therefore the data from the nearby room can be used, since during the nucleation experiments no air-condition or heating devices were used. Average indoor temperature ranged from 19.6 °C to 28.5 °C, while indoor relative humidity ranged from 42% to 55% depending on the time of the year that the experiments were conducted. Furthermore, the air exchange rate between the laboratory room and the outdoor environment was measured using CO₂ as a trace gas and the average value for all the experimental periods was 0.16 h⁻¹.



Figure 4.1. Testing of experimental setup for emission from painting materials.

The indoor number and PM₁₀ concentrations were measured with several instruments: DustTrak (8520, TSI), DustTrak II (8532, TSI) for particulate matter, and NanoScan SMPS (3910, TSI) for determination of particle number concentration and particle size distribution. The outdoor particle concentration was measured using the SMPS+C (CPC Model 5.403 and M-DMA, Grimm). The outdoor measurements were located in an urban background site located at the University campus (Lazaridis et al.,

4.1. New Particle Formation Events from Painting Materials

2008; Kopanakis et al., 2012). Additionally, the total volatile organic compounds (TVOC) were measured with a PhoCheck Tiger (ION Science) instrument. During the measurements, the instruments were placed on the bench next to each other (Figure 4.1.). At the first two experiments, two persons were present in the laboratory during the emission period and only one person was present in the laboratory during the rest of the experiments.

The painting materials consisted of water mixable oil medium (Artisan Series, Winsor & Newton) (linseed oil) and turpentine medium (Winsor & Newton) (composed mainly from monoterpenes alpha-pinene and beta-pinene). Oil colours (Old Holland) were used during the first two experiments for painting on linen canvas. However, it was observed in separate experiments that solely the use of oil colours did not result to an increase of the indoor number size concentration and therefore the ten experiments performed using only oil medium and turpentine. Ten bottles of 250 ml each were used (5 with oil medium and 5 with turpentine). During oil painting is a common practise to use turpentine for diluting the oil colors in conjunction with linseed oil.

4.1.3. Measurement Protocol

The experiments were performed in two periods, each consisting of 5 experiments (10 experiments in total). The measurements were conducted in 3 stages:

| | | | |
|-----------------|------------------|---------------|----------------------------------|
| <u>Stage 1:</u> | Background: | 0 - 60 min | (Empty laboratory) |
| <u>Stage 2:</u> | Emission period: | 60 - 150 min | (Painting and/or opened bottles) |
| <u>Stage 3:</u> | Removal period: | 150 - 330 min | (Empty laboratory) |

During stages 1 and 3 no person was present in the laboratory, whereas, during stage 2 only one person was present. Only on the experiments conducted on 26/09/13 and 02/10/13, two persons were present during stage 2. In these two experiments, the activity period (stage 2) consisted of painting a picture on a canvas with painting oil colours with a simultaneous opening of the medium and turpentine oils bottles. The

4.1. New Particle Formation Events from Painting Materials

emission period in the other experiments consisted of opening 10 bottles with oil medium and turpentine, which, were brought in the laboratory just before the start of stage 2 (emission period). The bottles with turpentine oils were placed close to the instrumentation for a time period of 90 minutes. After the emission period, the bottles were closed and removed from the laboratory room. The door and window were closed during all three stages.

4.1.4. Calculation of Growth and Formation Rates

The particle growth rate (GR) and formation rate (J_D) were calculated for each event. The growth rate (nm/h) represents the increase in particle size, whereas, the formation rate ($\text{cm}^{-3}\text{s}^{-1}$) represents the increase in particle concentration during the nucleation event. The methodology followed for calculating GR and J_D was first to identify the particles that participate in the nucleation event. For this purpose, every distribution of each time interval was examined manually. In the cases where nucleation was present indoors, the size distribution of particles had always a maximum at particle diameter lower than 50 nm. Particles up to this maximum considered to participate to the nucleation burst. Then, the mean particle diameter was obtained from the equation:

$$\overline{D_p} = \frac{\sum_{i=1}^k N_k D_k}{N_t} \quad (\text{Eq. 4.1})$$

where, k is the number of size bins in the distribution, N_k is the number of particles which belong to diameter D_k and N_t is the sum of particles which belong to the modes of the diameter. Since, the mean particle diameter is known the growth rate can be calculated by the following equation:

$$GR = \frac{\Delta \overline{D_p}}{\Delta t} \quad (\text{Eq. 4.2})$$

4.1. New Particle Formation Events from Painting Materials

where, $\Delta\overline{D}_p$ is the size range of the particles from \overline{D} to \overline{D}_{max} and t is the time required for the particles to reach \overline{D}_{max} . The formation rate was obtained as:

$$J_D = \frac{\Delta N}{\Delta t} \quad (\text{Eq. 4.3})$$

where, ΔN is the change in particle number concentration at a specific time period and Δt is the time period (or nucleation period). The duration of the nucleation event was considered as the period where the concentration of particles with sizes close to 20 nm started to increase along with particle size and time, and as long as the total number concentration of particles inside the laboratory was increasing.

4.1.5. Estimation of Deposition Losses

The particle deposition on indoor surfaces for particles with mobility diameters less than 50 nm was estimated using the model of Lai and Nazaroff (2000), which incorporates equations for the deposition velocity on upward, downward and vertical surfaces. In order to estimate the deposition on surfaces, a calculation of the total available area for deposition was made by measuring the dimensions of all the objects inside the laboratory room during the painting experiments. Friction velocity is a key parameter for the computation of deposition velocity and the value of 0.5 cm/s was used in the current study, which is characteristic for indoor environments with a surface to volume ratio equal to 2 and with low indoor air speed (Lai and Nazaroff, 2000).

4.1.6. Indoor Particle Number and Mass Concentrations

A comparison of indoor PN and PM₁₀ concentrations during the experimental procedure is presented in Table 4.1a. The average background concentration (BC) and emission period concentration is listed for each experiment. Table 4.1a suggests that the major impact from the oil mediums and turpentine is on PN concentration. Aerosol formation has been associated to ozone/terpenes reactions in many studies conducted in chambers

4.1. New Particle Formation Events from Painting Materials

under controlled indoor conditions (Weschler and Shields, 1999; Rohr et al., 2003; Coleman et al., 2008; Sarwar and Corsi, 2007; Chen and Hopke, 2009; Waring et al., 2011).

In this study, the ozone concentration ranged, during the measurement's periods, from 57 ppb to 70 ppb while the average values for each experiment ranged from 58 ppb to 68 ppb. The indoor ozone concentration was lower than the outdoor since ozone is diffused in the building skeleton while penetrating in the indoor environment. The indoor ozone concentration was determined by the outdoor ozone because there were no ozone sources (e.g. ionizers) and the laboratory room was mainly used, before the experiments, for storing the instrumentation. Coleman et al. (2008) conducted experiments in a chamber and studied nucleation events from terpene-rich household products. They reported that these events can be recorded for low ozone concentrations if these are combined with high terpene emissions, which corresponds to experiments presented herein. The emission rates of the substances emitted from painting bottles cannot be measured since an effort was made to achieve realistic conditions (just opening the bottles) in a real indoor environment. Nevertheless, the increase in TVOC's concentrations indicated the high emissions from the bottles.

The concentrations of TVOC's presented average values of 3.25 ppm at the end of the emission periods (stage 2) while the maximum background values were 0.005 ppm. The results confirm that the oil medium and turpentine are important sources of VOCs which act as precursors for new particle formation. Immediately after the emission period has begun, dramatic increase in TVOCs was observed and lasted on average for 30 min. Then, the TVOC concentration started decreasing on average 60 min before the end of emission period. At the end of the experiments and 3 h after the end of emission period, the concentration was still 0.250 ppm, which is 50 times more than an initial value recorded during the background measurements.

4.1. New Particle Formation Events from Painting Materials

Table 4.1. (a) Average number and PM₁₀ concentrations during background (BC) and emission period measurements; (b) Characteristics of the nucleation events and post nucleation period for each experiment.

| a) | Number Concentration | | Mass Concentration | | |
|----|----------------------|-------------------------|--------------------------------------|-------------------------|--------------------------------------|
| | Experiment | BC (#/cm ³) | Emission period (#/cm ³) | BC (µg/m ³) | Emission period (µg/m ³) |
| | 26/09/13 | 2.6×10 ³ | 1.6×10 ⁴ | 23 | 26 |
| | 02/10/13 | 2.2×10 ³ | 1.3×10 ⁴ | 17 | 19 |
| | 16/10/13 | 3.2×10 ³ | 6.3×10 ³ | - | - |
| | 24/10/13 | 4.4×10 ³ | 1.0×10 ⁴ | 32 | 36 |
| | 01/11/13 | 4.5×10 ³ | 1.0×10 ⁴ | 56 | 61 |
| | 27/01/14 | 1.8×10 ³ | 5.6×10 ⁴ | 9 | 12 |
| | 28/01/14 | 4.7×10 ³ | 1.7×10 ⁴ | 18 | 26 |
| | 29/01/14 | 2.2×10 ³ | 2.5×10 ⁴ | 10 | 12 |
| | 30/01/14 | 3.1×10 ³ | 1.6×10 ⁴ | 8 | 11 |
| | 31/01/14 | 6.6×10 ³ | 1.4×10 ⁴ | 14 | 18 |

| b) | Nucleation Period | | | Post nucleation period | | |
|----|-------------------|--------------|-----------|--|--------------|-----------|
| | Experiment | Duration (h) | GR (nm/h) | J _D (cm ⁻³ s ⁻¹) | Duration (h) | GR (nm/h) |
| | 26/09/13 | 0.7 | 34.0 | 13.2 | 3.9 | 10.4 |
| | 02/10/13 | 0.8 | 21.7 | 18.6 | 1.7 | 12.3 |
| | 16/10/13 | 0.9 | 33.8 | 26.1 | 2.5 | 8.9 |
| | 24/10/13 | 1.0 | 33.7 | 15.3 | 3.8 | 10.4 |
| | 01/11/13 | 0.8 | 22.6 | 10.0 | 3.9 | 13.8 |
| | 27/01/14 | 0.4 | 45.8 | 289.9 | 4.1 | 10.5 |
| | 28/01/14 | 0.8 | 34.2 | 25.7 | 1.4 | 13.0 |
| | 29/01/14 | 0.5 | 51.4 | 131.7 | 2.0 | 18.0 |
| | 30/01/14 | 0.8 | 31.0 | 37.0 | 2.5 | 9.0 |
| | 31/01/14 | 1.1 | 31.4 | 23.1 | 1.5 | 9.6 |

The PN and PM₁₀ concentrations during the experiment on 24/10/13 are plotted in Figure 4.2. Both PN and PM₁₀ concentrations increased from the beginning of the event. Specifically, the PN concentration reached 1.3×10^4 #/cm³ after 1 h of emission period with average background concentration equal to 4.4×10^3 #/cm³. On the other hand, the average PM₁₀ concentration of particles increased from 32 µg/m³ to 36 µg/m³. Although, the increase in PM₁₀ concentration was much lower than the increase in PN concentration, it is observed that also the PM₁₀ concentration is affected by the emission

4.1. New Particle Formation Events from Painting Materials

of particles from the painting materials. Similar increase on PM_{10} concentrations was observed in all the experiments. Lamorena et al. (2007) reported a simultaneous increase in both mass and number concentrations during emissions from natural paint by ozone initiated reactions. Possible condensation from painting materials on the already existing particles is likely to happen, thus, increasing the indoor PM_{10} concentration.

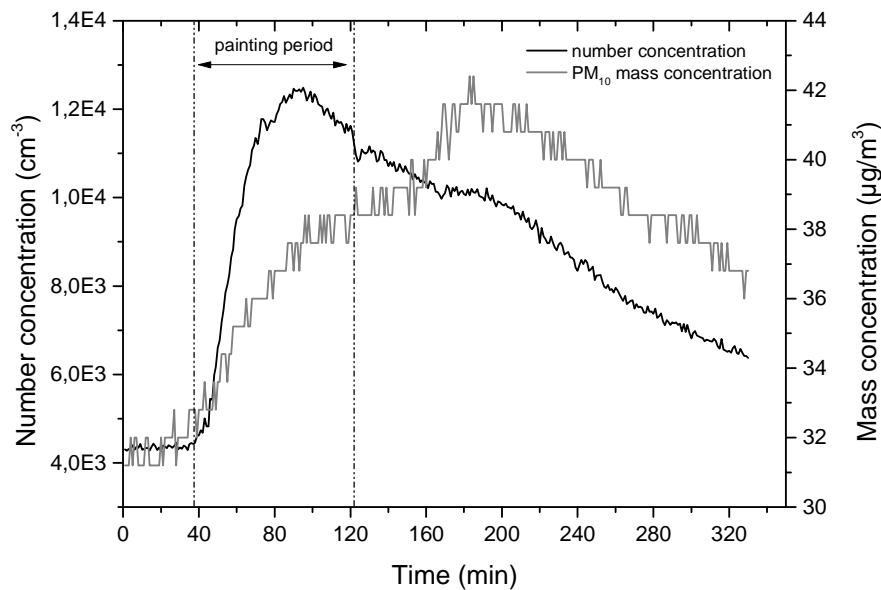


Figure 4.2. Number and PM_{10} concentration versus time during experiment on 24/10/13.

Figure 4.3 shows a comparison between the 5 experiments of the second data set. The second set was chosen due to the same profile followed during the emission period (stage 2) for all 5 experiments. The BC indoors was on average $3.6 \times 10^3 \text{ \#/cm}^3$ (Table 4.2). An intensive increase in PN concentration was observed along with the opening of the bottles. The average PN concentration during the emission period in the second set varied between 1.4 to $5.6 \times 10^4 \text{ \#/cm}^3$ (Table 4.2). Although, the painting materials used in every experiment were the same, higher number concentration was measured on the experiment on 27/01/14. A possible reason could be that the bottles with turpentine oils were closed tight for almost a week and stored in an office room at higher air temperature than in the laboratory, which resulted to a burst of new particles with three times higher concentration than the average. This assumption is supported by the fact that the

4.1. New Particle Formation Events from Painting Materials

background measurements before the experiment showed an average number concentration $1.8 \times 10^3 \text{ \#/cm}^3$. Moreover, the indoor concentration was always decreasing during the emission period indicating that the effective emission period lasted less than 90 min (usually 20–40 min).

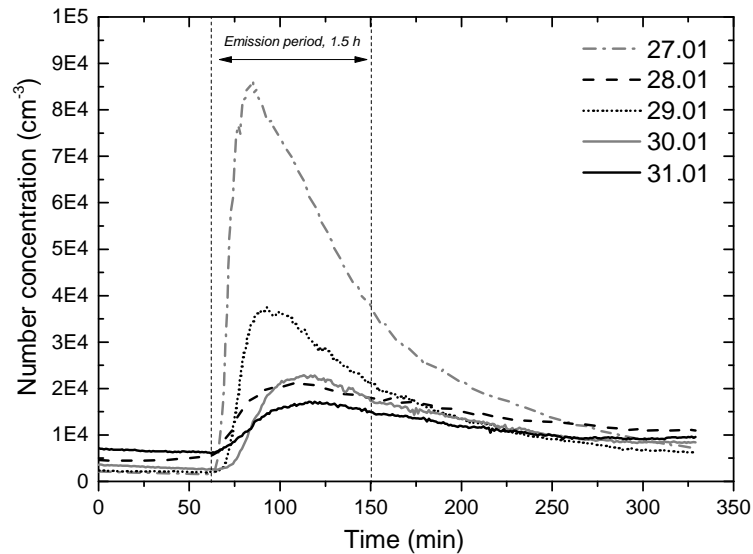


Figure 4.3. Total particle number concentration of indoor particles versus time for the 5 experiments of the second set.

4.1.7. Particle Size Distribution

In order to evaluate the particle size distribution (PSD) characteristics, the total number concentration of particles was separated into 3 classes. The first class includes particles of the lowest measured particle size up to 50 nm. This class (N_{10-50}) corresponds to particle sizes that involve particles at the nucleation mode. The second class obtained at particle sizes between 50 and 100 nm (N_{50-100}), where the PN concentration was still high, and the last class includes the remaining particle sizes from 100 to 350 nm ($N_{100-350}$), which is characterized by the accumulation mode of particles.

4.1. New Particle Formation Events from Painting Materials

Table 4.2. Average number concentrations (NC) of different particle fractions for background (BC) and emission period of all experiments.

| Experiment | | Total NC (#/cm ³) | N ₁₀₋₅₀ (#/cm ³) | N ₅₀₋₁₀₀ (#/cm ³) | N ₁₀₀₋₃₅₀ (#/cm ³) |
|------------|----------|----------------------------------|--|---|--|
| 26/09/13 | BC | 2.6×10 ³ | 5.4×10 ² | 1.5×10 ³ | 6.6×10 ² |
| | Emission | 1.6×10 ⁴ | 1.3×10 ⁴ | 2.7×10 ³ | 6.0×10 ² |
| 02/10/13 | BC | 2.2×10 ³ | 1.2×10 ³ | 9.5×10 ² | 9.7×10 ¹ |
| | Emission | 1.3×10 ⁴ | 9.9×10 ³ | 2.8×10 ³ | 2.7×10 ² |
| 16/10/13 | BC | 3.2×10 ³ | 1.2×10 ³ | 1.7×10 ³ | 3.2×10 ² |
| | Emission | 6.3×10 ³ | 4.2×10 ³ | 1.8×10 ³ | 3.2×10 ² |
| 24/10/13 | BC | 4.4×10 ³ | 9.2×10 ² | 2.5×10 ³ | 9.2×10 ² |
| | Emission | 1.0×10 ⁴ | 4.4×10 ³ | 5.1×10 ³ | 8.3×10 ² |
| 01/11/13 | BC | 4.5×10 ³ | 5.4×10 ² | 2.4×10 ³ | 1.4×10 ³ |
| | Emission | 1.0×10 ⁴ | 4.6×10 ³ | 4.4×10 ³ | 1.2×10 ³ |
| 27/01/14 | BC | 1.8×10 ³ | 8.6×10 ² | 7.6×10 ² | 2.0×10 ² |
| | Emission | 5.6×10 ⁴ | 3.8×10 ⁴ | 1.7×10 ⁴ | 1.1×10 ³ |
| 28/01/14 | BC | 4.7×10 ³ | 2.4×10 ³ | 1.9×10 ³ | 4.1×10 ² |
| | Emission | 1.7×10 ⁴ | 9.3×10 ³ | 7.5×10 ³ | 4.5×10 ² |
| 29/01/14 | BC | 2.2×10 ³ | 1.3×10 ³ | 7.3×10 ² | 1.8×10 ² |
| | Emission | 2.5×10 ⁴ | 1.5×10 ⁴ | 1.1×10 ⁴ | 2.6×10 ² |
| 30/01/14 | BC | 3.1×10 ³ | 1.8×10 ³ | 1.1×10 ³ | 2.1×10 ² |
| | Emission | 1.6×10 ⁴ | 1.1×10 ⁴ | 5.1×10 ³ | 1.6×10 ² |
| 31/01/14 | BC | 6.5×10 ³ | 3.6×10 ³ | 2.6×10 ³ | 3.5×10 ² |
| | Emission | 1.4×10 ⁴ | 7.5×10 ³ | 5.9×10 ³ | 2.9×10 ² |

Figure 4.4 presents the PN concentration for different size fractions versus time during a typical event (30/01/14). The N₁₀₋₅₀ particle fraction increased at the beginning of the emission period, whereas the N₅₀₋₁₀₀ fraction increased after a short period during the emission period. On the other hand, the emission from the painting materials had no significant impact on the N₁₀₀₋₃₅₀ particles. A slight increase on N₁₀₀₋₃₅₀ particles was observed at the beginning of the activity period. Although, the increase is minimal it is believed that the increase originates from the direct emission at this size fraction. The same behavior of the different particles sizes was observed in all experiments. Similar PSDs were reported in studies correlating the emissions from VOCs to PSD characteristics (Rohr et al., 2003; Sarwar et al., 2004; Fan et al., 2005; Coleman et al., 2008).

4.1. New Particle Formation Events from Painting Materials

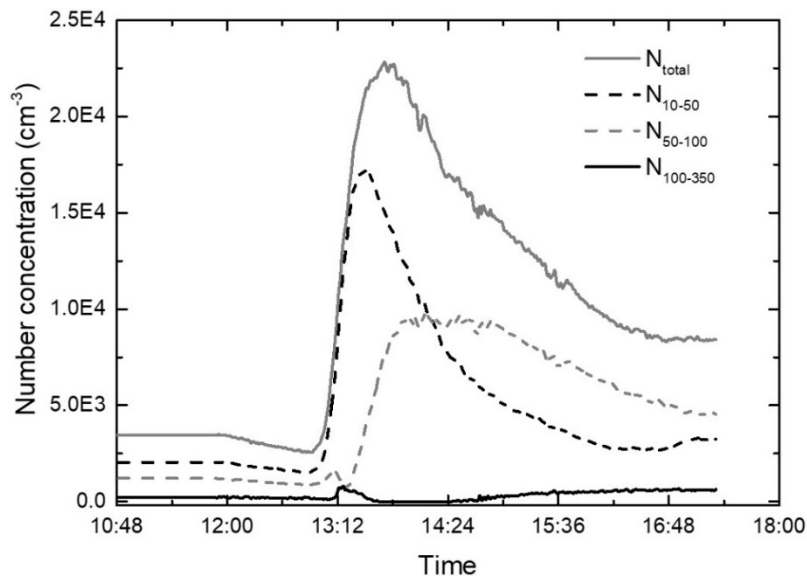


Figure 4.4. Number concentration of particles during an event on 30/01/14 for different particle size modes.

The rapid increase of N_{10-50} particles from the beginning of the emission indicates a burst of N_{10-50} particles inside the laboratory in the first minutes of the emission period. This burst, provoked by the medium materials and turpentine, underlines that the emission of new particles corresponds to particles sizes lower than 50 nm. However, an increase of N_{50-100} particles was observed several minutes later. The duration of this period usually varied between 10 and 40 min. This is in accordance with previous works studying the formation of ultrafine particles from VOC emissions (Fan et al., 2005; Lamorena et al., 2007). Moreover, the N_{50-100} number concentration increased shortly before the N_{10-50} particles reached the maximum value. Therefore, it was assumed that the increase in N_{50-100} particles is due to coagulation of smaller particles besides the direct emission of particles at this size range. Considering that the emission period had minimal impact on $N_{100-350}$ concentration, it is likely that the major impact on indoor PN concentration originates from emissions of the painting materials that correspond to a size range of particles between 10 and 100 nm.

Table 4.2 compares the average number concentration of different particle classes during the period before the emissions (BC) and during the emission periods for all experiments. Background N_{10-50} concentration inside the laboratory was higher than N_{50-}

4.1. New Particle Formation Events from Painting Materials

N_{100} and $N_{100-350}$ particles. The average BC for all 10 experiments was 1.4 and $1.6 \times 10^3 \text{ \#/cm}^3$ for N_{10-50} and N_{50-100} , respectively, indicating that N_{10-50} particles is the fraction of particles that contributes mostly to indoor PN concentration. The lowest concentration observed on $N_{100-350}$ particles with average BC $4.8 \times 10^2 \text{ \#/cm}^3$. The same behavior of the different particle sizes applies for the emission period. The highest concentrations measured for N_{10-50} particles with average emission concentration at $1.2 \times 10^4 \text{ \#/cm}^3$ and lowest for $N_{100-350}$ particles with average number concentration during the emission period at $5.5 \times 10^2 \text{ \#/cm}^3$ confirming that the ultrafine particles were the major fraction of the indoor particulate matter.

4.1.8. Characterization of New Particle Formation Events

New particle formation events were observed in all 10 experiments conducted in the laboratory. During the nucleation, the major contribution to the total indoor concentration was the particles at the size range of 10–65 nm. A typical particle formation event inside the laboratory is presented in Figure 4.5. The characteristic banana shape with a simultaneous increase of both PN concentration and particle size with time indicates the nucleation event. The nucleation events usually lasted for one hour (Table 4.1b) and ended always before the end of the emission period. Table 4.1b lists the calculated growth and formation rates for each nucleation event. The average GR and J_D for the first set of measurements was $29.2 \pm 6.4 \text{ nm/h}$ and $16.6 \pm 6.1 \text{ cm}^{-3}\text{s}^{-1}$, respectively, whereas, for the second set of measurements the values were $38.5 \pm 9.4 \text{ nm/h}$ and $101.9 \pm 114.1 \text{ cm}^{-3}\text{s}^{-1}$, respectively. Overall, the average GR and J_D of the 10 nucleation events inside the laboratory was $33.9 \pm 9.1 \text{ nm/h}$ and $21.1 \pm 8.7 \text{ cm}^{-3}\text{s}^{-1}$, respectively. The highest values of GR and J_D obtained on 27/01/14 and 29/01/14 (second set) and were mainly affected by the high indoor concentration measured in the laboratory during these two experiments.

Calculations of loss coefficients due to deposition were performed for particles with diameters from 10 to 50 nm. The computed values ranged from 0.3 h^{-1} for 10 nm particles to 0.009 h^{-1} for 50 nm particles, which suggests that in the current study the deposition losses might affect the nucleation process and reduce the intensity of the

4.1. New Particle Formation Events from Painting Materials

phenomenon. Nevertheless, since maximum indoor PN concentrations were achieved in a time period less than 10 min, it is expected that the effect of deposition in the particle concentration was not significant. High GR and J_D compared to outdoor nucleation events were observed in all the experiments conducted in the laboratory. The high GR and J_D values were encountered due to the abrupt burst of organic substances inside the laboratory along with the small scale of the phenomenon due to the volume of the laboratory (54 m^3). Moreover, the duration of the nucleation event plays a significant role for the calculation of the GR and J_D .

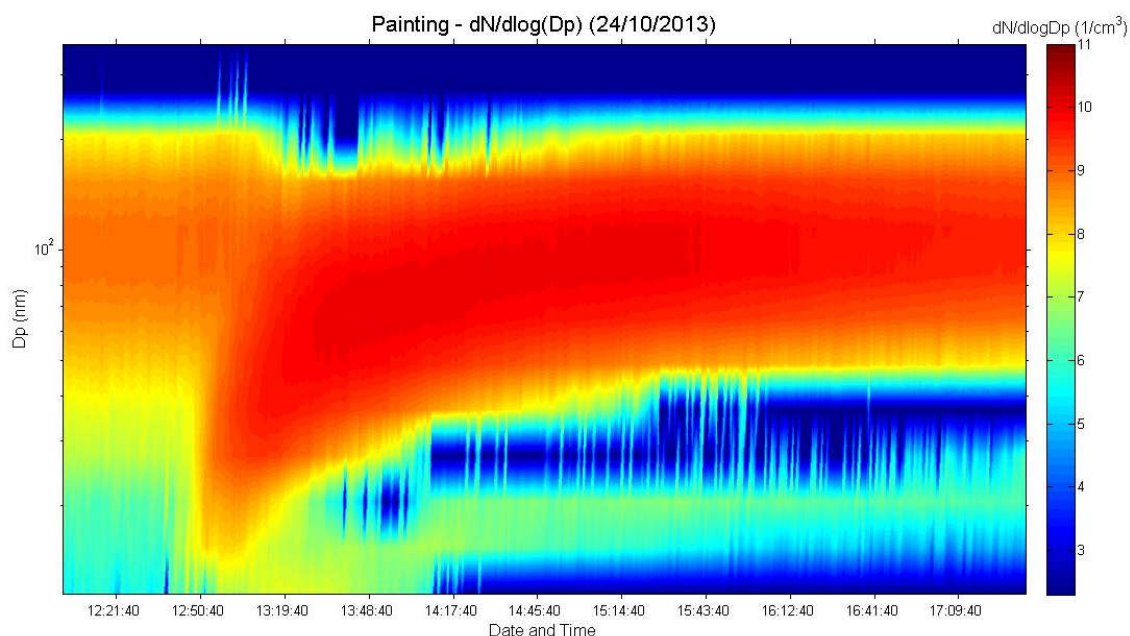


Figure 4.5. Particle number concentration inside the laboratory versus time during an experiment on 24/10/13.

Outdoor nucleation at the same site (Akrotiri station) usually lasted for several hours. The reported duration of the nucleation events outdoors varied between 4 and 21 h (Kopanakis et al., 2013), whereas in the presented study the duration of the nucleation events indoors usually lasted for less than an hour. This feature has a significant impact on the calculated GR and J_D . In Kopanakis et al. (2013) the average GR and J_D found at $6 \pm 4 \text{ nm/h}$ and $13 \pm 10 \text{ cm}^{-3}\text{s}^{-1}$, respectively. Similar studies close to the coastal area of the Mediterranean revealed growth and formation rates considerably lower than the ones

4.1. New Particle Formation Events from Painting Materials

presented here. Kalivitis et al. (2008) reported the formation rate was at $1.1\text{--}1.7\text{ cm}^{-3}\text{s}^{-1}$, while Cusack et al. (2013) observed the growth rate of the nucleation events ranging between 1.3 and 6.9 nm/h. Hovorka and Braniš (2011) observed nucleation events that took place in large indoor space and the reported growth rates were close to 2.6 nm/h. Moreover, it was found that after the end of the nucleation event, condensational growth of the indoor particles took place for several hours.

The average particle diameter, as calculated by Eq. (4.1), continued increasing for a few hours. Hovorka and Braniš (2011) also reported condensational growth of indoor particles after the end of the nucleation event. It should be noted that the particle condensational growth took place exactly after the end of the nucleation event. Considering that all nucleation events lasted for maximum one hour and the emission period (stage 2) lasted for 1.5 h, condensational growth observed usually at the end of stage 2 (emission period) and for a few hours during stage 3 (removal period). Table 4.1b also presents the growth rates derived after the end of the nucleation event for each experiment. Significant differences between nucleation period and post nucleation period were observed. The growth rate during the nucleation events lasted for maximum 1 h, whereas, particle condensation lasted for several hours (1.4–4.1 h). Moreover, the rate of condensation during the nucleation event was always higher than the rate of condensation indicating that the condensation after the end of the nucleation was less intensive. The average condensational growth rate was 11.6 nm/h. A coagulation of indoor particles is also to be considered since at the removal period the indoor particle concentration was decreased.

In order to confirm that the new particle formation events originated from indoors due to the emissions from the painting materials, the outdoor PN concentration, measured at Akrotiri meteorological station, was also examined. No new particle formation events were recorded before, during and after the end of the experiments for each day of the first measurements' period. As an example, Figure 4.6 presents the fluctuations of the outdoor PN concentration at Akrotiri station on 24/10/13. It is obvious that there was no new particle formation event during the sampling period on that day. Consequently, the nucleation event observed inside the laboratory, started and evolved indoors. Even if there was penetration of particles from the ambient atmosphere inside the laboratory, the

4.1. New Particle Formation Events from Painting Materials

measured low outdoor number concentration suggests that outdoor particles were not associated with the nucleation event observed indoors. In conclusion, no new particle formation events occurred in the outdoor environment and low outdoor concentrations were measured in all sampling periods.

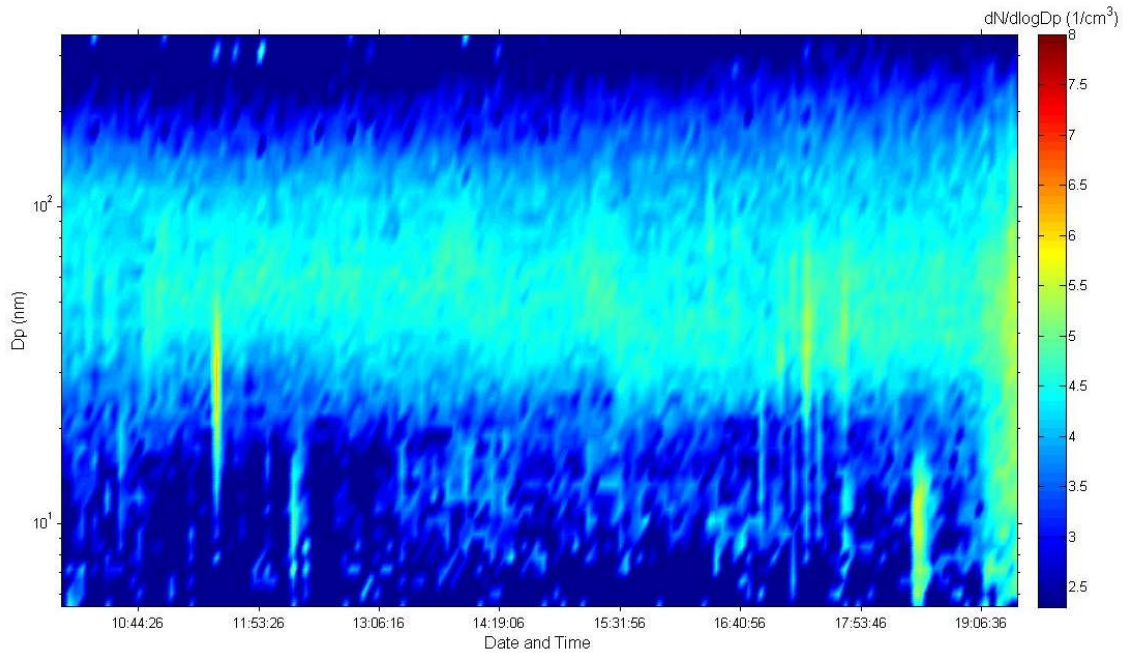


Figure 4.6. Outdoor number concentration of particles at Akrotiri station on 24/10/13.

Moreover, a comparison of the indoor and the outdoor concentration on the same day (24/10/13) is presented in Figure 4.7. Average outdoor concentration of particles on 24/10/13 was $4.8 \times 10^4 \pm 9.1 \times 10^4 \text{ \#/cm}^3$, whereas average indoor particle concentration was $7 \times 10^4 \pm 1.9 \times 10^4 \text{ \#/cm}^3$. Temporal increases of outdoor concentration were observed at noon or late afternoon. During these periods, the outdoor concentration reached values sometimes as high as indoors. Temporal increases of outdoor particle concentration at this site is associated with local sources (traffic, domestic heating) or transport of polluted air masses (Lazaridis et al., 2005; Kopanakis et al., 2013). Since the duration of these increases usually lasted only for a few minutes (10–20 min), it is believed that they are mainly affected by the local sources. Therefore, there is no correlation between the fluctuations of outdoor particle concentration and the indoor one.

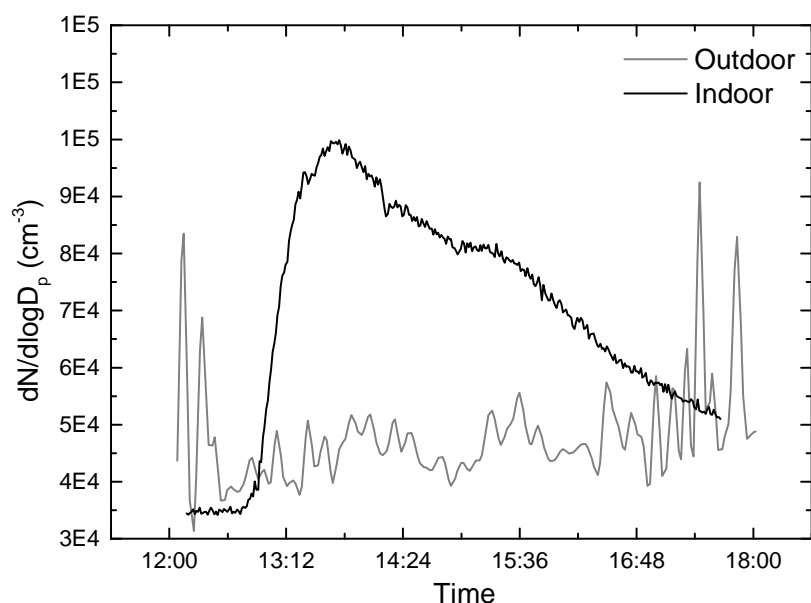


Figure 4.7. Comparison of outdoor and indoor particle number concentrations during an indoor nucleation event on 24/10/13.

4.1.9. PSD during Different Stages of the Experiment

The PSD was obtained for different periods through the total duration of the experiments. Each experiment was separated into 5 periods (background, emission periods A, B, and removal periods A, B) and the average values for each period were calculated. In practice, each period corresponds to a stage of the experiment (background (stage 1), emission period A, B (stage 2) and removal period A, B (stage 3)). Stages 2 (emission) and 3 (removal) were divided into two periods (A and B) in order to isolate the changes on the characteristics of the PSD through the progress of the experiments. The duration of periods A and B were equally distributed depending on the total duration of each stage of each experiment. In general, the PSDs showed similar characteristics for all experiments with exceptions in emission period A. Additionally, the PSD was examined through the progress of the new particle formation events. PSD during the emission period was closely related to the new particle formation event. There is an evolution of the size distribution with time. Although the PSDs from the two experimental sets had similar behavior, certain differences apply on the evolution of the distribution through the duration of the particle generation periods. The study of the evolution of the new

4.1. New Particle Formation Events from Painting Materials

particle formation events essentially demonstrates the differences in emission period A between the two sets of experiments.

In general, the beginning of the new particle formation event was characterized by a size distribution with two dominant modes: the first one located at nucleation particle mode (~ 20 nm) and the second one located at higher particle sizes. This is indicating that the dominant particle modes were two: one at small particle sizes responsible for the start of the event and one at larger particle sizes, which characterizes the major particle size contribution inside the laboratory. During the first minutes of the nucleation event, the second and dominant particle mode was present at higher number concentrations. However, as the phenomenon started evolving (burst of new particles) the nucleation mode increased rapidly along with time reaching high PN concentrations.

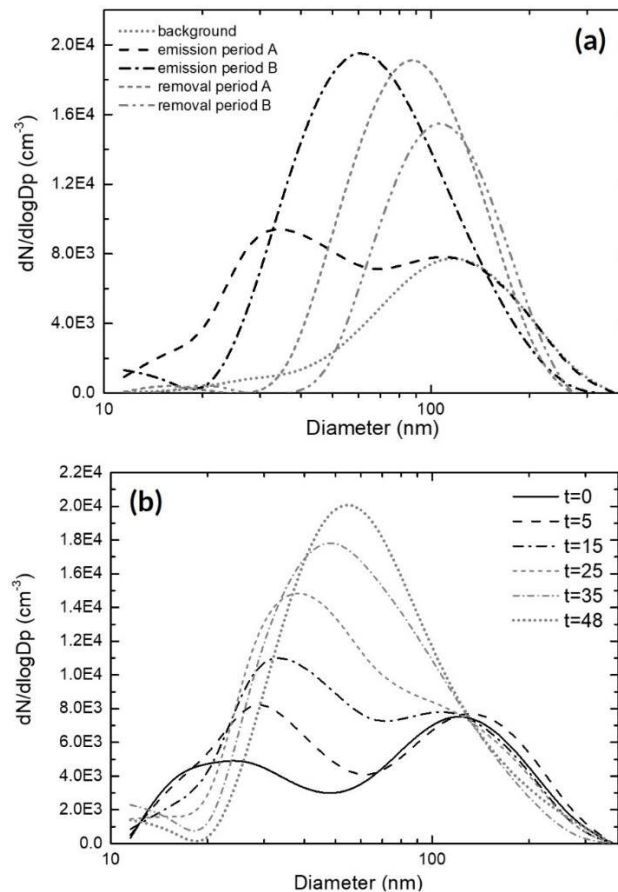


Figure 4.8. Particle size distribution on 01/11/13: a) different stages of the experiment; and b) evolution of the particle size distribution during the nucleation period (in minutes).

4.1. New Particle Formation Events from Painting Materials

Figure 4.8a presents a typical PSD of the first set of measurements for an experiment on 01/11/13. The size distribution of BC was characterized by a dominant mode located at 115 nm. However, in emission period A two dominant modes were observed, located at 36 nm and 115 nm, respectively. At this period, the nucleation mode was present in the indoor air due to the burst of new particles from the painting materials. Particles started to grow by condensation resulting in continuous increase of indoor PN concentration. During emission period B, the PSD presented one dominant mode (65 nm) due to coagulation of the indoor particles and it was characterized by the highest average number concentration ($1.9 \times 10^4 \text{ \#/cm}^3$). During the removal periods A and B, no other activities took place inside the laboratory, and the size distribution was characterized again by one dominant mode. However, during these periods the indoor PN concentration decreased with time due to deposition and coagulation. The dominant particle diameter shifted to bigger particle sizes (65–115 nm). The results are consistent with the study presented by Lamorena et al. (2007).

On the other hand, Figure 4.8b plots the evolution of the PSD only during the new particle formation event for the same experiment (01/11/13). The PSD is presented at different times during the nucleation burst, starting from $t=0$ until the end of the formation period at $t=48$ min. At the beginning ($t=0$), the distribution was characterized by two modes: the nucleation mode at 20 nm with particle concentration $4.8 \times 10^3 \text{ \#/cm}^3$ and the accumulation mode at 115 nm with particle concentration at $7.9 \times 10^4 \text{ \#/cm}^3$. However, after 5 min, the nucleation particle mode shifted towards bigger diameter (27 nm) and higher particle concentration ($8.2 \times 10^3 \text{ \#/cm}^3$), which was higher than the concentration at the accumulation mode ($7.5 \times 10^3 \text{ \#/cm}^3$). This is indicating a burst of new particles inside the laboratory. From $t=5$ to $t=48$ min, particles at nucleation mode grew by condensation and coagulation until the end of the new particle formation event resulting in the shift of the original distribution to PSD with one dominant mode. Particle size and number concentration increased along with the evolution of the event and reached the highest value at $t=48$ min with dominant mode located at 50 nm.

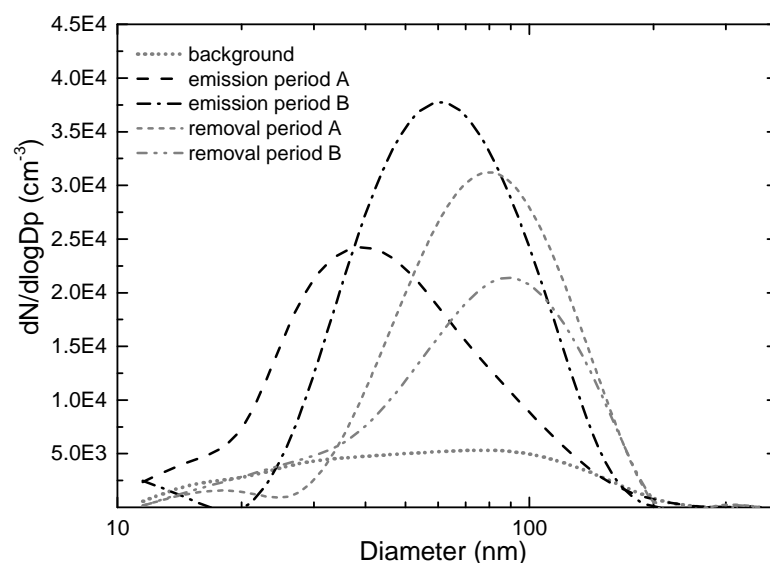


Figure 4.9. Particle size distribution at different stages during an experiment (28/01/14).

The major difference of the PSD at the second set of measurements was observed at the emission period A. The particle distribution was characterized by a dominant mode in all 5 experiments and this is probably associated with higher PN concentrations (Table 4.2) and nucleation characteristics (growth/formation rate, Table 4.1b). However, the size distribution of BC in 3 experiments (29/01/14, 30/01/14 and 31/01/14) was characterized by two dominant modes, one at particle size < 50 nm and a second mode at sizes between 50 and 100 nm. Figure 4.9. presents the PSD on 28/01/14, where a dominant particle mode located at 90 nm was observed in background period.

In contrast to Figure 4.8a, the size distribution at the emission period A presented one dominant particle mode located at 37 nm. However, the values presented on Figures 8 and 9 were obtained from the average number concentration of each particle size. This is indicating that the final result is dominated by the characteristics of each size distribution. In fact, the nucleation fraction of particles was present in the first minutes of the emission period (emission period A), but was observed in the second set of measurements due to high growth and formation rates. Thus, the initial mode observed at nucleation fraction embedded faster to the total size distribution. As a result, the size distribution at emission period A in the second set of measurements was found to be dominated by one mode.

4.1. New Particle Formation Events from Painting Materials

In agreement with Figure 4.8a, in emission period B the PN concentration was the highest with $3.8 \times 10^4 \text{ \#/cm}^3$ at the particle size close to 65 nm. During the removal periods A and B, the dominant particle size moved to 87 nm with a simultaneous decrease in the PN concentration ($3.1 \times 10^4 \text{ \#/cm}^3$ and $2.1 \times 10^4 \text{ \#/cm}^3$, respectively). It is likely that deposition and coagulation determined the particle characteristics at removal period. The indoor PN concentration decreased due to deposition of particles on indoor surfaces, while coagulation forced the indoor particles to collide with each another and form bigger particles (Hinds, 1999; Glytsos et al., 2010).

Additionally, Figure 4.9 plots the evolution of the new particle formation from the experiment on 28/01/14. At $t=0$, the size distribution is characterized by the nucleation particle mode at 15 nm and a second mode at 37 nm with number concentration $1.0 \times 10^4 \text{ \#/cm}^3$ and $9.7 \times 10^3 \text{ \#/cm}^3$, respectively. After 5 min, the PN concentration at nucleation mode increased significant ($1.8 \times 10^4 \text{ \#/cm}^3$) and shifted to higher particle sizes (20 nm) indicating the burst of ultrafine particles to the indoor air. Nucleation mode became dominant at $t=10$ min due to the formation of the new particles and the growth by condensation. The dominant mode was located at 27 nm with PN concentration $3.0 \times 10^4 \text{ \#/cm}^3$. However, at $t=15$ min the size distribution was dominated by one mode located at 36 nm (in contrast to Figure 4.8b).

Moreover, it was found that all nucleation events of the second set of measurements shifted towards size distribution with a dominant particle mode earlier than the first set of measurements. This is strongly associated with the higher growth rates observed in the second set of measurements. The growth rate on 28/01/14 was 34.2 nm/h, whereas on 01/11/13 it was 22.6 nm/h, indicating a difference of more than 10 nm/h between the two experiments. Higher growth rate corresponds to higher condensation rate. Moreover, at $t=15$ min the PN concentration at the dominant particle mode (37 nm) was $3.5 \times 10^4 \text{ \#/cm}^3$ ($1.1 \times 10^4 \text{ \#/cm}^3$ on 01/11/13), indicating higher coagulation rate (Hinds, 1999). Thus, a size distribution characterized by one dominant mode is observed earlier in the second set of measurements. From $t > 15$ min until the end of the nucleation event, PN concentration increases with time reaching the highest indoor concentration ($3.7 \times 10^4 \text{ \#/cm}^3$, $dN/d\log D_p$) with dominant particle mode located at 50 nm.

4.1.10. Conclusions

The presented study focused on emissions from painting materials in an indoor microenvironment. Painting activity and use of different turpentine oils were selected as a source of emission. Painting itself (oil paints) did not evoke significant changes neither in PN nor in PM₁₀ concentration. On the other hand, emissions from the turpentine oils used for painting were identified as a significant source of indoor emissions resulting in a burst of new particles inside the laboratory. In general, the new particle formation events were characterized by high growth and formation rates. On average, the particle growth rate was 33.9 ± 9.1 nm/h, whereas the particle formation rate was 21.1 ± 8.7 cm⁻³ s⁻¹. The high formation and growth rates was caused by the abrupt burst of organic substances along with the small volume area of the laboratory. In conjunction with the high TVOC concentrations measured after the opening of the bottles, there is a satisfactory evidence that the new particle formation events were triggered by the painting materials. On the other hand, low PN concentration measured outdoors without recording any new particle formation event ensures that the new particle formation events were of indoor origin. Subsequent particle condensational growth underlines the major impact of the organic substances to the indoor particle interactions. Although, new particle formation event is a crucial issue for the outdoor air particle dynamics, results presented in this chapter provides an evidence that nucleation is possible as a micro-scale phenomenon when the necessary gaseous precursors are present.

4.2. Evaluation of Nanoparticle Emissions from Laser Printers

4.2.1. Introduction

Indoor contaminants involve a variety of chemical compounds and gaseous pollutants. As the main component of particulate matter, indoor pollutants essentially influence indoor air quality (IAQ) with human occupational health being on the focus for improving environmental conditions. Accordingly, several studies have investigated the effect of ventilation and air-condition system (HVAC) to indoor concentration of particles (Fisk et al. 2000; Liddament et al. 2000; Quang et al. 2013; Park et al. 2014; Chatoutsidou et al. 2015). These studies indicate the effective removal of outdoor particles through the ventilation system, thus reduce human exposure to ambient pollutants. Nonetheless, human occupation itself can cause particle generation and release of numerous chemical compounds by indoor activities (Nazaroff and Weschler, 2004; Wu et al., 2012; Sangiorgi et al., 2013; Hussein et al., 2015).

In general terms, pollutants may be considered as outdoor or indoor origin. Outdoor originated pollutants include all compounds that are transported indoors mainly by natural convection. In this case, technical characteristics of the buildings play an important role such as mechanical ventilation, filters, insulation from doors and windows (Taylor et al., 1999; Liu and Nazaroff, 2001; Tian et al., 2009; Lai et al., 2012). Indoor concentrations are then closely associated with the outdoor ones. Alternatively, pollutants may originate from indoor sources as the product of human occupation, where chemical composition and characteristics of indoor pollutants are directly linked with primary sources. IAQ in office environments is highly affected by photocopier equipment as shown by numerous studies (Lee and Hsu, 2007; Kagi et al., 2007; Koivisto et al., 2010; McGarry et al., 2011), whilst the physical presence of the occupants can contribute as well (Fisk et al., 2000; Chatoutsidou et al., 2015).

Multi-zone environments have been investigated the last years in order to examine the impact from particle transport and airflows indoors (Miller and Nazaroff, 2001; Kao et al., 2009; Ng et al., 2013; Rim et al., 2013; McGrath et al., 2014). It was found that multi-zone environments and the relevant concentrations are affected by several factors, those belong to building design and those to the primary emissions.

4.2. Evaluation of Nanoparticle Emissions from Laser Printers

Accordingly, primary emissions and the related source characteristics (concentration, size distribution, duration of emission) affect IAQ with enrichment of the indoor air with pollutants, with the location of the source playing a significant role. On the other hand, building design and operation of the ventilation system has major impact to airtightness of the building and inter-zone distribution through exhaust or supply flows (Ng et al., 2013). Higher exchange rates are recommended in cases of higher pollutant concentrations, where, inhalation exposure can be considerably reduced. Internal layout, airflows or door configuration determine particle transport to indoor areas and dilution of the indoor concentrations (McGrath et al., 2014). Printers release mostly nanoparticles and since the toxicity and health effects of nanoparticles do not necessarily depend on their mass (Muller et al., 2005; Donaldson et al., 2006; Poland et al., 2008; Dhawan and Sharma, 2010), particulate mass as a parameter to assess material toxicity is not of such importance as it was considered in the past years.

Elemental, physicochemical and morphological composition of 40 metals and 100 semi-volatile organic compounds (SVOC) were assessed by Bello et al. (2013) for nanoparticles emitted from printer. Their study shows that engineered nanoparticles, including titanium dioxide, iron oxide and fumed silica, and several metals were found in toners and airborne nanoscale fraction, and that the chemical composition of examined nanoparticles reflected toner chemistry, which is consistent with previous studies (Barthel et al., 2011; Castellano et al., 2012). Results from few studies reported that the nanoparticles generated from printers originated from secondary formation processes, rather than from toner powder (Kagi et al., 2007; Wensing et al., 2008). Morawska et al. (2009) suggested that the nanoparticles generated from laser printers are rather secondary organic aerosol (SOA) formed from reactions between VOCs from laser printers and ozone present in the office where also heat plays an important role. Wolkoff et al. (1993) pointed out that the increase of TVOC after the finished printing might be due to the high temperature inside and outside the printer after completion of the print task.

A significant aspect that needs to be investigated with more detail is the formation mechanisms and the processes inside the printers leading to nanoparticle emissions. Wang et al. (2011a) characterized the nanoparticle formation mechanisms and found that nanoparticles were primarily emitted during cold startup or cold printing if the laser

4.2. Evaluation of Nanoparticle Emissions from Laser Printers

printer had enough time to cool down the internal surfaces. Furthermore, the results revealed that the nanoparticles are presumably generated from ion-induced nucleation of vapor-phase organic compounds, which are released from the toner powder during the rapid heating of internal printer surfaces. Most studies dealing with the impact of particle emissions from printers on IAQ are conducted under controlled conditions (He et al., 2010; Koivisto et al., 2010) or in an environmental chamber (Schripp et al., 2008; Wang et al., 2012b). There is still lack of field studies concerning the printer emission characteristics, especially combination of a field study (McGarry et al., 2011; Castellano et al., 2012) with a detailed chamber study (Shi et al., 2015) in conjunction with an evaluation of actual human exposure to printer emissions under real conditions (Tang et al., 2012).

Although, emission characteristics from laser printers are widely investigated, experimental studies in real working environments are scarce; hence, occupational exposure to these contaminants is still limited. This chapter presents the results from investigation of the influence of printer emissions to the indoor environment and to examine the particle concentrations in the IT & Communications Center of Technical University of Crete equipped with a print room (PR). The influence of human occupation was examined in conjunction with printer emissions in an office nearby, whilst the contribution of the outdoor environment was also investigated. Additionally, evaluation of the nanoparticle emissions from a chosen printer obtained from PR, and characterization of the processes that lead to increased nanoparticle concentrations was studied as well. Measurements were conducted in a small stainless steel environmental chamber under controlled conditions, where evolution of particle size distribution (PSD) with time and printed pages is studied in detail.

4.2.2. Sampling Site and Experimental Chamber

Indoor/outdoor one-week sampling campaign was conducted at the Technical University of Crete in period of 18-25 of May 2015 and the indoor sampling was performed in a building, which is a part of the School of Environmental Engineering. Outdoor PM₁₀ sampling was sited 50 m away from the under study building in approximately 1.5 m

4.2. Evaluation of Nanoparticle Emissions from Laser Printers

above the ground. The area surrounding the university campus corresponds to an urban/semi-rural area and is 5 km NW of the city of Chania. Detailed description of the area can be found in Lazaridis et al. (2008) and in Kopanakis et al. (2013). The building consists of offices and computer rooms on the ground floor and offices and a few laboratories on the first floor. All offices and laboratories on both floors are connected to the main corridor, which has two exits, one on each end. The two floors are connected with an elevator, stairwell and there are also two square-shaped well-like floor openings (4 m^2).

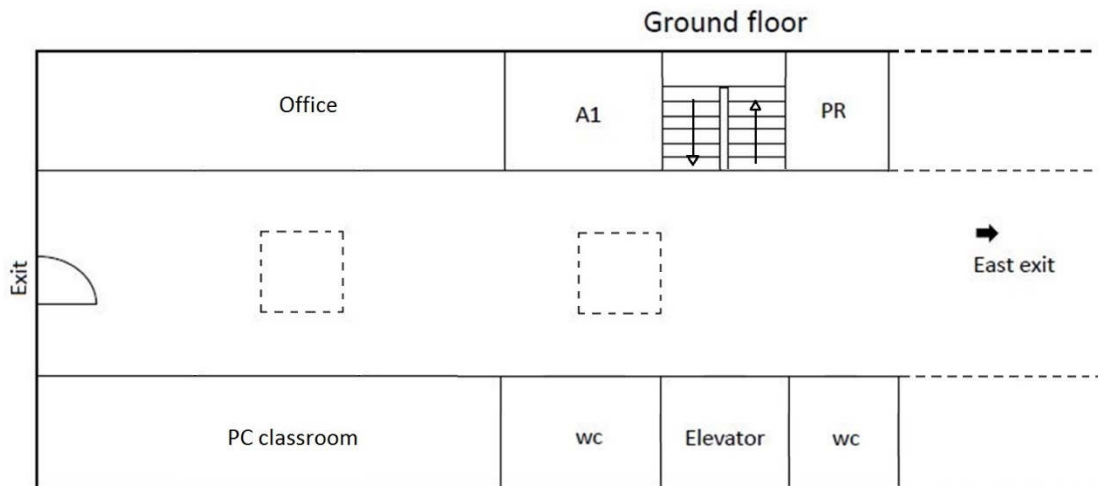


Figure 4.10. Floor plan and location of the print room (PR) and office (A1).

The building is occupied daily on weekdays from 09:00 to 21:00. The building is equipped with mechanical ventilation and separate A/C system, both of them operated manually by the occupants. Mechanical ventilation uses district ventilation ducts for entrance and exhaust of the airflows and does not have any filters to capture particles from outdoors. Therefore, the offices are connected with each other through ventilation ducts, depending on their location in the building. One office and a print room were selected on the ground floor. Figure 4.10 shows the simplified floor plan, the office (A1) and the print room (PR) are of rectangular shape (17 m^2) with one window and one door

4.2. Evaluation of Nanoparticle Emissions from Laser Printers

leading to the corridor. Mechanical ventilation was turned off during the campaign but the air condition system was selectively used by the occupants in A1 only.

Office A1 was occupied permanently by staff (1-3 persons), but also students entered the office occasionally for a short period. No hardcopy device was present inside A1, but common office equipment (computers, telephones) and furniture (desks, chairs, shelves). On the contrary, PR is a printer room with 4 professional printers (2x HP LaserJet 9050, Xerox 4110 PS and HP LaserJet 550) used by the university students during opened hours. PR is not permanently occupied, but several students enter the room briefly. Sampling in both A1 and PR were done in ~1.8 m height. Windows in PR and A1 were closed during the campaign, and the doors in PR and A1 were constantly opened during office hours. The printers' distances from the sampling point were 2 to 4 m. Temperature and relative humidity throughout the campaign were recorded to be $27 \pm 1^\circ\text{C}$ and $43 \pm 4\%$, respectively. The toner cartridge, fuser roller and the paper used in the chamber study were provided by IT & Communications Center, and are the same used by printers in the PR. During the field study, on average ~11,000 pages were printed daily, 67% of which by one printer (Xerox 4110 PS).

In order to maintain similar environmental conditions throughout the whole experiment in the chamber, temperature and was controlled with an A/C installed outside the chamber. The temperature during printing hours was kept on $26 \pm 1^\circ\text{C}$ and the average relative humidity was $60 \pm 5\%$. Chamber and sampling tubes were tested for leaks prior to the beginning of the measurements and the particle number and mass concentration were monitored at all times. The printers' emissions were sampled from one point, approximately 0.5 m from the printed page discharge outlet at the corner of the printer (Figure 4.11) so that it was also relatively close to the emitted particles from cooling fans (at the back of the printer). Instrument sampling the total VOC was placed inside the chamber, just above the discharge outlet.

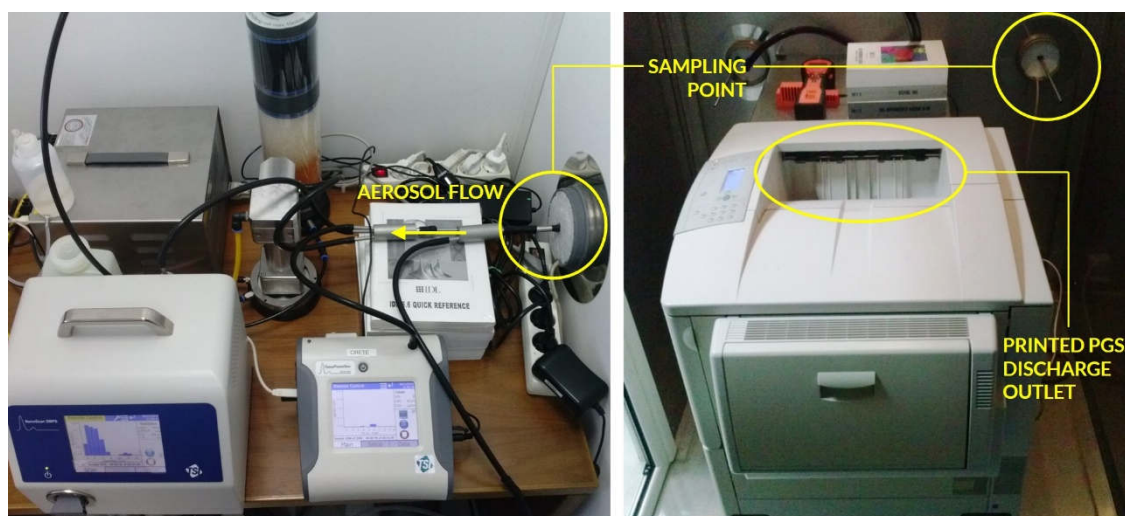


Figure 4.11. Experimental setup used to measure printer emissions in the chamber study.

4.2.3. Methods and Instrumentation

Based on printers' print statistics from one busy week in May (beginning of summer exam period) and October (freshmen registration) in 2015, one of the 4 printers from the PR was chosen to be tested in the chamber. HP LaserJet 9050 was equipped with the same refilled black toner cartridge was employed, which is used by printers in the PR (other than the one specified by the manufacturer). Prior to the beginning of the measurements a new (refilled) cartridge was inserted. The paper used for printing was for Office Deluxe white copy paper with weight of 80 g/m^2 and was stored outside the chamber.

According to the printer's statistics, this printer prints on average 2037 pgs./day and operates almost 11 hours every working day (opened hours 09:00-21:00, Monday-Friday). Table 4.3 shows the average distribution of printed pages and the times during a work day when the print jobs occurred. A typical printing day was simulated 3 times (on 16/11, 17/11 and 19/11), according to Table 4.3, and then once with a different schedule (18/11) where 226 pages of plain text were printed 3 times and afterwards 137 pages of text and figures were printed 3 times as well. Additionally, the cartridge and fuser were exchanged for new ones after the last print of the previous day in order to

4.2. Evaluation of Nanoparticle Emissions from Laser Printers

assess the emissions from printer startup and printing with the new installed parts (on 20/11). Two times 50 pages and then 100 pages of text were printed within 3 hours.

Table 4.3. Average distribution of print jobs for HP LaserJet 9050.

| Hours | Cumulative hours | Average percentage | Printed pages |
|---------------|------------------|--------------------|---------------|
| 09:00 - 10:00 | 1 | 5% | 110 |
| 10:00 - 11:00 | 2 | 8% | 159 |
| 11:00 - 12:00 | 3 | 13% | 255 |
| 12:00 - 13:00 | 4 | 11% | 229 |
| 13:00 - 14:00 | 5 | 10% | 208 |
| 14:00 - 15:00 | 6 | 16% | 322 |
| 15:00 - 16:00 | 7 | 10% | 197 |
| 16:00 - 17:00 | 8 | 8% | 153 |
| 17:00 - 18:00 | 9 | 8% | 154 |
| 18:00 - 19:00 | 10 | 7% | 151 |
| 19:00 - 20:00 | 11 | 3% | 63 |
| 20:00 - 21:00 | 12 | 2% | 35 |
| SUM | | 100% | 2037 |

Particle number (10-350 nm) and mass concentrations (0.3-10 μm) in PR was measured with NanoScan SMPS (3910, TSI) and OPS (3330, TSI), respectively. Additionally, number concentration of fine particles (< 1 μm) in office A1 was measured by P-Trak (8525, TSI). Indoor particle mass concentration in A1 was measured with DustTrak II (8532, TSI) and a DustTrak DRX (8534, TSI) was employed in PR. Outdoor particle mass concentration was measured with a DustTrak II (8530, TSI). Several instruments were used to measure particle concentration from printer emissions in the chamber study. More precisely SMPS (CPC Model 5.403 coupled with M-DMA - Vienna type, Grimm) for detailed particle number size distribution (5-350 nm) analysis, NanoScan SMPS for calculation of exposure doses and comparison with the field study, OPS for mass concentration measurements, and PhoCheck Tiger (ION Science) for the estimation of the TVOC.

In addition, average of total losses due to diffusion, inertial deposition and gravitational settling in the sampling tubing in the chamber measurements for the particle

4.2. Evaluation of Nanoparticle Emissions from Laser Printers

size range found in this study were negligible for NanoScan and OPS as they were estimated to be less than 2.4%. Finally, the first two days the sampling in the chamber was done only with CPC (due to M-DMA technical error) and the rest of the days were conducted with SMPS. Transport losses correction for CPC and SMPS were not applied because in the CPC only total particle number concentration is measured, so the particle loss correction cannot be applied without knowledge about particle size. In order to receive comparable results, the particle losses were not applied to SMPS data either. However, the losses were on average 17% and 2% for particles <20 nm and for particles 20-350 nm, respectively.

4.2.4. Two-Compartment Indoor Mass Balance Model

Consider a two-compartment indoor volume (i and j) with an AC operating system where particles are emitted only at compartment i . Assuming a well-mixed air volume, indoor particle concentration in compartment i can be described by a mass balance model:

$$\frac{dC_{in,i}}{dt} = PaC_{out} - aC_{in,i} - kC_{in,i} - \lambda C_{in}\eta + b_1C_{in,j} - b_2C_{in,i} + \frac{S}{V} \quad (\text{Eq. 4.4})$$

where, $C_{in,i}$ is the indoor particle number concentration ($\#/cm^3$) at i compartment, $C_{in,j}$ is the indoor particle number concentration ($\#/cm^3$) at j compartment, C_{out} is the outdoor particle number concentration ($\#/cm^3$), P is the penetration efficiency from outdoors, a is the air exchange rate (h^{-1}) with the outdoor environment, λ is the recirculation rate of the indoor air in the AC system (h^{-1}), η is the single-pass removal efficiency of the AC system, b_1 (h^{-1}) is the airflow rate from compartment j to i , b_2 (h^{-1}) is airflow rate from compartment i to j , k is the deposition rate (h^{-1}) in compartment i , S is the emission rate of particles (h^{-1}), V is volume of the area under study (cm^3) and t is the time (h). Coagulation was considered negligible since indoor PN concentration was rarely higher than $10^4 \#/cm^3$ in the present study (Hussein et al. 2009). Eq. (4.4) can be used to

4.2. Evaluation of Nanoparticle Emissions from Laser Printers

determine the total removal of particles in compartment i when no source is present ($S = 0$). Thus, Eq. (4.4) is rewritten:

$$\frac{dC_{in,i}}{dt} = PaC_{out} + b_1C_{in,j} - (a + k + \lambda\eta + b_2)C_{in,i} \quad (\text{Eq. 4.5})$$

where, the total removal rate is expressed by the quantity $a+k+\lambda\eta+b_2$, which corresponds to losses due to airflow from the under study volume to outdoors (a) or to compartment j (b_2), losses to filtration of the indoor air by the AC system ($\lambda\eta$) and losses due to particle deposition on indoor surfaces (k). On the contrary, the first two terms on the right hand side of Eq. (4.5) express the airflow into the under study volume from outdoors and from indoors respectively, thus, have a positive contribution to indoor particle concentration at compartment i . Eq. (4.5) can be solved analytically, therefore indoor PN concentration at any time t is given as:

$$C_{in,i}(t) = \frac{aPC_{out} + b_1C_{in,j}}{a + k + \lambda\eta + b_2} + \left[C_{in,i}(0) - \frac{aPC_{out} + b_1C_{in,j}}{a + k + \lambda\eta + b_2} \right] e^{-(a+k+\lambda\eta+b_2)t} \quad (\text{Eq. 4.6})$$

Eq. (4.6) suggests that the indoor PN concentration is exponentially decreasing with a rate equal to $a+k+\lambda\eta+b_2$. Subsequently, the first term in the right hand side of Eq. (4.6) represents the PN concentration that remains suspended indoors, but originates from penetration from outdoors or is transported from indoors. Eq. (4.4) was used as a mass balance model in order to evaluate the contribution from printer emissions inside PR. Therefore, the contribution from other internal areas into PR was incorporated as a common term in Eq. (4.4) -compartment j - considering that the major source of nanoparticles was located in PR (printers).

4.2.5. Particle Number Concentrations in the Print Room

In a controlled chamber study, all relevant parameters influencing printer emission are well defined and the characteristics of emitted particles can be studied in detail. This scenario, however, does not reflect the real situations where influences, such as environment background aerosol, occupants and other important factors playing a significant role. Therefore, field measurement is an important asset in evaluation of nanoparticle emissions from laser printers. For this reason, an intensive one-week campaign was performed in the print room of the IT & Communications Center, where the studied HP LaserJet 9050 is permanently located.

Figure 4.12 plots the particle number concentration in the size range of 10-350 nm in the PR with the total number of printed pages from all four printers. Average background concentration for both, nights (21:00-09:00) and weekend, was equally $3.1 \times 10^3 \text{ \#/cm}^3$, while the average PN concentration during printing was $5.4 \times 10^3 \text{ \#/cm}^3$. Similarly, as it was observed in the chamber measurements, there was a sharp increase in PN concentration every day during printers' startup where the maximum concentrations early in the morning (08:00-09:00) on workdays reached on average $4.4 \times 10^4 \text{ \#/cm}^3$ (see Table 4.4). Interestingly, the PN concentration at startup after the weekend on 25/05 was even higher than on last day before the weekend ($5.2 \times 10^4 \text{ \#/cm}^3$).

Table 4.4. Total particle number concentrations (\#/cm^3) during measurements in the PR.

| Conc./Date | *18/05 | 19/05 | 20/05 | 21/05 | 22/05 | Average |
|-------------------|--------------------|--------------------|--------------------|--------------------|--------------------|--------------------|
| Printed pages (#) | 5.06×10^3 | 1.69×10^4 | 9.28×10^3 | 1.26×10^4 | 1.04×10^4 | 1.08×10^4 |
| Night (before) | - | 3.79×10^3 | 2.12×10^3 | 3.01×10^3 | 3.31×10^3 | 3.06×10^3 |
| Startup (average) | - | 2.44×10^4 | 3.11×10^4 | 2.20×10^4 | 2.65×10^4 | 2.60×10^4 |
| Startup (max) | - | 4.07×10^4 | 4.63×10^4 | 4.13×10^4 | 4.59×10^4 | 4.36×10^4 |
| Printing | 5.59×10^3 | 4.92×10^3 | 3.62×10^3 | 6.06×10^3 | 7.02×10^3 | 5.44×10^3 |

*measurement campaign started at 12.00

There were 3 sharp PN concentration increases that may not relate to printing itself, two on 21/05 and one on 22/05 (see Figure 4.12). In the first case on 21/05 the PN concentration increase also might be caused by cleaning of the corridor just outside the

4.2. Evaluation of Nanoparticle Emissions from Laser Printers

PR. Emissions from cleaning agents usually involve nanoparticle generation as a product of SOA (Coleman et al., 2008; Huang et al., 2011; Nørgaard et al., 2014), but it was rather unlikely the cleaning was the cause of PN concentration increase in the other 2 cases due to duration, PN concentrations, dominant size modes and the actual time when the increases occurred. During the second event on 21/05 (late afternoon) the peak reached the same concentrations as during startup ($4.6 \times 10^4 \text{ \#/cm}^3$) and was certainly not caused by SOA from cleaning agents (cleaning usually takes place around noon).

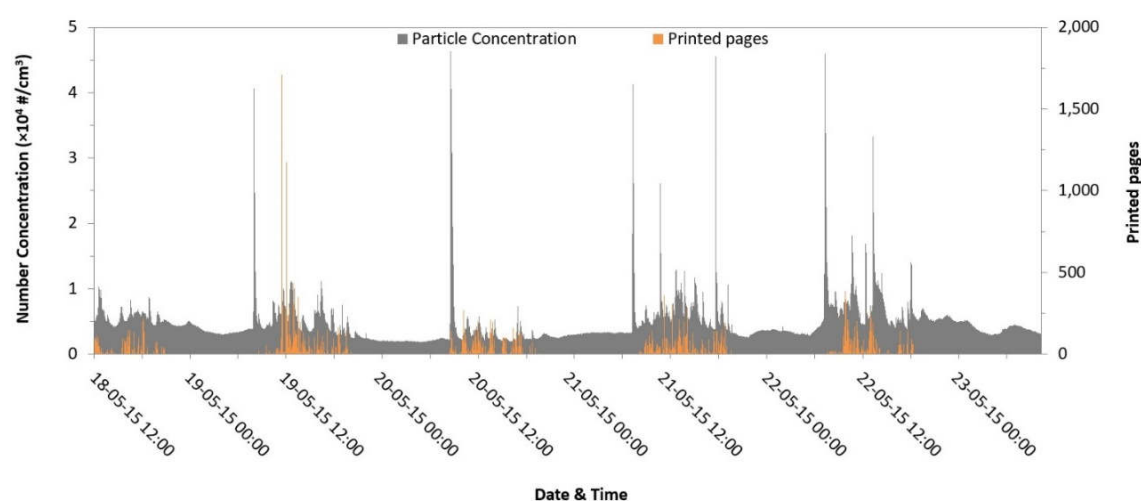


Figure 4.12. Total particle number concentration vs. printed pages in the PR.

All three events lasted around 2 minutes and were followed by immediate concentration decrease, probably caused by either warmup of one of the idling printers or a cool-down after a finished print job based on the events duration and the dominant particle size ($\sim 35 \text{ nm}$) in all 3 cases. This corresponds to the size fraction of particles emitted while startup and printer warmup (as discussed earlier in sections 3.1 and 3.2), where 68% of emitted particles were smaller than 50 nm, similarly as it was observed in the chamber measurements. On the contrary, particles ranging 50-100 nm were dominant during printing, most probably due to particle coagulation and deposition mechanisms. Another possible explanation of the sharp PN concentration increase on 22/05 is that according to the printers' statistics, all 4 printers received in relatively short time period

4.2. Evaluation of Nanoparticle Emissions from Laser Printers

of 5 minutes a total of 38 commands to print 674 pages and at the time of increase, all 4 printers were printing simultaneously.

As 3 out of 4 printers (same manufacturer and type) were identified as ‘initial burst’, suggesting that the last printer, responsible for 67% of all prints, could belong to printers with constant emission profile. It was not possible to prove a direct link between the number of printed pages from one of the printers and the nanoparticle emissions, which lead to a conclusion that, even though unequally, all 4 printers contributed to the emissions in the PR. Average PN concentration during printing hours in PR ($5.4 \times 10^3 \text{ \#/cm}^3$) is similar to the one observed in chamber measurements ($6.7 \times 10^3 \text{ \#/cm}^3$). Nonetheless, these values are not quantitatively comparable due to different conditions in PR, such as air exchange rate (larger room volume, opened door), background aerosol (also from other parts of the building, penetration and infiltration from outdoors), emission sources (4 printers and other sources), distance of sampling point from printers, and last but not least, the PR users.

In addition, Figure 4.13a shows that nanoparticle concentration varied temporarily with sharp increases leading to substantially higher indoor concentrations during day time (printing) when the printers were operating, compared to night time when no activity took place (Figure 4.13c). On average, concentration of 10-100 nm particles between 09:00 and 21:00 was 1.2-fold higher compared to night time during the campaign. In addition, particles in the size range 100-350 nm presented higher temporal fluctuations during day time (Figure 4.13b), although the corresponding concentrations were significantly lower than that of particles ranging 10-100 nm. The sharp increases of indoor nanoparticle concentration during printing are associated with primary emissions from printers. Hardcopy devices and printers are known for their effect on indoor PN concentration and especially in nanoparticle sizes (Schripp et al., 2008; Wensing et al., 2008; McGarry et al., 2011). Accordingly, indoor PN concentrations for fine particles ($< 1 \mu\text{m}$) are likely influenced by outdoors during night time.

4.2. Evaluation of Nanoparticle Emissions from Laser Printers

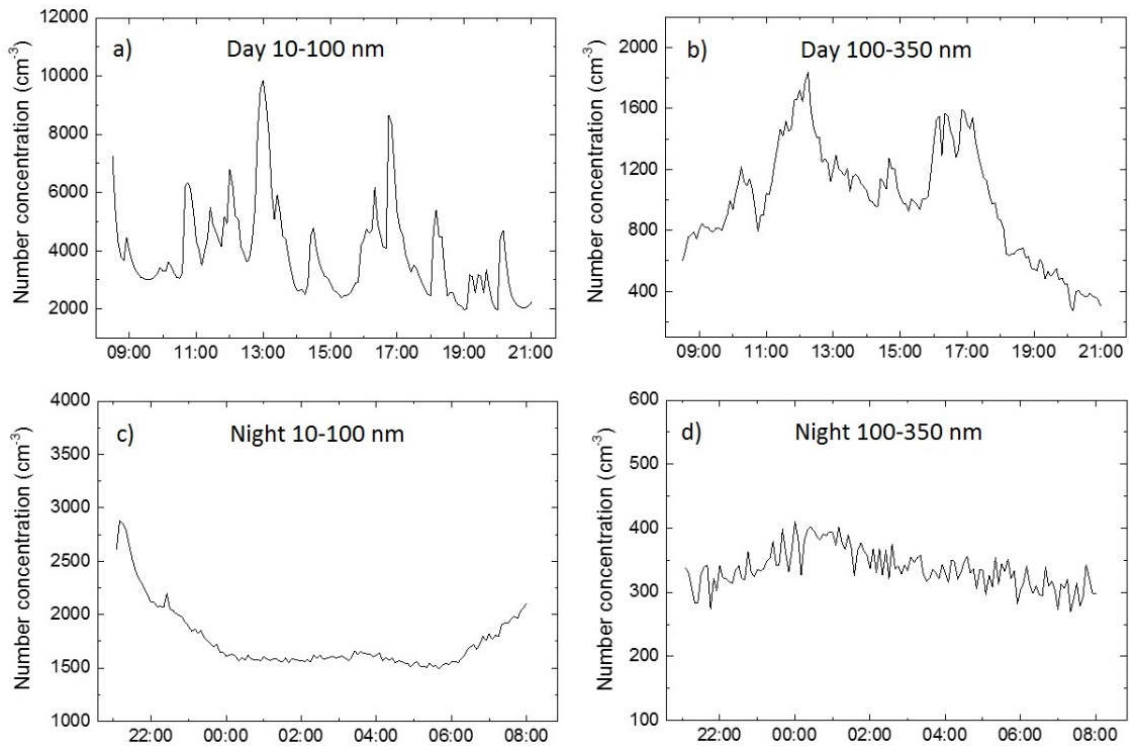


Figure 4.13. Particle number concentration in two size fractions in PR during day and night hours on 19/05: (a) 10-100 nm at day; (b) 100-350 nm at day; (c) 10-100 nm at night; and (d) 100-350 nm at night.

4.2.6. Contribution of Printer Emissions in the Print Room

Time-resolved PN concentrations in PR showed an exponential decrease of the indoor concentration after reaching a peak concentration on workdays during open hours (Figure 4.13a). The data after these peaks were used to determine the total removal rate ($a+k+\lambda\eta+b_2$) for nanoparticles, the particle size that was mostly affected by printer emissions. The total removal rate of nanoparticles was estimated for each day separately using Eq. (4.6). High removal rates were obtained for all days. Although it was not possible to estimate each variable separately, it is believed that the main contribution to the total removal rate in PR originates from b_2 , the exchange rate of PR with internal areas of the building. The door connecting PR with the main corridor was opened during day time, thus, air and particulate matter transport is easier and more effective. McGrath et al. (2014) conducted measurements in a room with different sources and found that the

4.2. Evaluation of Nanoparticle Emissions from Laser Printers

opened door scenario results in lower indoor concentrations, which is associated with easier escape of particles. Moreover, daily variations of the total removal rate are likely influenced by diurnal variations of the air currents inside the building. Higher estimate (12.84 h^{-1}) was obtained on 20/05, which corresponds to the day with the lower measured indoor PN concentrations among the working days (Table 4.5).

Table 4.5. Averaged total removal rate and suspended $< 1 \mu\text{m}$ particle concentration originating from other areas estimated for each workday in PR.

| Parameter | 18/05 | 19/05 | 20/05 | 21/05 | 22/05 | 25/05 |
|--|-------|-------|-------|-------|-------|-------|
| $a + k + \lambda\eta + b_2 \text{ (h}^{-1}\text{)}$ | 9.98 | 7.26 | 12.84 | 10.29 | 8.08 | 7.21 |
| $\frac{aPC_{out} + b_1C_{in,j}}{a + k + \lambda\eta + b_2} \text{ (\#/cm}^3\text{)}$ | 3,751 | 2,536 | 1,936 | 3,478 | 4,769 | 3,296 |

Subsequently, emissions from printers were estimated for fine particle concentration ($< 1 \mu\text{m}$) using Eq. (4.4) for each time interval. The emission rates were determined from the term S/V . Only, positive numbers were accepted when evaluating $dC_{in,i}/dt$ in order to represent the physical situation: emissions increase indoor particle concentration. Moreover, linear regression was used to correlate the estimated emissions rates with the corresponding indoor concentrations ($< 1 \mu\text{m}$). Accordingly, a least squares line was obtained for each day with $C_{in} = a S + b$. Table 4.6 presents the statistical indicators of the estimated emission rates along with the parameters of linear regression.

Table 4.6. Statistical indicators of the estimated nanoparticle emission rates S (10^8 min^{-1}) in PR.

| Date | Min | Max | 10 th | Median (50 th) | 90 th |
|-------|------|-------|------------------|----------------------------|------------------|
| 18/05 | 5.4 | 501 | 16 | 99 | 263 |
| 19/05 | 1.7 | 752 | 19 | 138 | 444 |
| 20/05 | 0.05 | 545 | 14 | 85 | 285 |
| 21/05 | 1.3 | 3,463 | 23 | 180 | 669 |
| 22/05 | 0.3 | 1,704 | 26 | 144 | 758 |
| 25/05 | 30 | 476 | 32 | 134 | 342 |

4.2. Evaluation of Nanoparticle Emissions from Laser Printers

Nanoparticle emission rates were scattered both in absolute values and from day to day. Higher values were obtained for 21/05 and 22/05 with 90th percentile at $669 \times 10^8 \text{ min}^{-1}$ and $758 \times 10^8 \text{ min}^{-1}$, respectively. In agreement with the measured indoor PN concentrations both days correspond to the higher averaged indoor concentration with $6 \times 10^3 \text{ \#/cm}^3$ and $7 \times 10^3 \text{ \#/cm}^3$ for 21/05 and 22/05, respectively. In agreement with other studies that evaluated emission from printers (He et al., 2007; Koivisto et al., 2010), median emission rates in the current study varied in the range $10^9 - 10^{10} \text{ min}^{-1}$, which corresponds to similar rates. Consequently, indoor PN concentrations were increased only by a few thousands (4 to $5 \times 10^3 \text{ \#/cm}^3$) during printing periods. Emissions from printers and the relevant indoor PN concentrations depends substantially on the printer and room characteristics (Wensing et al., 2008; Koivisto et al., 2010).

Table 4.7. Parameters of linear regression between emission rates (S) and indoor concentration of fine particles ($< 1 \mu\text{m}$) for PR.

| Date | N | a ($\times 10^{-8}$) | b | R^2 | P-value |
|-------------|----------|---|-----------------------|-------------------------|----------------|
| 18/05 | 45 | 9.0 | 3,804 | 0.91 | <0.05 |
| 19/05 | 46 | 9.8 | 2,764 | 0.82 | <0.05 |
| 20/05 | 43 | 6.4 | 2,010 | 0.87 | <0.05 |
| 21/05 | 51 | 6.1 | 4,084 | 0.95 | <0.05 |
| 22/05 | 42 | 9.1 | 4,879 | 0.87 | <0.05 |
| 25/05 | 14 | 10.2 | 3,368 | 0.81 | <0.05 |
| | average | 8.4 | 3,485 | | |
| | st. dev. | 1.8 | 1,011 | | |

Moreover, Table 4.7 suggests that the emissions from the printers were varying in time. This behaviour is associated with the use of the printers during the day. Multiple prints were performed during the opened hours the printed pages varying in number. Linear regression revealed that the two variables (C_{in} and S) are in good agreement, with R^2 being higher than 0.8, indicating that emission rates were well estimated from number concentration data. Emissions from printers and the relevant indoor PN concentrations depend substantially on the printer, room characteristics and indoor conditions (Wensing

4.2. Evaluation of Nanoparticle Emissions from Laser Printers

et al., 2008; Koivisto et al., 2010). As was said earlier, there is no specific trend between indoor PN concentrations and the number of printed pages (Figure 4.14). This was most probably associated with daily variations in removal rates inside PR.

The same observation is reported in Betha et al. (2011) in a study in a commercial print center. Variations in time are also associated with the use of the printers during the day. Multiple prints were performed during opened hours of the office with the printed pages varying considerably in number. Figure 4.14 demonstrates the complexity of a real working environment in office buildings and the difficulty to obtain a mathematically based correlation.

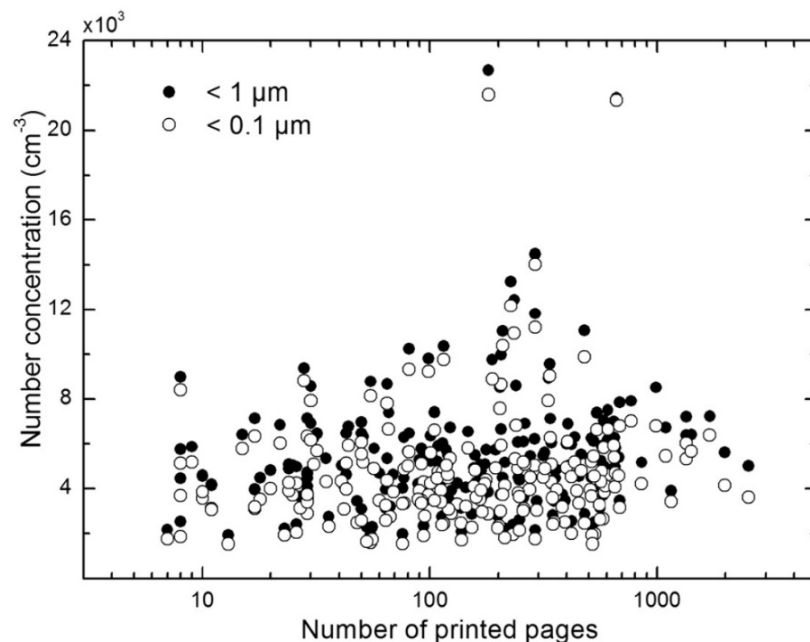


Figure 4.14. Variations of indoor PN concentrations with number of printed pages.

Additionally, Figure 4.15 present the correlation between A1 with PR using the number concentration data, where good agreement ($R^2=0.63$) was found between concentrations of particles $< 1 \mu\text{m}$. Although, parallel correlation with the outdoor data is missing in this case, the presented results confirm the impact of submicron particles that originated from PR but transported to the office nearby. Recall that A1 was occupied during opened hours; hence, human presence in A1 had a negligible impact to indoor PN

4.2. Evaluation of Nanoparticle Emissions from Laser Printers

concentration for submicron particles. Fine particles are not effectively escaped as coarse particles due to their smaller inertia that allows them to be influenced by airflow patterns of the building, momentum jets and eddies indoors (Kao et al., 2009). Internal airflows, location and magnitude of the emissions influence substantially particle transport indoors (McGrath et al., 2014), thus variations may be observed from day to day. Therefore, smaller particles are easily transported to internal areas of the building compared to bigger particles.

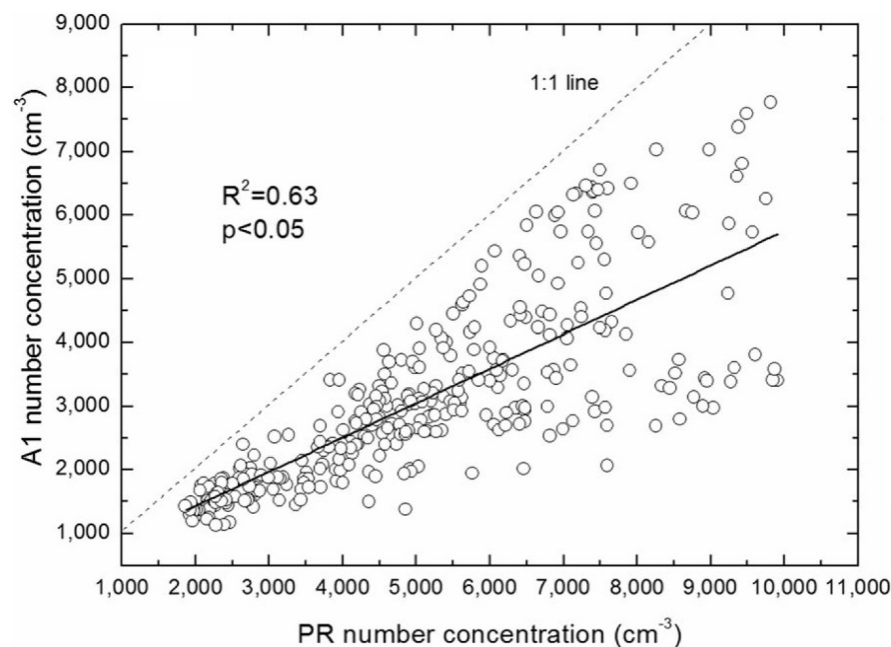


Figure 4.15. Correlation of particles concentrations (< 1 μm) in the Print Room (PR) with Office (A1).

4.2.7. PM Concentrations and I/O Ratio during the Field Study

Daily median PM_{10} mass concentrations inside PR and A1 are listed in Table 4.8. A comparison between the values indicates that higher median mass concentrations were measured in office B2. Additionally, comparing A1 and PR, higher daily median concentrations were measured for office A1. These results imply that office A1 is characterized by higher concentration of coarse particles compared to print room (PR)

4.2. Evaluation of Nanoparticle Emissions from Laser Printers

probably due to constant occupation by the employees. Other studies propose that human occupation in workplace environments is closely related with resuspension which mainly influence coarse particles (Fisk et al., 2000; Chatoutsidou et al., 2015; Hussein et al., 2015). The outdoor environment had significant impact to indoor PM levels in A1 with infiltration playing a dominant role, however, during opened hours temporal fluctuation indoors were dominated by indoor sources. In more detail, the sharp increase of indoor PM₁₀ concentration observed in all offices on 21/05 coincides with cleaning of the offices as recorder by the employees. The increased concentrations caused by cleaning of the offices is associated with activities such as vacuuming, dusting and walking that can considerably increase coarse particle concentration (Ferro et al., 2004).

Table 4.8. Indoor daily median PM₁₀ mass concentration for offices PR and A1.

| Room | 18/05 | 19/05 | 20/05 | 21/05 | 22/05 | 23/05 | 24/05 | 25/05 |
|------|-------|-------|-------|-------|-------|-------|-------|-------|
| PR | 24 | 19 | 11 | 19 | 18 | 18 | 9 | 10 |
| A1 | 37 | 26 | 17 | 27 | 25 | 25 | 12 | 13 |

In addition, Figure 4.16 presents PM_X ratios for PR. PM₁/PM₁₀ and PM_{2.5}/PM₁₀ ratios are plotted against time where ratios higher than 0.9 were obtained for periods when the building was not occupied (workdays 21:00-09:00 and weekend) for both cases. In practise, a diurnal variation for both ratios was observed during working days, whereas, during the weekend no diurnal variation was present. PM_{2.5}/PM₁₀ reached a ratio almost equal to 1 during the closed hours (21:00-09:00) on weekdays suggesting that indoor PM during night inside PR is dominated by smaller micron-sized particles and that coarse particle concentration (> PM_{2.5}) is negligible, i.e. not suspended in the air. The same behavior applies for PM₁/PM₁₀ but with lower ratios since PM₁ are included in PM_{2.5}. Similar results were obtained for the weekend where the A1 office was constantly unoccupied.

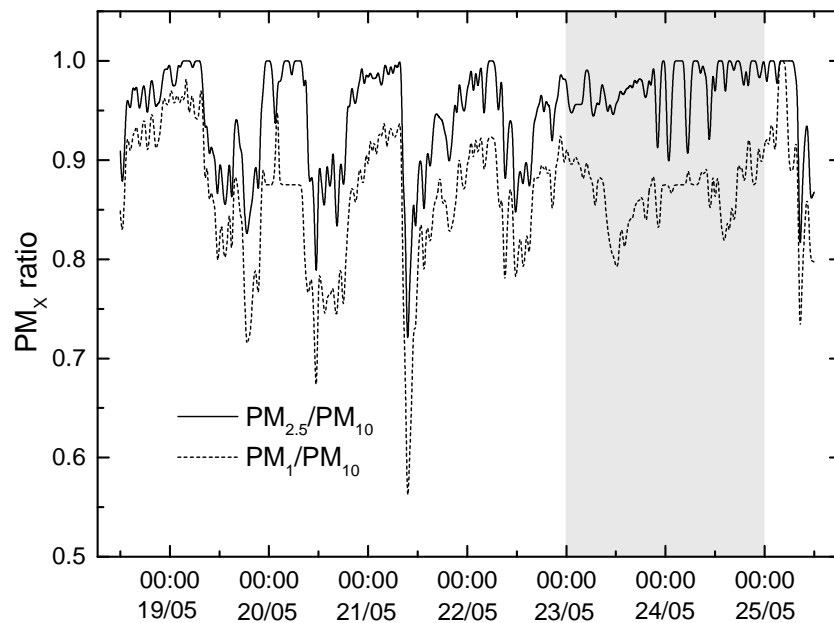


Figure 4.16. PM_X ratios (PM_1/PM_{10} and $PM_{2.5}/PM_{10}$) inside PR. The highlighted area corresponds to weekend.

Therefore, PM_1 particles most probably originate from outdoors during closed hours due to infiltration since the printers were not working, whereas, during day hours the contribution from coarse particles becomes important. In more detail, ratios < 0.9 both for PM_1/PM_{10} and $PM_{2.5}/PM_{10}$ were obtained only during opened hours (09:00-21:00), implying that coarse particles ($> 2.5 \mu\text{m}$) are significantly suspended during day time most notably due to particle resuspension. Particle size and resuspension are associated in many studies (Qian et al., 2008; Chatoutsidou et al., 2015; Hussein et al., 2015). Moreover, the good correlation between PN and PM_{10} concentration in PR using data when the office was not occupied (closed hours and weekend), further supports the conclusion that bigger particles ($> 2.5 \mu\text{m}$) are suspended in the air during opened hours. However, PM_1 particles are still dominating the indoor air with PM_1/PM_{10} being usually above 0.7.

4.2. Evaluation of Nanoparticle Emissions from Laser Printers

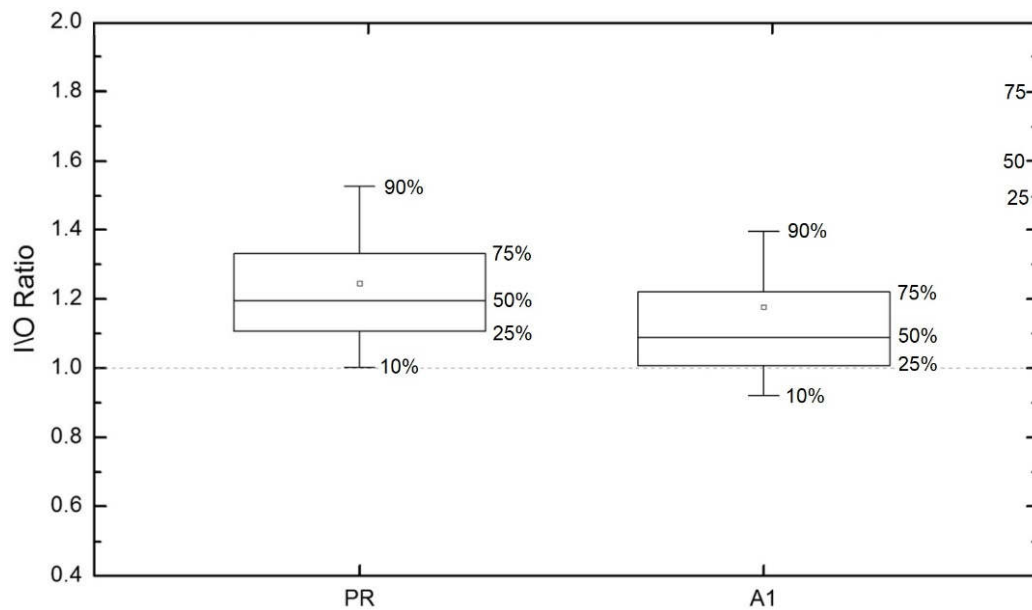


Figure 4.17. I/O ratio for PR and A1 obtained from mass concentration data. The box plots represent the 25th and the 75th percentile values, mean value and the horizontal line the median (50th percentile) value. The whiskers represent 10th and 90th percentile.

The PM₁₀ I/O ratios in A1 and PR found higher than 0.5 (10th percentile) suggesting that the indoor PM concentrations preserve values close to the outdoor levels (Figure 4.17). Mechanical ventilation was not operating, thus, high ratios are attributed to effective penetration of outdoor PM₁₀ particles indoors. Although the mechanical ventilation in the studied building does not have filters, studies which investigated the impact of mechanical ventilation confirm that the operation of the HVAC system results in reduced I/O ratios indoors due to effective capture of coarse particles from filters (Quang et al., 2013). A comparison between offices PR and A1 (occupied spaces) suggests that PR was characterized by slightly higher I/O ratios. Mean values were 1.24 and 1.18 for PR and A1, respectively. I/O ratios higher than 1 for PM₁₀ are also reported in a study inside copy centres (Vicente et al., 2017). The difference between the two offices is associated with printer emissions and especially the PM₁ fraction.

4.2.8. Effect of Printer's Startup on PN Concentration in the Chamber

The mechanism of the printer operation is summarized in the HP LaserJet 9050 Service Manual. When a print command is sent from the formatter, the engine controller drives the main motor to rotate the photosensitive drum, primary charging roller, developing cylinder, transfer charging roller, and pressure roller. The primary charging roller applies a uniform negative charge to the photosensitive drum surface. Toner on the developing cylinder develops the latent image formed on the photosensitive drum into a visible image, which is transferred onto media by the transfer charging roller. The paper passes between a heated fuser element and a soft pressure roller. This melts the toner and presses it into the paper and the printed page is delivered to the discharge outlet. The cleaning blade is in contact with the surface of the drum at all times. As the drum rotates during printing, excess toner is scraped off and stored in the waste toner reservoir. Therefore, possible sources of nanoparticles in such a process could involve toner powder agglomerates from the printer cartridge, particulate coatings released from the paper, and evaporated VOCs emitted from the toner powder on the page and from toner residue from previous printings.

Table 4.9. Average, maximum and minimum total particle number concentrations ($\#/cm^3$) during the printer chamber measurements.

| PN concentration | 16/11 | 17/11 | *18/11 | 19/11 | Average |
|--------------------------|--------------------|--------------------|--------------------|--------------------|--------------------|
| Background | 8.70×10^1 | 2.09×10^2 | 1.25×10^2 | 1.09×10^2 | 1.33×10^2 |
| Startup (15-min average) | 1.35×10^4 | 5.20×10^4 | 7.43×10^4 | 1.00×10^5 | 6.00×10^4 |
| Startup (15-min max) | 1.88×10^4 | 7.67×10^4 | 9.90×10^4 | 1.59×10^5 | 8.85×10^4 |
| Printing (average) | 6.48×10^3 | 6.01×10^3 | 4.58×10^3 | 9.78×10^3 | 6.73×10^3 |
| Printing (max) | 1.75×10^4 | 2.98×10^4 | 1.73×10^4 | 3.89×10^4 | 2.59×10^4 |
| Printing (min) | 2.45×10^3 | 6.82×10^2 | 6.87×10^2 | 9.84×10^2 | 1.20×10^3 |

*different printing schedule

The first printing of each day was at least 30 minutes after the printer was turned on, thus, the effect of 'cold' start printing was not investigated. Increased particle number (PN) concentration was observed almost instantly after the printer startup on every

4.2. Evaluation of Nanoparticle Emissions from Laser Printers

printing day. As shown in Table 4.9, half an hour before the printer startup, the average background concentration was measured to be 133 \#/cm^3 while the average PN concentration during startup was $6 \times 10^4 \text{ \#/cm}^3$ and the maximum observed concentration on any given day during startup was $1.6 \times 10^5 \text{ \#/cm}^3$. The maximum concentration in every measurement appeared within 5 minutes from startup and was decreasing afterwards. In fact, the maximum concentration during startup was at least two times higher than during printing in all cases with exception of 16/11 (see Table 4.9).

A study conducted by Schripp et al. (2008) in an emission test chamber investigated time-dependent characterization of particle release from laser printers and found that the 9 tested printers can be identified by two emission profiles: constant and initial burst. The printers with a constant emission profile generated particles throughout the entire printing task. However, printers identified as ‘initial burst’ stopped emitting particles soon after the printing started, or as it was in the case of this study, after the initial startup. Note that peak concentrations during startups on any given day were much higher than the concentrations generated while printing, suggesting that the major source of nanoparticles is the residual toner on the fuser rather than the evaporation of the toner powder on the paper.

As shown in Table 4.9, the very first day the total PN concentration was the lowest among all days and the maximum concentration at startup was almost equal to the maximum concentration during printing. The cause of this low initial PN concentration on the first printing day was most probably the transport of the printer from another building, where the excess toner from previous printings got shook off from the printer’s components. New fuser and cartridge were used and checked repeatedly prior to the beginning of measurements on the first day so the waste toner was then accumulating in the reservoir and on the fuser roller ever since.

Wensing et al. (2008) examined the printers’ startup with and without inserted toner cartridge with no obvious difference in particle concentration suggesting that residual toner deposited on the fuser roller from previous printing jobs contribute to the nanoparticle emissions at the printer startup. To confirm this, the fuser and the cartridge were changed over 1 h after the last print job on 19/11. After that the printer was turned on again and 5 test pages were printed. Although the particle number concentration at

4.2. Evaluation of Nanoparticle Emissions from Laser Printers

startup increased from $9 \times 10^3 \text{ \#/cm}^3$ to $1.7 \times 10^4 \text{ \#/cm}^3$, printing itself did not increase the PN concentration and was decreasing instead. However, the maximum PN concentration at startup on 20/11 ($3 \times 10^4 \text{ \#/cm}^3$) was lower by factor of 5 in comparison with the previous day ($1.6 \times 10^5 \text{ \#/cm}^3$), but still higher than it was on startup on the very first day ($1.9 \times 10^4 \text{ \#/cm}^3$) or the night before when the fuser and the cartridge were changed. This leads to a conclusion that the nanoparticles were deposited also on the other components of the printer considering that there were no toner residues on the fuser roller. Moreover, the waste toner reservoir where the scraped off excess toner is stored is a part of the toner cartridge, which was also exchanged for a new one.

4.2.9. Effect of Printing and Idling on PN Concentration in the Chamber

Whenever an increase in particle number concentration was observed after startup, it was associated with activated fans or rotating fuser, respectively. This was usually in the beginning or the end of the print job, occasionally when the printer was in standby mode. In order to look at this assumption thoroughly, a different printing schedule was used for this purpose where 226 pages of plain text were printed 3 times and afterwards 137 pages of text and figures were printed 3 times as well, and the printers' fans activity was recorded. As can be seen on Figure 4.19, printing of 226 pgs. of text was completed in 20 minutes (with exception of the third print, which was cancelled due to printers' cable misplacement after 60 printed pgs. and the printer had to be restarted) and the printing of 137 pgs. of text and figures was done in 53 minutes.

Continuous increase in PN concentration was not observed due to printing process, but there was an increase in PN concentration on the beginning of the print job on several occasions. More details are distinguishable when particle number concentration is plotted against time and particle diameter in lognormal mode, as showed in Figure 4.20. Note that the last print on 18/11, where no fan activity was recorded, the printing itself did not emit considerable amount of particles (on average $2.3 \times 10^3 \text{ \#/cm}^3$) and PN concentration continued to decrease until the end of the printing day, even though the last three print jobs (text and figures) on 18/11 each print took almost an hour to complete. After the startup on 19/11, the first increased particle number concentration

4.2. Evaluation of Nanoparticle Emissions from Laser Printers

was observed after 5 hours of printing, at which point ~1000 pages were already printed (see Figure 4.20). After the #6 print job of the day, fluctuations in particle number concentrations were observed before, during and after the printings. Investigation of the particle size fractions suggests that the particle sizes contributing the most to the increase in PN concentration on 18/11 were in range of 10-50 nm, similarly as it was on 19/11 (shown in Figure 4.18).

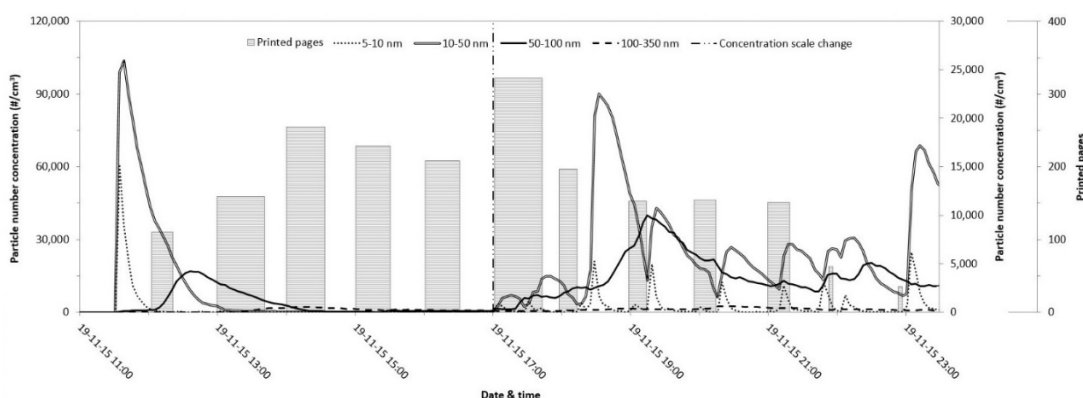


Figure 4.18. PN concentrations of different size fractions during printing on 19/11.

Now, while in standby, the printer's fuser control keeps the temperature of the fuser roller on 180°C, the pressure roller temperature on 140°C, and 5 out of 6 fans are half-speed rotating and the last one is off. In the case the standby state lasts 5 minutes or more, the fuser/delivery motor is rotated for about 0.08 seconds to prevent the pressure roller from becoming deformed. This could explain the presence of nanoparticles and the temporary small increase in particle number concentration between print jobs when the printer was idling. Although these local peaks, which usually lasted less than 1 minute, are not visible on a big scale, they are however noticeable with a 1 second resolution of CPC. When a print command is received, fuser roller temperature rises to 190°C and pressure roller to 180°C, all 6 fans are working on full-speed and all the motors controlling the fuser, scanner and drum are rotating as well, similarly, as it is at the end of the print (last rotation). In this process, scraped off excess toner (stored in the waste toner reservoir of the cartridge), and the residual toner deposited on the fuser roller and

4.2. Evaluation of Nanoparticle Emissions from Laser Printers

other internal printer components are released from the printer into the environment by rotating fans and fuser roller, which could explain the increase of concentration on the beginning of the printing.

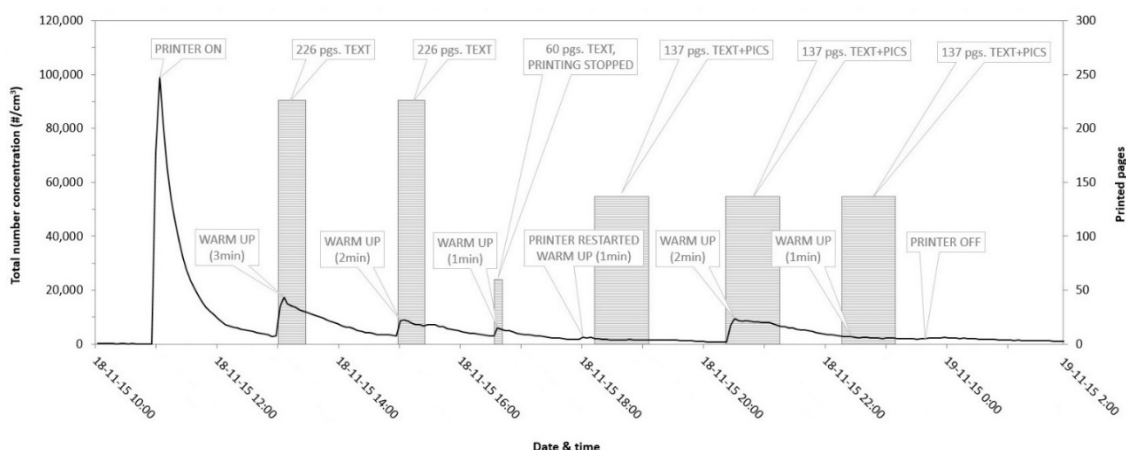


Figure 4.19. Total particle number concentration versus printed pages on 18/11.

This, however, does not explain why the nanoparticle emissions at startup are higher by several factors in comparison with the decreasing concentrations during the continuous printing process. Wang et al. (2011a) measured the temperatures inside the printer, VOCs and particle concentrations during printing and proposed that the decrease of particle concentration might be due to a combination of several mechanisms: (1) neutralization of free charges with the increasing interior printer temperature; (2) Suppressed nucleation due to elevated interior printer temperatures in the vicinity of the fuser where the VOCs are emitted; (3) enhanced dilution effect of VOCs with increasing interior printer air temperature; (4) thermally enhanced agglomeration of the nanoparticles (coagulation) into fewer, larger particles; as was in the case of this study (see Figure 4.21), and (5) reduced emission of VOCs from a hot fuser (cold fuser may cause adhering of toner residue particles).

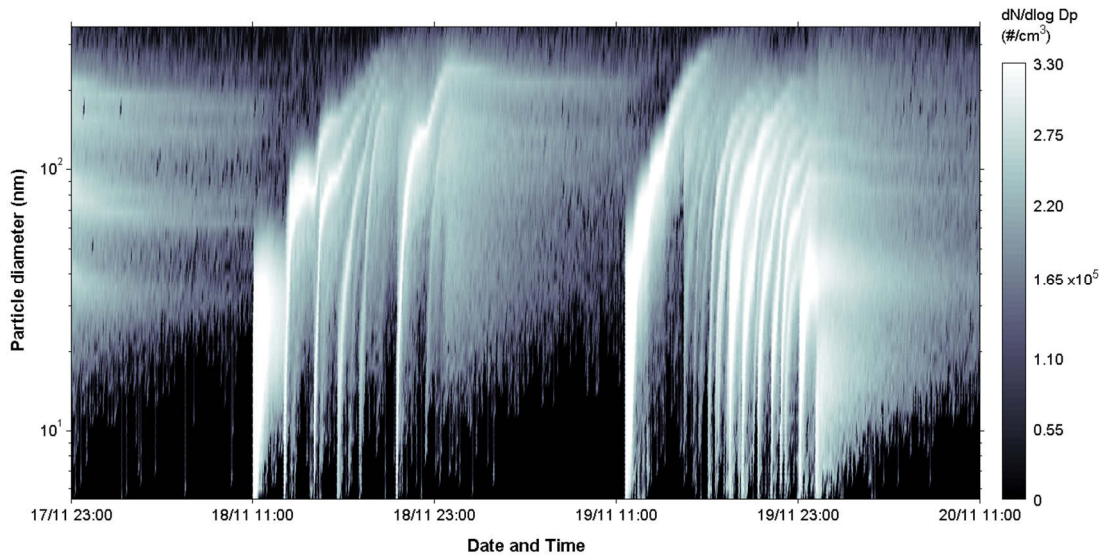


Figure 4.20. Particle number concentration vs. time in the chamber on 18/11 and 19/11.

4.2.10. Effect of Printer Startup and Printing on PSD in the Chamber

After the printer is turned on, all 6 fans are rotating for 30 seconds, the duplexer fan for 3 seconds, and the fuser heaters turn on. To investigate the particle sizes responsible for the PN concentration increase, particles were divided into 4 size fractions (5-10, 10-50, 50-100 and 100-350 nm). It was found that during the startup vast majority of the emitted particles ranged from 10-50 nm and then 5-10 nm (see Figure 4.18). Approximately 30 min after the startup when concentration of particles < 50 nm decreased, an increase of 50-100 nm particles was observed. This trend was noticed also during the printing process, but with lower concentrations. Whereas in the case of particles ranging between 100-350 nm, there were almost no particles till 2 h after the startup ($\sim 50 \text{ \#/cm}^3$), when the concentrations slightly increased and reached on average $1.2 \times 10^3 \text{ \#/cm}^3$. The PSD did not undergo significant changes even after the start of printing (Figure 4.21a).

4.2. Evaluation of Nanoparticle Emissions from Laser Printers

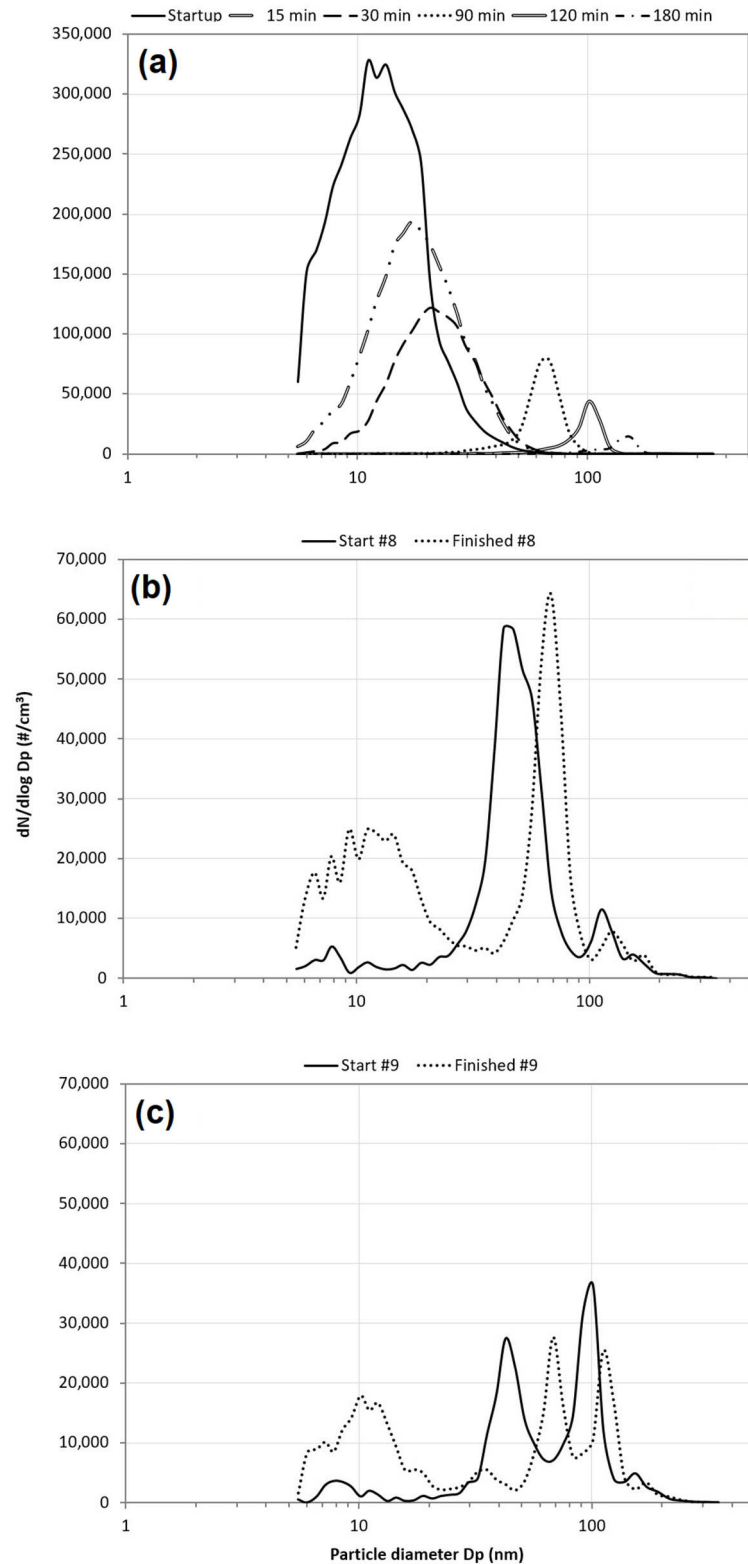


Figure 4.21. Particle size distributions on 9/11: printer's startup (a); first and last scan of print #8 (b), and print #9 (c).

4.2. Evaluation of Nanoparticle Emissions from Laser Printers

Within 1 h from startup the particle size mode shifted from 10 to 50 nm and to 150 nm in 3 h from startup. The growth in particle size and decrease of PN concentration of particles < 50 nm with time suggest that this mode shifting was a result of particle coagulation and deposition losses mechanisms of particles emitted by printer at startup rather than particles being emitted by printer in the printing process. Moreover, as discussed previously, the printer emitted nanoparticles during the printing primarily in the beginning or the end of printing jobs regardless of number of printed pages. The size mode of these emitted particles was ~15 nm, similarly as it was at startup. This caused multimodal size distributions with two dominant size modes, rapidly shifting towards bigger particle sizes with lower concentrations (Figure 4.21b and 11c), which made it difficult to obtain reproducible size distributions from printer emitted PN concentrations.

4.2.11. Effect of Printing on Mass and TVOC in the Chamber

Concentration of nanoparticles (with low mass contribution) ranging 10-100 nm contributed to PN concentration by 80%, while particles smaller than 10 nm and particles ranging 100-350 nm altogether on average by 20%. Therefore, mass concentration of particles in the size range of 0.3-10 μm (as obtained by OPS) were of minimal importance (see Table 4.10). Because the vast majority of particles were smaller than 300 nm (even smaller than 100 nm), particles of this size have negligible contribution to the particulate matter. Nonetheless, as shown in Figure 4.22, each of the 12 print jobs on 17/11 can be identified by increase in mass concentration of particles 0.3-10 μm (unlike PN concentration), even though the average mass concentration was only 0.51 $\mu\text{g}/\text{m}^3$ (max. concentration 1.75 $\mu\text{g}/\text{m}^3$). Similar trend in mass concentration was also observed during printing processes on every printing day.

Several studies suggest that the major VOC source is off-gassing from the printer components, such as toner powder, paper, plastics or circuit boards (Wolkoff et al., 1993; Lee et al., 2001; Lee et al., 2007; Destailats et al., 2008). Examining the TVOC in this study revealed that the increase in concentrations (see Table 4.10) did not entirely correspond to the amount of printed pages on any printing day. Concentrations reached maximum at 0.36 and 0.38 ppm, respectively, even though on 16/11 and 17/11 more than

4.2. Evaluation of Nanoparticle Emissions from Laser Printers

double number of pages were printed (~2000 pgs. in 11 h) in comparison with 18/11 (~900 pgs. in 10 h). Moreover, on 17/11 the concentration was increasing after the first print job was done and slightly decreased during the print #4 after the TVOC concentration reached 0.288 ppm and started to increase again after the #9 print was completed. In this time interval (between prints #4 and #9) nearly 1000 pgs. were printed. The TVOC concentration then continued to increase and reached its maximum between prints #11 and #12 at 0.38 ppm and then the same value was reached more than 1 hour after the last printing of the day.

Table 4.10. Average total mass and number concentrations of 0.3 – 10 μm particles obtained from OPS and median values of TVOC during printers' chamber measurements.

| Concentration | 16/11 | 17/11 | *18/11 | 19/11 | Average |
|---|--------------|--------------|---------------|--------------|----------------|
| Mass concentration ($\mu\text{g}/\text{m}^3$) | 0.55 | 0.51 | 0.22 | 0.47 | 0.44 |
| Number concentration ($\#/\text{cm}^3$) | 4 | 8 | 2 | 5 | 5 |
| TVOC (maximum; ppm) | 0.36 | 0.38 | 0.38 | - | 0.37 |
| TVOC (average; ppm) | 0.23 | 0.25 | 0.24 | - | 0.24 |

*different printing schedule

TVOC samples were taken only during the printing process, thus, neglecting the decay concentration. Several studies (Morawska et al., 2009; Koivisto et al., 2010; Wang et al., 2011a) reported immediate decrease of PN and TVOC concentrations after the printing finished. This is in contrary with our observation where on every printing day when the printer was turned off after the last print job was completed, the TVOC retained its concentration for ~1.5 hours. Furthermore, there was almost an hour time gap between prints #2 and #3, and between prints #3 and #4, where the TVOC was increasing instead of decreasing (see Figure 4.22). Wolkoff et al. (1993) suggested that the increase of TVOC after the finished printing might be due to the high temperatures inside and outside the printer after the completion of the print task.

4.2. Evaluation of Nanoparticle Emissions from Laser Printers

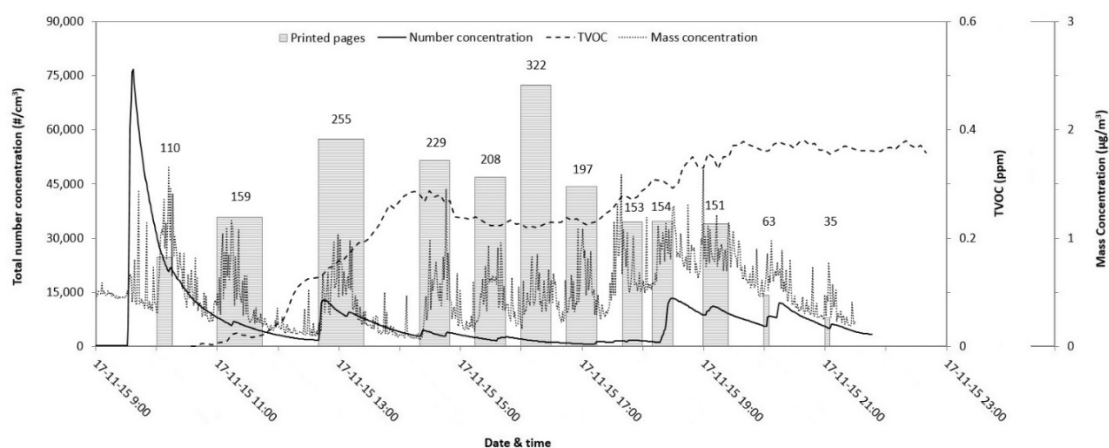


Figure 4.22. Total particle number concentration, TVOC and mass concentration (0.3-10 μm) versus printed pages on 17/11.

4.2.12. Conclusions

One-week sampling was also done in the print room of the IT & Communications Center where 4 printers are located (included the one examined in the chamber study). The impact from human occupation and printing was studied in two different rooms, an office and a print room. Particle number (PN) and mass (PM) concentrations were measured on-line both indoors and outdoors. Different occupation scheme characterized both rooms, however, common sources were identified as the product of human occupation. The major contribution to indoor PN concentrations originated from printer emissions in terms of long exposure, which affected nanoparticle concentrations ($< 100 \text{ nm}$) with direct impact in the print room.

Average PN concentration during opened hours was measured to be $5.4 \times 10^3 \text{ \#/cm}^3$. Printers' startup on every day was characterized by sharp increase in PN concentrations, similarly as it was observed in the chamber study, reaching on average $4.4 \times 10^4 \text{ \#/cm}^3$. Regression analysis provided high correlations (R^2) between the indoor PN and PM concentrations in PR and the corresponding concentrations in A1. On the contrary, in periods where the offices were closed and no printing took place (night, weekend), indoor concentrations were influenced by the outdoor concentration. Human occupation during workdays had secondary impact in the occupied offices. Human

4.2. Evaluation of Nanoparticle Emissions from Laser Printers

presence without particle generation was associated with resuspension activities that caused increased concentration indoors for particles higher than 2.5 μm . I/O ratios higher than 1 that were obtained for two of the selected offices (A1, PR). Overall, particle number and mass concentrations in the under study building are influenced primarily by indoor sources (printers) during working days.

Additionally, evolution of particle size distributions with time and printed pages was also studied in detail in an experimental chamber. Printer was generating nanoparticles ($< 50 \text{ nm}$) primarily during cold startup (1.9×10^4 to $1.6 \times 10^5 \text{ \#/cm}^3$), whereas the average PN concentration during printing was only $6.7 \times 10^3 \text{ \#/cm}^3$. Scraped off excess toner and the residual toner deposited on the fuser roller were released from the printer into the environment by rotating fans and fuser roller, which was probably the cause of increase in nanoparticle concentration with mode on $\sim 15 \text{ nm}$ in the beginning or the end of print jobs. Maximum concentration at startup, after the cartridge and fuser roller were changed, was lower by factor of 5 in comparison with the previous day suggesting that the nanoparticles were deposited also on the other components of the printer.

Due to greater distance of sampling point from printers, taking into account also higher number of sources, larger room volume in PR measurements, in comparison with the chamber study, it is estimated that the PN concentration, and thus the exposure dose of print room users, would be much higher at distances closer to the printers. Adding a low pressure HEPA filters into the existing mechanical ventilation, a filter or adsorbent to the printers' air outlets and also that staying more than 1 m away from the printer could reduce the exposure to high nanoparticle concentrations from printers' emissions.

4.3. Particle Resuspension during Walking in an Indoor Microenvironment

4.3.1. Introduction

The indoor air quality (IAQ) has very important implications to human health since people spend most of their time indoors (80-90%) (Robinson and Nelson, 1995). Human exposure to ambient particulate matter (PM) can cause serious health problems on the respiratory and cardiovascular system or even mortality (Morawska et al., 2003; Pope et al., 2006; Anderson et al., 2009). Many studies have focused on determining the impact of particle exposure to human health (Franck et al., 2011; Morawska et al., 2013). The results suggest that PM health effects depend both on exposure time and exposure concentration (Pope et al., 2006). Particles generated by indoor sources found to have the dominant role on human exposure (Morawska et al., 2013), however, significant correlation found between the outdoor originated particulate matter indoors (Janssen et al., 2000). The particle size is also highlighted as a major issue in risk assessment of human exposure (Cao et al., 2012).

Hence, the determination of indoor sources characteristics and origin of indoor particles are necessary in order to investigate the impact of indoor PM to everyday life. The pathogenic effect of dust inhalation on respiratory tissues can be attributed to the direct physical action of dust particles on the epithelium of the human airways and may be exacerbated by the toxic effects of both trace elements and of biologically active compounds (Leski et al., 2011). There is an increasing body of epidemiological evidence that high particulate levels in the air also cause cardiovascular disease (Brook et al., 2010), including myocardial infarction, stroke, heart failure, arrhythmias, and venous thromboembolism (Martinelli et al., 2013). Much dust storm material is silt-sized quartz, and it has been argued that this can, if inhaled over a sustained period, cause non-occupational silicosis (also called desert lung syndrome) to develop in human lungs (Goudie, 2014).

Characterization of indoor particulate matter in respect to chemical composition depends on the precursor material or source. Personal exposure and health effects is highly associated with chemical composition of atmospheric particles (Pöschl, 2005; Sarigiannis et al., 2011). Elemental carbon, heavy metals and organic compounds are

4.3. Particle Resuspension during Walking in an Indoor Microenvironment

usual components of the suspended particulate matter (Srivastava and Jain, 2007; Kopanakis et al., 2012; Bzdek et al., 2012). Moreover, dust particles can be easily transported, thus, particulate matter characteristics and chemical composition depends significantly on the origin region (Koçak et al., 2012; Karanasiou et al., 2009). Hence, the knowledge of the origin of particles and the associated chemical composition is a crucial issue both on in terms of IAQ and human exposure.

Airborne particles in the indoor environment can be derived either from outdoors or from indoor sources (Abt et al., 2000; Nazaroff, 2004; Chen et al., 2011). The indoor concentration of particulate matter is arising from ambient particles that penetrate indoors (Qian et al., 2014; Tian et al., 2009) and by emission of particles originating from indoor activities. Common activities such as printing, painting, cooking, burning wood, burning candles and smoking can generate new particles in the indoor environment (Pagels et al., 2009; Slezakova et al., 2009; Glytsos et al., 2010; Torkmahalleh et al., 2012; Zhang et al., 2012).

Particle resuspension from indoor surfaces is a crucial issue that affects indoor particle dynamics. Many studies investigated particle resuspension experimentally or using theoretical models. The experiments were conducted in controlled conditions using chamber or wind tunnels (Goldasteh et al., 2013a; Wang et al., 2012a; Tian et al., 2014) whereas, several real environments were used to study the impact of resuspension activities to indoor particle concentration (Rosati et al., 2008; Shaughnessy and Vu, 2012). Hence, particle resuspension was investigated throughout two aspects: the influence of human activities and when a fluid flow acts on the deposit particles.

Considering the first case, it was found that particle resuspension depends on many factors such as the amount of particle size, number of present people, the type of the floor, the walking style, the type of the shoes, bottom roughness, walking velocity and foot size (Zhang et al., 2008). Two types of mechanical forces are proposed, foot tapping on the floor and displacement due to foot penetration (Kubota and Higuchi, 2013; Oberoi et al., 2010). Moreover, indoor conditions were examined (infiltration system, presence of fan, relative humidity) in regard to their impact on resuspension, but still uncertainties exist on how they are affecting the resuspension rate of indoor particles (Shaughnessy and Vu, 2012).

However, insight to resuspension in relation to particle dynamics and interactions between external and intermolecular forces proposed by several models. Reeks and Hall (2001) considered a kinetic approach of particle resuspension where the bound particle oscillates about a pivot on the surface under the influence of the drag and lift force of the fluid flow. Lazaridis et al. (1998) adopted the same kinetic approach but modeling the particle-surface interaction using the Lennard-Jones intermolecular potential. Guingo and Minier (2008) and Goldasateh et al. (2013b) used Monte Carlo computations to simulate surface roughness and distribution of the adhesion forces.

The proposed models share common features such as the stochastic description of particle resuspension, the strong dependence on surface roughness and the importance of interaction between the deposit particles and the surface. It was found that high surface roughness corresponds to easier detachment (Soltani and Ahmadi, 1995) due to a significant reduction in adhesion forces (Zisking et al., 1995). Moreover, particle size plays an important role by enhancing resuspension, since the removal forces (drag and lift) depend strongly on it (Hinds, 1999). It was also proposed (Reeks and Hall, 2001) that resuspension depends on time with high resuspension rates at a short-term regime followed by a long-term regime with reduced rates. The time dependence observed also experimentally (Wang et al., 2012a).

The aim of this work was to evaluate the particle resuspension rate induced by walking inside an indoor microenvironment using continuous measurements of indoor particle mass/number concentration. The main objectives were to determine the impact of different dust loadings on the floor, the indoor particle concentration and the resuspension rate and to investigate the impact of different walking patterns, style and walking speed to the resuspension rate.

4.3.2. Experimental setup

The measurements were carried out in the period between June to September 2013 in a laboratory at the Technical University of Crete. The area of the laboratory is 18.5 m² of rectangle shape and its volume is 53.7 m³ with one door and one window placed opposite of the door. The effective volume was estimated to be ~77 % of the total volume, thus

4.3. Particle Resuspension during Walking in an Indoor Microenvironment

41.5 m³. The effective surface area was equal to 6 m² (4.3×1.4 m). During the resuspension measurements, the instruments were placed at the farther end of the paper pool with inlets 1.38 ± 0.03 m above the ground. The selected height of the instruments (1.38 m) corresponds to the breathing zone of the person performing the walking.

During the experiments only one person was present in the laboratory, with the window and the door closed all times. To determine the reproductivity, all 8 variations (combination of rectangle and line paths with different dust loadings – 25, 15, 5 and 1 g/m²) of resuspension experiments were performed twice. Additional measurements were conducted with increased and decreased walking speed in order to investigate the effect of walking speed on resuspension rate. Two experiments were performed with 20% higher walking speed, whereas, two experiments performed with 20% lower walking speed. Thus, four additional experiments with different walking speed. The experiments were conducted following a line path and only in the case 5 g/m² and 1 g/m² of dust loading. The increased or decreased speed was obtained based on the average walking speed on each set of measurements (5 g/m² and 1 g/m² in the present case). The materials used to build the paper pool were a simple plotter paper (0.94 m width, $\rho = 80 \text{ g/m}^2$) and a masking paper tape. The footwear used during the walking were a classic long stripe cotton socks, 3 pairs (75 % cotton, 25 % polyester).

4.3.3. Instrumentation and Measurement Protocol

Several instruments were used in order to measure indoor particle concentration. More precisely a Dust Trak (8520, TSI) was used for mass concentration of PM₁₀, and a P-Trak (8525, TSI) for particle number concentration of fine particles (< 1 μm). OPS (3330, TSI) was employed for the determination of the mass size distribution. The air temperature and relative humidity during the resuspension measurements were recorded by four Tiny Tag data loggers placed in the corners of the laboratory. Scheme of the laboratory and the instrumentation is depicted in Figure 4.23. The average air temperature in the laboratory during the measurements period was recorded to be 30 ± 1°C and the relative humidity 45 ± 4%. Nonetheless, the PM₁₀ mass concentration data obtained by Dust Trak were corrected based on work of Chalvatzaki et al. (2010) where comparative

4.3. Particle Resuspension during Walking in an Indoor Microenvironment

measurements of PM₁₀ concentrations by the Beta attenuation monitor (FH 62 SEQ) and the Dust Trak were performed at an urban background site close to the laboratory for a period of 12 months. The Dust Trak instrument measurements were then corrected based on these comparative measurements.

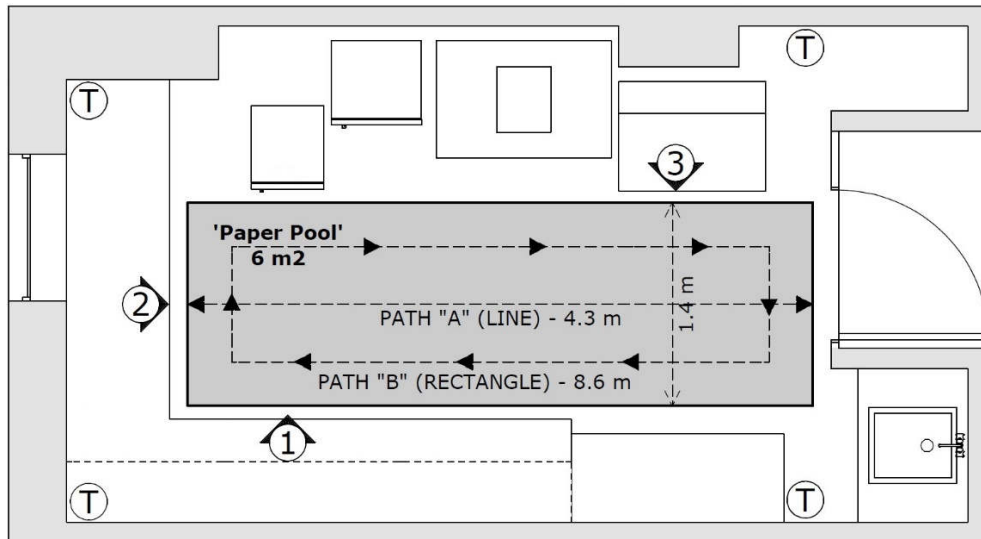


Figure 4.23. Scheme of the laboratory and the instrumentation around the paper pool: (1) DustTrak, (2) P-Trak, (3) OPS, and (T) Temperature and Relative Humidity.

At the beginning, two testing measurements were conducted using 25 g/m² dust on the floor of the paper pool, one in a rectangle (Figure 4.24) and another in a line path for a walking period of 30 minutes. The other experiments were conducted using a walking period of 20 minutes. Each resuspension experiment (20 experiments in total) lasted 5 hours and 30 minutes and were completed in 3 stages:

- Stage 1: Empty laboratory: 0 - 60 min (background measurement)
- Stage 2: Walking period: 60 - 80 min (resuspension - emission period)
- Stage 3: Post walking period: 80 - 330 min (empty laboratory - particles removal)

4.3. Particle Resuspension during Walking in an Indoor Microenvironment

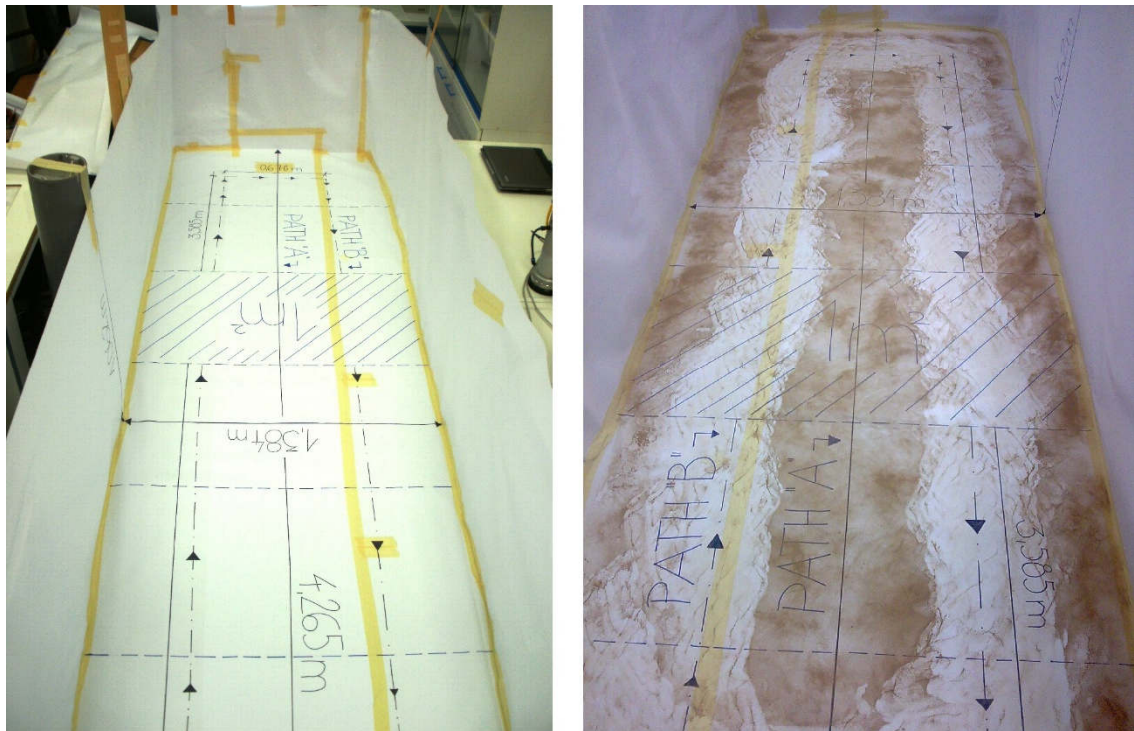


Figure 4.24. Paper pool before (left) and after walking (right) in rectangular pattern on 25 g/m^2 of dust load.

The 20 minutes of the emission period were used to determine the resuspension rate, since it was the only period of activity inside the laboratory room. However, only the last 10 minutes of background period and the first 210 minutes of the removal period used to evaluate the background and the removal period respectively. Hence, 4 h in total for each experiment. The background period was evaluated only at the last 10 minutes, since, no significant temporal fluctuations of the indoor concentration observed during the pre-activity period. The removal period was evaluated only for the first 210 min because the indoor concentration maintained similar values after the chosen period. During stages 1 and 3 no one was present in the room and all the windows and doors were closed. During the stage 2 only one person was present in the room with the door and window closed. Two walking paths were used for the experiments. Path A in which the person was walking in a line path 4.3 m long in the middle of the paper pool and path B in which the person was walking in a rectangle shaped path of 8.6 m long around the edge of the paper pool in a clockwise direction.

4.3.4. Dust analysis

The dust used in all the experiments was collected with a scoop into a 10-liter container outside the laboratory window from the sidewalk on 05/06/2013 between K1 and K2 buildings of School of Environmental Engineering. It is the same dust that could possibly get inside the indoor environment during air exchange while opening the window or by penetration. The collected dust was then sieved on a laboratory sieve with an aperture of 53 μm and stored in an air-tight box at a room temperature in the laboratory. With the same sieve the dust was spread manually on the floor of the paper pool with extreme care in order to maintain a uniform layer. The dust was spread at 15 ± 5 cm height above the ground at the most 4 - 5 h before the measurements. Prior to new measurement, the paper with a dust loading at the bottom of the paper pool was overlaid twice from the top with a new paper (during the experiments with 25 and 15 g/m^2 of dust loading the bottom was overlaid four times with a new paper in order not to affect the next measurements) and the walls were cleaned with a piece of semi-wet cloth.

Heavy metals analysis (Na, Mg, Al, Si, K, Ca, Fe, Ti, V, Cr, Mn, Ni, Cu, Zn, As, Se, Cd, Ba, Hg, Pb) was performed to determine the metal content of the dust used by Inductively coupled mass spectrometry (ICP-MS 7500cx coupled with Autosampler Series 3000, Agilent Technologies). The collision (He) and reaction modes of the instrument were used during the analysis procedure in order to eliminate possible isotopes interferences (e.g. interference of $^{40}\text{Ar}^{12}\text{C}$ in the ^{52}Cr analysis). The results were calibrated using an external calibration curve (at least 5 levels of concentration, with a correlation coefficient $r = 0.99$ for each element) and the corresponding Merck standards. Although, the results did not reveal any significant levels of major crustal elements (Al, Si, Fe, Ca, K, Mg, Ti) which were all below 0.62% with exception of Calcium where the analysis showed a high concentration equal to 14.94%. On the other hand, trace elements (Zn, Pb, Cu, Ni, Cd, Cr) and other element (Na, V, Mn, As, Se, Ba, Hg) concentrations were not higher than 0.01%, except Sodium (0.81%).

4.3.5. Model Description

Resuspension rate model

A resuspension model was used for the analysis of the resuspension experiments and the calculation of the resuspension rate. The resuspension of an indoor aerosol is usually defined by the resuspension rate r (min^{-1}), which is the fraction of particles removed from the surface per unit of time (Nicholson, 1988):

$$r = \frac{R}{L} \quad (\text{Eq. 4.7})$$

where R is the resuspension flux ($\mu\text{g}/\text{m}^2\text{min}$) and L ($\mu\text{g}/\text{m}^2$) is the particle surface concentration. Considering a room of well-mixed air volume, the particle concentration can be described by a dynamic mass balance model (Chen and Zhao, 2011):

$$\frac{d(VC_{in})}{dt} = PaVC_{out} + S - aVC_{in} - kVC_{in} \quad (\text{Eq. 4.8})$$

where C_{in} is the particle concentration inside the laboratory ($\mu\text{g}/\text{m}^3$), C_{out} is the particle concentration outside the laboratory ($\mu\text{g}/\text{m}^3$), V is the effective volume of the laboratory (m^3), P is the penetration efficiency, a is the air exchange rate (min^{-1}), k is the deposition rate (min^{-1}), S is the emission of the particles indoors ($\mu\text{g}/\text{min}$) and t is the time (min^{-1}). In particular, in respect to particle emissions by resuspension (S), the emission rate can be written as:

$$S = r A_r L \quad (\text{Eq. 4.9})$$

4.3. Particle Resuspension during Walking in an Indoor Microenvironment

where r is the resuspension rate (min^{-1}), A_r is the floor surface area used for resuspension (m^2) and L is the floor loading ($\mu\text{g}/\text{m}^2$). Thus, Eq. (4.8) can be rewritten as follows:

$$V \frac{dC_{in}}{dt} = PaVC_{out} + rA_rL - (a+k)VC_{in} \quad (\text{Eq. 4.10})$$

Introducing a mass balance model on the surface, the change in aerosol mass concentration on the floor can be written as (Qian and Ferro, 2008):

$$A \frac{dL}{dt} = -rA_rL + kVC_{in} \quad (\text{Eq. 4.11})$$

where A is the total surface area of the room (m^2). Thus, the change in particle concentration indoors is described by a set of two equations, namely Eq. (4.10) and (4.11). During the resuspension experiments, the total surface area of the laboratory was used. In this case, A_r can be substituted with A , and a simplified version of the system of Eq. (4.10) and (4.11) yields:

$$V \frac{dC_{in}}{dt} = PaVC_{out} + rAL - (a+k)VC_{in} \quad (\text{Eq. 4.12})$$

$$A \frac{dL}{dt} = -rAL + kVC_{in} \quad (\text{Eq. 4.13})$$

Eq. (4.12) describes the change in mass concentration indoors and Eq. (4.13) is describing the change in particle mass concentration on the floor. The resuspension rate r is estimated by Eq. (4.12) using a forward difference approximation, while, Eq. (4.13)

4.3. Particle Resuspension during Walking in an Indoor Microenvironment

can be solved analytically. Thus, the resuspension rate and the particle surface loading for each time step are given by:

$$r(t+dt) = \frac{V}{AL(t)} \left[\frac{C_{in}(t+dt) - C_{in}(t)}{dt} + (k+a)C_{in}(t) - aPC_{out}(t) \right] \quad (\text{Eq. 4.14})$$

$$L(t) = \frac{kV C_{in}(t)}{rA} (1 - e^{-rt}) + L(0) e^{-rt} \quad (\text{Eq. 4.15})$$

The requirements for solving the above system are the initial values of mass loading $L(0)$ and the change in concentration $C(t)$ with time. Given the initial mass loading $L(0)$ and the change of aerosol concentration, r can be estimated for time step one using Eq. (4.14). Since r is known, Eq. (4.15) is then used to estimate the surface loading at the first time step, $L(1)$. The same procedure is followed for every time step. Moreover, the particle concentration in the indoor air can be predicted from Eq. (4.12) (Qian et al., 2008):

$$C_{in}(t+dt) = r \frac{A}{V} L(t) dt + C_{in}(t) [1 - (a+k)dt] + aPC_{out}(t) dt \quad (\text{Eq. 4.16})$$

The first term on the right side of the Eq. (4.16) is the resuspension contribution to indoor air concentration, the second term refers to the reduction of indoor concentration by deposition and air exchange rate and finally the third term is the penetration of outdoors origin particles indoors.

4.3. Particle Resuspension during Walking in an Indoor Microenvironment

Infiltration rate

The particle indoor dynamic model for a well-mixed air volume is given by Eq. (4.12). The infiltration rate of outdoor origin particles can be estimated using Eq. (4.12) for a period without any activity inside the laboratory. Thus, Eq. (4.12) is written as:

$$V \frac{dC_{in}}{dt} = P a V C_{out} - (a + k) V C_{in} \quad (\text{Eq. 4.17})$$

The analytical solution of the above equation is:

$$C_{in}(t) = \frac{a P C_{out}}{a + k} + \left(C_{in}(0) - \frac{a P C_{out}}{a + k} \right) e^{-(a+k)t} \quad (\text{Eq. 4.18})$$

The right side of Eq. (4.18) consists of two terms. The first term is the steady state concentration of the particles inside the laboratory which can be defined as the fraction of particles that penetrates from outdoors and remain suspended indoors. The second term represents the total losses of the indoor aerosol due to deposition and air exchange from indoors to outdoors. The infiltration rate was calculated based on Eq. (4.18) after the end of the activity, where, the particle concentration is exponentially decreasing with time. Due to lack of outdoor data, the infiltration was estimated as the fraction of particles that remain suspended inside the laboratory (the steady state particle concentration or infiltration concentration C_{inf}):

$$C_{inf} = \frac{a P C_{out}}{a + k} \quad (\text{Eq. 4.19})$$

Air exchange rate

The air exchange rate was estimated based on the exponential decay of CO₂ inside the laboratory. The concentration of CO₂ after the emission period is described by the following equation:

$$\frac{dC_{CO_2}}{dt} = -a C_{CO_2} \quad (\text{Eq. 4.20})$$

where a is air exchange rate (h⁻¹). Thus, CO₂ concentration at any time inside the laboratory is given by:

$$C_{CO_2}(t) = C_{CO_2}(0) e^{-at} \quad (\text{Eq. 4.21})$$

The average air exchange of the laboratory calculated to be 0.16 h⁻¹ during the experiments.

4.3.6. Indoor Particle Concentration

Indoor particle number and mass concentration was measured simultaneously during the walking experiment. The number concentration was measured in the size range of 0.02 - 1 μm, whereas, the measured mass concentration corresponded to the size range of 0.1 - 10 μm. Figure 4.25 presents the indoor mass and number concentration versus time during the experiment on 04/07. The mass concentration is influenced from the beginning of the activity with an increase in the indoor concentration which is followed by a decreasing period after the end of the walking. The background average indoor mass concentration was 73 μg/m³, while, during the walking the average mass concentration was 3,320 μg/m³ indicating 45-fold increase. On the other hand, the number

4.3. Particle Resuspension during Walking in an Indoor Microenvironment

concentration maintained similar concentration levels before and during the walking. Average background concentration was $2 \times 10^3 \text{ \#/cm}^3$, whereas, average concentration during the walking was $2.1 \times 10^3 \text{ \#/cm}^3$. The same characteristic found in all experiments. Thus, the three periods (background, walking period, post-walking period) were strongly correlated only with the indoor particle mass concentration.

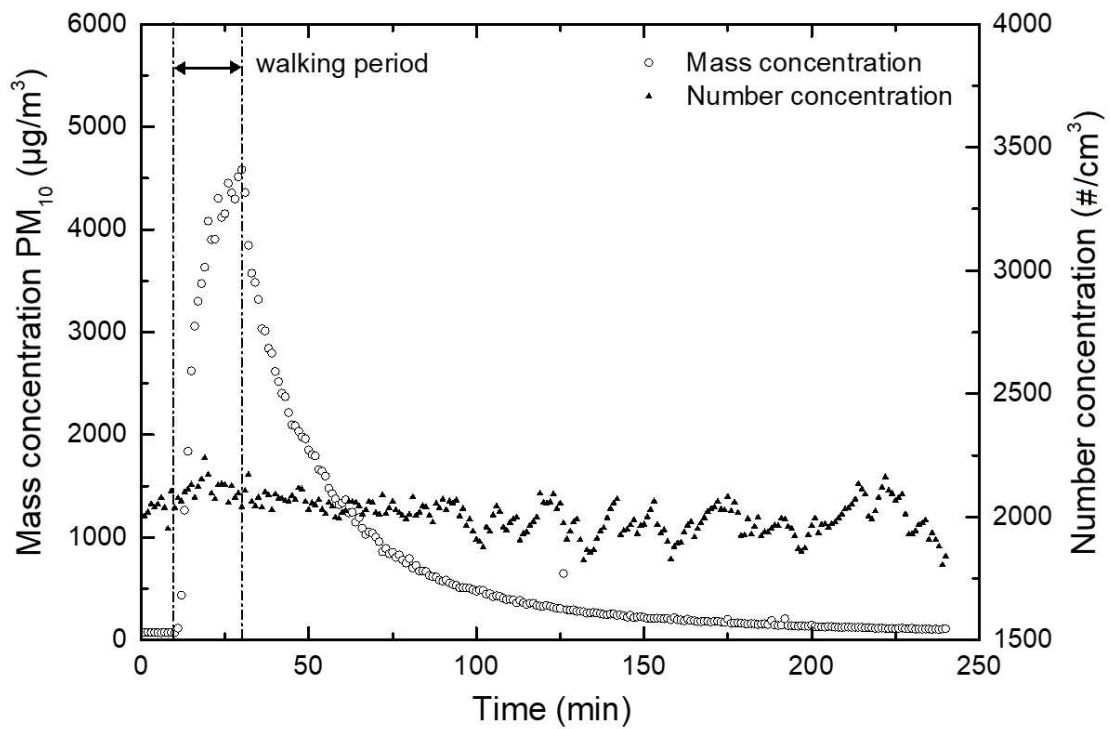


Figure 4.25. Mass and number concentration versus time during walking in rectangle pattern inside the paper pool with dust loading 25 g/m^2 (R2 on 04/07).

Although particle resuspension from indoor surfaces depends on particle size (Wang et al., 2012a), larger particles detach more easily from the surface (Boor et al., 2013). Previous studies verify that small particles ($< 1 \text{ \mu m}$) are not easily resuspended or not resuspended at all (Tian et al., 2014). Moreover, studies on resuspension by human walking concluded that resuspension rate increases with particle size (Qian et al., 2008; Shaughnessy and Vu, 2012). Results of this study indicate that in terms of mass concentration the walking influences strongly the PM_{10} indoor particle concentration. On

4.3. Particle Resuspension during Walking in an Indoor Microenvironment

the other hand, in terms of number concentration the indoor particles are not affected by the walking in the laboratory room inside the measured particle size range. Considering the different size range used for the mass and number concentration, the presented results imply that the resuspension of indoor particles takes place at particle sizes higher than 1 μm . It is likely that particles at size that correspond to the measured number concentration (0.02 - 1 μm) is not resuspend at all. Since, the measured size range of the mass concentration corresponds to higher particle sizes (0.1 - 10 μm), it is believed that the resuspended particulate matter lies in the size range of 1 - 10 μm .

Table 4.11 summarizes the average PM_{10} concentration for background and activity periods during all experiments. Indoor PM_{10} mass concentration during the activity period indicate on average 75-fold, 40-fold, 14-fold and 0.6-fold increase of mass concentration in the case of 25, 15, 5 and 1 g/m^2 , respectively. This is indicating a considerable change in indoor mass concentration inside the laboratory. Indoor mass concentration is increased by one or two orders of magnitude in a period of few minutes (20 minutes). On the other hand, particle number concentration maintained values close to the background level in all experiments as indicated in Figure 4.25.

No dependence of indoor PM_{10} concentration found in respect to the two different walking profiles followed during the activity. Walking in a rectangular manner or in line inside the laboratory had no effect on indoor aerosol concentration and therefore on the resuspension rate. Qian and Ferro (2008) examined the effect of different walking paces and weight of the person while walking inside a chamber and found that the main contribution in resuspension rate is walking style. In the presented study walking style, walking duration, dust type, foot wear and walking person were the same in all experiments and the only variable during the activity was the walking pattern which had no effect on the indoor particle concentration.

4.3. Particle Resuspension during Walking in an Indoor Microenvironment

Table 4.11. Comparison between average background concentration and average walking concentration for different dust loadings (R-Rectangular, L-Line pattern).

| Date & Walking Pattern | PM₁₀ background concentration (µg/m³) | PM₁₀ concentration (µg/m³) | Increase (%) | Emission Rate (mg/min) |
|--|--|---|---------------------|-------------------------------|
| Dust Loading 25 g/m² | | | | |
| 04/07-R | 73 | 3,320 | 4,452 | 17.3 |
| 10/07-L | 58 | 3,205 | 5,471 | 14.6 |
| 26/07-R | 39 | 3,839 | 9,654 | 17.6 |
| 30/07-L | 32 | 3,463 | 10,561 | 19.4 |
| Average | 51 | 3,457 | 7,535 | 17.2 |
| Dust Loading 15 g/m² | | | | |
| 21/06-R | 47 | 1,433 | 2,957 | 6.5 |
| 26/06-L | 36 | 1,579 | 4,317 | 7.1 |
| 08/08-R | 42 | 1,690 | 3,902 | 7.8 |
| 10/08-L | 35 | 1,716 | 4,843 | 9.2 |
| Average | 40 | 1,605 | 4,005 | 7.7 |
| Dust Loading 5 g/m² | | | | |
| 02/07-R | 38 | 462 | 1,104 | 2.0 |
| 28/06-L | 42 | 573 | 1,260 | 2.4 |
| 12/08-R | 41 | 556 | 1,268 | 3.5 |
| 13/08-L | 49 | 642 | 1,222 | 2.9 |
| ^A 10/09-L | 34 | 680 | 1,924 | 2.8 |
| ^B 11/09-L | 39 | 573 | 1,370 | 4.1 |
| Average | 41 | 581 | 1,358 | 3.0 |
| Dust Loading 1 g/m² | | | | |
| 12/07-R | 47 | 215 | 362 | 0.9 |
| 24/07-L | 27 | 325 | 1,089 | 2.2 |
| 15/08-R | 52 | 259 | 399 | 1.2 |
| 14/08-L | 50 | 240 | 378 | 1.4 |
| ^A 12/09-L | 35 | 381 | 976 | 2.6 |
| ^B 13/09-L | 24 | 156 | 563 | 1.0 |
| Average | 39 | 263 | 628 | 1.6 |

(A) Walking Speed +20%; (B) Walking Speed -20%

4.3.7. Indoor PM₁₀ Concentration at Different Dust Loadings

Figure 4.26 presents the PM₁₀ indoor mass concentration versus time for different dust loadings. One experiment from each dust loading (thus 4 in total) was chosen in order to compare the indoor mass concentration and examine the effect of the dust loading to the

4.3. Particle Resuspension during Walking in an Indoor Microenvironment

measured PM₁₀ mass concentration. All chosen experiments corresponded to walking in a line path in order to isolate the impact of using different dust loadings on the floor. Higher surface loading is leading to higher indoor mass concentration. Increased concentration on the floor corresponds to higher initial dust loading, which, can be potentially removed from the surface. In fact, calculating the emission rate S from Eq. (4.9) for each surface loading reveals that the emission rate increases with increasing initial dust loading on the floor (Table 4.11). The average emission rates for 25, 15, 5 and 1 g/m² dust loading were 17.2, 7.7, 3.0 and 1.6 mg/min, respectively. Gomes et al. (2007) also observed increased mass of resuspended particles at higher dust loadings and Tian et al. (2014) reported that higher dust emission rates were provoked by higher surface dust loadings. Moreover, Qian et al. (2014) reported that the emission rates of particle mass due to walking were in the range 10⁻² - 10² mg/min, which is in agreement with the findings presented hereby.

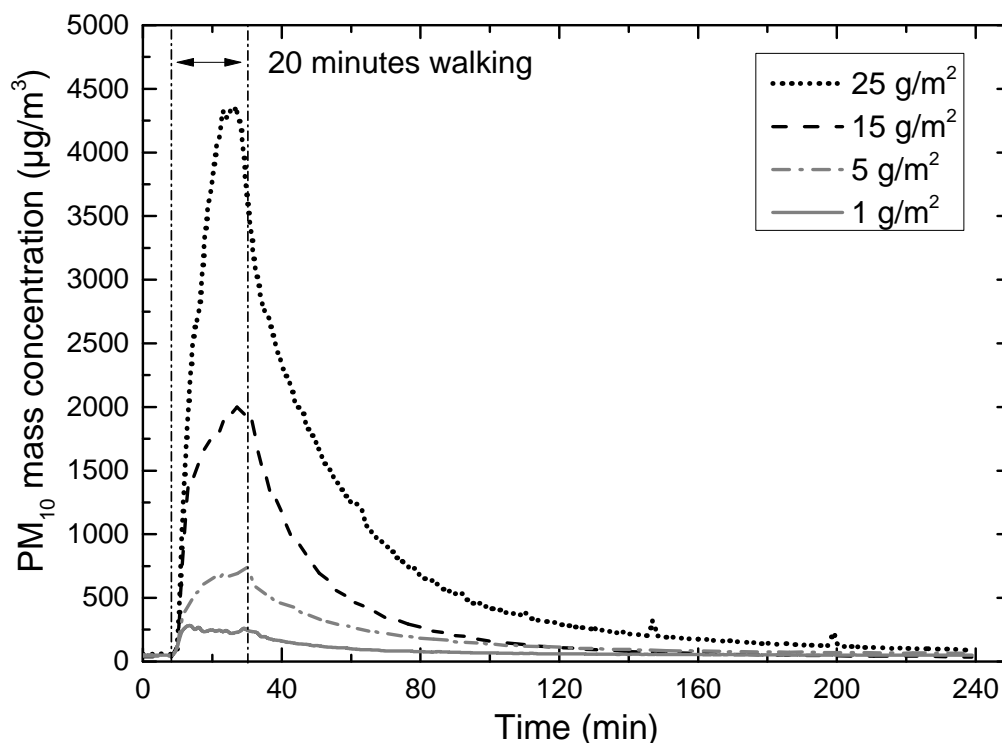


Figure 4.26. Mass concentration versus time for different dust loadings. Line path was used in all experiments (10/07, 26/06, 28/06, 14/08).

4.3.8. Estimation of Infiltration Rate

In the absence of indoor sources, the indoor particle concentration is the net result of particle penetration from outdoors, particle deposition on indoor surfaces and air exchange rate of the studied room (Hussein et al., 2009; Rim et al., 2013). Thus, the total indoor particles losses include deposition by Brownian diffusion and gravitational settling (Nazaroff, 2004) and the indoor/outdoor air exchange rate (Chen and Zhao, 2011). In the presented study the post-walking period was evaluated using the Eq. (4.17), which reflects the indoor particle concentration inside the laboratory in the absence of indoor sources. Applying Eq. (4.18) to the experimental data after the end of the activity and using also Eq. (4.19), the infiltration rate and total losses inside the laboratory can be estimated. Figure 4.27 presents a comparison between the experimentally measured and calculated PM₁₀ mass concentrations after the end of the walking period where the same pattern was found in all experiments.

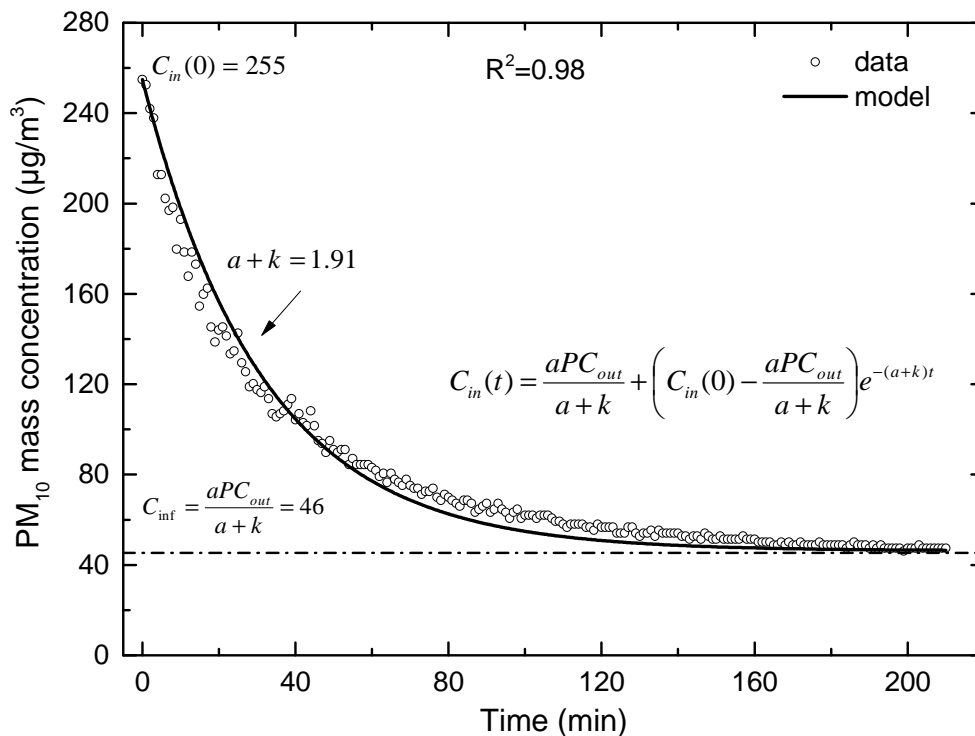


Figure 4.27. Observed and calculated mass concentration after the end of walking in rectangle pattern inside the paper pool with 25 g/m² dust loading (R5 on 12/07).

4.3. Particle Resuspension during Walking in an Indoor Microenvironment

Additionally, in Table 4.12 lists the infiltration concentrations C_{inf} and total losses as they were calculated by Eq. (4.18) for each experiment. The correlation between the calculated indoor concentration for the experiment R5 (Figure 4.27) and the experimental one is high ($R^2 = 0.98$). This indicates that Eq. (4.18) describes well the measured indoor particle concentration starting with the initial value of $255 \mu\text{g}/\text{m}^3$ and ending at the steady state mass concentration of $46 \mu\text{g}/\text{m}^3$ inside the laboratory.

Table 4.12. Results of the calculated indoor concentrations after the end of the walking.

| Date | Dust load (g/m^2) | Initial Conc. $C(0)$ ($\mu\text{g}/\text{m}^3$) | Steady state Conc. C_{inf} ($\mu\text{g}/\text{m}^3$) | Total losses $a+k$ (h^{-1}) | R^2 |
|--------------------|--|--|---|--|-------|
| 04/07 | 25 | 4.6×10^3 | 95 | 2.60 | 0.97 |
| 10/07 | 25 | 4.0×10^3 | 63 | 2.35 | 0.97 |
| 21/06 | 15 | 2.0×10^3 | 48 | 2.39 | 0.99 |
| 26/06 | 15 | 3.9×10^3 | 48 | 2.91 | 0.97 |
| 02/07 | 5 | 6.6×10^2 | 39 | 2.25 | 0.98 |
| 28/06 | 5 | 7.6×10^2 | 59 | 2.36 | 0.94 |
| 12/07 | 1 | 2.6×10^2 | 46 | 1.91 | 0.98 |
| 24/07 | 1 | 2.9×10^2 | 25 | 2.90 | 0.95 |
| 26/07 | 25 | 4.2×10^3 | 48 | 3.46 | 0.98 |
| 30/07 | 25 | 3.9×10^3 | 44 | 3.04 | 0.97 |
| 08/08 | 15 | 2.0×10^3 | 38 | 3.24 | 0.98 |
| 10/08 | 15 | 1.9×10^3 | 43 | 3.00 | 0.98 |
| 12/08 | 5 | 6.2×10^2 | 36 | 2.78 | 0.97 |
| 13/08 | 5 | 7.4×10^2 | 46 | 3.27 | 0.94 |
| 15/08 | 1 | 2.7×10^2 | 62 | 3.00 | 0.99 |
| 14/08 | 1 | 2.7×10^2 | 48 | 2.91 | 0.95 |
| ^A 10/09 | 5 | 8.0×10^2 | 31 | 2.65 | 0.98 |
| ^B 11/09 | 5 | 7.5×10^2 | 33 | 4.20 | 0.91 |
| ^A 12/09 | 1 | 4.4×10^2 | 27 | 2.69 | 0.98 |
| ^B 13/09 | 1 | 1.9×10^2 | 26 | 3.13 | 0.97 |
| Average | | | 46 | 2.85 | 0.98 |

(A) Walking Speed +20%; (B) Walking Speed -20%

High correlation between the experimental and the calculated indoor concentration was found in all experiments with R^2 ranging between 0.91 – 0.99. The C_{inf} is independent from the initial surface dust loading. According to Eq. (4.19) the

steady state indoor concentration is a function of penetration of outdoor particles and total losses inside the laboratory. Moreover, no correlation was found between total losses ($a+k$) and the initial surface loading. The average of total losses inside the laboratory were estimated on $2.85 \pm 0.5 \text{ h}^{-1}$, which is consistent with other studies dealing with indoor particle dynamics (Lai, 2002; He et al., 2005).

4.3.9. Dust Loading

The most important factor for determining the resuspension rate is the surface dust loading for every time interval. The resuspension rate and surface loading are irreversibly proportional (Eq. (4.14) and (4.15)) and cannot be derived independently. An increase of indoor mass concentration is increasing the resuspension rate and reducing the dust loading on the floor. The $L(t)$ can be estimated only by knowing the resuspension rate at that specific moment. Giving the initial value $L(0)$, a repeated numerical procedure is followed by estimating at each time step the resuspension rate and then the instant dust loading on the floor.

Several variations of dust loading were taking place while the experiment was performed. A typical example of surface concentration variations versus time during the activity period is shown in Figure 4.28. The initial dust loading on the floor was estimated at 24.57 g/m^2 and this value is compared with the calculated dust loading derived from Eq (9). The data points under the line, which shows the initial surface concentration, indicate an increase in indoor mass concentration, whereas, the data points above the line indicate a decrease in indoor mass concentration (various temporal fluctuations took place in most of the experiments). Numerically, the first case is related with a positive number in the calculation of resuspension rate, while the second case is related with a negative number. Moreover, the mass concentration on the floor shows small variations.

In Figure 4.28 the dust loading fluctuations varied between $24.5 - 24.6 \text{ g/m}^2$. Even though the indoor PM_{10} concentration increases up to two orders of magnitude, the surface dust loading $L(t)$ retains values close to the initial dust loading. The same behavior was observed in all experiments. The average variance of the relative fluctuations of the surface concentration was found 0.013%, confirming that a very small

4.3. Particle Resuspension during Walking in an Indoor Microenvironment

fraction of the deposited dust on the floor is actually resuspended. These findings are in agreement with Tian et al. (2014) where the authors also suggested that only a small fraction of particles is resuspended. Nevertheless, indoor PM_{10} concentration increases drastically with higher dust loading during the walking period resulting in higher mass concentration. A reasonable explanation is that the higher the dust loading on the floor, the higher the potential fraction of particles that can detach from the surface and consequently resuspend.

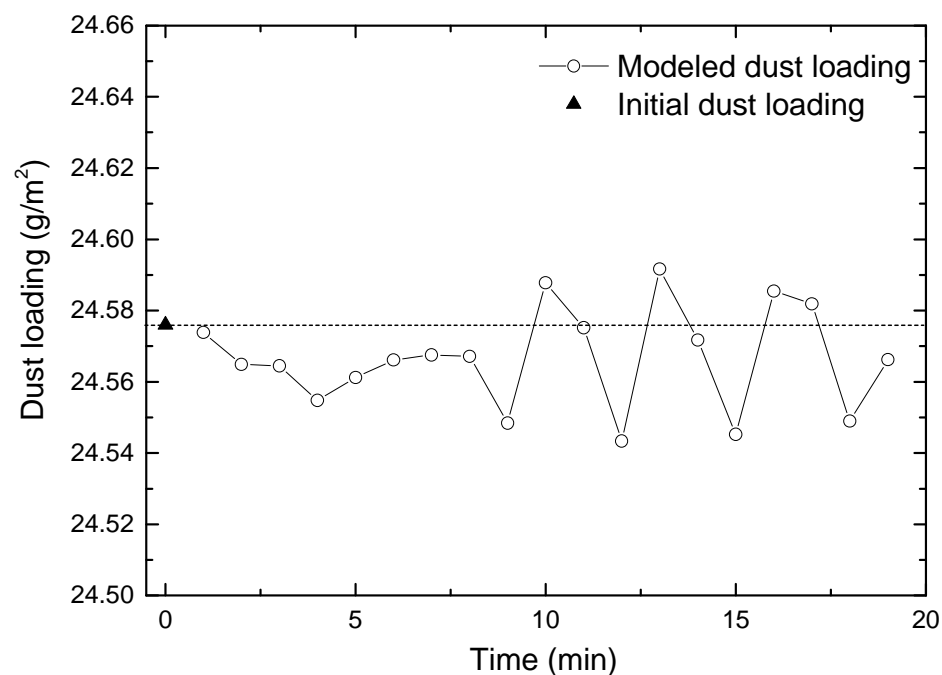


Figure 4.28. Initial and the calculated dust loading on the floor versus time during the activity period, $Lo = 24.57 g/m^2$ (R2 on 04/07).

Particle detachment is closely related with resuspension and it depends both on the adhesive and removal forces (Zhang et al., 2008; Ibrahim et al., 2003). Moreover, resuspension occurs easily for larger particles (Boor et al., 2013, Rosati et al., 2008). In human induced particle resuspension, particle detachment is caused by mechanical forces, such as foot tapping (Kubota and Higuchi, 2013) or displacement due to foot penetration (Oberoi et al., 2010). Moreover, Goldasteh et al. (2014) proposed that the

main mechanism for particle resuspension is the high speed airflow generated at the gap of the shoe sole during the upward and downward motion of the foot. Considering that the walking style was the same for all experiments, particle detachment happened under the same conditions. Removal forces that are connected with these conditions were likely in the same order of magnitude and responsible for the fraction of particles leaving the surface.

4.3.10. Resuspension Rate

The resuspension rate was calculated using the coupled set of Eq. (4.14) and (4.15). Table 4.13 summarizes the resuspension rate for all the experiments. On average the resuspension rate for all the experiments was $6.61 \times 10^{-3} \text{ h}^{-1}$. In general, the range of the resuspension rate was between $10^{-2} - 10^{-3} \text{ h}^{-1}$. These results are in agreement with other studies for resuspension by walking in a chamber or in real environment which found values in the range $10^{-2} - 10^{-6} \text{ h}^{-1}$ (Qian and Ferro, 2008; Shaughnessy and Vu, 2012; Tian et al., 2014). Table 4.13 also suggests that resuspension rate is independent from the initial dust loading on the floor. The different dust loadings are affecting the indoor PM_{10} concentration but not the resuspension rate.

Factors such as walking speed, weight of person, number of persons inside the room, type of shoes and floor, or walking style contribute differently on the resuspension rate (Qian et al., 2014; Boor et al., 2013). In the case of the herein presented analysis, different walking patterns had no effect on indoor concentration nor on resuspension rate. Even though different walking speeds were examined in 4 experiments (10/09, 12/09 higher walking speed, 11/09, 13/09 lower walking speed), no correlation was found between the walking speed and the resuspension rate. Probably, the effect of walking speed on particle resuspension should have an effect for a wider range of speeds.

The air temperature and relative humidity had no effect on resuspension rate for the range of the environmental conditions occurred in the laboratory. The average temperature inside the laboratory for all the experiments was $30 \pm 1^\circ\text{C}$ and the average relative humidity was $45 \pm 4\%$. The relative humidity was found to affect the adhesion force between the particle and the substrate through capillary forces (Bateman et al.,

4.3. Particle Resuspension during Walking in an Indoor Microenvironment

2014). However, the influence of relative humidity on particle detachment becomes significant on wider ranges of 20% - 90% RH (Bateman et al., 2014). Qian and Ferro (2008) also found no effect on resuspension rate for RH range 26.4 % - 51%, while, Tian et al (2014) found a dependence on resuspension for two levels (40% and 70%) of RH.

Table 4.13. Resuspension rate for different dust loadings.

| Date | Resuspension rate r (h^{-1}) |
|--|---|
| Dust loading 25 g/m² | |
| 04/07 | 7.15×10^{-3} |
| 10/07 | 6.64×10^{-3} |
| 26/07 | 7.31×10^{-3} |
| 30/07 | 8.60×10^{-3} |
| Average | 7.43×10^{-3} |
| Dust loading 15 g/m² | |
| 21/06 | 4.46×10^{-3} |
| 26/06 | 5.05×10^{-3} |
| 08/08 | 5.28×10^{-3} |
| 10/08 | 6.19×10^{-3} |
| Average | 5.25×10^{-3} |
| Dust loading 5 g/m² | |
| 02/07 | 4.05×10^{-3} |
| 28/06 | 4.63×10^{-3} |
| 12/08 | 6.65×10^{-3} |
| 13/08 | 6.48×10^{-3} |
| ^A 10/09 | 5.56×10^{-3} |
| ^B 11/09 | 8.38×10^{-3} |
| Average | 5.96×10^{-3} |
| Dust loading 1 g/m² | |
| 12/07 | 7.81×10^{-3} |
| 24/07 | 2.06×10^{-2} |
| 15/08 | 1.10×10^{-2} |
| 14/08 | 1.35×10^{-2} |
| ^A 12/09 | 2.39×10^{-2} |
| ^B 13/09 | 9.60×10^{-3} |
| Average | 1.44×10^{-2} |

(A) Walking Speed +20%; (B) Walking Speed -20%

4.3. Particle Resuspension during Walking in an Indoor Microenvironment

The resuspension rate of indoor particles was estimated for each time step of every experiment using the set of Eq. (4.14) and (4.15). In order to find the time dependence of resuspension rate, the walking period was further divided. This was due to the fact that in several experiments fluctuation of indoor mass concentration was observed, thus, the activity period divided into two stages. In stage 1, which is the burst of particle emission, the first 4 minutes of the activity were chosen due to higher rates observed at this period, and in stage 2 the remaining time of the activity was chosen. Figure 4.29 presents the resuspension rate for the two stages for all the experiments.

Figure 4.29 demonstrates a strong dependence of resuspension rate versus time. The first minutes of the event are characterized by higher resuspension rate than the remaining time. The resuspension rate at stage 1 is higher by 68% in comparison to stage 2. Strongly adhered particles are more difficult to detach from the surface. Thus, in the first minutes of the walking resuspension occurs for particles which are less adhered on the surface. Similar results were found both in cases of human-induced particle resuspension (Qian et al., 2008) or in wind tunnel studies (Wang et al., 2012a; Ibrahim et al. 2003). Turbulent air flow generated by human walking, adhesion forces and type of deposit (monolayer or multilayer) are responsible for the fluctuation on resuspension rate through exposure time (Boor et al., 2013).

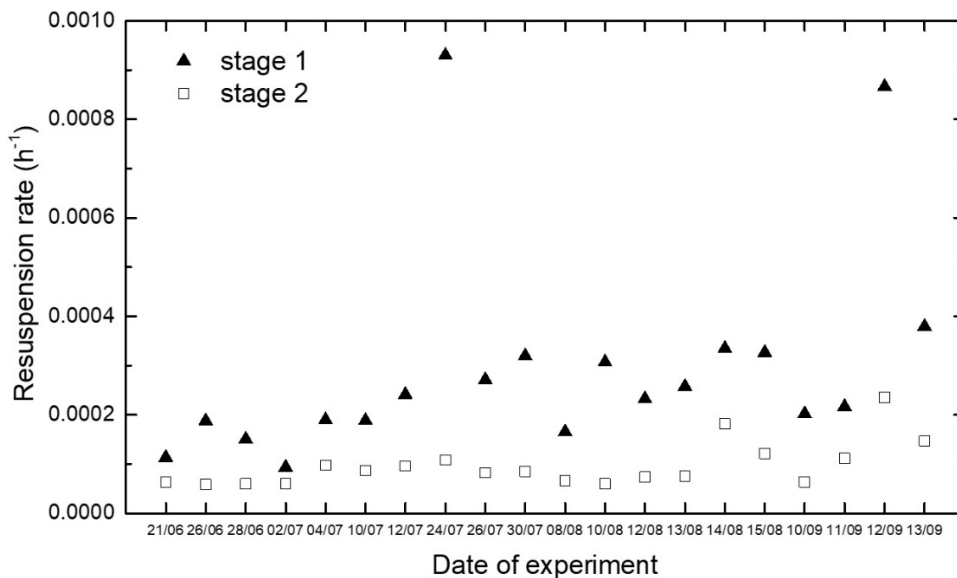


Figure 4.29. Comparison of resuspension rate for stage 1 and 2 for all the experiments.

4.3. Particle Resuspension during Walking in an Indoor Microenvironment

Using the Eq. (4.16) the indoor PM_{10} concentration can be predicted for each time step. The resuspension rate r and surface loading L , are already known (Eq. (4.14) and (4.15)), thus, the indoor concentration of aerosol is derived by setting the values for every time interval. The results are presented in Figure 4.30 for different surface dust loadings. The calculated indoor mass concentration is based on coupled differential Eq. (4.12) and (4.13), which refer to a mass balance in the air and on the floor, respectively. The physical processes taken into account are penetration of particles from outdoors, exchange rate of the indoor air, deposition of particles onto surfaces and emission by resuspension. Coagulation and condensation are assumed to have no major effect on indoor particle dynamics. The coagulation process influence directly the particle number distribution and has minor effect in total mass concentration of particles (Nazaroff, 2004). Moreover, it is important only in high number concentrations and therefore, can be neglected when total number concentration is lower than 10^4 cm^{-3} (Hussein, 2009). The number concentration of indoor aerosol in all experiments was under that limit and independent of any walking, supporting the assumption of negligible coagulation during walking experiments inside the laboratory.

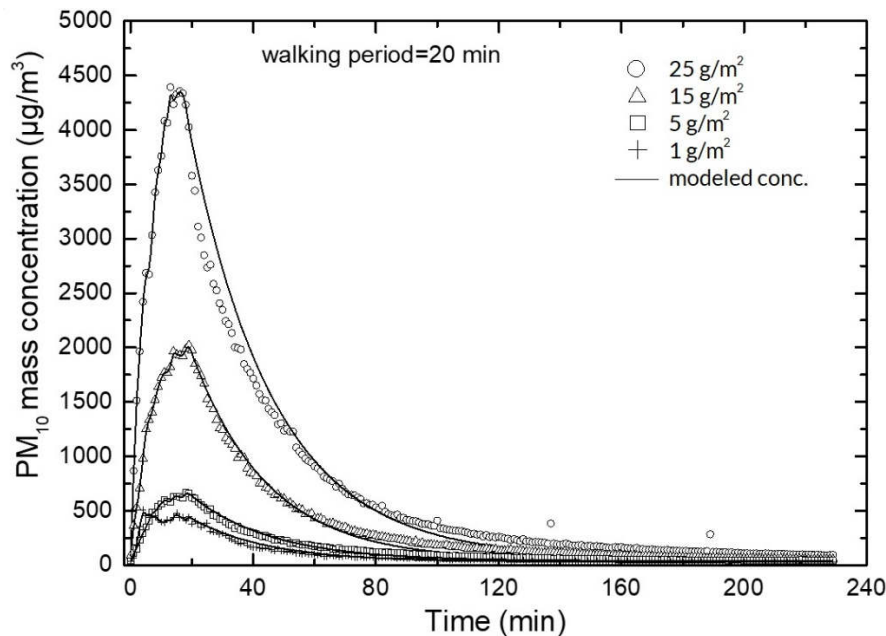


Figure 4.30. Comparison of experimentally obtained and calculated PM_{10} concentrations for different dust loadings (data correspond to Figure 4.25).

The deposition found to be dominant in the calculations of the total loss rate inside the laboratory. Although the air exchange rate was one order of magnitude lower than the deposition rate, it was significant enough to neglect it. The net result from infiltration of outdoor particles, air exchange of indoor particles and deposition on the surfaces of the laboratory led to a steady state concentration (C_{inf}) and as defined by Eq. (4.19) represents the fraction of particles penetrating from outdoors and remain suspended indoors. The C_{inf} is directly correlated with the background PM₁₀ concentration inside the laboratory before the activity period. The indoor PM₁₀ decreases after the activity period tending to reach the background concentration. Indoor concentration reached the background concentration ~3 h after the end of the experiment (Figure 4.30).

4.3.11. Conclusions

The current study focused on the estimation of resuspension rate by human-induced walking inside a laboratory. Different dust loadings were used to cover the floor while the walking style was the same for all the experiments. The resuspension rate for PM₁₀ induced by human walking estimated in the range of $10^{-2} - 10^3 \text{ h}^{-1}$. Different dust loadings on the floor contribute directly to the indoor mass concentration of particles but have no effect on the resuspension rate. Although higher dust loading resulted in higher emission rates and was associated with higher potential of dust particles than can detach from the surface, the fraction of particles leaving the surface is related to the magnitude of the removal forces.

Further investigation on this is needed in order to illustrate the nature of removal forces induced by human walking. Moreover, it is believed that the resuspension rate depends mainly on walking speed rather than on walking pattern or dust loading. Wider walking speed range should be examined in order to investigate the impact of the removal forces. The indoor mass balance model used in this study well-predicted the indoor particle concentration in both activity and post-activity period. However, resuspension of indoor particles is a complicated physical process dealing with the adhesion forces of particles on the floor and the removal forces acting upon them, thus a simultaneous investigation on particle dynamics both on the floor and the ambient air is necessary.

4.4. Estimation of Emission Rates from Arc Welding and Cutting

4.4.1. Introduction

Arc welding is a common unit operation in the construction industry, where frequent changes in location and welding position make it more difficult to control fume exposures than in industries where fixed locations are common. Shielded Metal Arc Welding (SMAW; also known as Manual Metal Arc Welding—MMAW or ‘stick’ welding), is a manual arc welding process that uses a consumable electrode of a proper composition for generating arc between itself and the parent work piece (Figure 4.31). In SMAW, the electrode is a metal rod or stick held in the torch with a small clamp. The rod has a solid coating of inert materials which vaporizes during welding. This creates an inert cloud or gases which protect the molten metal and displace any oxygen that might come into contact with it. The gas cloud settles on the pool of molten metal as it cools, and is referred to as ‘slag’. The disadvantage to SMAW is that the slag must be chipped off of the weld after it cools, and can sometimes infiltrate the weld causing weakness.

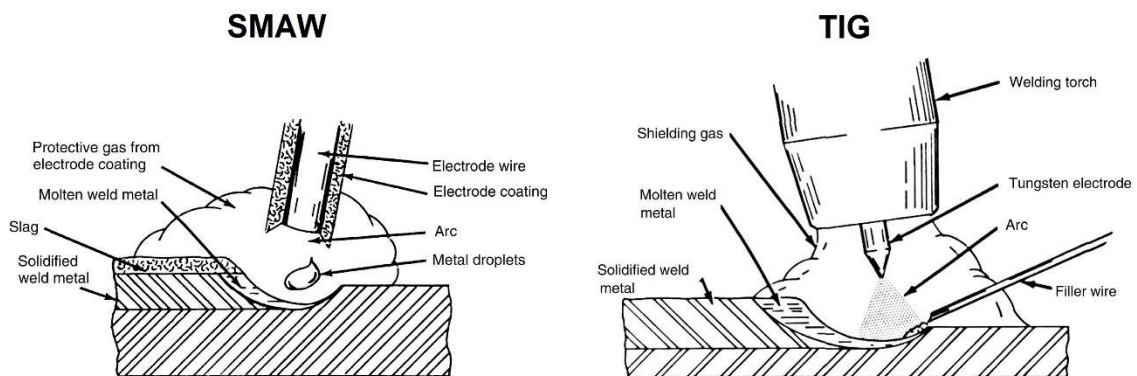


Figure 4.31. Arc welding processes (adapted from Antonini, 2014).

Tungsten Inert Gas (TIG; also known as Gas Tungsten Arc Welding—GTAW), is an arc welding process in which heat is generated by an electric arc struck between a non-consumable tungsten electrode and the work piece. Flux is not used in the process and the weld pool is shielded by an inert gas (Ar, He, N or as mixture with CO₂) protecting the molten metal from atmospheric contamination. The heat produced by the

4.4. Estimation of Emission Rates from Arc Welding and Cutting

arc melts the edges of work pieces and joins them, filler rod/wire may be used, if required. Tungsten withstands the heat of welding, significantly less fume is generated in comparison with SMAW, and is usually reserved for specialized types of welds (Antonini, 2014).

Welding fumes appear when the arc between a special electrode and a weld material produces evaporation of the welding consumables. The high-temperature multicomponent vapor is then forced up from the bottom area of the arc column to the low-temperature environmental air and forms a vapor–gas mixture as a result of mixing with air (Tashiro et al., 2010). The vapor–gas mixture cools down during mixing with air, and reaches a temperature of phase transition, when the primary particles of welding fumes are formed. Their chemical composition and size distribution are of great importance since they determine the physicochemical properties of the welding fume (Berlinger et al., 2011; Oprya et al., 2012).

The dusty plasma behavior (strong ionization of the environment created by electric-arc discharge formed between the electrode and the weld material) was studied by Vishnyakov et al. (2014a) in the process of coagulation of the primary particles, which are formed as a result of the nucleation and nuclei growth in the condensable high-temperature vapors. The study found that the coagulation of the ultrafine particles (~2 nm) occurred in two stages: at first the chain-like agglomerates were formed rapidly, and then they associated with the cluster-like agglomerates, and the final agglomerates (inhalable particles) had bimodal size distribution with different chemical compositions and fractal dimensions. The agglomerates are kept together by van der Waals, electrostatic and magnetic forces (Antonini, 2006). These agglomerates, as shown in Figure 4.32, consisting of long chains, frequently of hundreds of fine particles, are rather stable and retain their agglomerate structure in the process of their separation with an electrostatic classifier of SMPS or with a cascade impactor.

Ennan et al. (2013) demonstrated that the inhalable particles of the welding fume have three-modal particle size distribution, when electrodes with rutile (such as the one used in this study) and carbonate-fluorite covers are applied. The first mode (content of 80–90%) is represented by the agglomerates (~0.22 μm) of small primary particles, which are formed as a result of nucleation and growth of the nuclei in the liquid phase.

4.4. Estimation of Emission Rates from Arc Welding and Cutting

The second mode ($\sim 0.33 \mu\text{m}$) is a product of association of the small primary particles with the large primary particles, which are formed as a result of the coagulation of the nuclei in the liquid phase (10–20%). The third mode (0.02–0.2%) is the coarse fume particles ($> 1 \mu\text{m}$).

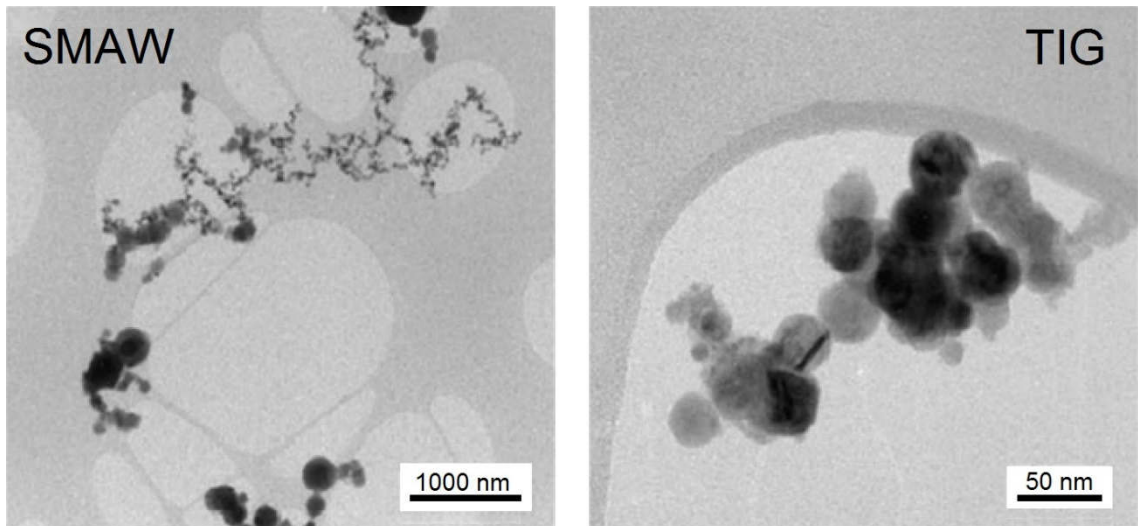


Figure 4.32. Typical TEM bright-field images of the investigated welding aerosols (adapted from Berlinger et al., 2011).

Welding exposure is also a common cause of work-related asthma (WRA), which includes both occupational asthma (OA, new-onset asthma related to sensitizers or irritant work exposures) and work-exacerbated asthma (WEA, preexisting asthma that worsens on work exposures). Banga et al. (2011) found that exposure to welding fumes was the fifth leading cause of WRA among workers in Michigan, US. Antonini et al. (2011) reported respiratory effects among welders including bronchitis, airway irritation, lung function changes, and a possible increase in the incidence of lung cancer. This issue of occupational UFP exposures is of increasing importance as evidence suggests that UFPs are potent triggers of oxidative stress, systemic inflammatory and may contribute to adverse respiratory outcomes as specific exposure to welding fumes is known to cause respiratory health problems (Järvelä et al., 2013; Kauppi et al., 2015).

4.4. Estimation of Emission Rates from Arc Welding and Cutting

Computational fluid dynamics (CFD) was used by Tian et al. (2016) to investigate the transport and deposition of welding fume agglomerates in a realistic human nasal airway. The authors found that a very small fraction of the inhaled welding fume agglomerates was dispersed into the nasal olfactory mucosa, and did not reach the olfactory bulb within the brain. The deposition was extremely low and the majority of considered particles passed through the nasal barrier and penetrated deep into the lungs.

This chapter presents the results from estimation of emission rates, and human dose and retention from two arc welding processes, SMAW and TIG. Additionally, cutting of stainless steel (SS) was also investigated as this process is many times accompanying the welding. In a simulated confined workspace of experimental chamber under controlled conditions, 4 different exposure scenarios were considered, including staying in the workspace with and without use of filtering facepiece respirator (FFR) during the emission, leaving the workspace or staying in the workspace after the emission. In this study, total deposited dose in the RT was assessed for the extrathoracic and the thoracic region (the lungs), subsequently, cumulative retention in extrathoracic and thoracic regions, GI tract and blood was also calculated. Dose and retention from SMAW, TIG and cutting of SS were calculated for time period of 4 h and 4 different scenarios where the emission period occurred in the first 5 min.

4.4.2. Experimental Setup

Measurements were conducted in a small stainless steel environmental chamber (Figure 4.33) with volume of 7.56 m³. The flow through the chamber was 5.3 L/min measured with Gilibrator-2 (Standard cell, Sensidyne, USA), thus, the air exchange rate equaled 0.044 h⁻¹. Additional pump to increase the air exchange rate was intentionally not employed in order to simulate confined welding workspace. The inlet of the sampling point was in distance of 1.2 m from the emission source. Chamber and the sampling tubes were tested for leaks prior to the beginning of the measurements and the particle number (PN) and mass concentration were monitored at all times. Uniform particle concentration was ensured by fan operating at 1200 rpm. The air temperature and relative humidity inside the chamber during all the measurements was on average 25 ±1°C and 45 ±1%,

4.4. Estimation of Emission Rates from Arc Welding and Cutting

respectively. Metal used to weld and cut in all experiments was stainless steel tube (10-15 cm) with rectangular profile and wall thickness of 2.5 mm.

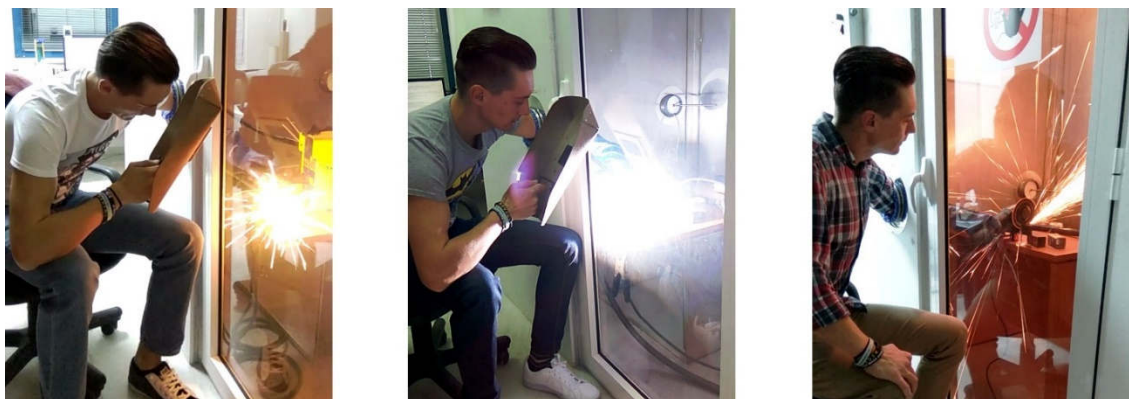


Figure 4.33. SMAW (on left), TIG (center) and cutting (on right) of SS in experimental chamber.

SMAW was performed by Gysmi 164 Inverter (Gys, France) with Fincord-M (35 cm, $\text{\O} = 4$ mm) rutile medium coated electrodes (Oerlikon, Switzerland) at 90 A of direct current (DC), which was sufficient enough considering the SS tube wall thickness. In total 1 electrode was used for both SMAW welding processes (1/2 electrode per process). In this study TIG welding by fusion (i.e. without a filler rod) was performed by Fronius Magic Wave 2000 (Fronius, Austria) with argon (100% Ar) as an inert gas at DC of 90 A. For the cutting experiments AG 115 SS-DC angle cutter (Kraft Tech, China) equipped with Speed Plus 200 Green cutting disc for stainless steel (Zebra, Würth, Germany) was employed to cut the SS tube.

The net duration of the emission source was approximately 3x 20 s and 2x 60 s (in total time period of 5 min per experiment) for welding processes and cutting, respectively. These relatively short emission periods are based on limitations of the used instrumentation where after certain concentration limit flowrate and coincidence error occurs. Each experiment was done two times in a row for each process on a same day with a minimum of 4-6 h between the processes, and measurements of different processes were conducted on different days. The effect of different current, welded metal, welding duration, distance of sampling point or air exchange rate was not examined.

4.4. Estimation of Emission Rates from Arc Welding and Cutting

Condensation Particle Counter (CPC 3775) was employed to measure the total PN concentration, an OPS to measure the mass concentrations of different particles sizes (both TSI, Inc., USA) and PhoCheck for the estimation of the total volatile organic compound (TVOC). In addition, average of total losses due to diffusion, inertial deposition and gravitational settling in the sampling tubing (Hinds, 1999) in the chamber measurements for the particle size range found in this study were negligible for CPC as they were estimated to be less than 4% for the particle size range detectable by the instrument. Although the average loss for fine mode particulate mass measured by OPS was also less than 4%, for the coarse mode it was 56% on average, thus loss correction factor was applied for each of the 16 size bins separately for the whole size range measured by the instrument.

4.4.3. Calculation of Deposition Losses inside the Chamber Volume

In this study the air exchange rate is a known parameter (0.044 h^{-1}). In order to estimate the loss rate β (h^{-1}) comprising all deposition mechanisms, analyses needed to be performed also on the overall particle loss rate from the PN and mass concentration decays. Overall particle loss rate (λ^*) includes the deposition rate of aerosol particles (β) and air change rate (λ):

$$\lambda^* = \lambda + \beta \quad (\text{Eq. 4.22})$$

The overall particle loss rate can be derived from a simple mass balance equation (Smolík et al., 2005) describing the change in concentration of aerosol particles in an indoor environment:

$$V \frac{dC_i}{dt} = V \lambda (PC_o - C_i) + Q - S \quad (\text{Eq. 4.23})$$

4.4. Estimation of Emission Rates from Arc Welding and Cutting

where V is the volume of the room, C_i and C_o are the concentrations of aerosol particles indoors and outdoors, t is time, λ is the air exchange rate, P is the penetration factor, Q represents possible particles sources and parameter S represents total sink strength of aerosol particles. Assuming that there are no indoor particle sources, that particles are not resuspended, are physically and chemically stable, and there is no coagulation, the sink strength S can be simplified to $S = C_i V \beta$, where β is the deposition rate in the room comprising all deposition mechanisms and all surfaces. Eq. (4.23) can be simplified under the following conditions: (1) after the emission period there is no other source of aerosol particles in the room; (2) there is no resuspension of deposited aerosol particles; (3) particle coagulation can be neglected, (4) the initial aerosol particles concentration C_i is equal to the initial condition $C_i(0) = C_o$. Then the equation describing the loss of aerosol particles becomes:

$$C_i(t) = C_\infty + (C_0 - C_\infty) e^{-\lambda^* t} \quad (\text{Eq. 4.24})$$

The experimental curves were then fitted with the model utilizing the constrained Nelder-Mead Simplex method to find parameters of the model equation which minimize the sum of squares of residuals between theoretical prediction and experimental data.

4.4.4. Effect of Welding and Cutting on PN Concentration

In all cases the total PN concentration reached its peak within 5 min from the start of the emission and ranged from 2.4 to $3.6 \times 10^6 \text{ \#/cm}^3$ (see Figure 4.34). The 1 h average total PN concentration varied from 2.4 to $5.2 \times 10^5 \text{ \#/cm}^3$ and was the highest in the case of SMAW and the lowest in the case of cutting process (Table 4.14). It was not possible to measure the size distributions of the particles emitted during the processes due to technical error of the SMPS and the only available particle size distribution is from SMAW testing on SS at 70 A in size range of 5-350 nm. Note that all the experiments were conducted with DC of 90 A, thus, the concentration would reach higher number

4.4. Estimation of Emission Rates from Arc Welding and Cutting

concentrations since the emission of airborne fine particles and fume formation rate increases with the current intensity (Guerreiro et al., 2014).

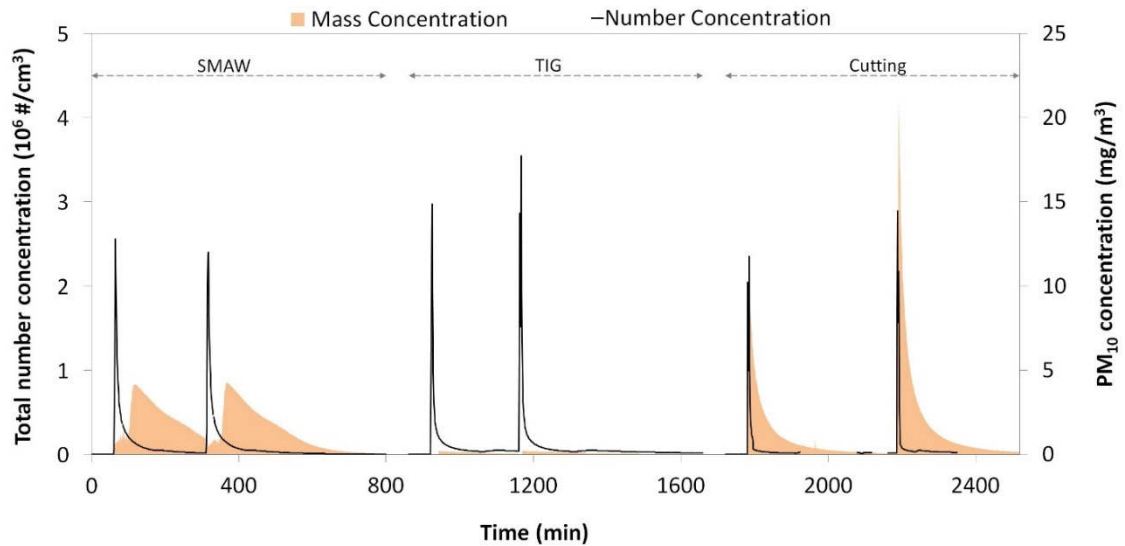


Figure 4.34. Total particle number and PM₁₀ concentration during welding (SMAW, TIG) and cutting of SS.

As it can be seen in Figure 4.35, there is a burst of new particles in the whole measured size range at the start of the emission with dominant mode on 13 nm (Figure 4.35a). Within 10 min the size distribution shifts towards particles with bigger diameters and higher concentration with dominant mode on 242 nm and reaches its maximum after 15 min from the beginning of the emission. Even 4 h after the end of the emission, the shape of the size distributions remained almost unchanged, but the particle concentration decreased with time (Figure 4.35b). Berlinger et al. (2011) showed that during TIG welding, most particles have mobility diameters in the range of 15-160 nm, while SMAW particle diameters are larger, ranging between 100-600 nm.

4.4. Estimation of Emission Rates from Arc Welding and Cutting

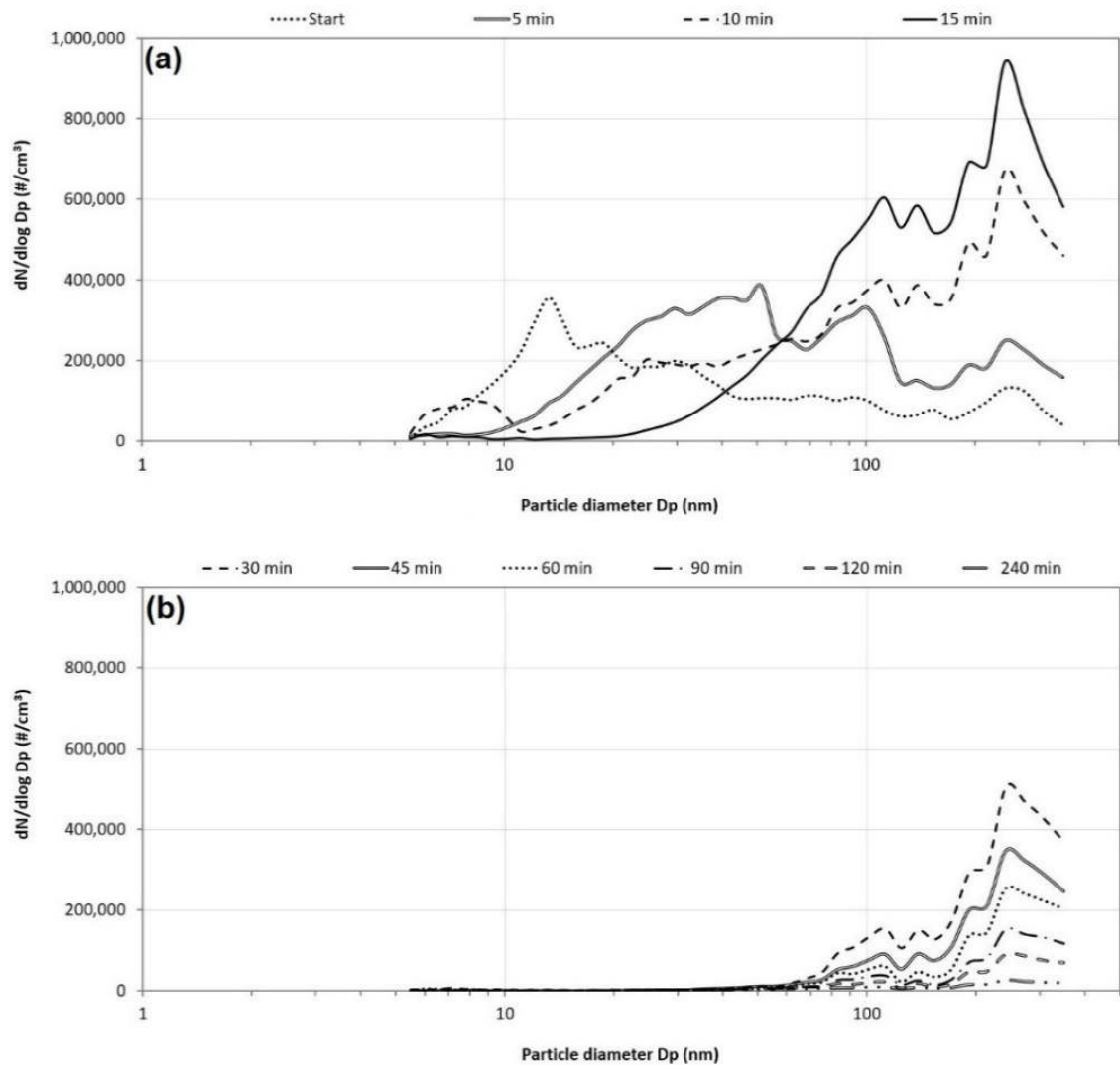


Figure 4.35. Size distributions of 5-350 nm particles during SMAW test at 70 A: (a) Within first 15 min from start; and (b) From 30 to 240 min from start of the welding.

Multicomponent condensation in the low-temperature plasma, which forms at SMAW, was investigated by Vishnyakov et al. (2014b). The liquid particles after the start of nucleation of the predominant component (iron) had bimodal size distribution, with a nano-sized mode of the nuclei and a larger-sized mode of the aggregated droplets. Consequently, the condensation of the accompanying low-boiling components on these droplets caused the termination of nucleation earlier than conditions for the condensation growth of the equilibrium nuclei arise. Therefore, the growth of the nuclei occurred only

4.4. Estimation of Emission Rates from Arc Welding and Cutting

by their coalescence (large number density of nuclei in a liquid state causes their intensive Brownian coagulation). Thus, size distributions in the beginning of the welding process are undergoing rapid changes, hence, SMPS with low-time resolution is not sufficient and spectrometer, such as Fast Mobility Particles Sizer (FMPS) with time resolution of 1 s might be required (Brand et al., 2013; Avino et al., 2015).

4.4.5. Effect of Welding and Cutting on Particulate Mass

The 1 h average PM₁₀ concentrations during cutting were the highest among all processes (Figure 4.34) and reached their maximums (11 and 22 mg/m³ for the first and second experiment, respectively) within 5 min from the start of the emission, similarly, as it was in the case of TIG, which had the lowest PM concentrations. Note that due to OPS's coincidence error (when the particle concentration reaches the limit of $3 \times 10^3 \text{ \#/cm}^3$), the instrument stopped sampling for ~ 10 min from the start of the emission in both cases.

As shown in Table 4.14, the fine particles (PM_{2.5}) dominated in both welding processes, whereas the coarse particles in the cutting process. SMAW and cutting mass concentration values found in this study are consistent with study of Lin et al. (2014) where the authors characterized aerosol particle sizes in workplace of fitness equipment manufacturing. PM₁₀ concentration from SMAW reached maximum peak (4.14 mg/m³ on average) 1 h after the start of emission in both cases, with 1 h average PM₁₀ concentration of 1.55 mg/m³.

Table 4.14. Average, maximum and minimum number and mass concentration values for period of 1 h from start of the welding (SMAW and TIG) and cutting of SS.

| Process | Number Concentration (#/cm ³) | | Mass Concentration (mg/m ³) | | | |
|------------|---|-------------------|---|------|--------------------------------|-------|
| | Aver. | Max. | Fine (PM _{2.5}) | | Coarse (PM _{2.5-10}) | |
| | | | Aver. | Max. | Aver. | Max. |
| SMAW I | 5.1×10^5 | 2.6×10^6 | 1.56 | 4.08 | 0.07 | 0.12 |
| SMAW II | 5.2×10^5 | 2.4×10^6 | 1.46 | 4.19 | 0.05 | 0.09 |
| TIG I | 3.9×10^5 | 3.0×10^6 | 0.18 | 0.21 | 0.01 | 0.01 |
| TIG II | 4.8×10^5 | 3.6×10^6 | 0.19 | 0.21 | 0.01 | 0.01 |
| Cutting I | 2.4×10^5 | 2.4×10^6 | 1.03 | 1.64 | 3.35 | 9.41 |
| Cutting II | 2.9×10^5 | 2.9×10^6 | 1.63 | 2.64 | 6.06 | 19.28 |

4.4. Estimation of Emission Rates from Arc Welding and Cutting

Figure 4.36 illustrates the formation of the three fractions of agglomerates in the welding fume from SMAW consisting mostly of $PM_{1-2.5}$ fraction. As mentioned earlier, when the high-temperature multicomponent vapor is forced up from the bottom area of the arc column to the low-temperature environmental air, it forms a vapor-gas mixture and reaches a temperature of phase transition when the large primary particles of welding fumes are formed, and at the same time the concentration of the small primary particles decreases. The PM_1 fraction represents the result of the small primary particles' agglomeration, and the structures with uniform dense core, which are formed as a result of association of the small primary particles and the large primary particles. The $PM_{1-2.5}$ and $PM_{2.5-10}$ fractions are the coarse fume particles (Tashiro et al., 2010; Berlinger et al., 2011; Ennan et al., 2013; Vishnyakov et al., 2014a).

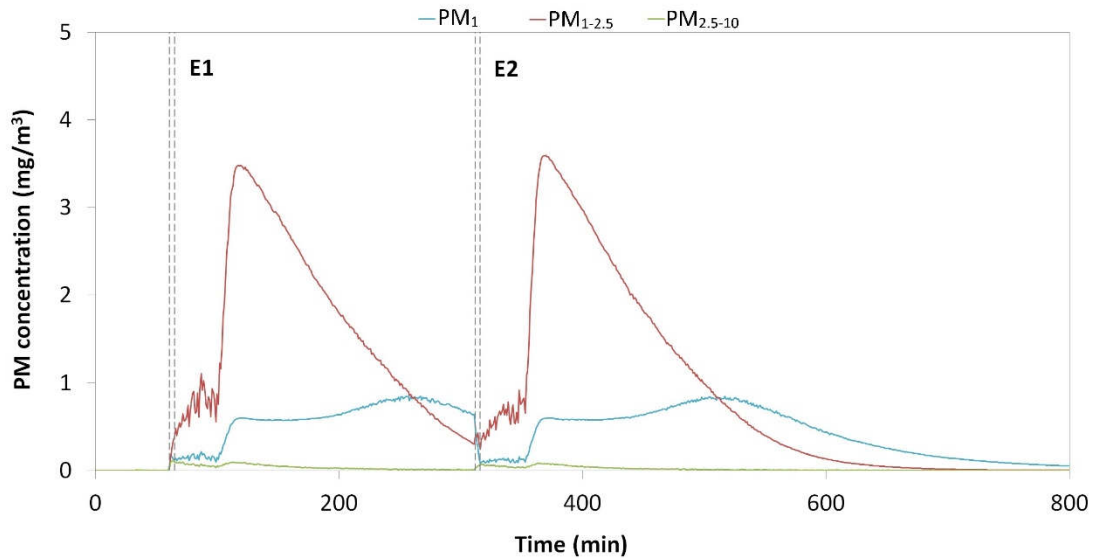


Figure 4.36. Concentration of PM_1 , $PM_{1-2.5}$ and $PM_{2.5-10}$ during SMAW. E1 and E2 represents the first and the second emission period, respectively.

4.4.6. Deposition Loss Rate in the Chamber Volume

Deposition loss rate calculated from the particle mass and number concentration decays after the end of the emission (see Table 4.15) shows that particulate mass from cutting process had the highest deposition loss rate for both, fine and coarse mode. On the other

4.4. Estimation of Emission Rates from Arc Welding and Cutting

hand, particles from SMAW process were deposited faster due to the highest particulate mass, which enhanced the coagulation of fine particles, thus, increased the loss rate. Although there were very low concentrations of coarse particles at welding processes, coarse particles had lower deposition loss rates than the fine particles.

Particulate mass generated from TIG welding process had the lowest deposition loss rate (not taking into account the coarse particles due to its very low contribution to PM_{10}) and the highest deposition loss rate calculated from number concentration decay suggesting that these particles were smaller in diameter and had lower mass than the particles generated from SMAW or cutting. Number concentration 16 h after the end of TIG emission was still $3.4 \times 10^3 \text{ \#/cm}^3$, while the number concentration for particles generated from SMAW dropped below $2 \times 10^3 \text{ \#/cm}^3$ 8 h after the end of emission and decreased on 60 \#/cm^3 after 16 h.

Table 4.15. Deposition loss rate β (h^{-1}) calculated from particle number and mass concentration decays after the end of emission in a simulated confined workspace.

| Process | Number Conc. ($\leq 3 \mu\text{m}$) | Mass Concentration | |
|------------|--|---------------------|--------------------------|
| | | Fine ($PM_{2.5}$) | Coarse ($PM_{2.5-10}$) |
| SMAW II | 1.334 | 0.445 | 1.030 |
| TIG II | 3.274 | 0.247 | 1.844 |
| Cutting II | 1.337 | 1.093 | 3.480 |

4.4.7. Effect of Welding and Cutting on TVOC concentration levels

As can be seen in Table 4.16, SMAW produced higher average TVOC and also had the highest maximum concentration. Average total volatile organic compound (TVOC) was found to be 3.21 and 2.31 ppm for SMAW and TIG, respectively, and was higher than the average TVOC during cutting of SS (0.03 ppm). This difference can be attributed to the different nature of the welding and cutting processes. The iron oxide particles generated at the process of friction of cutting disc and the SS do not produce high TVOC, whereas in the welding process, much higher temperatures at the melting of electrode and metal produce also higher TVOC values. Berlinger et al. (2011) examined the physicochemical characteristics of different welding aerosols and found clear size

4.4. Estimation of Emission Rates from Arc Welding and Cutting

dependency of the elemental composition in particles generated in SMAW welding. Small particles with diameters below ~50 nm are mostly metal oxides, in contrast to larger particles which also contain more volatile elements, which seemed to increase with increasing particle size, which explains higher TVOC during SMAW in comparison with cutting.

Table 4.16. TVOC concentrations (ppm) in the chamber for period of 12 h.

| Process | Average | St. deviation | Maximum | Minimum |
|----------------|----------------|----------------------|----------------|----------------|
| SMAW II | 3.21 | 0.32 | 23.17 | 2.91 |
| TIG II | 2.31 | 0.41 | 6.86 | 1.89 |
| Cutting II | 0.03 | 0.03 | 0.08 | 0.00 |

4.4.8. Conclusions

The results of this study present experimental measurements of emissions from SMAW and TIG arc welding processes and cutting of SS in a simulated confined workspace. All 3 investigated processes generated high PN concentrations ranging from 2.4 to 3.6×10^6 #/cm³. Among all 3 processes, PM₁₀ concentrations from cutting reached the highest mass concentrations (11 and 22 mg/m³), while SMAW had the highest contribution of fine particles (~4.1 mg/m³), consisting mostly of PM_{1-2.5}. As demonstrated in this chapter, where the total duration of emission was only 1 min for welding processes and 2 min for cutting (in total time period of 5 min per experiment), even a short emission period can cause a great increase of respirable particle concentrations, thus increasing the actual human dose.

5. Size-Resolved Penetration of Filtering Facepiece Respirators

5.1. Introduction

Many workplaces are associated with increased aerosol particle concentrations of various origins. These may be related to adverse health effects in those working in such polluted environments. Thus, workers in industrial applications and workplaces may be exposed to a broad range of aerosol particles possibly causing adverse health effects (Flanagan et al., 2003; Muller et al., 2005; Donaldson et al., 2006; Poland et al., 2008). Dust inhalation and deposition in the bronchioles and on the parenchyma can result in pneumoconiosis, such as silicosis caused by the inhalation of silicon (SiO_2) dust (Flynn and Susi, 2003). Great attention should be paid to exposure to ultrafine particles (<100 nm), which may have detrimental impact to human health. Once deposited into the upper airways, nanoparticles can cross the epithelial and endothelial cells into the blood and lymph circulation, spleen, and heart, and can be translocated to the central nervous system and ganglia along axons and dendrites of olfactory neurons (Oberdörster et al., 2005; Churg, 2000). In recent years, great progress in nanotechnology has led to the spread of engineered nanomaterials in workplaces. For example, carbon nanotubes (CNTs) are used in wide range of applications, such as electron field emitters, conductive plastics, semiconductor devices, and medical devices (Chen et al., 2014; Wang et al., 2011b; Endo et al., 2008). Consequently, the performance of filtering facepiece respirators (FFR) is the topic of extensive studies and is well characterized for a wide size range of biological and non-biological aerosol particles (Harnish et al., 2013; He et al., 2013; Balazy et al., 2006a; Coffey et al., 1999).

In Europe, the Personal Protective Equipment directive (89/686/EEC) requires that personal protective equipment (PPE) placed within the European market is certified by European Norm (EN) and marked with 'Conformité Européen' (CE), indicating European Community (EC) conformity. All respirators must be approved and tested to the performance requirements of the corresponding European Standard (ES), which forms the following categories: filtering half masks, half masks and quarter masks, full face masks, powered air respirators, and supplied air respirators. A filtering half mask

5. Size-Resolved Penetration of Filtering Facepiece Respirators

is a facepiece that consists entirely or substantially of filter material or comprises a facepiece in which the main filter(s) form an inseparable part of the device. Legislation of European Standards for filtering half masks is covered by EN 149:2001.

There are three categories of filtering facepieces (FFP) classified according to their maximum total inward leakage (TIL) and filter efficiency: FFP1 (80%), FFP2 (94%), and FFP3 (99%), which are designed to protect against solid, non-volatile water-based, and oil-based aerosol particles. Therefore, all respirators have to meet both the solid and liquid filter performance requirements. This norm was followed by the amended version EN 149:2001+A1:2009 (further referred to in this article as EN 149) in July 2009. This amendment introduced two usability classes of disposable respirators: single shift only (non-reusable, marked 'NR') and reusable (marked 'R'). Moreover, all reusable respirators must endure cleaning and disinfection as described by the manufacturer and pass the dolomite test for clogging (giving the user better and longer lasting breathing resistance), which is indicated by the printing of the letter 'D' on the mask (previously only required on FFP1 and FFP2 respirators) (BS EN, 2001).

Performance tests include filter penetration, extended exposure (loading), flammability, breathing resistance, TIL, and dolomite dust clogging (optional). EN 13274-7:2008 (Determination of particle filter penetration) is used for testing filter penetration, and dictates the use of a non-neutralized, polydisperse 1% solution of sodium chloride (NaCl) against solid particles and paraffin oil against oil based aerosol at flow rate of 95 L/min. The test aerosol is fed into the chamber where the examined filtering device is mounted in a leaktight way on an adaptor. The NaCl aerosol is generated by a Collison atomizer under pressure of 3.45 bar at flow rate of 13 L/min, with a particle size range of approximately 40-1200 nm and a mass median diameter (MMD) of ~600 nm. The output is mixed with 82 L/min of dry dilution air (to give total of 95 L/min) in a chamber with volume of $\geq 1750 \text{ cm}^3$. The generated polydisperse NaCl upstream and downstream of the respirator is then vaporized through a hydrogen flame and the intensity of light emitted at 589 nm, proportional to sodium concentration, is subsequently measured by flame photometry and penetration based on mass concentration ratio is obtained.

5. Size-Resolved Penetration of Filtering Facepiece Respirators

For testing against liquid and oil aerosol particles, paraffin oil (paraffinum perliquidum CP 27 DAB 7) is atomized at 100°C under a pressure of 4 bar, diluted with 50 L/min of filtered air, the generated test aerosol is reduced to concentration of $20 \pm 5 \text{ mg/m}^3$, by releasing a fraction of oil mist, and further dilution in the cyclone with 83 L/min of filtered air. Under these conditions the particle size distribution is lognormal with a median Stokes diameter of 400 nm and geometric standard deviation (GSD) of 1.82. The mass concentration of aerosol is measured upstream and downstream of the respirator by a 45° light scattering photometer (BS EN, 2008). Throughout the years, the performance of the FFRs has been the topic of extensive studies, resulting mainly in the characterization of aerosol penetration through filters using aerosols that are thought to be similar to those encountered in workplaces (Myojo and Sugimoto, 1997; Lee et al., 2005; Rengasamy et al., 2008; Jung et al., 2014, Rengasamy et al., 2015; Vo et al., 2015; Gao et al., 2016), while other studies were aimed at determining the most penetrating particle size (MPPS) and to examine whether biological aerosols were collected in a similar manner to inert aerosols of the same particle size distribution (Lee et al., 2008; Eninger et al., 2008; Rengasamy et al., 2010; Lore et al., 2012; Zuo et al., 2013; Rengasamy et al., 2014a). Nonetheless, these studies of respirator penetration were focused mainly on N95 facepieces (not oil-proof with filtering efficiency $\geq 95\%$) or other type of facepieces approved by the National Institute for Occupational Safety and Health (NIOSH), rather than on CE-marked respirators.

Even though EN and NIOSH certifications are widely recognized in many parts of the world, they employ different test protocols for the certification process. Nowadays, the N95 facepieces are certified according to regulations in NIOSH 42 CFR 84, which dictate that filters are tested with charge-neutralized NaCl at 85 L/min. For these tests the particle size of ~300 nm in diameter thought to be the MPPS (NIOSH, 1997). However, before first significant changes were made and the NIOSH regulation 42 CFR 84 was revised in 1990s, Moyer (1986) suggested 'worst-case' type aerosol for testing of electret filter penetration, including using dried, charge neutralized test aerosol (NaCl and DOP) of different sizes and a CMD based measurement method. Further studies on filter efficiency as a function of particle size and flow rate proved the

5. Size-Resolved Penetration of Filtering Facepiece Respirators

shortcomings of the former NIOSH regulation 30 CFR 11 (Stevens and Moyer, 1989; Moyer and Stevens, 1989a; Moyer and Stevens, 1989b). Some studies urged the need to employ methods and conditions allowing the measurement of fractional penetration over a range of particle sizes under a 'worst-case' scenario and pointed out the importance of particle size and flow rate in particle capture by electret filter (Brosseau et al., 1989; Chen et al., 1990; Chen et al., 1992; Brosseau et al., 1993). Other studies focused on surgical masks penetration or the use of an inert aerosol to predict the collection of a biological aerosol by respirators (Chen and Willeke, 1992; Weber et al., 1993; Brosseau et al., 1994; Chen et al., 1994).

All this research had a significant impact and contribution to the improvement of the filter penetration testing and certification process of NIOSH-approved respirators. These issues are somehow similar to those in EN 149 and yet, up to this day, EN 149 still lacks critical updates in methodology used for CE-marked facepieces certification, taken by NIOSH over 20 years ago. There are limited number of studies in the literature reporting CE-marked respirator performance (Huang et al., 2007; Plebani et al., 2010; Plebani et al., 2012; Ciotti et al., 2012; Penconek et al., 2013). Although in vast majority of these studies a MPPS of 30-60 nm was found, and charge-neutralized test aerosol and detection method relying on CMD were used, these studies investigated the penetration through the entire half masks in an experimental chamber (or with human subjects) using their own test method (or with a commercially available filter tester) focusing on a specific problem (diesel exhaust particles, oily aerosol, bioaerosol, filtering material properties, particle collecting mechanism, etc.).

Although these studies primarily address the filtering performance of the respirators, other studies evaluate the aspects directly affecting the overall facepiece performance, such as total inward leakage (TIL), which consists of three components: face seal leakage, exhalation valve leakage (if fitted), and filter penetration. Rengasamy et al. (2014b) examined the TIL of N95 filtering facepieces and showed that filter penetration is critical to the TIL of different particle sizes. The study also demonstrated that relatively high efficiency respirators might produce lower TIL values. In another study, Rengasamy and Eimer (2012) pointed out that the induced leakage allowed the test aerosols inside the FFR (regardless of particle size), while filter penetration

5. Size-Resolved Penetration of Filtering Facepiece Respirators

determined the TIL for different size particles. Authors also concluded that a good-fitting respirators with lower filter penetration values would provide better protection against nanoparticles. Coffey et al. (2004) studied the fitting characteristics of FFRs and their findings demonstrate that it may be more beneficial to wear a respirator that fits well and has not undergone fit-testing than to wear a respirator with poor-fitting characteristics that has passed a fit-test. Nonetheless, using a respirator that has passed a fit-test enhances a worker's probability of receiving an adequate level of protection. Additionally, the use of exhalation valves has been proven useful in dissipating humidity, heat, and carbon dioxide from the dead space of FFRs, and decreasing exhalation resistance, thereby making the respirator more comfortable (Roberge, 2012). Brosseau (1998) examined the penetration behavior of inhalation and exhalation respirator valves with 300 and 800 nm particle sizes and found that, in the absence of valve failure, the valves behave differently when challenged with different sized particles.

For CE-marked FFRs fitted in accordance with the manufacturer's information, at least 46 out of the 50 individual exercise results (i.e. 10 subjects x 5 exercises) for TIL shall be not greater than 25%, 11%, and 5% for FFP1, FFP2, and FFP3 masks, respectively. Additionally, at least 8 out of the 10 individual wearer arithmetic means for the TIL shall be not greater than 22%, 8%, and 2% for FFP1, FFP2, and FFP3 masks, respectively (BS, 2001). Moreover, all respirators have to meet both the solid and liquid filter penetration performance requirements. The EN 149 differs from National Institute for Occupational Safety and Health (NIOSH) regulation 42 CFR part 84 in that it does not require separate measurement of exhalation valve leakage. Exhalation valve leakage is assessed as part of the TIL, which is included in all European Standards. However, testing of the valve fitted in the respirator is inherently subjecting the valve to a continuously varying pressure drop (Kuo et al., 2005). Bergman et al. (2012) carried out a study on the impact of multiple consecutive donnings on the fit of six N95 respirators. Head strap and nosepiece breaks were taken into account and work shifts were assumed to be 10-hours long with 20 donnings per shift. The data suggest that 5 consecutive donnings can be performed before the fit factor drops consistently.

5. Size-Resolved Penetration of Filtering Facepiece Respirators

In vast majority of cases, most of the aerosol contaminants that enter a respirator worn by human test subjects are not due to filtration performance, but face seal leakage (Grinshpun et al., 2009). Therefore, a FFR cannot provide optimal protection unless it fits properly, with a good seal around the face (Rengasamy et al., 2015). In another study Rengasamy et al. (2009) compared the penetrations of eight N95 and P100 masks with FFP2 and FFP3 masks by using monodisperse particles ranging from 4 to 400 nm. The findings provided expected levels of penetrations and the MPPS was found to be between 30 and 60 nm (CMD). Penetrations of different types of diesel exhaust particles (DEP) through FFP2 and FFP3 respirators were studied by Penconek et al. (2013). Their results suggest that, due to their size and morphology, the tested commercially available respirators may not ensure the required level of protection against DEP. FFP1, FFP2, and FFP3 penetrations by respirable solid particles were examined by Grima-Olmedo et al. (2014), the results revealed that the performance of all these facepieces was considerably poorer than it is demanded by the EN 149.

The penetration performance was compared from 47 mm filters cut out of 13 commercially available filtering facepieces from FFP1, FFP2, and FFP3 filtering classes by utilizing 9 sizes of charge-neutralized monodisperse ammonium sulfate. EN 149 sets the MPPS on ~600 nm MMD (40-1200 nm) as a certification criterion for the respirator penetration tests, while study presented in this chapter is focused on the size range 20-400 nm (CMD). Measurements of 9 chosen FFRs were also conducted in an experimental chamber (0.43 m³) in a manikin-based study and the results were compared to penetrations of 47 mm filters cut out from identical FFRs. EN 149 method tests the respirator's penetration with the FFRs tightened on a specimen in a chamber with a volume of ≥ 1750 cm³ with non-neutralized polydisperse aerosol detected by flame photometry. Hence, the results from the standard method and the method used in this study are not directly comparable. The goal of this research is (1) to obtain information about size-resolved penetration of FFRs in order to examine whether the FFRs are efficient in respiratory protection against workplace aerosols discussed in previous chapter; and (2) to demonstrate the disadvantages and shortcomings of the currently valid European Norm and show that for the particle size range 20-400 nm the penetration is much higher than it would be by following the CE certification protocol.

5.2. Materials and Methods

5.2.1. Filtering Facepieces

Thirteen CE-marked commercially available FFRs from five different brands were selected (3M, Refil, Moldex, Respair, and Segre) from all three protection classes: FFP1 (3 respirators), FFP2 (4 respirators), and FFP3 (6 respirators). Two replicates of each FFR were purchased and randomly marked from 1 to 13. Two representative 47 mm diameter samples were cut out from each FFR as received (i.e. without any conditioning) in order to determine the penetration performance of the material throughout the respirator. The samples were cut from all masks always from the same position, one from the right nose side and one from the left side. Some of the respirators had a plastic mesh keeping the structure and shape of the respirator, and this was removed prior to inserting the filter into the filter holder.

Table 5.1. List of filtering facepiece respirator and their characteristics.

| FFR test # | FFR model | Protection class | Certification | Respirator characteristics | | |
|------------|---------------------------------------|------------------|---------------|----------------------------|---------------|-----------------|
| | | | | Filter Layer Material | Disposability | Dolom. clogging |
| 1 | ^a Refil 511 | FFP1 | CE 1024 | Polypropylene | Non-R | No |
| 2 | ^b Moldex 3505 | FFP3 | CE 0121 | Polypropylene | Non-R | No |
| 3 | ^c 3M 9312 ⁺ | FFP1 | CE 0086 | Polypropylene | Non-R | Yes |
| 4 | ^d Respair C | FFP3 | CE 0086 | Polypropylene | Non-R | No |
| 5 | ^a Refil 831 | FFP2 | CE 1024 | Polypropylene | Non-R | No |
| 6 | ^c 3M 8835 | FFP3 | CE 0086 | Polypropylene | Reusable | Yes |
| 7 | ^b Moldex 3405 | FFP3 | CE 0121 | Polypropylene | Reusable | Yes |
| 8 | ^e Segre CN P3 | FFP3 | CE 0194 | Polypropylene | Reusable | Yes |
| 9 | ^b Moldex 2405 ⁺ | FFP2 | CE 0121 | Polypropylene | Non-R | Yes |
| 10 | ^c 3M 9310 | FFP1 | CE 0086 | Polypropylene | Non-R | Yes |
| 11 | ^c 3M 9322 | FFP2 | CE 0086 | Polypropylene | Non-R | Yes |
| 12 | ^a Refil 731 | FFP2 | CE 1024 | Polypropylene | Non-R | No |
| 13 | ^e Segre CN P3 V | FFP3 | CE 0194 | Polypropylene | Reusable | Yes |

(a) Refil spol. s.r.o., Karlovy Vary, Czech Republic; (b) Moldex, Culver City, CA, USA; (c) 3M, Maplewood, MN, USA; (d) Respair, Aylesbury, Buckinghamshire, UK; (e) Segre AB, Örebro, Sweden

5. Size-Resolved Penetration of Filtering Facepiece Respirators

In order to measure the penetrations of the FFRs, a chamber with a manikin was used and the respirators were tested as received (i.e. without any conditioning). All of the respirators were sealed around to the face of the manikin and the respirator exhalation valve (if fitted) was sealed so that no face seal leakage nor exhalation valve leakage would occur. Moreover, the reproducibility of the results was examined by measuring two identical facepieces from each of nine FFR models, for a total of 18 respirators. Table 5.1 contains the list of filtering facepieces used in this study and their characteristics.

5.2.2. Experimental Setup

The filter tester used in this study was an automated system developed in the Laboratory of Aerosol Chemistry and Physics (LACP) of the Institute of Chemical Process Fundamentals, v.v.i. (ICPF) of The Czech Academy of Sciences. The program operating the experiments employed an algorithm developed in the LACP laboratory and ran in LabView (National Instruments Co., Austin, TX, USA), which controlled the whole test system, the data recording, and the data analysis. Figures 5.1.-5.3. present the schematics of the experimental setup used to measure particle penetration through the filters and FFRs in the experimental chamber. In order to reveal any system leakage, zero volts were applied to the differential mobility analyzer (DMA) as a zero count check prior to each measurement. Two blank tests (without a filter in the filter holder) were also performed; one occurred before the launch of the very first measurement and one was at the end, after the measurements of all filters were done.

In order to generate the challenge monodisperse aerosol particles, clean, dry, pressurized air was delivered to the particle generator and salt solution was dispersed by a nebulizer (AGK 2000, Palas GmbH, Karlsruhe, Germany) under pressure of 2.5 and 3 bar, in filter tests and manikin-based tests, respectively. A 1 g/L solution of ammonium sulfate ($(\text{NH}_4)_2\text{SO}_4$) (0.1 g/L in chamber study) was chosen as the challenge aerosol over sodium chloride, which is used for the certification tests of CE-marked facepiece half masks (according to EN 13274-7:2008). This was due to the dodecahedron shape of generated ammonium sulfate particles, which represent the

5. Size-Resolved Penetration of Filtering Facepiece Respirators

sphere shape better than the cubic crystals of sodium chloride (being closer to the theoretical assumption for particle sizing in electrostatic classifier). A sample flow of 2 L/min of generated polydisperse ammonium sulfate passed through a liquid droplet separator to remove the larger drops and the polydisperse aerosol was then dried in a diffusion dryer (homemade, ICPF workshop, Prague, Czech Republic). Due to higher flow rates in the manikin-based study, sample flow of 2.5 L/min was used. The aerosol flow rate was checked prior to the start of each experiment with a Gilibrator-2 flow calibrator (Standard cell, Sensidyne LP, St. Petersburg, FL).

In the next step a Boltzmann charge equilibrium was imparted on the particles in the ^{85}Kr neutralizer (10 mCi, 370 MBq). The monodisperse aerosol particles of the required mobility diameter were subsequently selected in the electrostatic classifier of the DMA (homemade, Vienna type, ICPF workshop, Prague, Czech Republic) with active length of 22 cm. During all experiments the sheath airflow inside the DMA was maintained at ~ 10 L/min and ~ 97 L/min for filter tests and experimental chamber, respectively, and was recorded by a mass flow meter (Model 4040, TSI Inc., Minneapolis, MN, USA) along with pressure and temperature. The monodisperse particles then went through another ^{85}Kr neutralizer and the sample was diluted by 8 L/min of clean, dry air before entering the mixing volume. This was checked by another mass flow meter (Model 4040, TSI Inc., Minneapolis, MN, USA) prior to each measurement. In the case of chamber measurements, the sample was diluted by 94.5 L/min of air.

Afterwards, the generated monodisperse ammonium sulfate particles passed through the stainless steel filter holder (homemade, ICPF workshop, Prague, Czech Republic) with the tested 47 mm filter in it (Figure 5.1a and 5.2). Filter holder consists of two 1-inch stainless steel tubes with customized tri-clamp ferrule add-ons placed on the end. The filter is then placed between two customized ferrules. The two tubes are connected with a simple clamp, which can be removed in order to disconnect the tubes to insert/remove the filter. Instead of a classical gasket there are two customized PTFE rings ensuring perfect fit and seal of the filter in the filter holder. All filters were challenged under a flow of 9 L/min, which corresponded to a face velocity of 10.56 cm/s (with effective filter area 14.27 cm²). In order to maintain the same face

5. Size-Resolved Penetration of Filtering Facepiece Respirators

velocity for the cut sample and the whole respirator, the flow rate of 9 L/min through the sample was calculated from flow rate of 95 L/min (representing heavy work breathing conditions) with assumption of uniform effective filter area estimated to 150 cm² for all FFRs. In the case of manikin-based study, the filter holder was replaced by 0.43 m³ (430 liters) experimental chamber with the manikin (Figure 5.1b and 5.3).

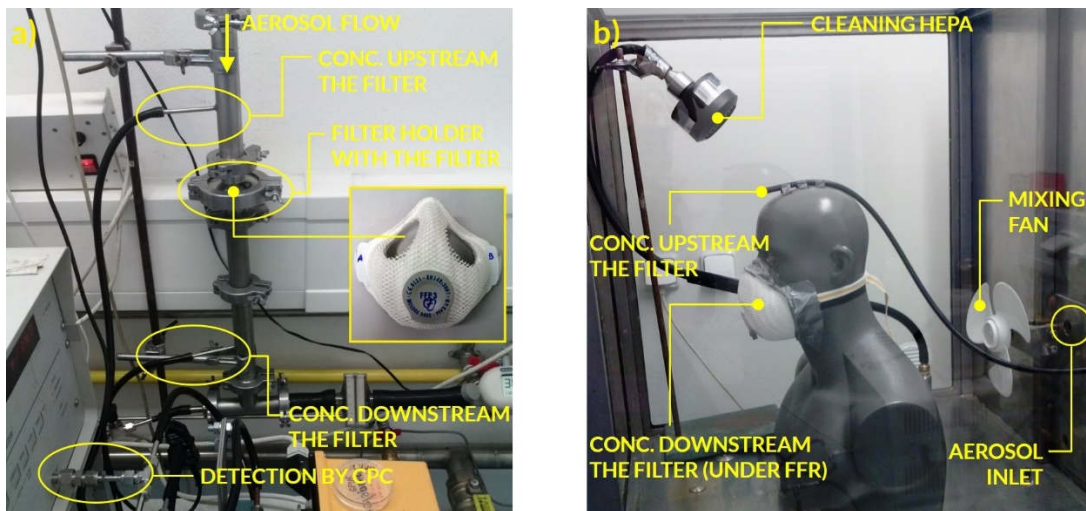


Figure 5.1. (a) Experimental setup used to measure the particle penetration through: filters in the filter holder; and (b) Identical FFR on a manikin in a chamber test.

All of the respirators in the experimental chamber were challenged under a flow of 95 L/min (corresponding to a face velocity of 10.56 cm/s with effective filter area of 150 cm²) instead of 9 L/min used for filters. Particle number concentrations upstream and downstream of the filter were simultaneously measured by two ultrafine condensation particle counters (UCPC 3025A, TSI Inc., Minneapolis, MN, USA), which were sampling on low flow mode at 0.3 L/min, and 1.5 L/min (high flow mode) in manikin-based experiments. Additionally, test system included two three-way electromagnetic switching valves that altered the position of the two CPCs after each particle size measurement in order to compensate for possible differences in the readings of the two CPCs. Thus, each size was measured twice both upstream and downstream of the filter with alternating measurement position of the two CPCs.

5. Size-Resolved Penetration of Filtering Facepiece Respirators

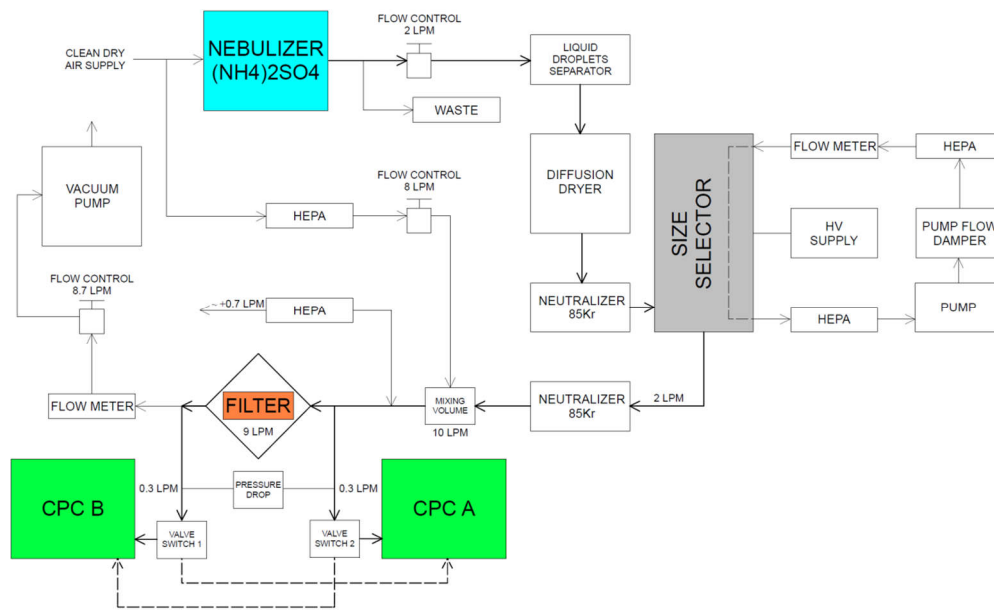


Figure 5.2. Schematics of experimental setup used in this study to measure the particle penetration through the filters.

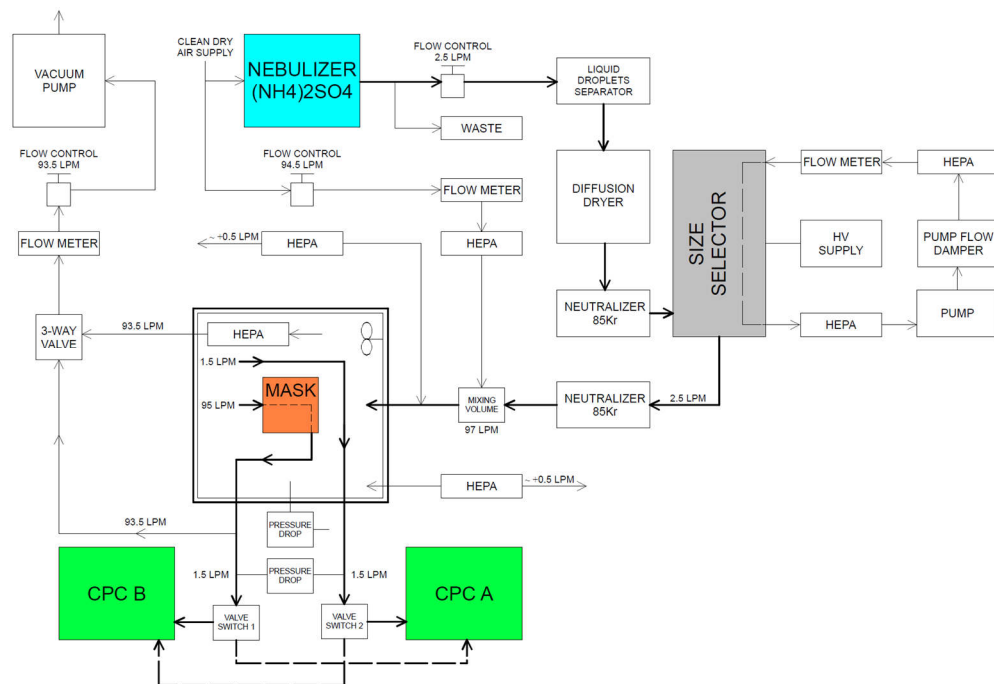


Figure 5.3. Schematics of experimental setup used in this study to measure the particle penetration through the respirators.

5. Size-Resolved Penetration of Filtering Facepiece Respirators

As a steady-state particle concentration during every scan is crucial for the correct calculation of the penetration of filtering materials and for the estimation of the MPPS, a regular concentration stability check was done after every change in the particle size and during every single measurement. In addition to the flow rate and the upstream and downstream concentrations, the pressure drop across the filter was also recorded by a pressure sensor (GMSD 25MR-K31, Greisinger Electronic GmbH, Regenstauf, Germany) connected to a pressure measuring device (GMH 3155, Greisinger Electronic GmbH, Regenstauf, Germany). Measuring the pressure drop across the filter also gave us an indication of the leak-free placement of the filter in the filter holder.

5.2.3. Data Analysis

The calculation and data analysis of penetration and standard deviation were performed by the program algorithm that controlled the entire test system. Penetration (P) can be expressed as:

$$P (\%) = \frac{c_2}{c_1} 100 \quad (\text{Eq. 5.1})$$

where P is the penetration defined as the ratio of the concentrations downstream (2) and upstream (1) of the filter. Taking into account the altering of the CPCs' position, the aerosol particle penetration through the filter and the standard deviation σ_P of the measured penetration were determined for each particle size as follows:

$$P(\%) = \sqrt{\frac{c_{2B} \cdot c_{2A}}{c_{1B} \cdot c_{1A}}} 100 \quad (\text{Eq. 5.2})$$

5. Size-Resolved Penetration of Filtering Facepiece Respirators

$$\sigma_P(\%) = \frac{1}{2} \sqrt{\frac{c_{2B} \cdot c_{2A}}{c_{1B} \cdot c_{1A}}} \sqrt{\frac{\sigma_{C1A}^2}{C_{1A}^2} + \frac{\sigma_{C2A}^2}{C_{2A}^2} + \frac{\sigma_{C1B}^2}{C_{1B}^2} + \frac{\sigma_{C2B}^2}{C_{2B}^2}} 100 \quad (\text{Eq. 5.3})$$

where c_{1A} , c_{1B} , c_{2A} , and c_{2B} represent the concentrations upstream (1) and downstream of the filter (2) measured by the CPCs (A or B) and σ_{C1A} , σ_{C2A} , σ_{C1B} , and σ_{C2B} are the corresponding standard deviations to these measurements. Eq. (5.3) was calculated by the error propagation principle from the Eq. (5.2), similarly to work of Zikova *et al.* (2015). The previously mentioned variables in the Eq. (5.2) are the median values calculated from all the scans done while measuring a certain particle size for the specific variable (c_{1A} , c_{1B} , c_{2A} , c_{2B}). The length of each scan was one minute. Certain time delay was given to the system to stabilize after changing the size of the particles. This delay depends on number concentration measured by downstream CPC (starting from 5 seconds for concentrations $> 1000 \text{ \#/cm}^3$ and going up to 5 minutes for concentrations $< 1 \text{ \#/cm}^3$). After this time delay the system checks the stability prior to the measurement - taking the measurements for the whole selected measurement period and checking if the concentration changes more than 5% during the scan. If the change in concentration is larger than 5% than it continues checking until this criterion is met for both upstream and downstream CPC.

Moreover, before the set of scans for given particle size the concentration on downstream CPC is measured and based on the measured concentration, the number of scans for this particular particle size is set (again starting from 2 scans per size for concentrations $> 1000 \text{ \#/cm}^3$ and going up to 10 scans for concentrations $< 1 \text{ \#/cm}^3$). This procedure should improve statistics in the case of lower concentrations of testing particles. The last stability check is done after measuring every single scan. The data from both CPC downstream and upstream the filter are checked in similar way like during the pre-measurement check and if the criterion is not met, the measurement continues until the total number of pre-set correct scans is reached.

Furthermore, each scan could have theoretically been repeated an infinite number of times. The algorithm compares the stability of the concentration upstream

5. Size-Resolved Penetration of Filtering Facepiece Respirators

and downstream of the filter at the end of each scan and evaluates it as sufficient or insufficient; in the latter case, the scan was repeated until a stability criterion was met. After the selected particle size was measured successfully in CPC position A-B the program altered the switchers into B-A position and this particle size was measured again the same way. In the chamber measurements, when the particle number concentration upstream of the respirator dropped below 10 \#/cm^3 for a period of at least 60 seconds the 1 hour filling protocol was initiated. The total length of the manikin-based tests in the experimental chamber ranged from 12 to 18 h and the maximum particle number concentrations upstream of the filter in all measurements were between 1800 and 3000 \#/cm^3 . Uniform particle concentration in the chamber was ensured by a mixing fan operating at 1000 rpm.

The nine particle sizes selected for the comparison of the filter penetrations ranged from 20 to 400 nm (20-35-50-70-100-140-200-280-400 nm) of count mobility diameter (CMD). This size range, as well as the particle sizes, remained the same for all the measurements. The selection of the particle size range for the size-resolved measurements, and the lower and upper size limits (20 and 400 nm), were given by the used aerosol generator. Particles with smaller and bigger diameters were generated with too low concentrations to overcome the CPCs' minimum counting limit downstream, and, therefore, they were under the detection limit of the filter testing system. The calculated MPPS were determined using the lognormal fit for each separate penetration curve. Measured MPPS can differ from the fitted one up to 10 nm, which is a considerable difference in some cases.

Even though the resolution of size-resolved method allows to measure with better resolution, in order not to make the single measurement unnecessary long only limited amount of sizes was selected. Thus this information does not offer in detail where exactly the real MPPS is, the lognormal fitting can estimate the position of MPPS reliably. All presented results of MPPS, as well as penetrations, are the median values of individual filters representing the specific FFRs. Median values were chosen over mean values in all calculations mainly due to the fact that the mean values of the repeated measurements do not reflect the prevailing penetration values while median value is less burdened with the possible outliers in the results. This test system has

several advantages over commercial automated testers. As the system was developed in the LACP laboratory, there is full control of the key parameters, and all important parts of the system are exchangeable. Thus, the system is adaptable for various testing needs, gives detailed size-resolved penetration results, and allows for the determination of the real MPPS. Corrections for possible differences in measurement of the two detectors are not dependent on any initial calibration or estimation of a correction factor.

5.2.4. Evaluation of the System with Standard Filter Medium

The system was regularly used over the last few years to measure penetrations of filtration materials for several companies and manufacturers with excellent repeatability. So far the only published work proving the stability and advantages of this testing system and measurement method was published by Zíková et al. (2015) where the results had very good repeatability. In order to verify the performance of filter testing system, repeated tests were performed using standard filter medium HB 5893 (Hollingsworth & Vose, East Walpole, MA, USA). This test was performed at the same conditions as all the tests of the commercial FFRs, flow rate through the filter 9 L/min (face velocity 10.56 cm/s) and the diameter of the cut sample of 47 mm. The test was performed using ammonium sulfate particles (1 g/L solution). The main reason of this setup is the limitation of the system, especially the face velocity of 2.5 cm/s (as described in HB 5893 technical data sheet), which would be on the edge of the measurement range of used testing system.

As can be seen in Figure 5.4, the measured penetration during repeated measurements are close to each other suggesting very good homogeneity of the standard material and very good repeatability of the measurement system. The MPPS of HB 5893 is close to 100 nm and the corresponding maximum penetration in this case was 0.02-0.03%. The comparison of these standard filter medium results obtained by system used on this study with the values given in the HB 5893 technical data sheet was not possible due to several important factors:

5. Size-Resolved Penetration of Filtering Facepiece Respirators

1. Different measurement procedures—the standard test measures overall penetration (one penetration value), one the other hand, hereby presented test system gives detailed size-resolved penetration.
2. Different detection systems used—standard test uses photometers, whereas size-resolved method uses single count CPCs.
3. Different face velocities (due to the limitations of system in this study).

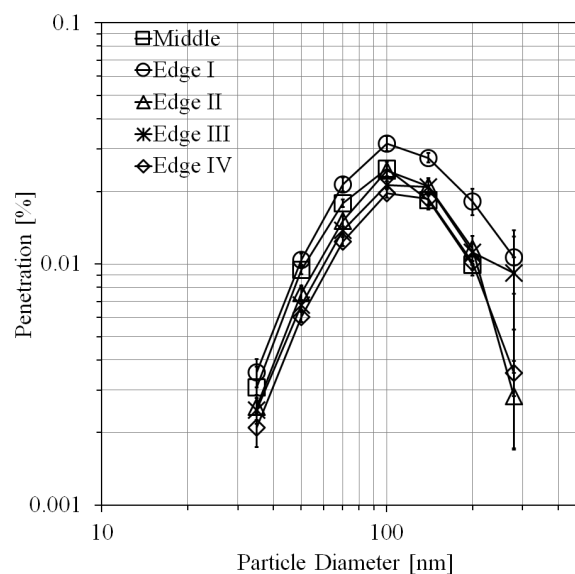


Figure 5.4. Penetration of ammonium sulfate through standard filter material HB 5893. The error bars represent the standard deviation.

5.3. Results

5.3.1. Filter Penetrations

Three facepiece respirators were challenged from the filtering class FFP1; Figure 5.5a demonstrates the results from these measurements. Although all three respirators were within the FFP1 maximum penetration limit of 20% (at 600 nm MMD), the measurements showed a rather wide differences between filters from respirator 1, which had median penetration (CMD) at MPPS equal to 13.9%, and filters from FFRs 3

5. Size-Resolved Penetration of Filtering Facepiece Respirators

and 10, which had penetrations reaching 4.9 and 4.1%, respectively. Differences in the FFRs penetration and performance were also observed in the FFP2 class (see Figure 5.5b). The percentage penetration criterion of this filtering class is $\leq 6\%$ (at 600 nm MMD). With exception of FFR 12, penetrations of all the filters from FFRs in this class ranged from 3.5 to 6.4% (CMD). Respirator 12 had, in all four filter measurements penetrations $> 6\%$, with a median penetration of 17.7% (11.8-34.3%) at MPPS. Considering that the FFP3 has the highest protection level, requiring a maximum penetration $\leq 1\%$ (or a filtration efficiency 99% at 600 nm MMD), 6 half masks were chosen to be tested. 4 out of 6 respirators showed median penetration higher than 1%, as seen in Figure 5.5c. It is also worth mentioning that none of the 13 filters among these four respirators met the $\leq 1\%$ criteria. On the other hand, filters from respirators 4 and 6 provided results with median penetrations of 0.4% and 0.03% (CMD), respectively.

5.3.2. Comparison of Within-Respirator Penetration and MPPS

As two filter samples from each respirator were examined, comparison of within-respirator penetrations from these filters between two identical respirators is presented as well (see Figure 5.6). In some cases (FFRs 2II, 4, 5, 6, 7II, 8, 8II, 9, 9II, 10, 11 and 13II) the penetration difference between two samples from the same respirator varied from 0.02-0.8%, which is less than 1%, and in other cases, the penetration difference was found to be over 1%, between 1.3-6.8% (FFRs 1, 1II, 3, 5II, 11II, 12 and 13). Results from respirator 12II from FFP2 reached exceptionally high penetrations (equal to 17.9 and 34.3%) and also had wide difference (16.4%) between the two examined samples. Penetration also varied between two identical respirators and ranged from 0.02 to 2.5% (see Figure 5.6c). The highest penetration difference, however, was found between respirators 12 and 12II, and was equal to 11%. Comparing the total penetrations from all the examined filters representing the individual FFRs show that the percentage penetration results from filtering classes FFP1, FFP2, and FFP3 overlap (3.2-16.3% for all filters from the FFP1, 2.4-34.3% for all filters from the FFP2, and 0.02-3.3% for all filters from the FFP3). The MPPS was

5. Size-Resolved Penetration of Filtering Facepiece Respirators

determined from the position of the maximum on the penetration curve by fitting lognormal peak shape and the hereby presented results are the median values for all filters representing the FFRs (see Table 5.2). The MPPS range for all the FFRs was found to be between 28-47 nm with exception of respirator 1 (FFP1), 2 (FFP2) and 9 (FFP3) ranging from 52 to 59 nm.

Table 5.2. Median values of MPPS, pressure drop, and the filter performance.

| FFR test # | Protection class | MPPS - lognormal fit [nm] | MPPS - measured [nm] | MPPS % penetration [%] | Pressure drop [kPa] |
|------------|------------------|---------------------------|----------------------|------------------------|---------------------|
| 1 | FFP1 | 58 | 50 | 13.9 | 0.07 |
| 2 | FFP3 | 52 | 50 | 1.9 | 0.15 |
| 3 | FFP1 | 28 | 35 | 4.9 | 0.07 |
| 4 | FFP3 | 43 | 50 | 0.4 | 0.21 |
| 5 | FFP2 | 43 | 50 | 6.4 | 0.11 |
| 6 | FFP3 | 37 | 35 | 0.03 | 0.23 |
| 7 | FFP3 | 47 | 50 | 2.0 | 0.15 |
| 8 | FFP3 | 44 | 50 | 1.6 | 0.21 |
| 9 | FFP2 | 59 | 50 | 4.1 | 0.18 |
| 10 | FFP1 | 33 | 35 | 4.1 | 0.08 |
| 11 | FFP2 | 33 | 35 | 3.5 | *0.12 |
| 12 | FFP2 | 40 | 50 | 17.7 | *0.04 |
| 13 | FFP3 | 39 | 35 | 2.4 | *0.19 |

*pressure drop data available only for one of the measurements

5. Size-Resolved Penetration of Filtering Facepiece Respirators

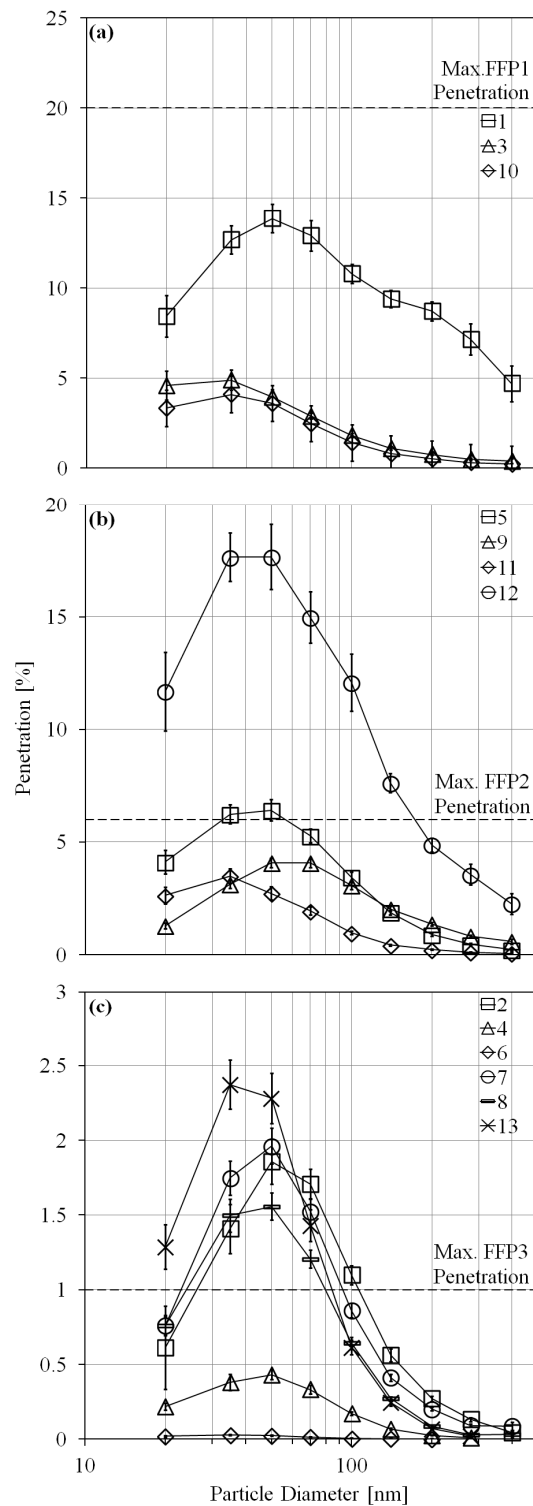


Figure 5.5. (a) FFP1, (b) FFP2, and (c) FFP3 filtering classes median size-resolved penetrations. The error bars represent the standard deviation.

5. Size-Resolved Penetration of Filtering Facepiece Respirators

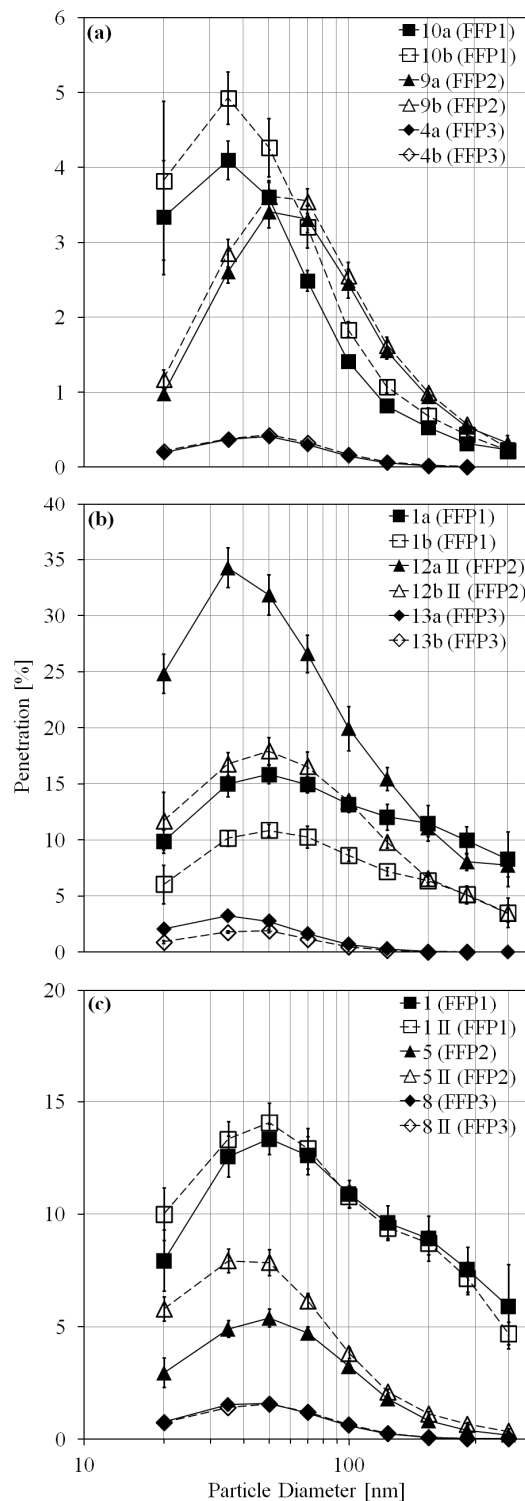


Figure 5.6. Penetration difference: (a) <1%, (b) >1%, and (c) between 2 identical respirators. Letters ‘a’ and ‘b’ indicate two filters from the same FFR, and ‘II’ indicates filters from the second (identical) FFR. Error bars represent the st. deviation.

5.3.3. FFP Penetrations and Comparison to Filter Measurements

Figure 5.7a depicts the results of median penetrations from these measurements. The maximum penetration limit in this filtering class was 20% (at 600 nm MMD). The most notable difference was observed in the case of respirator 10. FFR 10A reached a maximum penetration (CMD) of 5.5%, while the maximum penetration of 10B was 10.2%. Although all three respirators from FFP1 class were within 20%, measurements from respirator 1 showed an almost 4% difference between the manikin-based (18.0%) and of filtering material measurements from the previous study (13.9%). Differences in the FFRs' penetration were also observed in the FFP2 class. The percentage penetration criterion of this filtering class is $\leq 6\%$ (at 600 nm MMD), this was fulfilled only by respirator 11, which had even lower median penetration (2.8%) than the filter penetrations (3.5%) from identical FFR (see Figure 5.7b). Respirator 9 reached median penetration of 6.5% (CMD), whereas filter measurements from FFR 9 showed median penetration of 4.1%. Similarly, FFR 5 showed median penetration at a MPPS equal to 6.5% and had had only minor differences in comparison with measurements of corresponding filters from identical FFRs (6.4%).

The FFP3 filtering class has the highest protection level, requiring maximum penetration of $\leq 1\%$ (or a filtration efficiency of 99% or higher at 600 nm MMD). The results are presented in Figure 5.7c, where it is seen that respirator 2 and 6 were within $\leq 1\%$ (CMD). In fact, respirator 2 reached a significantly lower penetration level (0.6%, determined on 1 respirator only) than those found in the filter measurements from the same type of facepiece (1.9%, the median of 3 filters from 2 facepieces), which could be explained by the lower homogeneity of the material of FFR 2. Pressure drop during manikin-based and filter measurements were almost identical. Notably, it was possible to conduct only one measurement with respirator 2. It is also noteworthy that neither of the respirators from FFR 8 had penetrations of $\leq 1\%$. This was also the case with filter measurements from respirator 8, where all four filters reached penetration over 1% (with a median penetration of 1.6%). On the other hand, respirator 6 had median penetration of 0.1% – three times higher than it was in the filter penetration experiments (0.03%).

5. Size-Resolved Penetration of Filtering Facepiece Respirators

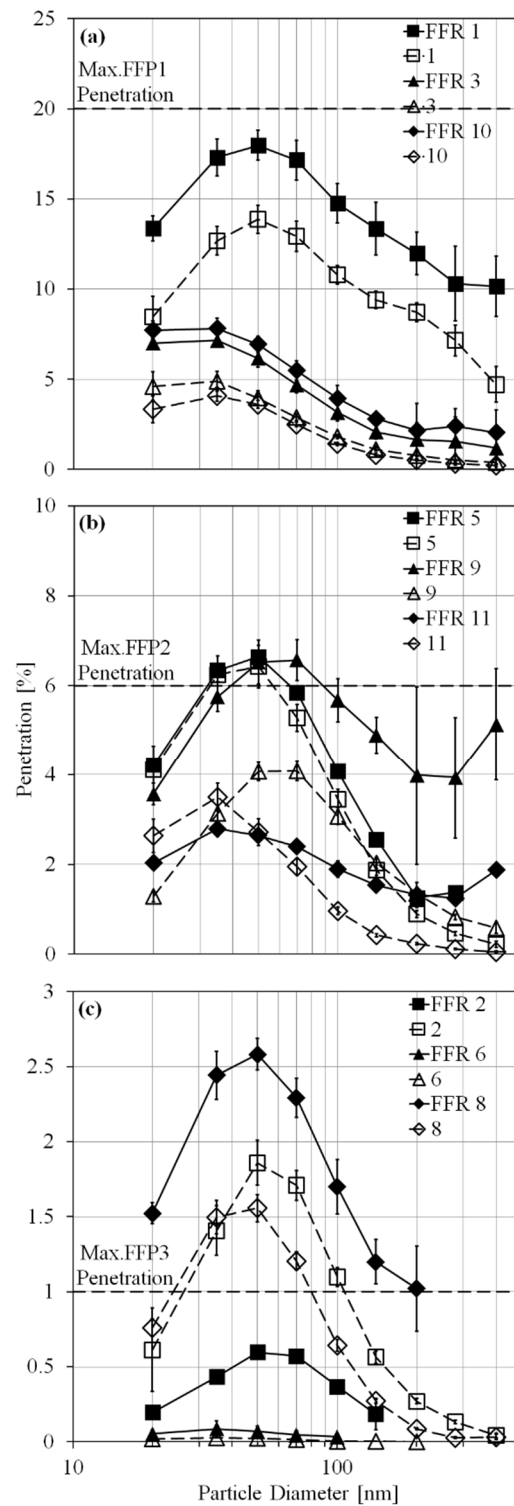


Figure 5.7. (a) FFP1, (b) FFP2, and (c) FFP3 filtering classes median size-resolved penetrations. The dashed lines represent the penetration of filtering material from identical FFR and the error bars represent the standard deviation.

5. Size-Resolved Penetration of Filtering Facepiece Respirators

Furthermore, variations were found in the MPPS (CMD). The MPPS was determined from the position of the maximum on the penetration curve by fitting lognormal peak shape and the hereby presented results are the median values. Generally, the MPPS ranged 25-48 nm with exception of respirator 1 (FFP1), 2 (FFP2) and 9 (FFP3) ranging from 53 to 64 nm. These findings are consistent with the previous results, where the MPPS of measured filters were almost identical for all filters from identical FFR models (28-47 nm), again with exception of the same FFR models (1, 2 and 9) ranging from 52 to 59 nm (see Table 5.3).

Table 5.3. Comparison of MPPS, pressure drop, and the respirators performance of manikin-based study and filter measurements.

| FFR # | Protect. class | Respirators | | | Filters | | |
|-------|----------------|--------------------------|------------------------|-------------------|--------------------------|------------------------|-------------------|
| | | MPPS – lognorm. fit [nm] | MPPS % penetration [%] | Press. drop [kPa] | MPPS – lognorm. fit [nm] | MPPS % penetration [%] | Press. drop [kPa] |
| 1 | FFP1 | 52.8 | 18.0 | 0.07 | 57.8 | 13.9 | 0.07 |
| 2 | FFP3 | 54.7 ^B | 0.6 | 0.12 ^A | 52.4 | 1.9 | 0.15 |
| 3 | FFP1 | 25.0 | 7.2 | 0.08 | 28.1 | 4.9 | 0.07 |
| 5 | FFP2 | 44.4 | 6.6 | 0.12 | 42.5 | 6.4 | 0.11 |
| 6 | FFP3 | 36.0 | 0.1 | 0.15 ^A | 36.7 | 0.03 | 0.23 |
| 8 | FFP3 | 48.1 | 2.6 | 0.17 | 43.8 | 1.6 | 0.21 |
| 9 | FFP2 | 64.4 | 6.6 | 0.15 | 58.7 | 4.1 | 0.18 |
| 10 | FFP1 | 26.5 | 7.8 | 0.06 | 32.5 | 4.1 | 0.08 |
| 11 | FFP2 | 43.0 ^B | 2.8 | 0.10 ^A | 32.7 | 3.5 | 0.12 ^A |

FFRs with test numbers 4, 7, 12 and 13 are missing, as these FFR were excluded from comparison with the filter tests.

(A) pressure drop data available only for one of the measurements; (B) only one successful FFR measurement conducted.

5.3.4. Comparison of Within-Respirator Penetration

The results from respirator 10 (FFP1) suggest a rather wide differences in the within-model penetration performance, with 5.5 and 10.2% (CMD) for 10A and 10B, respectively. Similarly, FFR 5 from the FFP2 filtering class showed relatively poor within-respirator performance (4.8 and 8.5% for FFRs 5A and 5B, respectively), as was

5. Size-Resolved Penetration of Filtering Facepiece Respirators

also observed in the filter measurements (5.4 and 7.9%). On the other hand, good within-respirator performance was found in the case of FFR 6, with percentage penetration values equal to 0.1% for 6A and 6B, respectively (see Figure 5.8a). Additionally, better understanding of within-respirator variation may be demonstrated by comparing the results from respirator 8 (FFP3).

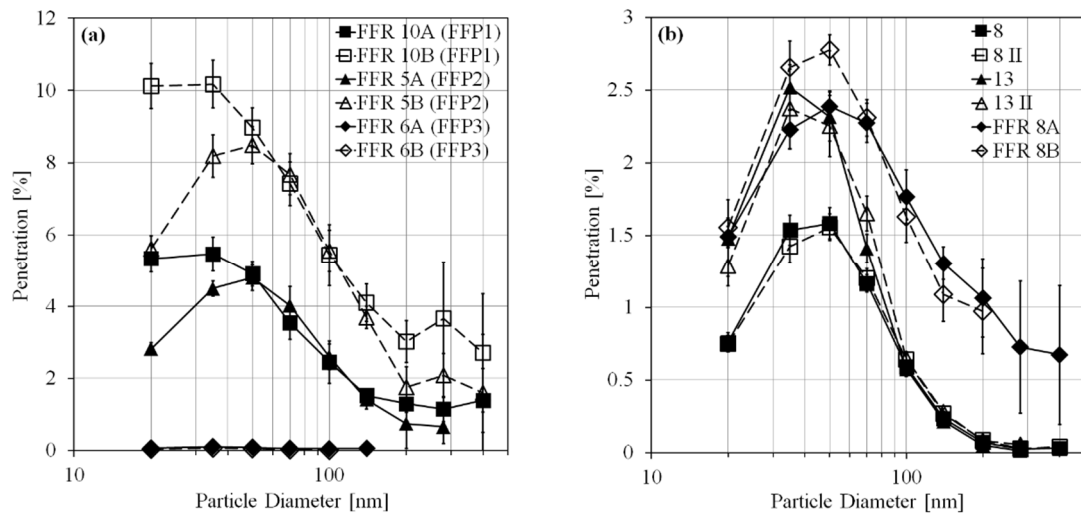


Figure 5.8. (a) Penetration difference between 2 identical respirators; (b) Penetration variations of FFRs 8 and 13 (both FFP3) from filter and manikin-based study. Letters ‘A’ and ‘B’, two identical FFRs (‘II’ indicates filters from an identical FFR from filter measurements). The error bars represent the standard deviation.

As shown in Figure 5.8b, the two FFRs 8 examined in the manikin-based study and the two identical respirators tested in filter measurements were accompanied, for comparison purposes, by FFR 13, which was examined during the filter measurements, as the only difference from FFR 8 is the fitted exhalation valve. Penetration results from the exact same filtering material should be very similar considering that these FFRs belong to the highest protection class (maximum penetration 1%). However, the penetrations found in this comparison varied from 1.6 to 2.8% (CMD). Relatively small differences were observed between FFR 8A and 8B examined in manikin-based study and two FFRs 13 from filter measurements (2.4-2.8%), while two FFR 8 examined from filter measurements had lower penetration values (1.6%). As was also seen in the

5. Size-Resolved Penetration of Filtering Facepiece Respirators

filter measurements, differences between percentage penetrations of FFRs were observed within the FFP1, FFP2, and FFP3 classes. Examining the performance of all the FFR models revealed that the tested filtering facepieces penetrations are overlapping (5.5-19.3% for all FFRs in FFP1, 2.8-8.5% in FFP2, and 0.1-2.8% in FFP3).

5.3.5. FFR Leakage Test

Additionally, FFR 6 was challenged, as the respirator with the best penetration results from filter measurements and from the manikin-based measurements in the chamber, with the test aerosol under varying conditions. Figure 5.9 illustrates the results from these experiments. The results suggest that the highest penetration levels were reached when the respirator had a sealed exhalation valve, but was not sealed around the face (line C, penetration ~50%) and when neither the face seal nor the exhalation valve were sealed (line A, penetration ~40%). Line B represents the condition when the respirator was sealed around the face, but the exhalation valve was left free. In this case the penetration was found to be ~10% and the maximum penetration was equal to 400 nm.

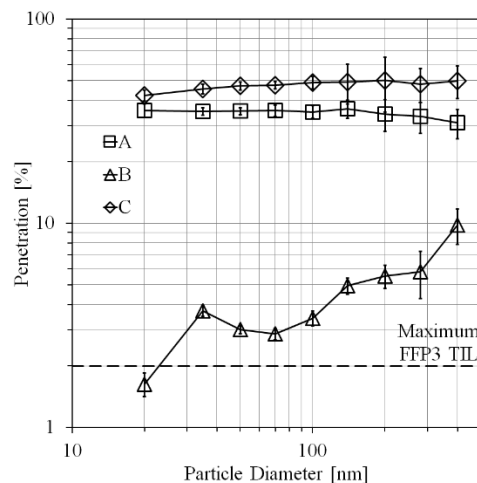


Figure 5.9. FFR 6 size-resolved penetrations: A – respirator not sealed around the face, exhalation valve not sealed; B – respirator sealed around the face, exhalation valve not sealed; C – sealed exhalation valve, not sealed around the face. The error bars represent the standard deviation.

5. Size-Resolved Penetration of Filtering Facepiece Respirators

The median percentage penetration performance (CMD) observed in filter measurements and manikin-based measurements of FFR 6 were 0.03% and 0.09% (with a filtration efficiency of 99.97% and 99.91%), respectively. Penetration levels increased when the respirator was not sealed around the face of the manikin and reached ~50% with a sealed exhalation valve and ~40% when the exhalation valve was not sealed. According to Grinshpun et al. (2009), most of the aerosol contaminants that enter a respirator are not due to filtration performance, but face seal leakage. Therefore, a filtering facepiece cannot provide optimal protection unless it fits properly, with a good seal around the face. In general, comparison of the two experimental methods (manikin-based and filter measurement method) for measuring penetration of filtering materials from FFRs are in good agreement, with a significant correlation of $R^2=0.91$. In addition to providing a more comprehensive evaluation of the penetration performances of CE-marked filtering facepieces, using two methods also allows for the inter-comparison of the methods themselves.

5.4. Discussion

Conditions and test protocol for measurements in this study were different than those used for CE certification, thus the results obtained in this study may not predict the results that would be obtained by the CE certification test method. It is acknowledged that the method used in this study to evaluate the penetration performance of the filtering half masks is based on both, isolated measurement of 47 mm filtering material cut out of the FFRs, and measurement of identical FFRs in manikin-based tests in an experimental chamber. The EN 149 method, which tests the FFRs only in a test chamber tightened on a specimen, thus, the results presented in this article represent the percentage penetrations obtained by the size-resolved measurement method against the FFP limits set by the EN 149. This method offers several advantages. First, penetration measurement of any specific part of the chosen respirator and adjustment of the diameter of the filter is possible according to the special needs of the measurement. Second, comparing the performance of several filters from the same facepiece would allow for the possibility of determining the homogeneity of the FFR filtering material if

5. Size-Resolved Penetration of Filtering Facepiece Respirators

needed. As was previously mentioned, detailed size-resolved penetration results allow for the determination of the real MPPS based on CMD. Hence, this method provides more critical results in regards to leak control, non-charged particles, and finding the real MPPS.

One could argue that hereby presented results were obtained by a method that is not based on the European Norm. EN 149 uses a protocol where the FFRs are challenged with non-neutralized polydisperse aerosol nebulized from a 1% solution of polydisperse NaCl (40-1200 nm) with MMD on ~600 nm. However, utilizing non-neutralized polydisperse NaCl for the certification of filtering facepieces does not represent the worst-case scenario, i.e. maximum penetration (the filter fibers are charged and the aerosol particles challenging the filter are in Boltzmann charge equilibrium) for testing of the electret filter and the use of polydisperse test aerosol does not provide with detailed size-resolved penetration, thus, it is not possible to find the real MPPS.

Neutralization of the test aerosol is of a great importance; when both the filter fibers and aerosol particles are charged, the Coulombic forces significantly enhance the capture of the particles and reduce the particles penetration. On the other hand, for a mechanical filter (i.e. with non-charged filter fibers) with low efficiency there are no significant differences between penetrations of charged and non-charged aerosol particles (Balazy et al., 2006b). For a charged filter fiber (electret filter) the MPPS of 300 nm (or > 300 nm) is insufficient as a limit for FFRs to pass the penetration test, and usage of a non-neutralized test aerosol may lead to distorted results of protection level. Based on the Single Fiber Filtration Theory, NIOSH accepts the size of 300 nm in diameter as the MPPS for particulate filters. Investigations have demonstrated that the MPPS is quite dependent on the operational conditions, and for non-charged filter fibers MPPS would be indeed ~300 nm, but the particle penetration peak would reach as high as ~80%. In order to provide adequate filter efficiencies, electret filters rely heavily on their electrostatic charge. Therefore, when compared to mechanical filters with non-charged filter fibers, the polarization force on the charged filter fiber with a fiber charge density of 13 nC/m would decrease the filter penetration from ~80% to

5. Size-Resolved Penetration of Filtering Facepiece Respirators

~5% and cause the shift of MPPS towards ~50 nm (Martin and Moyer, 2000; Balazy et al., 2006b).

According to the Fuchs theory (Fuchs, 1963), in the size range where the MPPS occurred in all measurements (30-60 nm) less than 2% of particles have a double charge while over 20% of 60 nm particles are single charged (> 4.4%). Therefore, the penetration results are more sensitive at these particle sizes (~15% of 400 nm particles have double charge and only about ~20% have a single charge), which can cause uncertainty in the penetration measurement. Nevertheless, the mode of the aerosol size distribution produced by the aerosol generator, under the operational conditions and with given ammonium sulfate solution, is around 70 nm, which means that particles bigger than 70 nm will have every time much higher concentration than their doublets (doubly charged particles). Even though in the case of this study it rather caused an overestimation of the penetration for particles bigger than 100 nm, the position of MPPS was little affected by double charged particles and was still within the allowed uncertainty limit of the measurement.

EN 149 sets the criterion for the respirator penetration tests even lower; it is on ~600 nm (MMD). Interestingly, for all the measured filters from FFRs in this work, the MPPS occurred in the range of 30-60 nm (CMD) at 9 L/min flow rate (with a face velocity equal to 10.56 cm/s, which is equivalent to 95 L/min aerosol flow at 150 cm² of effective filter area). The current findings are consistent with previous studies that report MPPS in the same range during CE-marked and NIOSH-approved half masks penetration measurements (Huang et al., 2007; Rengasamy et al., 2008; Rengasamy et al., 2009). Under the assumption that the generator dispersing the NaCl has a lognormal size distribution with a GSD of 1.90 and taking into account the change from aerodynamic to mobility particle diameter of NaCl particles ($\rho_p = 2.16 \text{ g/cm}^3$), the Hatch-Choate equations (Hinds, 1999) can be applied to calculate the CMD used in this study, which would be ~80 nm (equivalent to ~600 nm of MMD).

Although it may appear that ~80 nm is much closer to the MPPS results found in this study, the results from these two methods are not comparable and, therefore, the previously mentioned calculation has an informative character only. The MPPS, however, is characterized as the size of a particle with the highest relative particle

5. Size-Resolved Penetration of Filtering Facepiece Respirators

number concentration passing through a specific filtering material and is also dependent on the detection method and operational conditions. The particle mass size distribution downstream of the filter shifts the MPPS towards particles with smaller diameter (< 400 nm) and lower mass, while the filtering material retains a larger part of bigger particles (~ 400 - 1200 nm). Subsequently, this leads to underestimation of the particle penetration, as the flame photometry detection method is less sensitive to particles with smaller diameters (due to their lower mass contribution), which results in a misleading estimation of penetration. Thus, detection methods based on MMD should not be used for estimation of the penetration and MPPS of filtering facepieces.

Additionally, toxicity and health effects of nanoparticles do not necessarily depend on their mass. Aerosol of biological origins, such as viruses and bacteria, can be highly infectious if inhaled even at a very low dose and the related health effects may depend on the number of inhaled particles, not particle mass (McCullough and Brosseau, 1999; Donaldson et al., 2006; Poland et al., 2008; Jones and Brosseau, 2015). Furthermore, Huang et al. (1998) suggest that the aerosol penetration of the MPPS may locally be higher than the required penetration limit because of the fiber structure of the respirator. This may be caused by the non-homogeneity of the filter medium, which could be explained by manufacturing process, different chemical composition of the filter media, or different methods of introducing electric charge onto the filter fibers.

The MPPS of the respirators in this study was found to be in the range of 25-65 nm (CMD), which is in agreement with other studies reporting MPPS in CE-marked and NIOSH-approved FFR penetration measurements (Rengasamy et al., 2009; Huang et al., 2007; Balazy et al., 2006b). The obtained penetration results indicate that 7 out of 9 FFR models compared in this study reached higher penetrations during manikin-based respirator measurements than during measurements of filters from the same respirators. This could be caused by several factors. First, in the filter measurements (effective diameter 42.54 mm, effective filter area 14.27 cm^2), flow rate of 9 L/min was used, with face velocity equal to 10.56 cm/s, which is equivalent to a 95 L/min aerosol flow with an assumed effective filter area of 150 cm^2 for the respirator. Therefore, all of the filters had uniform effective areas. During the respirator measurements, aerosol flow of 95 L/min was used with an assumed effective filter area

5. Size-Resolved Penetration of Filtering Facepiece Respirators

of 150 cm² for all the respirators. However, this area varies from respirator to respirator, as does the respirator style (flat fold or cup shaped, see Table 5.1), which could cause the discrepancy in the face velocities and, therefore, also the percentage penetration results. Second, some respirators might have a rather non-homogeneous distribution of the filtering material. Although the method of homogeneity examination is not applicable in the manikin-based measurements, the higher percentage penetrations of manikin-based measurements could be partly explained by a non-homogeneous distribution of the filtering material.

Furthermore, due to the perfect fit of the filter in the filter holder, the inward leakage through the exhalation valve and face seal leakage was not relevant during filter measurements. Thus, the penetration results obtained might have higher accuracy than the respirator measurements, despite the fact that the respirators were precisely sealed around the face of the manikin and the exhalation valve (if fitted) was sealed as well. Measuring the pressure drop across the respirator and the filter gave an indication of proper fit of the respirator on the manikin and the fit of the filter in the filter holder. Indeed, the recorded values of pressure drop during filter measurements were very similar or slightly higher than the values recorded during the manikin-based measurements (see Table 5.2). The influence of filter loading on the penetration was considered negligible for two reasons. First was the relatively short time of exposure, which was 3-6 h in the case of filters and 12-18 h in the respirator measurements (consider that half of this time consisted of the chamber cleaning). Second, once the filter loading achieves a certain level, an electret filter begins acting as a mechanical filter and its efficiency increases, while the pressure drop across the filter increases during loading (Barrett and Rousseau, 1998). In this case the pressure drop during all the measurements ranged from 0.06 to 0.17 kPa and was constant, with insignificant fluctuations and without increasing filter efficiency.

According to the experiments, when FFR 6, as the respirator with the best test results from filter measurements and from experimental chamber measurements, was sealed around the face of the manikin and the exhalation valve was left free the penetration decreased from ~50% to ~10%, which is still far above the allowed $\leq 2\%$. Although the maximum particle number concentrations upstream of the filter in all

5. Size-Resolved Penetration of Filtering Facepiece Respirators

measurements were between 1800 and 3000 #/cm³, the particle concentration can be much higher in a real work environment. Martin and Moyer (2000) studied the penetration of NaCl particles through the face seal leakage of N95 respirators and their results suggested that the penetration can increase beyond 5% even at a low level loading, and the actual respiratory protection level may be even lower if the respirator does not have a perfect fit. The filter penetration is critical to the TIL of different particle sizes. Relatively high efficiency respirators produce lower TIL values (Rengasamy et al., 2014ab), but filter efficiency is rather insignificant once a leakage is introduced into the facepiece. However, EN 149 does not require separate measurement of exhalation valve leakage, which is assessed as part of the TIL examination, which shall be not greater than 22%, 8%, and 2% for FFP1, FFP2, and FFP3 masks, respectively (BS, 2001).

Based on the 89/686/EEC directive, during the process of CE certification in the country where the respirators are manufactured the notified body conducts the tests under EN 149 and EN 13274 and is responsible for both, type examination and checks on the final product (or monitoring of production). All respirators tested in this study were already CE-certified, i.e. passed the EN 149 penetration tests, assuming all notified bodies follow the same norm for examining and certifying the filtering facepieces. Therefore, it is rather unclear why all the filters and respirators from only one particular manufacturer had satisfactory maximum penetration levels according to the size-resolved method used in this study, and to EN 149 as well (since the FFRs were already certified).

In overall, 21 out of 46 filters tested with the size-resolved method in this study exceeded the percentage penetration limit set by EN 149. On the contrary, only 4 out of 16 respirators exceeded the percentage penetration limit in the manikin-based chamber measurements. This difference once again points out the disadvantage of testing the filter penetration on a whole FFR. There is clearly a need for modification in relation to a more sophisticated testing method and conditions in the currently valid European Norm for testing of filter penetrations. Additionally, the information about size-resolved penetration has particular importance (especially in the nanoparticle size range), and should be provided by the manufacturers on the datasheet of the FFRs.

5.5. Conclusions

The percentage penetrations of CE-marked filtering facepieces were experimentally measured by a size-resolved method (20-400 nm CMD) of measuring penetrations 47 mm filters cut out from CE-marked FFRs and measurements of identical FFRs tested in a manikin-based study. Penetration difference between 2 filter samples from same respirator was in most cases up to 6.8%, and between 2 identical respirators up to 2.5%. Comparison of the total penetrations from all the examined filters showed percentage penetration ranged 3.2-16.3% (FFP1), 2.4-34.3% (FFP2), and 0.02-3.3% (FFP3). The MPPS determined from lognormal fitting of the penetration curves was found to be between 25 and 65 nm (CMD) in all measurements. Also, in this study 7 out of 9 FFR models reached higher penetrations from manikin-based respirator measurements than during measurements of filters from the respective respirators. These two experimental methods for measuring penetrations of filtering materials from FFRs are in good agreement ($R^2=0.91$), however, penetration levels increased up to ~50% when the respirator was not sealed around the face of the manikin.

The real protection level provided by these filtering facepieces may be even lower if the respirator does not have a perfect fit. Therefore, considering that a poor filtration efficiency and a poor fit may increase under real work conditions, the particle penetration is even higher than it was found in this study. As expected, in many cases the real penetration of these respirators was beyond of what is allowed by the European Standards, which is mainly due to usage of non-neutralized, polydisperse test aerosol, inadequate detection method relying on the particulate mass, and the assumption that the MPPS is on ~600 nm (MMD) as the criterion for FFRs to pass the penetration test. These conditions and test methods lead to underestimation of particle penetration, especially in the nanoparticle size range (< 100 nm). Based on this study, it is concluded that the recently valid EN 149:2001+A1:2009 is neither sufficient nor efficient for estimation of particle penetration through filtering half masks and may need modification in relation to a more sophisticated testing method and conditions. Thus, the CE-marked respirators examined in this study may not be efficient in providing the expected respiratory protection for workers exposed to nanoparticles.

6. Calculation of Human Dose

6.1. Introduction

The inhalation rate, particularly in industrial environments, depends mainly on the working conditions, specifically the physical load, which can vary considerably. Retention of particles deposited in the respiratory tract (RT) depends on the properties of the aerosols and also on the load of work (Ruzer et al., 1995) and it is usually not known accurately. Workplace related concentrations and workload are rather unspecified parameters and depend on the nature of work since workers during the work day are mostly at several different places and locations characterized by different concentration levels. Analogous situation occurs with indoor exposure since the measurements of concentration in many occupational settings may be performed only infrequently. Therefore, one cannot expect consistent correlation between exposures estimated from spatially varying measurements and actual personal exposures (Ruzer et al., 2013). However, mathematical modeling of the deposition and distribution of inhaled aerosols within human lungs is an invaluable tool in predicting the health risks associated with inhaled environmental aerosols (Martonen and Guan, 2001).

Particle deposition in the human respiratory system is an extremely complex phenomenon (Rosati et al., 2013), governed by a wide variety of overlapping and interacting factors. Simulation studies can be used to predict the deposition of inhaled particles on differing spatial scales of resolution. Models can be developed that predict total respiratory system deposition or deposition in each of the regional compartments (Comer et al., 2001; Kim and Hu, 2006). In addition, models can predict deposition efficiencies in each individual airway generation or simulate the dose to a specific anatomical location within a respiratory passage (Asgharian et al., 1995). Exposure time series combined with other physiological characteristics of the simulated person may be used as an input to a modified version of the empirical dosimetry model to predict deposited particle dose, thus, used as a risk assessment of respirable particulate matter. An example of such a model is an empirical ICRP model developed by the International Commission on Radiological Protection based on works of Rudolf et al. (1983, 1986, 1988, 1990).

6. Calculation of Human Dose

Workers in many occupational settings are exposed to variety of aerosol emissions of diverse origin, concentration and chemical composition. Emissions from these workplace related aerosol sources can result in adverse health effect in means of long-term exposures. In work environment where it is not possible to secure clean air or the ventilation is not feasible, personal respiratory protection should be used. Deposited dose and cumulative retention in the RT in this study were assessed in ExDoM2 model. Different work scenarios including use of respiratory protection were considered for 4 different emission sources discussed in Chapter 4. Additionally, exposure prevention and possible adverse health effects of these sources are discussed in this chapter as well.

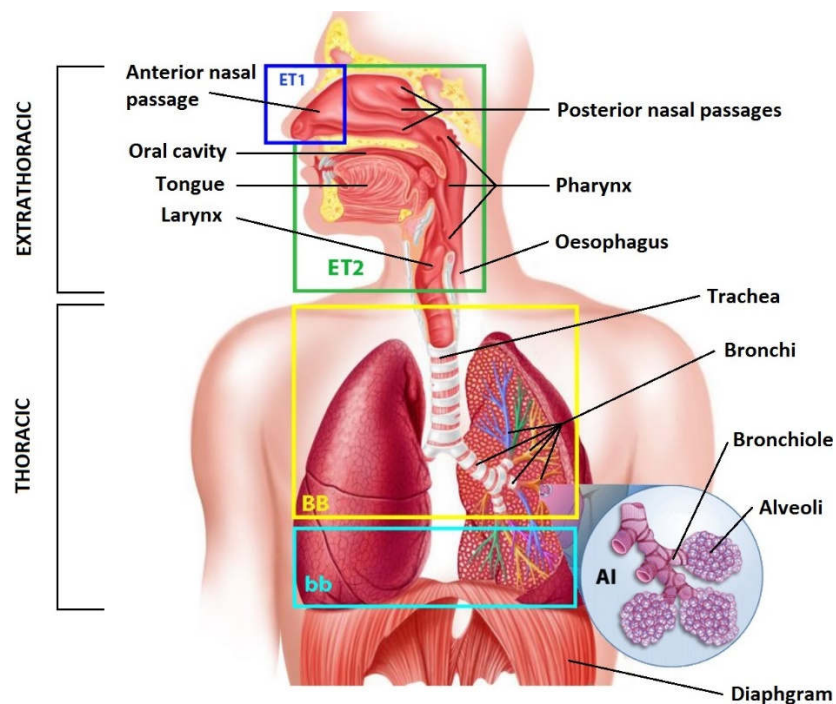


Figure 6.1. Human respiratory tract (adapted from www.anatomywrap.com/respiratory-system-without-labels).

6.2. Exposure Dose Model

ExDoM2 is a model used in this study for calculating the human exposure and the deposition dose, clearance, and retention of aerosol particles in the respiratory tract (RT) from. ExDoM2 is an updated version in respect to the ExDoM incorporating new particle

clearance mechanisms in the Human Respiratory Tract Model (HRTM) (ICRP, 2012) and it was developed using the Matlab software (Mathworks, Inc., USA) in the Laboratory of Atmospheric Aerosol at the Technical University of Crete. The RT (Figure 6.1) is treated as two regions: the extrathoracic regions (ET) and the thoracic regions (TH). The extrathoracic regions are further divided into the ET1 (anterior nasal passage) and ET2 (posterior nasal passages, pharynx and larynx) regions. The thoracic region (the lungs) is divided into the BB (trachea and bronchi), bb (bronchiolar) and AI (alveolar–interstitial).

6.2.1. Human Dose Calculation

The ExDoM2 model estimates the individual's dose rate H ($\mu\text{g}/\text{h}$) of particles in different size fractions by Equation (3.1) as the product of the exposure concentration, the ventilation rate and the deposition fraction of particles in the respiratory tract (Chalvatzaki and Lazaridis, 2015):

$$H = \sum B C_i n_{i,j} \quad (\text{Eq. 6.1})$$

where B (m^3/h) is the ventilation rate of the exposed individual (depending on the breathing frequency and tidal volume), C_i the exposure concentration ($\mu\text{g}/\text{m}^3$) for particles in the size fraction i , and $n_{i,j}$ the deposition fraction in region j of the respiratory tract for particles in the size fraction i . The deposition efficiency n_j depends on aerodynamic deposition efficiency n_{ae} (due to impaction and gravitational settling) and thermodynamic deposition efficiency n_{th} (due to diffusion). The deposition efficiency of region j is calculated as:

$$n_j = (n_{ae}^2 + n_{th}^2)^{1/2} \quad (\text{Eq. 6.2})$$

where both the aerodynamic and thermodynamic efficiencies are expressed as:

$$n = 1 - \exp(-a R^p) \quad (\text{Eq. 6.3})$$

where a and p are dimensionless constants and R has a characteristic functional form that is different in each region and depends on the particle size (aerodynamic and thermodynamic) and the relevant respiration parameters.

6.2.2. Clearance and Retention Calculation

The model also calculates the clearance and retention of particles in the RT. The amount of particles in each region of the lungs after an acute intake is given by the mass balance equation (Aleksandropoulou and Lazaridis, 2013):

$$\frac{dR_i(t)}{dt} = -[m_i(t) + s_i(t)] R_i(t) \quad (\text{Eq. 6.4})$$

where, $m_i(t)$ and $s_i(t)$ are the instantaneous clearance rates of the deposit in compartment i due to mechanical movement and absorption into blood, respectively, and $R_i(t)$ the retained mass after time t . In addition, absorption into blood is assumed to occur at the same rate in all the regions considered.

The mass of particles in each compartment of the RT during and after continuous exposure to particles and their fraction transferred to the gastrointestinal (GI) tract, lymph nodes, and blood. The retained mass in each compartment of the RT and their mass fraction transferred to the oesophagus and blood is estimated by Equation (3.5) for fraction of particles dissolving relatively rapidly and Equation (3.6) for fraction of particles dissolving slowly, and are solved independently using exponential substitution and Gauss elimination (Chalvatzaki and Lazaridis, 2015):

$$\frac{dI_j(t)}{dt} = \sum_{k=1}^{13} [m_{k,j} I_k(t) + (m_{j,k} + s_r) I_j(t)] + f_r H_j(t) \quad (\text{Eq. 6.5})$$

6. Calculation of Human Dose

$$\frac{dT_j(t)}{dt} = \sum_{k=1}^{13} [m_{k,j} T_k(t) + (m_{j,k} + s_s) T_j(t)] + (1 - f_r) H_j(t) \quad (\text{Eq. 6.6})$$

where m is the mechanical movement rate of particles from compartment k to j ($m_{k,j}$) or the opposite ($m_{j,k}$), f_r the fraction dissolved rapidly, $(1 - f_r)$ the fraction dissolved slowly, s_r the rapid dissolution rate, s_s the slow dissolution rate, H_j the instantaneous dose applied to the compartment j at time t , I the retained mass of particles dissolving relatively rapidly after time t in compartments k and j , T the retained mass of particles dissolving slowly after time t in compartments k and j . Hence, the retained mass after time t in compartment j is calculated as the sum of the $T_j(t)$ and $I_j(t)$. The fractions f_r and $(1 - f_r)$ depend on the type of the absorption behavior. The system is solved per 1/(breathing frequency) during exposure and per minute post-exposure to determine retention.

6.3. Methodology

Exposure dose rates from background concentration during nights in the laboratory (prior to emissions from painting materials, resuspension and welding) and in the print room (12 h period without printing and occupants) were considered as ‘clean environment’ for the purposes of this study and taken as the reference. Particle density of 1.5 g/cm^3 (approximation for ambient aerosol) was used for the exposure dose calculation of the background concentration. In all calculations particles were assumed to be spherical (shape factor of 1). The dose rates were calculated for an adult Caucasian male with ventilation rate $1.5 \text{ m}^3/\text{h}$ (light work scenario, nose breathing, moderate blood absorption behavior). Exposure time step calculated for dose from number concentrations (emissions from painting materials and printers) was 5 min, and 1 h in the case of dose calculated from mass concentrations (resuspension and arc welding).

The particle density is used in the model to convert between different equivalent diameters and was assumed to be 1.5 g/cm^3 for emissions from painting materials. In the case of printers’ emissions, the same refilled black toner cartridge was employed, which is used by printers in the PR. Although the chemical composition of the toner cartridge was not investigated in this study, generally, most of the commercially available printers’

6. Calculation of Human Dose

toner powder particles have an outer layer from copolymer (possibly including styrene, $\rho=0.9 \text{ g/cm}^3$) enchaining the toner particles to the paper and an iron oxide ($\rho=5.2 \text{ g/cm}^3$) core material carrying charges. There is lack of studies in the literature confirming the particle density of the nanoparticles from printer emissions, therefore, an assumed default uniform particle density of 3 g/cm^3 was used, since the toner powder consists of approximately 50% of iron oxide and 50% of copolymer (Wang et al., 2011).

Since the ExDoM2 model is based on Andersen cascade impactor, prior to human dose calculations from mass concentrations, conversion (Hinds, 1999) from optical diameter (data from OPS) to aerodynamic diameter was necessary. For this purpose, uniform value of particle density equal to 2.65 g/cm^3 (Arizona Road Dust) was used for emissions from resuspended dust, and 3.7 g/cm^3 (Avino et al., 2015) was considered for the arc welding emissions (SMAW, TIG and cutting).

Scenarios involving use of FFR were based on filter efficiencies of FFR #3, and FFR #6, which were chosen as both had satisfactory results in all the size-resolved penetration tests in filter measurements and in manikin-based tests as well. FFR #3 (FFP1 filtering class) was used for emissions from painting materials and printing. FFR #6 (from FFP3) was used for emissions from dust resuspension and arc welding since, according to initial calculations, respirators from lower filtering classes did not offer sufficient protection against particles from these two emission sources. Deposited dose from particle number concentration was examined for two scenarios: emission and post-emission period in the case of painting material emissions, and for startup and printing in the case of emissions from printers in the PR. The dose rates from resuspension and welding were calculated for total of 4 h exposure time and 4 different scenarios where the emission occurred in the first 20 min in the resuspension experiments and the first 5 min during arc welding:

1. Stay the entire time period (4 h) in the polluted workspace without use of FFR.
2. Stay the entire time period in the polluted workspace; use of FFR only during the emission period (first 20 or 5 min, respectively).
3. Stay in the polluted workspace only for the time period of emission without a use of FFR and then leave the polluted workspace.
4. Stay the entire time period in the polluted workspace with use of FFR.

6.4. Calculation of Deposited Dose (#) from Number Concentration

6.4.1. Human Dose from Painting Material Emissions

The painting oils used for the experiments (Chapter 4.1) consisted of water mixable oil and turpentine medium composed mainly from monoterpenes (α - and β -pinenes). Turpentine is a clear or yellowish highly flammable fluid obtained by steam distillation of wood resins, mainly from pine trees and it is a mixture of monoterpenes: α and β -pinenes, carene, camphene and dipentene. As a solvent, turpentine serves as a thinning component for oil-based paints, therefore, it is widely used by art painters, and can be the cause of turpentine-induced occupational asthma (Dudek et al., 2009). Individuals who work with pine in the furniture industry may be exposed to monoterpenes, the most abundant of which are α -pinene, β -pinene, and Δ^3 -carene (Hagström et al., 2012; Edman et al., 2003).

Monoterpenes are among most ubiquitous VOCs to be detected in indoor air while human presence and specific pattern of behavior strongly influences presence and concentrations of monoterpenes in the indoor environment (Król et al., 2014). These can easily penetrate the different barriers of the body and uptake of pinenes can occur through the lungs, the gastrointestinal tract and intact skin (Cavender, 1994). In secondary organic aerosols (SOAs) formation with ozone (O_3) in indoor environments monoterpene plays reactive role. Such ozonolysis can be influenced by the presence of gaseous pollutants such as ammonia (NH_3) penetrated from outdoor environment (Talbot et al., 2017). Niu et al. (2017) demonstrated the toxicities of the indoor SOA formed from the ozonolysis of a monoterpene and found that there was 22–39% stronger pulmonary inflammatory effect on the particles generated with NH_3 .

Human dose model for 10 experiments with turpentine oil emissions (NPFE) was estimated in the presented study. The results show that the average total human dose during the experiments (Table 6.1) without a use of a FFR was 1.2×10^9 and 5.1×10^8 # for the NPFE and post-emission period, respectively. It represents 4.6 and 1.3-fold increase compared to the exposure dose at background concentration, which was calculated to be 2.2×10^8 #. According to the calculations, > 96% of turpentine oil particles deposited in the alveolar–interstitial (AI) region (68% of all deposited particles)

6. Calculation of Human Dose

of the lungs from emission or post-emission period were particles smaller than 100 nm. On the other hand, average exposure dose from the NPFE emissions and post-emission period with the use of FFR were estimated to be 7.5 and 2.4×10^7 # representing 0.7 and 0.9-fold decrease with respect to the exposure dose at background concentration for the NPFE and post-emission period, respectively.

The MPPS of FFR #3 used for the calculations is on ~30 nm, which means that every particle size on the left and right of the MPPS on the penetration curve will have lower penetration values, and the filter's efficiency increase with particle size. As can be seen on Figure 6.2 (doughnut charts), FFR retained mostly particles > 50 nm and narrowed the percentage ratio of particles smaller than 50 nm, but in turn also captured $\geq 95.1\%$ of these particles. The FFR effectively retained large part of nanoparticles in all cases (Figure 6.2), except for one where human dose even with use of FFR was 1.3-fold higher compared to background concentration of the same day (27-Jan). This value is, however, the average of 18 time steps (90 min emission period per 5 min time steps), thus, the concentrations could be locally even higher. Although FFR from FFP1 filtering class may not be efficient in preventing against airborne contaminants and FFR of higher filtering class may be required, use of FFR is highly suggested when working with solvents containing monoterpenes, such as painting oils.

Table 6.1. Average exposure dose (#) in respiratory tract (RT) regions for 5 min time step and increase in respect to background (BC) exposure dose (in the laboratory prior to emission period) with exposure dose during NPFE and post-emission period with and without use of FFR.

| Process | RT region | | | | | Total dose (#) | +/- (%) |
|----------------|-------------------|-------------------|-------------------|-------------------|-------------------|-------------------|---------|
| | ET1 10% | ET2 6% | BB 2% | bb 17% | Al 65% | | |
| - BC | 2.1×10^7 | 1.1×10^7 | 4.7×10^6 | 3.4×10^7 | 1.5×10^8 | 2.2×10^8 | - |
| No NPFE | 1.1×10^8 | 6.1×10^7 | 2.5×10^7 | 1.9×10^8 | 8.3×10^8 | 1.2×10^9 | +459% |
| FFR Post-emis. | 4.7×10^7 | 2.5×10^7 | 1.1×10^7 | 7.6×10^7 | 3.5×10^8 | 5.1×10^8 | +134% |
| FFR NPFE | 7.0×10^6 | 3.8×10^6 | 1.6×10^6 | 1.2×10^7 | 5.1×10^7 | 7.5×10^7 | -66% |
| FFR Post-emis. | 2.2×10^6 | 1.2×10^7 | 4.9×10^5 | 3.5×10^6 | 1.6×10^7 | 2.4×10^7 | -89% |

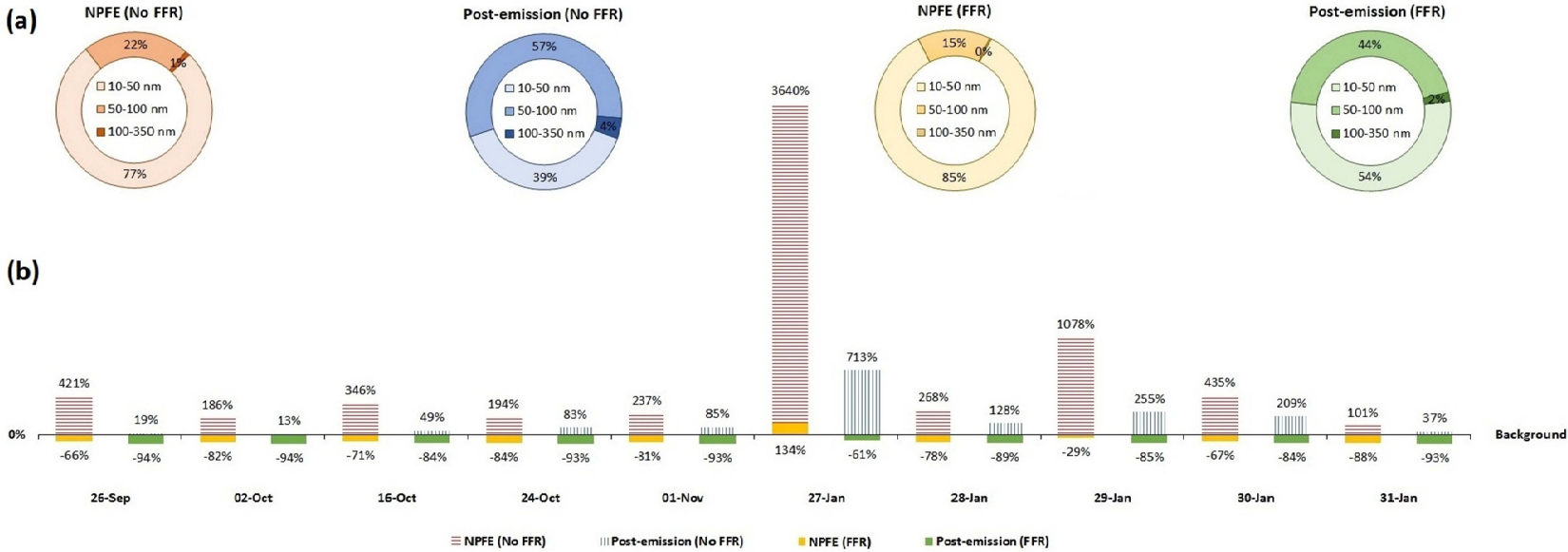


Figure 6.2. Average percentage increase of human dose (#) in RT with and without FFR during NPFE (90 min) and post-emission period (180 min) (columns); and size fractions of particles deposited in AI region of the RT (doughnut charts).

Indoor air quality (IAQ) may also be improved with portable air cleaner, which is capable of removing ultrafine particles. However, none of the air cleaners remove all pollutants and some may introduce harmful emissions into the indoor environment such as ozone (Britigan et al., 2006; Niu et al., 2001). Therefore, air cleaners based on filtration technique, i.e. HEPA (and preferably also active carbon) are a fair and effective solution. Nevertheless, air cleaners should not replace ventilation in any case, but rather may supplement this solution. Indoor sources such as resuspension from dust or SOA may be the major contributors in increased particle concentration (Almeida et al., 2011; Fromme et al., 2007).

On the contrary, natural ventilation prevents air filtration of incoming outdoor air, hence expose the occupant to outdoor pollution (Bekö et al., 2008; Sultan et al., 2007). Waring et al. (2008) tested HEPA filters and electrostatic precipitators (ESP) and found that they remove particles much more effectively than the ion generators (IG) for the measured particle diameter range of ~10–500 nm. In addition, ozone emitted by ion generators (and printers) can, react with terpenes to produce harmful SOA in the ultrafine and fine size ranges, thus worsen the air quality. Furthermore, the authors suggest that technologies such as the portable HEPA filters are effective at particle removal and do not generate ozone or other harmful byproducts. Mølgaard et al. (2014) studied several air cleaners at chosen settings where the filter-based air cleaners performed best for all particle diameters above 100 nm.

6.4.2. Human Dose from Laser Printer Emissions

Recently, Khatri et al. (2017) collected nasal lavage and urine samples for over 3 weeks from six permanent employees from three copy centers and eleven controls, which participated in the study, and found chronic upper airway inflammation and systemic oxidative stress in photocopier operators, chronically exposed to nanoparticles. On the contrary, another recent controlled exposure study conducted by Karrasch et al. (2017) investigated the health effects of laser printer emissions during 75 min exposure, where examinations before and after exposures also included bronchial and alveolar nitric oxide. They concluded that the experimental acute responses to short but very high-level

6. Calculation of Human Dose

exposures were small and did not indicate clinically relevant effects compared to low particle number concentrations.

For purposes of this calculations, experimental data from one-week measurement campaign in a university printer center (Chapter 4.2) was used to calculate the human particle dose. The results from the human dose model (Table 6.2) from the laser printer emissions show that the average total human dose during printers' startup and printing was 2.0×10^9 and 3.5×10^8 #, respectively. It represents 14.3 and 1.2-fold increase for the printers' startup and printing, respectively, compared to the exposure dose at background concentration (3.1×10^3 #/cm³), which was calculated to be 1.4×10^8 #. The model also showed that 65% of all particles from printer emissions during startup end up in the alveolar–interstitial (AI) region of the lungs (of which 82% were UFPs < 50 nm, see Figure 6.3), where the oxygen and carbon dioxide exchange takes place.

Furthermore, data obtained by Sisler et al. (2015) indicate that particles emitted from printer even at low, non-cytotoxic exposure levels are bioactive and affect cellular responses in an alveolar–capillary co-culture model, which could possibly lead to adverse health effects. Average exposure dose from the printer emissions during the printing were estimated to be 3.0×10^8 # representing 1.2-fold increase with respect to the exposure dose at background concentration. As shown in Table 6.2, the human dose significantly decreased when a FFR was used, and was equal to the human dose at BC during printers' startup, while 0.9-fold decrease was observed during printing.

Table 6.2. Average human dose (#) in RT regions during printers' startup and printing with and without use of FFR in the PR, and increase in respect to background (BC).

| Process | RT region | | | | | AI | Total dose (#) | +/- (%) |
|---------|-------------------|-------------------|-------------------|-------------------|-------------------|-------------------|----------------|---------|
| | ET1 10% | ET2 6% | BB 2% | bb 17% | | | | |
| - BC | 1.3×10^7 | 7.1×10^6 | 3.0×10^6 | 2.1×10^7 | 9.5×10^7 | 1.4×10^8 | - | |
| No FFR | | | | | | | | |
| Startup | 2.1×10^8 | 1.1×10^8 | 4.8×10^7 | 3.4×10^8 | 1.3×10^9 | 2.0×10^9 | +1339% | |
| Print. | 3.1×10^7 | 1.7×10^7 | 6.7×10^6 | 4.7×10^7 | 2.0×10^8 | 3.0×10^8 | +117% | |
| FFR | | | | | | | | |
| Startup | 1.5×10^7 | 8.0×10^6 | 3.4×10^6 | 2.4×10^7 | 8.9×10^7 | 1.4×10^8 | -1% | |
| Print. | 1.6×10^6 | 8.7×10^5 | 3.6×10^5 | 2.6×10^6 | 1.0×10^7 | 1.6×10^7 | -89% | |

6. Calculation of Human Dose

Additionally, the increase in human dose without use of FFR in PR was lower than it was observed in the chamber giving 24.1 and 5.2-fold increase during the printers' startup and printing, respectively. This was probably due to greater distance of printers from the sampling point and also higher air exchange rate. Wang et al. (2011) measured particle number concentrations and VOCs simultaneously directly above the printer, and at distances of 1 and 2 m away from the printer, and the results showed that at distance of 1 m away from the printer the concentration was reduced to 5% of that at the source. Note that the distance of the sampling point from printers in PR (49 m³, opened door) was 2-4 m, whereas in the chamber study (7.6 m³) it was only 0.5 m. Hence, taking into account also higher number of sources (4 printers instead of just 1), the emission concentrations in the PR would likely be much higher at distances closer to the emission source. Consequently, the exposure dose of the PR users and the staff (especially during printers' startup), staying next to the printers would be also much higher than it is estimated in this study where the exposure dose is calculated for average 5 min time step.

After 6 h of acute exposures in a busy photocopy center led to upper airway inflammation and systemic oxidative stress in 9 healthy subjects, which for certain markers took longer than 24–36 h post-exposure to clear (Khatri et al., 2013). Comprehensive in vitro analysis conducted by Pirela et al. (2016) reported preliminary evidence of epigenetic modifications that might translate to pulmonary disorders as an effects of nanoparticles emitted from laser printers. In addition, Grminski et al. (2011) evaluated the genotoxic potential of three black toner powders and their results suggest that metals and metalloids as components of magnetite, or polycyclic aromatic hydrocarbons (PAHs) as components of the carbon-bearing material, are responsible for the genotoxic effects (damaging the genetic information within a cell causing mutations, which may lead to cancer) rather than cytotoxic.

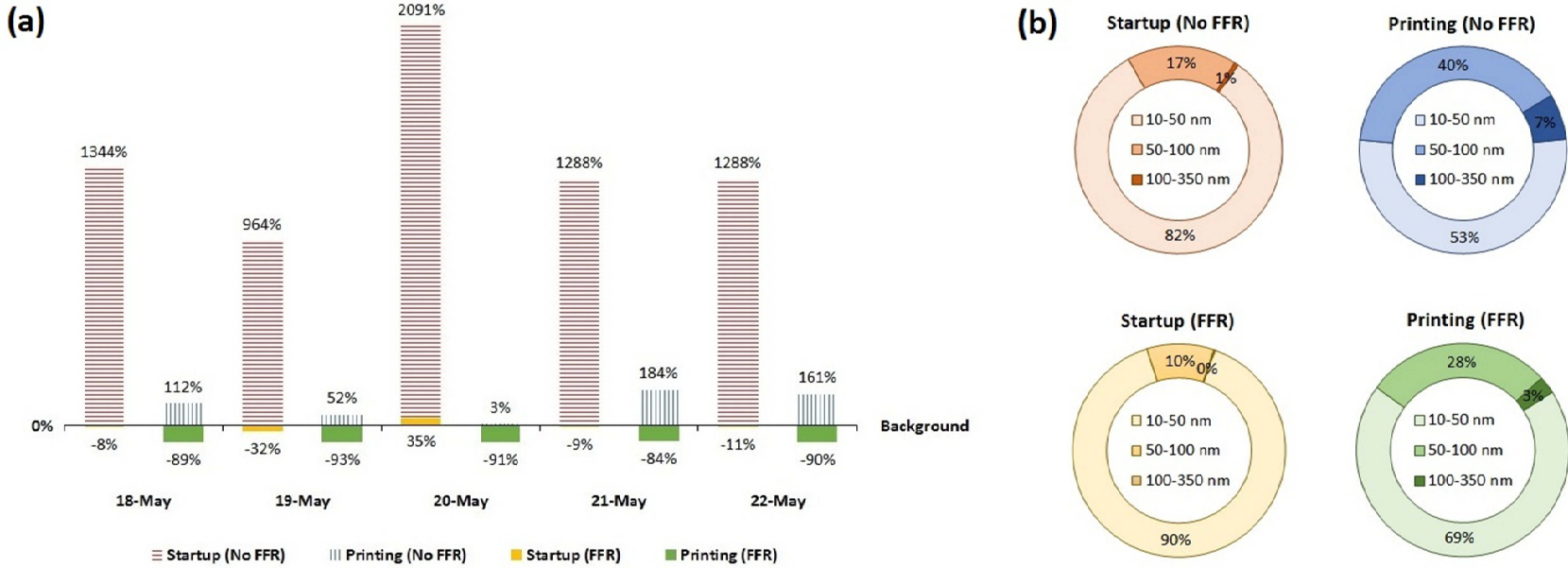


Figure 6.3. (a) Average percentage increase of human dose (#) in RT with and without FFR during printers' startup and printing in PR; and (b) size fractions of particles deposited in AI region.

6. Calculation of Human Dose

In contrast to use of FFR when working with turpentine painting oils, where ventilation is many times not feasible, in cases such as printing in a print room, solutions involving use of FFR should be avoided and focus should be on ventilation systems and providing good IAQ in general. Natural ventilation has become a key component in sustainable building design and may reduce the cost of air handling systems of the building, but it is also preventing the use of air filtering technologies. Study by Khaleghi et al. (2011) show that average particle number concentrations for sub-micron particles are higher in spaces with natural ventilation. There is lack of knowledge in differences for two identical spaces operating with either natural or mechanical ventilation. Both mechanical and natural ventilation systems were examined by Montgomery et al. (2015). Their results revealed that the mechanical ventilation was more effective in controlling the total VOCs and CO₂ levels regardless of occupants' load and also that the particulate mass (PM) I/O ratios were significantly higher while operating with the natural ventilation.

As shown previously, the emissions from printers were the major source of high nanoparticle concentrations in the PR and it might be solved by the air cleaner, ventilations system or by removing one of the printers in PR (ideally the combination of all three). The existing mechanical ventilation in the buildings where the measurements were taken, was not working during the campaign. Despite the fact that it does not have any filters for particle capture, rather cheaper and easier solution would be adding low pressure HEPA filters into the mechanical ventilation instead of installing a new one. Wang et al. (2011) also propose adding a filter or adsorbent to the printers' air outlets, which could be helpful in mitigating the VOCs release, and also that staying more than 1 m away from the printer can greatly reduce the exposure to high nanoparticle concentrations.

6.5. Cumulative Deposited and Retained Dose (μg) from Mass Concentration

6.5.1. Human Dose from Dust Resuspended during Walking

Personal activity sources, such as particle resuspension during walking, often represent strong source for exposure. Ferro et al. (2004) found that simply walking around indoors increased personal exposure to both fine and coarse particles. Cumulative deposited and retained dose in this work was estimated for experimental data from 25, 15 and 5 g/m^2 of dust resuspended during walking. Generally, the human dose was decreasing with the decreasing dust load in similar manner to the resuspension rate discussed in Chapter 4.3 (25>15>5 g/m^2). Exceptions were the second and the third scenario where the use of FFR or leaving the polluted workplace played a significant role in further human dose, clearance and retention. As can be seen in Figure 6.4a, human dose in the first scenario, staying in the polluted workspace for the entire time period without a use of FFR was the 'worst case' scenario. The increase in total deposited dose compared to the BC was 166-fold, 81-fold and 25-fold for 25, 15 and 5 g/m^2 of resuspended dust, respectively.

In contrast to the previous, the last scenario, accounting for use of FFR for the entire time period, was the 'best case' scenario where the total deposited dose was much lower than that of the background (Table 6.3). Examination of the second and third scenario revealed that the human dose would be much lower if the exposed simulated subject not wearing FFR at the duration of emission (20 min), would leave the polluted workspace immediately after the end of emission rather than stay the entire time period in the polluted workplace (4 h) and use FFR only during the emission period (Figure 6.4b). In such a case the decrease in total cumulative human dose after 4 h was estimated to be between 29 and 45% in these two scenarios.

The transport of particles from one region to another and to the gastrointestinal (GI) tract and lymph nodes is performed mechanically by the airway secretions and cilia movement (mucociliary escalator), airway macrophages, and extrinsic means, such as coughing and nose blowing. Particles deposited in the RT are cleared by three main routes: by absorption to the GI tract (via the pharynx), to lymph nodes (via lymphatic channels), and by absorption into blood (depending on the chemical form of the particle). Particles can be distributed from the blood circulation system to other organs or tissues

6. Calculation of Human Dose

like liver, kidneys, heart, brain, muscle and bone. Absorption into blood is assumed to occur at the same rate in all regions, except for anterior nasal passage (ET1) where no absorption takes place. However, due to the complex geometries present in the oral and nasal regions, little theoretical modeling has been done in the extrathoracic compartment.

Total cumulative deposited dose in the extrathoracic region represented ~96%. ~60% of this dose was deposited in the anterior nasal passage. The particles deposited in the extrathoracic region were retained (~48%), entered the GI tract (~45%) or were cleared by nose blowing (~7%). As was said earlier, particles smaller than 1 μm are not easily resuspended or not resuspended at all since the removal forces (drag and lift) depend strongly on the particle size. Due to very small contribution of fine particles in the resuspended dust, only ~4% of total dose were deposited and ~2% were retained in the thoracic region. It is concluded that airborne dust produced by emission source (depends also on chemical composition) would possibly pose greater health risk rather than resuspended dust since it contains a little fraction of fine particles that could be deposited and retained in the thoracic region.

Table 6.3. Cumulative deposited and retained dose (μg) in extrathoracic and thoracic region, GI tract and blood after 4 h for resuspension from: (a) 25 g/m^2 , (b) 15 g/m^2 , and (c) 5 g/m^2 of dust.

| Scenario/Region | Cum. Deposited Dose | | Cum. Retention | | | |
|--|---------------------|----------|----------------|----------|-------|-------|
| | Extrathor. | Thoracic | Extrathor. | Thoracic | GI | Blood |
| (a) 25 g/m^2 | | | | | | |
| Stay (No FFR) | 12,273 | 420 | 6,076 | 256 | 5,723 | 56 |
| Stay (20 min FFR) | 7,138 | 306 | 3,575 | 200 | 3,305 | 35 |
| Leave after 20 min | 5,199 | 121 | 2,539 | 63 | 2,442 | 21 |
| Stay (FFR) | 8 | 0 | 4 | 0 | 4 | 0 |
| (b) 15 g/m^2 | | | | | | |
| Stay (No FFR) | 6,021 | 214 | 2,989 | 133 | 2,802 | 28 |
| Stay (20 min FFR) | 3,878 | 166 | 1,945 | 109 | 1,793 | 19 |
| Leave after 20 min | 2,206 | 54 | 1,082 | 29 | 1,033 | 9 |
| Stay (FFR) | 4 | 0 | 2 | 0 | 2 | 0 |
| (c) 5 g/m^2 | | | | | | |
| Stay (No FFR) | 1,878 | 81 | 938 | 53 | 871 | 9 |
| Stay (20 min FFR) | 1,162 | 63 | 589 | 44 | 534 | 6 |
| Leave after 20 min | 779 | 25 | 387 | 15 | 362 | 3 |
| Stay (FFR) | 1 | 0 | 1 | 0 | 1 | 0 |

6. Calculation of Human Dose

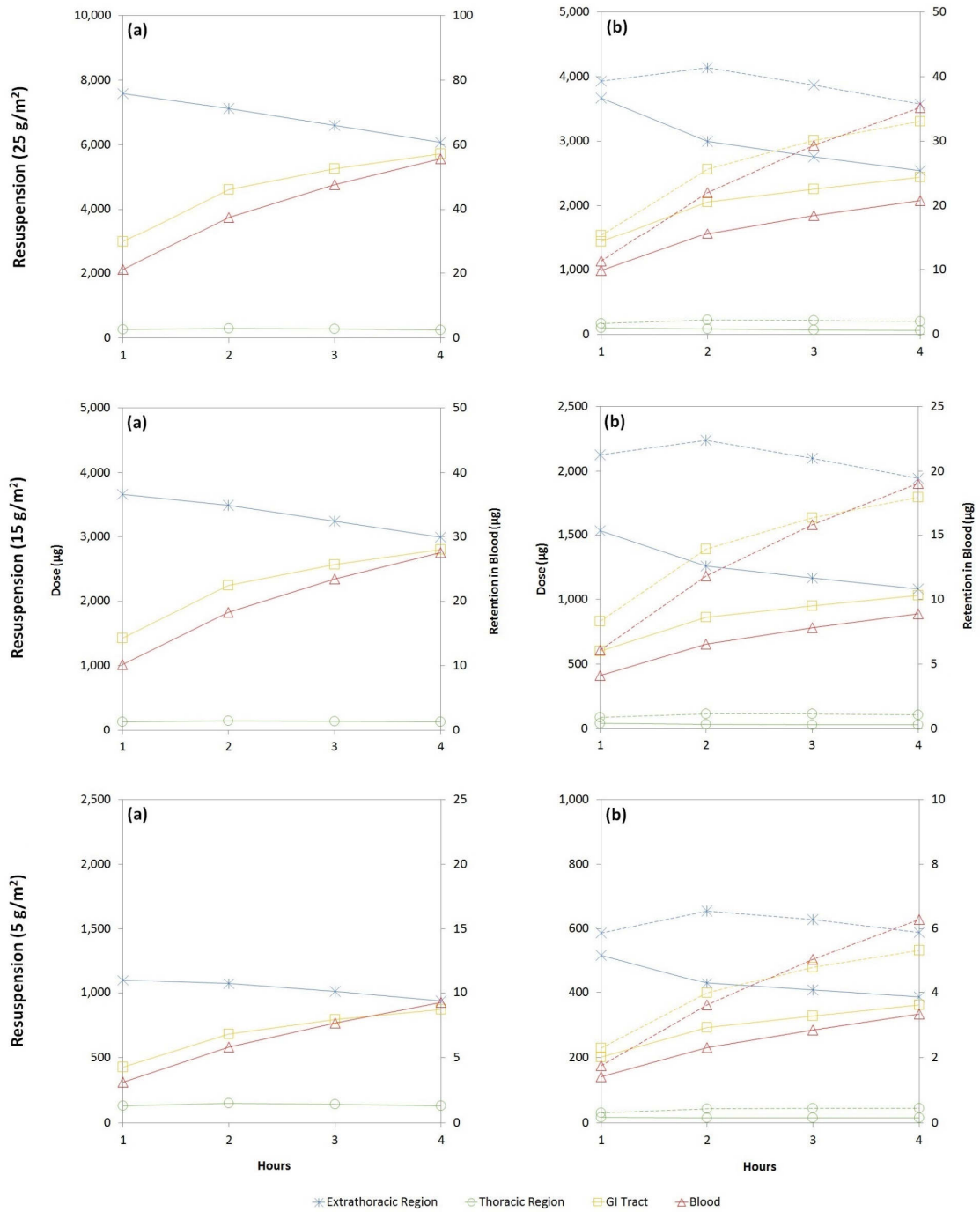


Figure 6.4. Cumulative retention (μg) in extrathoracic and thoracic regions, GI tract, and blood: (a) Stay the entire time period—No FFR; (b) Stay only for the time period of emission—No FFR and then leave (full line), and Stay the entire time period—FFR only during the emission period (dashed line).

6. Calculation of Human Dose

Occupational exposure to respirable crystalline silica (SiO_2) dust particles occurs in many industries (shipbuilding, ironworkers, construction, mining, mills, pottery, glass production, etc.). In spite of optimal regulation in the developed countries, exposure to respirable silica is still a major occupational health problem (Steenland and Ward, 2014). Silicosis is a disabling disease caused by inhalation of crystalline silica and is mostly incurable (Sen et al., 2016). Mycobacterial diseases, airway obstruction, and lung cancer are also associated with silica dust exposure (Leung et al., 2012). Silica, also known as quartz or cristobalite, is made up of fine particles and mainly constitutes of crystalline silica with a diameter less than $10\ \mu\text{m}$ and is easily trapped in the respiratory tract. Most critical problems in diagnosis of silicosis is that patients may develop symptoms even after a long gap from exposure and therefore it is crucial for the clinicians to be aware of occupations with potential silica exposure (Steenland and Ward, 2014).

Mineralogy, particle size distribution and chemical composition of the soil samples were studied jointly with the nutrient content of soil solution from study areas of Crete, including four types of parent rocks with different geological origin, from acidic to ultramafic (Moraetis et al., 2006). Regarding the current research study presented herein, no interrelation between the chemical composition of dust used in the resuspension experiments and the Cretan soil dust was found. This leads to a conclusion that the used dust is not of natural soil origin. More likely, it is attributed to road dust because soil particles as well as anthropogenic metals like Pb and Cr (Watson et al., 1994; Karanasiou et al., 2009) were included in the chemical profile of dust used in the experiments. Furthermore, the high percentage of Ca in the used dust implies the influence of construction activities in the area since sulfate salts such as CaSO_4 and $\text{Al}_2(\text{SO}_4)_3$ are typical cement components. Hence, the dust used in this study most likely originated from construction works on the K2 building (School of Environmental Engineering, TUC) in the time period when the dust collection took place, as suggested also by the chemical analysis.

6.5.2. Human Dose from Arc Welding and Cutting of Stainless Steel

This work estimated the cumulative deposited and retained dose from two arc welding processes (SMAW and TIG) and cutting of stainless steel in a simulated confined workplace. Human dose assessed in ExDoM2 was calculated for 4 different work scenarios including use of respiratory protection. In the first scenario, staying in the polluted workspace for the entire time period without a use of FFR was the ‘worst-case’ scenario and reached the highest values of deposited, and thus retained dose during all processes (Table 6.4 and Figure 6.5). Nonetheless, in the second scenario, when staying in the polluted workspace for the entire time period and FFR is used only for the duration of the emission period (5 min) and then is taken off, deposited dose was somewhat lower, but very similar to the first scenario (especially in the thoracic region), giving 174-fold, 123-fold and 5-fold increase in total deposited dose compared to BC (76 μg) for cutting, SMAW and TIG, respectively.

In the third scenario, as demonstrated in Figure 6.5, it would be more beneficial in respect to deposited dose if the exposed simulated subject not wearing a FFR at the duration of emission, would leave the polluted workspace immediately after the emission period (5 min). In such a case, the increase in total deposited dose was estimated to be 19-fold, 1-fold and 0.3-fold for cutting, SMAW and TIG, respectively, in comparison with the dose from BC. Note that in the case of SMAW in this scenario, compared to the previous two scenarios, the deposited dose decreased significantly because the average PM_{10} concentration during the emission period (when the simulated subject was still present in the polluted workspace) was only 0.45 mg/m^3 , continued increasing and reached its maximum 1 h later (4.19 mg/m^3). The last scenario, accounting for use of FFR for the entire time period while staying in the polluted workspace, was the ‘best-case’ scenario as in this particular case the total deposited dose was much lower than that of BC.

The vast majority of dose in all processes was deposited in the extrathoracic region of the RT (Table 6.4), where the particles were retained (~53%), entered the oesophagus (GI tract) via pharynx (~44%) or were cleared by nose blowing (~3%). From all 3 processes, deposited dose in extrathoracic region from cutting (~91%) was higher

6. Calculation of Human Dose

in every scenario compared to welding processes (~77%). On the contrary, due to higher concentration of fine and ultrafine particles, retained dose in the thoracic region was higher for SMAW and TIG welding processes (~20%) in comparison to cutting (~7%). As can be seen in Figure 6.5a (as the most likely scenario in real life), the cumulative retention in the thoracic region was stable after the cutting, while in the case of SMAW and TIG the retention in thoracic region was increasing with time due to higher contribution of respirable particles. Consequently, 16%, 21% and 8% of the total cumulative dose was deposited in the AI region (where the gas exchange takes place) from SMAW, TIG and cutting, respectively. From dose retained in the thoracic region from both welding processes ~6% was absorbed to blood, while in the case of cutting it was ~10%. Nevertheless, the total deposited dose from cutting after the first 1 h (in which the emission occurred) was 3-fold higher than that from SMAW, after 4 h they had very similar values of blood retention (~100 µg). After 8 h blood retention from SMAW reached 234 µg, while in the case of cutting it was only 180 µg. More importantly, one must consider also the different chemical composition of particles from these two processes deposited and retained in the thoracic region.

Table 6.4. Cumulative deposited dose and cumulative retention (µg) in extrathoracic and thoracic region, GI tract and blood after 4 h: (a) Cutting II, (b) SMAW II and (c) TIG II.

| Scenario/Region | Cum. Deposited Dose | | Cum. Retention | | | |
|-----------------------|---------------------|----------|----------------|----------|-------|-------|
| | Extrathor. | Thoracic | Extrathor. | Thoracic | GI | Blood |
| (a) Cutting II | | | | | | |
| Stay (No FFR) | 13,408 | 1,296 | 6,790 | 1,011 | 6,194 | 106 |
| Stay (5 min FFR) | 12,051 | 1,233 | 6,129 | 970 | 5,552 | 98 |
| Leave after 5 min | 1,414 | 78 | 696 | 54 | 665 | 9 |
| Stay (FFR) | 8 | 1 | 4 | 1 | 4 | 0 |
| (b) SMAW II | | | | | | |
| Stay (No FFR) | 7,540 | 1,942 | 4,238 | 1,725 | 3,176 | 102 |
| Stay (5 min FFR) | 7,497 | 1,931 | 4,217 | 1,715 | 3,155 | 101 |
| Leave after 5 min | 114 | 18 | 63 | 15 | 48 | 1 |
| Stay (FFR) | 5 | 1 | 3 | 1 | 2 | 0 |
| (c) TIG II | | | | | | |
| Stay (No FFR) | 344 | 110 | 189 | 98 | 149 | 6 |
| Stay (5 min FFR) | 331 | 106 | 182 | 95 | 142 | 6 |
| Leave after 5 min | 88 | 10 | 50 | 9 | 35 | 1 |
| Stay (FFR) | 0 | 0 | 0 | 0 | 0 | 0 |

6. Calculation of Human Dose

General ventilation systems, consisting of both supply and exhaust, can be mechanical, natural, or a mixture of both might prevent or minimize the respiratory hazards of welding fume. The most efficient and economical method of welding contaminant control in the breathing zone of the welder is local exhaust that captures the contaminants at or near the source (Flynn and Susi, 2012). When ventilation controls fail to reduce the air contaminants produced by welding to allowable levels (Pouzou et al., 2015) or when the use of ventilation is not feasible (e.g. welding in confined spaces), personal respiratory protective equipment should be used (Lehnert et al., 2012). When welding in a confined space (area with poor ventilation that has limited space, entry or exit, such as storage tanks, holds of ships, boilers, furnaces, tunnels), all the hazards that are associated with welding are amplified (Bowler et al., 2007; Hanley et al., 2015). However, up to this day, there is just a limited research on emission rates and resulting exposure dose from welding in confined workspaces in regards to both, field and simulated studies.

High concentrations of Mn, especially in a confined workspace, can cause a disease known as ‘manganism’, characterized by tremor, muscle weakness and rigidity, extreme slowness of movements, or may cause a progression of parkinsonism (Racette et al. 2017). The amount of Mn in welding rods can vary, but most welders are exposed to mixed metal fumes that contain a small percentage of Mn, which was 0.5% in the electrode used for the experiments in this study (Chapter 4.4), according to the manufacturer. However, latest studies on neurological outcomes associated with low-level Mn exposure suggest that changes can be detected in the brain even at very low levels of exposure among humans before any clinically evident deficits (Baker et al., 2015; Lee et al., 2016), where type and route of exposure play an important role in the extent of Mn-induced toxic effects on the brain (Long et al., 2014). Although the occupational exposure limit (OEL) for Mn vary within the authorities, the American Conference of Governmental Industrial Hygienists (ACGIH) advised threshold limit value (TLV) for Mn to be $20 \mu\text{g}/\text{m}^3$ for respirable and $100 \mu\text{g}/\text{m}^3$ for inhalable PM, which however, can be easily exceeded in a confined workspace (Hanley et al., 2015).

On the other hand, metal fumes that contain iron oxide generated at the cutting of SS are considered a nuisance dust with little likelihood of causing chronic lung disease

6. Calculation of Human Dose

after inhalation. Accumulation of iron oxide in the lungs is called 'siderosis' and is not usually associated with pulmonary fibrosis (lung scarring) and functional impairment of the lungs (Flors Blasco et al., 2010). Abnormalities are reversible and may resolve partially or completely after the worker is removed from the exposure. Moreover, differences between SMAW and TIG welding processes should be addressed with great care as well, even though during TIG significantly less fume is generated, mostly originating from base metal and the external filler metal if used. Brand et al. (2013) monitored the particle size distributions of various welding and joining techniques in standardized laboratory conditions and noted UFP composition differences between processes with high mass emission rates (SMAW) and welding processes with low mass emission rates (TIG). Despite the fact that in all scenarios total dose from TIG in this study had the lowest values, this welding process generates a high number concentration of heavy metal nanoparticles, such as Mn, Cr or Ni (Miettinen et al., 2016) in size range of 15-160 nm (Berlinger et al., 2011).

Although major concerns exist regarding the potential consequences of human exposure to UFP, no human toxicological data is currently available. Study of Andujar et al. (2014) strongly suggest that welding-related UFP could be responsible, at least in part, for the pulmonary inflammation observed in welders. Pr sum  et al. (2015, 2016), based upon metal oxide nanoparticles found in lung tissue sections of welders, investigated pulmonary effects in mice of repeated exposure to nanoparticles and demonstrated for the first time a potential risk for respiratory health posed by repeated exposure to nanoparticles at occupationally relevant doses. These results provide therefore the first evidence of a link between human exposure to nanoparticles and long-term pulmonary effects. Furthermore, Halatek et al. (2017) confirmed deleterious effect of transitory metals (Cr^{VI} , Mn, Ni) and particles during experimental inhalation exposure to welding dusts, evidenced in the lungs and brain in serum of rats. Their result confirms also the hypothesis about the effect of the welding dusts on the oxidative stress responsible for disturbed systemic homeostasis and impairment of calcium regulation.

6. Calculation of Human Dose

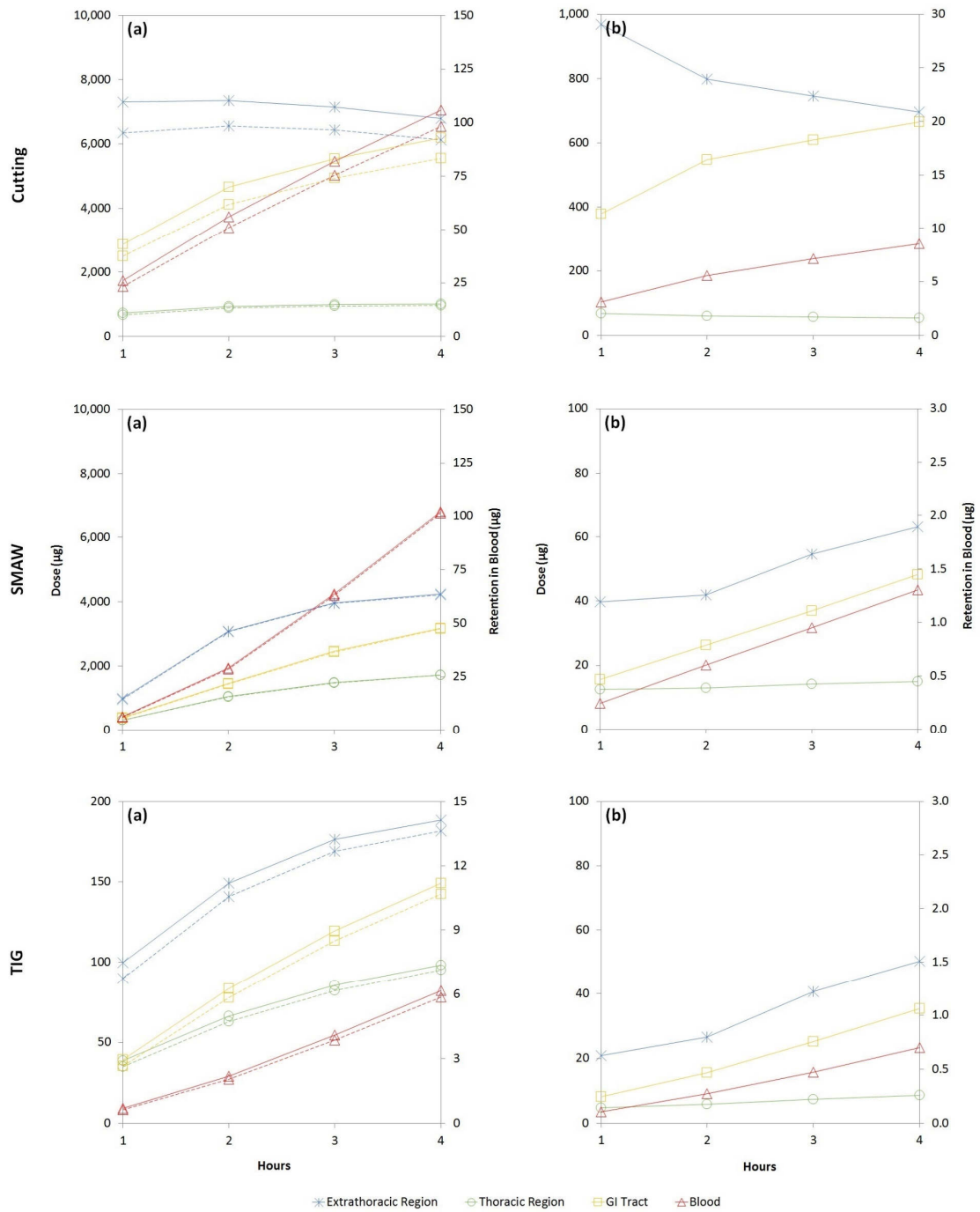


Figure 6.5. Cumulative retention (μg) in RT (extrathoracic and thoracic regions), Thoracic region, GI tract, and blood (sec. axis): (a) Stay all the time period—No FFR (full line), and Stay all the time period—FFR only during the emission period (dashed line); (b) Stay only for the time period of emission (first 5 min)—No FFR and then leave.

6.6. Study Limitations and Recommendations

There are several study limitations, mainly of experimental character, which must be addressed. Human dose calculated from particle number concentration was sampled by NanoScan SMPS. However, this instrument has low size resolution (13 size channels in size range of 10-350 nm) and many times low accuracy in estimating the particle size. In order to sample the particle size in detail with higher accuracy and wider size range, a SMPS (or FMPS) with high time and particle size resolution up to 1000 nm might be required. Furthermore, ExDoM2 lacks model calculations of clearance, retention and absorption from particle number concentration. Investigation of the mechanism of nanoparticle translocation is an active research area, which is exceptionally crucial. If the inhaled nanoparticles, particularly engineered, cross the lung epithelium and become bloodborne, they may have the potential to gain access to the blood–brain barrier, likely resulting in adverse health effects.

Mass concentration was sampled with an instrument based on 120° light scatter (i.e. depending on the particle's refraction index), hence, measured optical diameter needed to be converted to aerodynamic diameter in order to use the data as an input in the ExDoM2 model. The conversion was done under assumptions that optical diameter equals Stokes diameter, and that the particle density and shape factor are those of the sampled aerosol. This is in many cases (such as in this study) difficult to determine and approximate values are used, which in return, along with the conversion from optical to aerodynamic diameter, can result in incorrect estimation of the particle's diameter. These limitations could be eluded by cascade impactor sampling with an adequate filter, which allows for detailed chemical analysis of heavy metals (Mn, Cr, Ni, etc.) in the solid component of aerosols from the filter samples with destructive (e.g. ICP-MS) or non-destructive (e.g. XRF) analytical method (Korzhova et al., 2016).

Short emission periods in the case of welding processes were based on limitations of the used instrumentation where after certain concentration limit flowrate and coincidence error occurred. However, exposures are dependent on many influencing factors, and especially time-weighted proximity to the emissions from both distant and localized sources can encounter exposure scenarios that can produce significant human

6. Calculation of Human Dose

doses. This leads us to another limitation, which is the actual distance of the sampling point to the simulated subject's breathing zone. Although in this study the aerosol concentration in the chamber experiments was assumed to be uniform, the distance of the sampling point from the emission source was 0.5 m during measurements of printer emissions, and 1.2 m in the case of arc welding and cutting of SS. In the experiments conducted in the laboratory (NPFE and dust resuspension) the distance of the emission source from the sampling point was ~0.5 m. On the contrary, during sampling in the print room the sampling point was ~2 m to the closest printer and ~4 m to the farthest printer since closer distances were not feasible for practical reasons.

Distances 2-5 m from the emission source are sufficient to describe the general background of air pollution in a workroom, but are deficient for determination of personal exposure. The distance of sampling point should be in the radius of ~30 cm from the subject's head (Hariri et al., 2013), preferably sampled by personal sampling method (Quémerais et al., 2015), e.g. with Sioutas Personal Cascade Impactor, so that solution with fixed sampling position is avoided, especially in cases such as welding processes. Additionally, there were another ~1.2 m of horizontal tubing and flow splitters in the chamber experiments, and even though transport losses correction for mass concentration was accounted for, in the case of sampling by an impactor, such a sampling is incorrect. Moreover, the sampling would have to be done by an impactor placed inside the chamber (or by several impactors in order to obtain hourly size distributions) near the emission source, which was not feasible solution in the experiments conducted in this study.

The scenarios involving use of FFR were based on FFR filter efficiency only in means of model calculations, i.e. FFR was not challenged with actual emissions from painting materials, printers, dust nor welding fumes. Thus, pressure drop caused by accumulated dust or welding fumes on the filter (Cho and Yoon, 2012) and its effect on FFR's performance was not taken into consideration. Another assumption was that the filtering facepiece fits perfectly and there are no leaks around the face seal. However, penetration levels can increase up to ~50% when the respirator does not have a perfect fit, which is difficult to achieve especially in the nose-bridge area of the FFR. Nonetheless, scenario variant with FFR that does not have a perfect fit could not be examined due to lack of experimental data from FFR testing. In addition, as demonstrated

6. Calculation of Human Dose

earlier, most FFRs offer efficient protection against particles larger than ~400 nm, but may be ineffective in providing the expected respiratory protection for workers exposed to nanoparticles. Despite the fact that a poor filtration efficiency and a poor fit may increase under real work conditions, the use of FFR especially in a confined workspace can considerably reduce the exposure to nanoparticles and particulate matter.

Further limitations are rather of general character and include parameters, which are specific for each work environment. Including— gender, work scenario and type of breathing (nose breathing may change to mouth type breathing under heavy work conditions or higher air temperatures), blood absorption behavior (depending on the chemical composition and size of the particles), determination of adequate reference background concentration (if required for the comparison with the FFR efficiency), wind speed and/or air exchange rate of the workplace, or the time which the dose is calculated for. The latter refers to cumulative deposited and retained dose over rather longer time periods of exposure (months or years) and the health status of the subject, e.g. when the dose from the previous time period is not cleared, hence is accumulating in the organism in time, possibly resulting in adverse health effects (Hannu et al., 2007; Wittczak et al., 2012). Therefore, in order to estimate the relevant deposited and retained dose from any work environment with higher accuracy, all the parameters and conditions should be taken into consideration since generalization of these could result in false human dose estimation.

6.7. Conclusions

Human dose from various indoor workplace related aerosol sources was assessed for extrathoracic and thoracic region in ExDoM2 model. Dose rates were calculated for different scenarios for emissions from painting materials, printers, resuspended dust, and arc welding. During emissions from painting materials, the average increase of total dose represented 4.6 and 1.3-fold at emission and post-emission period, respectively, compared to the exposure dose from BC. On the other hand, increase of total dose in the PR represented 13.4 and 1.2-fold at printers' startup and printing, respectively, in

6. Calculation of Human Dose

comparison to the BC exposure. Vast majority ($\geq 93\%$) of all particles generated from both, painting material and printers' emissions, were in the ultrafine size range.

Cumulative deposited and retained dose from mass concentrations was estimated for 4 different scenarios and 2 types of emission sources, dust resuspended while walking, and arc welding processes. Examination of different scenarios revealed that: (1) In both emission cases, the first scenario, staying in the polluted workspace for the entire time period without a use of FFR was the 'worst case' scenario, while the last scenario, accounting for use of FFR for the entire time period, was the 'best case' scenario where the total deposited dose was much lower than that of BC; and (2) It would be more beneficial in respect to total deposited dose if the exposed simulated subject not wearing FFR at the duration of emission, would leave the polluted workspace immediately after the end of emission rather than stay the entire time period and use FFR only during the emission period. However, due to very small contribution of fine particles in the resuspended dust, only ~4% of total dose were deposited in the thoracic region. On the contrary, due to higher concentration of fine and ultrafine particles, retained dose in the thoracic region (the lungs) was higher for arc welding processes (~20%) compared to cutting (~7%) and resuspended dust.

The related health effects due to exposure to the hereby examined emission sources vary significantly and depend mainly on the concentration, time of exposure and chemical composition of the aerosol particles. As shown, FFRs examined in Chapter 5 would significantly reduce the exposure levels and protect the user in most of the cases (under assumption that the FFR has a perfect fit and there are no leaks) if worn at all times in the polluted workplace. Empirical aerosol particle deposition models, such as ExDoM2, can provide a quantitative estimate of the amount of material deposited in the RT under certain conditions. However, there are certain limitations which should be eluded in order to estimate the relevant deposited and retained dose from any work environment with higher accuracy.

7. Conclusions and Recommendations

7.1. General Conclusions

Estimation of emission rates of 4 different aerosol sources was presented in Chapter 4. Two aerosol emission sources that contribute to high particle number concentrations and two emissions that are characterized by high mass concentrations were examined. In the first part, emissions from painting materials in an indoor microenvironment were investigated. Painting activity and use of turpentine oils were selected as a source of emission. While painting itself did not increase the indoor particle concentration, emissions from opened turpentine oil bottles used for painting were identified as a significant source of indoor emissions resulting in a burst of new particles inside the laboratory. Second part of Chapter 4 presented a one-week sampling conducted in the print room of the IT & Communications Center where 4 printers are located. Additionally, evolution of particle size distributions with time and printed pages was also studied in detail in an experimental chamber. The results confirmed that the major contribution to indoor PN concentrations originated from printer emissions in long-term exposures. Printers' startup in PR was characterized by sharp increase in PN concentrations, similarly as it was observed in the chamber study. Printer examined in the chamber was generating nanoparticles (< 50 nm) primarily during cold startup.

Next study focused on the estimation of resuspension rate by human-induced walking inside a laboratory. Four different dust loadings were used to cover the floor and two walking pattern were applied. The resuspension rate for PM_{10} was estimated in the range of $10^{-2} - 10^3$ h^{-1} , which is in agreement with previous studies. As expected, different dust loadings on the floor contributed directly to the increase of indoor particle mass concentration, but had no effect on the resuspension rate. Last part of Chapter 4 describes SMAW and TIG arc welding processes and cutting of SS in a simulated confined workspace. Among all 3 processes, PM_{10} concentrations from cutting reached the highest mass concentrations, while SMAW had the highest contribution of fine particles, consisting mostly of $PM_{1-2.5}$ fraction. All 3 investigated processes generated also high PN concentrations ranging from 2.4 to 3.6×10^6 $\#/cm^3$.

7. Conclusions and Recommendations

Chapter 5 shows the study of percentage penetrations of CE-marked FFRs, which were experimentally determined by a size-resolved method (20-400 nm CMD) of measuring penetrations of filters cut out from FFRs, and measurements of identical FFRs tested in a manikin-based study. As expected, penetration differences between 2 filters from same respirator and between 2 identical respirators were identified as well as variations in total penetrations in all 3 protection classes. In overall, 21 out of 46 filters tested with the size-resolved method in this study exceeded the percentage penetration limit set by EN 149. Results presented in this chapter confirmed the disadvantages of standard filter penetration test method, which underestimates the particle penetration, especially in the nanoparticle size range. Size-resolved penetrations obtained in this study were then used for calculation of human dose in scenarios including FFR.

Last chapter of this dissertation deals with human dose from aerosol sources investigated in Chapter 4. Human dose was assessed in ExDoM2 model. Average increase of total dose during emissions from painting materials and printers was several folds higher compared to the exposure dose of background concentration. However, results also suggest that FFR would effectively protect the user in most cases during the emission period if worn at all times. Furthermore, cumulative deposited and retained dose from mass concentrations was estimated for different scenarios for dust resuspended while walking, and arc welding and cutting processes. As expected, results of different scenarios revealed that staying in the polluted workspace for the entire time period without a use of FFR was the ‘worst case’ scenario. On the contrary, results suggest that use of FFR for the entire time period in the polluted workplace can significantly reduce the exposure to harmful airborne contaminants. Empirical aerosol particle deposition models, such as the one used in this study, can provide a quantitative estimate of the amount of material deposited in the human respiratory tract under certain conditions.

7.2. Recommendations for Future Work

Estimation of emission rates is an important juncture in assessment of the indoor particle dynamics. However, in order to assess the exposure dose in real workplace environment, it is recommended that focus should be on detailed personal sampling. Particularly in

7. Conclusions and Recommendations

confined workspaces where ventilation controls fail to reduce the air contaminants to allowable levels or the use of ventilation is not feasible. As mentioned earlier, distances 2-5 m from the emission source are sufficient to describe the general background of air pollution in a workroom, as it was in the case of the research presented herein. Hence, determination of personal exposure with personal sampling method in real workplace environment (where solutions with fixed sampling position are avoided) in combination with detailed controlled study is necessary.

Although majority of the studies primarily address the filtering performance of FFRs, other studies evaluate the aspects directly affecting the overall facepiece performance, such as pressure drop, particle loading, and humidity effects under different flow rates. Given the high filtration efficiency and perfect fit of FFR, next thing to be concerned about is the performance of FFR under 'real-world' conditions. Studies of aforementioned filtering facepiece characteristics are conducted in the laboratory under controlled conditions, i.e. steady flow conditions, constant particle concentration, and flow rate. In reality, FFRs are used in situations where the flow rate, particle concentration, and relative humidity vary in time, but most importantly, test aerosol used to certificate these FFRs differs from nanoparticles, which workers are exposed to in their actual workplaces. Therefore, to prevent occupational diseases and their adverse effects on the workers' health, it is necessary to investigate the performance of filtering facepieces, especially filtration efficiency against engineered nanoparticles (such as carbon nanotubes) under different flow rates and humidity conditions, which represent the 'real-world' conditions better than laboratory set up used for FFRs certification.

Distribution of mainly metal components in airborne contaminants in the human respiratory tract is well studied in regards to both, dose modelling and toxicological studies. Models that can predict behavior of nanoparticles in the respiratory tract exist. However, in the context of empirical aerosol dose model employed in the current research, focus should be on development of an additional tool for calculation of deposition and retention of nanoparticles in the respiratory tract, which is missing in the current version of the model. One of the major concerns regarding the possible toxic effects of nanoparticles is the capacity of these materials to penetrate cells and potentially translocate to other cells, tissues, and organs remote from the portal of entry to the body.

REFERENCES

- Abt, E., Suh, H.H., Catalano, P. and Koutrakis, P. (2000). Relative contribution of outdoor indoor particle sources to indoor concentrations. *Environ. Sci. Technol.* 34, 3579-3587.
- ACGIH (2013). Manganese, Elemental and Inorganic Compounds. TLV Chemical Substances 7th Edition Documentation. Cincinnati, OH: ACGIH.
- Aleksandropoulou, V. and Lazaridis, M. (2013). Development and application of a model (ExDoM) for calculating the respiratory tract dose and retention of particles under variable exposure conditions. *Air Qual. Atmos. Health*, 6, 13-26.
- Almeida, S.M., Canha, N., Silva, A. et al. (2011). Children exposure to atmospheric particles in indoor of Lisbon primary schools. *Atmos. Environ.* 45, 7594–7599.
- Anderson, H.R. (2009) Air pollution and mortality: A history. *Atmos. Environ.* 43, 142-152.
- Andujar, P., Simon-Deckers, A., Galateau-Sallé, F. et al. (2014). Role of metal oxide nanoparticles in histopathological changes observed in the lung of welders. Part. *Fibre Toxicol.* 11, Art. no.23.
- Antonini, J.M. (2006). Design, construction and characterization of a novel robotic welding fume generator and inhalation exposure system for laboratory animals. *J. Occup. Environ. Hyg.* 3, 194–203.
- Antonini, J.M. (2014). Health Effects Associated with Welding. In *Comprehensive Materials Processing*, Volume 8 (pp. 49-70). Elsevier, ISBN: 978-0-08-096533-8.
- Antonini, J.M., Keane, M., Chen, B.T. et al. (2011). Alterations in welding process voltage affect the generation of ultrafine particles, fume composition, and pulmonary toxicity. *Nanotoxicol.* 5, 700-710.
- Aoki, T. and Tanabe, S.-I. (2007). Generation of sub-micron particles and secondary pollutants from building materials by ozone reaction. *Atmos. Environ.* 41, 3139-3150.
- Asgharian, B., Wood, R. and Schlesinger, R. B. (1995). Empirical modeling of particle deposition in the alveolar region of the lungs: A basis for interspecies extrapolation. *Fund. Appl. Toxicol.* 27, 232-238.
- Austin, J., Brimblecombe, P. and Sturges, W.T. (2002). *Air Pollution Science for the 21st Century*, First Edition, Elsevier. ISBN: 978-0-0805-2690-4.

- Avino, P., Manigrasso, M., Pandolfi, P., Tornese, C., Settimi, D. and Paolucci, N. (2015). Submicron particles during macro-and micro weldings procedures in industrial indoor environments and health implications for welding operators. *Metals* 5, 1045-1060.
- Baker, M.G., Criswell, S.R., Racette, B.A., Simpson, C.D., Seixas, N.S., Checkoway, H. and Sheppard, L. (2015). Neurological outcomes associated with low-level manganese exposure in an inception cohort of asymptomatic welding trainees. *Scand. J. Work. Environ. Health* 41, 94-101.
- Balazy, A., Toivola, M., Adhikari, A., Sivasubramani, S.K., Reponen, T. and Grinshpun, S.A. (2006a). Do N95 respirators provide 95% protection level against airborne viruses, and how adequate are surgical masks? *Am. J. Infect. Control* 34, 51-57.
- Balazy, A., Toivola, M., Reponen, T., Podgórski, A., Zimmer, A. and Grinshpun, S.A. (2006b). Manikin-based performance evaluation of N95 filtering-facepiece respirators challenged with nanoparticles. *Ann. Occup. Hyg.* 50, 259-269.
- Banga, A., Reilly, M.J. and Rosenman, K.D. (2011). A study of characteristics of Michigan workers with work-related asthma exposed to welding. *J. Occup. Environ. Med.* 53, 415-419.
- Barrett, L.W. and Rousseau, A.D. (1998). Aerosol loading performance of electret filter media. *Am. Ind. Hyg. Assoc. J.* 59, 532-539.
- Barthel, M., Pedan, V., Hahn, O., Rothhardt, M., Bresch, H., Jann, O., and Seeger, S. (2011). XRF analysis of fine and ultrafine particles emitted from laser printing devices. *Environ. Sci. Technol.*, 45, 7819-7825.
- Bateman, A.P., Belessein, H. and Martin, S.T. (2014). Impactor apparatus for the study of particle rebound: Relative humidity and capillary forces. *Aerosol Sci. Tech.* 48, 42-52.
- Bekö, G., Clausen, G., and Weschler, C.J. (2008). Is the use of particle air filtration justified? Costs and benefits of filtration with regard to health effects, building cleaning and occupant productivity. *Build. Environ.*, 43, 1647–1657.
- Bello, D., Martin, J., Santeufemio, C., Sun, Q., Lee Bunker, K., Shafer, M., and Demokritou, P. (2013). Physicochemical and morphological characterisation of nanoparticles from photocopiers: Implications for environmental health. *Nanotoxicology*, 7, 989-1003.
- Bergman, M.S., Viscusi, D.J., Zhuang, Z., Palmiero, A.J., Powell, J.B. and Shaffer, R.E. (2012). Impact of multiple consecutive donnings on filtering facepiece respirator fit. *Am. J. Infect. Control* 40, 375-380.

- Berlinger, B., Benker, N., Weinbruch, S. et al. (2011). Physicochemical characterisation of different welding aerosols. *Anal. Bioanal. Chem.* 399, 1773–1780.
- Betha, R., Selvam, V., Blake, D.R. and Balasubramanian, R. (2011). Emission characteristics of ultrafine particles and volatile organic compounds in a commercial printing center. *J. Air Waste Manage.* 61, 1093–1101.
- Boor, B.E., Siegel, J.A. and Novoselac, A. (2013). Monolayer and multilayer particle deposits on hard surfaces: Literature review and implications for particle resuspension in the indoor environment. *Aerosol Sci. Tech.* 47, 831-847.
- Bowler, R.M., Nakagawa, S., Drezgic, M. et al. (2007). Sequelae of fume exposure in confined space welding: A neurological and neuropsychological case series. *Neurotoxicology* 28, 298-311.
- Brand, P., Lenz, K., Reisinger, U. and Kraus, T. (2013). Number size distribution of fine and ultrafine fume particles from various welding processes. *Ann. Occup. Hyg.* 57, 305-313.
- Britigan, N., Alshawa, A., and Nizkorodov, S. A. (2006). Quantification of Indoor Ozone Levels in Indoor Environments Generated by Ionization and Ozonolysis Air Purifiers. *J. Air Waste Manage. Assoc.*, 56, 601–610.
- Brook, R.D., Rajagopalan, S., Pope, C.A. et al. (2010). Particulate matter air pollution and cardiovascular disease: An update to the scientific statement from the American Heart Association. *Circulation* 121, 2331-2378.
- Brosseau, L.M. (1998). Aerosol penetration behavior of respirator valves. *Am. Ind. Hyg. Assoc. J.* 59, 173-180.
- Brosseau, L.M., Chen, S.-K., Vesley, D. and Vincent, J.H. (1994). System design and test method for measuring respirator filter efficiency using mycobacterium aerosols. *J. Aerosol Sci.* 25, 1567-1577.
- Brosseau, L.M., Evans, J.S. and Ellenbecker, M.J. (1993). An empirical model for estimating the collection efficiency of dust-mist respirators. *Ann. Occup. Hyg.* 37, 135-150.
- Brosseau, L.M., Evans, J.S., Ellenbecker, M.J. and Feldstein, M.L. (1989). Collection Efficiency of Respirator Filters Challenged with Monodisperse Latex Aerosols. *Am. Ind. Hyg. Assoc. J.* 50, 544-549.
- BS EN (2001). Respiratory protective devices. Filtering half masks to protect against particles—Requirements, testing, marking. London, UK: BSI British Standards. BS EN 149.

- BS EN (2008). Respiratory protective devices. Methods for test—Part 7: determination of particle filter penetration. London, UK: BSI British Standards. BS EN 13274-7.
- Bzdek, B.R., Pennington, R. and Johnston, M.V. (2012). Single particle chemical analysis of ambient ultrafine aerosol: A review. *J. Aerosol Sci.* 52, 109-120.
- Cao, A.-G., Yu, G., Chen, Y.-S., Cao, Q.-M., Fiedler, H., Deng, S.-B., Huang, J. and Wang, B. (2012). Particle size: A missing factor in risk assessment of human exposure to toxic chemicals in settled indoor dust. *Environ. Int.* 49, 24-30.
- Carpenter, R.L. and Kimmel, E.C. (1999). Aerosol deposition modeling using ACSL. *Drug Chem. Toxicol.* 22, 73-90.
- Castellano, P., Canepari, S., Ferrante, R. and L'Episcopo, N. (2012). Multiparametric approach for an exemplary study of laser printer emissions. *J. Environ. Monit.*, 14, 446-454.
- Cavender, F. (1994). Alicyclic hydrocarbons. In: Clayton G.D. and Clayton F.E., eds. *Patty's industrial hygiene and toxicology, Vol II, Part B.* New York: John Wiley & Sons. pp. 1267-1300.
- Chalvatzaki, E. and Lazaridis, M. (2015). Development and application of a dosimetry model (ExDoM2) for calculating internal dose of specific particle-bound metals in the human body. *Inhal. Toxicol.*, 27, 308-320.
- Chalvatzaki, E., Kopanakis, I., Kontaksakis, M., Glytsos, T., Kalogerakis, N. and Lazaridis, M. (2010). Measurements of particulate matter concentrations at a landfill site (Crete, Greece). *Waste Manage.* 30, 2058-2064.
- Chatoutsidou, S.E., Ondráček, J., Tesař, O., Tørseth, K., Ždímal, V. and Lazaridis, M. (2015). Indoor/outdoor particulate matter number and mass concentration in modern offices. *Build. Environ.* 92, 462–474.
- Chatoutsidou, S.E., Serfozo, N., Glytsos, T., and Lazaridis, M. (2017). Multi-zone measurement of particle concentrations in a HVAC building with massive printer emissions: influence of human occupation and particle transport indoors. *Air Qual. Atmos. Health*, DOI: 10.1007/s11869-017-0461-4.
- Chen, C. and Zhao, B. (2011). Review of relationship between indoor and outdoor particles: I/O ratio, infiltration factor and penetration factor. *Atmos. Environ.* 45, 275-288.
- Chen, C.-C. and Willeke, K. (1992). Aerosol penetration through surgical masks. *Am. J. Infect. Control* 20, 177-184.

- Chen, C.-C., Lehtimäki, M. and Willeke, K. (1992). Aerosol penetration through filtering facepieces and respirator cartridges. *Am. Ind. Hyg. Assoc. J.* 53, 566-574.
- Chen, C.-C., Ruuskanen, J., Pilacinski, W. and Willeke, K. (1990). Filter and leak penetration characteristics of a dust and mist filtering facepiece. *Am. Ind. Hyg. Assoc. J.* 51, 632-639.
- Chen, S.-C., Wang, J., Bahk, Y.K., Fissan, H. and Pui, D.Y.H. (2014). Carbon nanotube penetration through fiberglass and electret respirator filter and nuclepore filter media: Experiments and models. *Aerosol Sci. Technol.* 48, 997-1008.
- Chen, S.-K., Vesley, D., Brosseau, L.M. and Vincent, J.H. (1994). Evaluation of single-use masks and respirators for protection of health care workers against mycobacterial aerosols. *Am. J. Infect. Control* 22, 65-74.
- Chen, X. and Hopke, P.K. (2009). A chamber study of secondary organic aerosol formation by linalool ozonolysis. *Atmos. Environ.* 43, 3935-3940.
- Cho, H.-W. and Yoon, C.-S. (2012). Workplace field testing of the pressure drop of particulate respirators using welding fumes. *Ann. Occup. Hyg.* 56, 948-958.
- Churg A. (2000). Particle uptake by epithelial cells. In *Particle-lung interactions*, P. Gehr, C. Mühlfeld, B. Rothen-Rutishauser, F. Blank (ed.). New York: Marcel Dekker, pp. 401–435.
- Ciotti, C., Pellissier, G., Rabaud, C., Lucet, J.-C., Abiteboul, D. and Bouvet, E. (2012). Effectiveness of respirator masks for healthcare workers, in France. *Med. Maladies Infect.* 42, 264-269.
- Coffey, C.C., Campbell, D.L. and Zhuang, Z. (1999). Simulated workplace performance of N95 respirators. *Am. Ind. Hyg. Assoc. J.* 60, 618-624.
- Coffey, C.C., Lawrence, R.B. Campbell, D.L., Zhuang, Z., Calvert, C.A. and Jensen, P.A. (2004). Fitting Characteristics of Eighteen N95 Filtering-Facepiece Respirators. *J. Occup. Environ. Hyg.* 1, 262-271.
- Coleman, B.K., Lunden, M.M., Destailats, H. and Nazaroff, W.W. (2008). Secondary organic aerosol from ozone-initiated reactions with terpene-rich household products. *Atmos. Environ.* 42, 8234-8245.
- Comer, J.K., Kleinstreuer, C. and Zhang, Z. (2001). Flow structures and particle deposition patterns in double-bifurcation airway models. Part 2. Aerosol transport and deposition. *J. Fluid Mech.* 435, 25-54.

- Corsi, R.L., Siegel, J.A. and Chiang, C. (2008). Particle resuspension during the use of vacuum cleaners on residential carpet. *J. Occup. Environ. Hyg.* 5, 232-238.
- Curtius, J. (2006). Nucleation of atmospheric aerosol particles. *C. R. Phys.* 7, 1027-1045.
- Cusack, M., Alastuey, A. and Querol, X. (2013). Case studies of new particle formation and evaporation processes in the western Mediterranean regional background. *Atmos. Environ.* 81, 651-659.
- Debia, M., Weichenthal, S. and Dufresne, A. (2014). Case study: Ultrafine particles exposure in apprentice welders. *J. Occup. Environ. Hyg.* 11, D1-D9.
- Destailhats, H., Maddalena, R.L., Singer, B.C., Hodgson, A.T. and McKone, T.E. (2008). Indoor pollutants emitted by office equipment: a review of reported data and information needs. *Atmos. Environ.* 42, 1371-1388.
- Dhawan, A. and Sharma, V. (2010). Toxicity assessment of nanomaterials: Methods and challenges. *Anal. Bioanal. Chem.*, 398, 589-605.
- Donaldson, K., Aitken, R., Tran, L., Stone, V., Duffin, R., Forrest, G. and Alexander, A. (2006). Carbon nanotubes: a review of their properties in relation to pulmonary toxicology and workplace safety. *Toxicol. Sci.*, 92, 5-22.
- Dudek, W., Wittczak, T., Świerczyńska-Machura, D., Walusiak-Skorupa, J. and Pałczyński, C. (2009). Occupational asthma due to turpentine in art painter - case report. *Int. J. Occup. Med. Environ. Health* 22, 293-295.
- Edman, K., Löfstedt, H., Berg, P. et al. (2003). Exposure assessment to α and β -pinene, Δ^3 -carene and wood dust in industrial production of wood pellets. *Ann. Occup. Hyg.* 47, 219-226
- Endo, M., Strano, M.S. and Ajayan, P.M. (2008). Potential applications of carbon nanotubes. *Topics in Appl. Physics* 111, 13-62.
- Eninger, R.M., Honda, T., Adhikari, A., Heinonen-Tanski, H., Reponen, T. and Grinshpun, S.A. (2008). Filter performance of N99 and N95 facepiece respirators against viruses and ultrafine particles. *Ann. Occup. Hyg.* 52, 385-396.
- Ennan, A.A., Kiro, S.A., Oprya, M.V. and Vishnyakov, V.I. (2013). Particle size distribution of welding fume and its dependency on conditions of shielded metal arc welding. *J. Aero Sci.* 64, 103-110.
- Fan, Z., Weschler, C.J., Han, I.-K. and Zhang, J. (2005). Co-formation of hydroperoxides and ultra-fine particles during the reactions of ozone with a complex VOC mixture under simulated indoor conditions. *Atmos. Environ.* 39, 5171-5182.

- Ferro, A.R., Kopperud, R.J. and Hildemann, L.M. (2004). Source strengths for indoor human activities that resuspend particulate matter. *Environ. Sci. Technol.* 38, 1759-1764.
- Fisk, W.J., Faulkner, D., Sullivan, D. and Mendell, M.J. (2000). Particle concentrations and sizes with normal and high efficiency air filtration in a sealed air-conditioned office building. *Aerosol Sci. Technol.* 32, 527–544.
- Flanagan, M.E., Seixas, N., Majar, M., Camp, J. and Morgan, M. (2003). Silica dust exposures during selected construction activities. *Am. Ind. Hyg. Assoc. J.* 64, 319-328.
- Flors Blasco, L., Domingo, M.L., Leiva-Salinas, C., Mazón, M., Roselló-Sastre, E., Vilar, J. (2010). Uncommon occupational lung diseases: High-resolution CT findings. *Am. J. Roentgenol.* 194, W20-W26.
- Flynn, M.R. and Susi, P. (2003). Engineering controls for selected silica and dust exposures in the construction industry - A review. *Appl. Occup. Environ. Hyg.* 18, 268-277.
- Flynn, M.R. and Susi, P. (2012). Local exhaust ventilation for the control of welding fumes in the construction industry - A literature review. *Ann. Occup. Hyg.* 56, 764-776.
- Franck, U., Herbarth, O., Röder, S. et al. (2011). Respiratory effects of indoor particles in young children are size dependent. *Sci. Total Environ.* 409, 1621-1631.
- Fromme, H., Twardella, D., Dietrich, S., Heitmann, D., Schierl, R., Liebl, B. and Rüden, H. (2007). Particulate matter in the indoor air of classrooms – exploratory results from Munich and surrounding area. *Atmos. Environ.* 41, 854–866.
- Fuchs, N.A. (1963). On the stationary charge distribution on aerosol particles in a bipolar ionic atmosphere. *Geofis. Pura Appl.* 56, 185-193.
- Gao, S., Kim, J., Yermakov, M. et al. (2016). Performance of N95 FFRs Against Combustion and NaCl Aerosols in Dry and Moderately Humid Air: Manikin-based Study. *Ann. Occup. Hyg.* 60, 748-760.
- Géhin, E., Ramalho, O. and Kirchner, S. (2008). Size distribution and emission rate measurement of fine and ultrafine particle from indoor human activities. *Atmos. Environ.* 42, 8341-8352.

- Glytsos, T., Ondráček, J., Džumbová, L., Kopanakis, I. and Lazaridis M. (2010). Characterization of particulate matter concentrations during controlled indoor activities. *Atmos. Environ.* 44, 1539-1549.
- Gminski, R., Decker, K., Heinz, C. et al. (2011). Genotoxic effects of three selected black toner powders and their dimethyl sulfoxide extracts in cultured human epithelial A549 lung cells in vitro. *Environ. Mol. Mutagen.*, 52, 296-309.
- Goldasteh, I., Ahmadi, G. and Ferro, A.F. (2013a). Wind tunnel and numerical simulation of dust particle resuspension from indoor surfaces in turbulent flows. *J. Adhes. Sci. Technol.* 27, 1563-1579.
- Goldasteh, I., Ahmadi, G. and Ferro, A.F. (2013b). Monte Carlo simulation of micron size spherical particle removal and resuspension from substrate under fluid flows. *J. Aerosol Sci.* 66, 62-71.
- Goldasteh, I., Tian, Y., Ahmadi, G. and Ferro, A.R. (2014). Human induced flow field and resultant particle resuspension and transport during gait cycle. *Build. Environ.* 77, 101-109.
- Gomes, C., Freihaut, J. and Bahnfleth, W. (2007). Resuspension of allergen-containing particles under mechanical and aerodynamic disturbances from human walking. *Atmos. Environ.* 41, 5257-5270.
- Goudie, A.S. (2014). Desert dust and human health disorders. *Environ. Int.* 63, 101-113.
- Graczyk, H., Lewinski, N., Zhao, J., Concha-Lozano, N. and Riediker, M. (2015). Characterization of Tungsten Inert Gas (TIG) Welding Fume Generated by Apprentice Welders. *Ann. Occup. Hyg.* 60, 205-219.
- Grima-Olmedo, C., Ramírez-Gómez, A., Medic-Pejic, L. and García-Torrent, J. (2014). The penetration of respiratory protective devices by respirable solid particles. *J. Aero Sci.* 74, 36-41.
- Grinshpun, S.A., Haruta, H., Eninger, R.M., Reponen, T., McKay, R.T. and Lee, S.-A. (2009). Performance of an N95 filtering facepiece particulate respirator and a surgical mask during human breathing: Two pathways for particle penetration. *J. Occup. Environ. Hyg.* 6, 593-603.
- Guerreiro, C, Gomes, J.F., Carvalho, P., Santos, T.J.G., Miranda, R.M. and Albuquerque, P. (2014). Characterization of airborne particles generated from metal active gas welding process. *Inhal. Toxicol.* 26, 345–352.

- Guingo, M. and Minier, J.-P. (2008). A new model for the simulation of particle resuspension by turbulent flows based on a stochastic description of wall roughness and adhesion forces. *J. Aerosol Sci.* 39, 957-973.
- Guo, Z., Sparks, L.E., Tichenor, B.A. and Chang, J.C.S. (1998). Predicting the emissions of individual VOCs from petroleum-based indoor coatings. *Atmos. Environ.* 32, 231-237.
- Hagström, K., Jacobsen, G., Sigsgaard, T., Schaumburg, I., Erlandsen, M. and Schlunssen, V. (2012). Predictors of monoterpene exposure in the danish furniture industry. *Ann. Occup. Hyg.* 56, 253-263.
- Halatek, T., Stanislawska, M., Kaminska, I., Cieslak, M., Swiercz, R. and Wasowicz, W. (2017). The time-dependent health and biochemical effects in rats exposed to SS welding dust and its soluble form. *J. Environ. Sci. Health A Tox. Hazard. Subst. Environ. Eng.* 52, 265-273.
- Hanley, K.W., Andrews, R., Bertke, S. and Ashley, K. (2015). Manganese Fractionation Using a Sequential Extraction Method to Evaluate Welders Shielded Metal Arc Welding Exposures during Construction Projects in Oil Refineries. *J. Occup. Environ. Hyg.* 12, 774-784.
- Hannu, T., Piipari, R., Tuppurainen, M., Nordman, H. and Tuomi, T. (2007). Occupational asthma caused by stainless steel welding fumes: A clinical study. *Eur. Respir. J.* 29, 85-90.
- Hariri, A., Leman, A.M. and Yusof, M.Z.M. (2013). Experimental study on welding fumes exposure from aluminum metal inert gas (MIG) process. *Adv. Mat. Res.* 701, 382-386.
- Harnish, D.A., Heimbuch, B.K., Husband, M., et al. (2013). Challenge of N95 filtering facepiece respirators with viable H1N1 influenza aerosols. *Infect. Control Hospit. Epidemiol.* 34, 494-499.
- He, C., Morawska, L. and Gilbert, D. (2005). Particle deposition rates in residential houses. *Atmos. Environ.* 39, 3891-3899.
- He, C., Morawska, L. and Taplin, L. (2007). Particle emission characteristics of office printers. *Environ. Sci. Technol.* 41, 6039-6045.
- He, C., Morawska, L., Hitchins, J. and Gilbert, D. (2004). Contribution from indoor sources to particle number and mass concentrations in residential houses. *Atmos. Environ.* 38, 3405-3415.

- He, C., Morawska, L., Wang, H. et al. (2010). Quantification of the relationship between fuser roller temperature and laser printer emissions. *J. Aerosol Sci.*, 41, 523–530.
- He, X., Yermakov, M., Reponen, T., McKay, R.T., James, K. and Grinshpun, S.A. (2013). Manikin-based performance evaluation of elastomeric respirators against combustion particles. *J. Occup. Environ. Hyg.* 10, 203-212.
- Hinds, W.C. (1999). *Aerosol Technology: Properties, Behavior, and Measurement of Airborne Particles*, Second Edition. John Wiley & Sons, New York. ISBN: 978-0-471-19410-1.
- Hobson, A., Seixas, N., Sterling, D. and Racette, B.A. (2011). Estimation of particulate mass and manganese exposure levels among welders. *Ann. Occup. Hyg.* 55, 113-125.
- Hofmann, W. (1996). Modeling techniques for inhaled particle deposition: The state of the art. *J. Aerosol Med.* 9, 369-388.
- Holmes, N.S. (2007). A review of particle formation events and growth in the atmosphere in the various environments and discussion of the mechanistic implications. *Atmos. Environ.* 41, 2183-2201.
- Housiadas, C., Drossinos, Y. and Lazaridis, M. (2004). Effect of small-scale turbulent fluctuations on rates of particle formation. *J. Aerosol Sci.* 35, 545-559.
- Hovorka, J., Braniš, M. (2011). New particle and condensational growth in a large indoor space. *Atmos. Environ.* 45, 2736-2749.
- Huang, C., Willeke, K., Qian, Y., Grinshpun, S.A. and Ulevicius, V. (1998). Method for measuring the spatial variability of aerosol penetration through respirator filters. *Am. Ind. Hyg. Assoc. J.* 59, 461-465.
- Huang, S.-H., Chen, C.-W., Chang, C.-P., Lai, C.-Y. and Chen, C.-C. (2007). Penetration of 4.5 nm to 10 µm aerosol particles through fibrous filters. *J. Aero Sci.* 38, 719-727.
- Huang, Y., Ho, K.F., Ho, S.S.H., Lee, S.C., Yau, P.S. and Cheng, Y. (2011). Physical parameters effect on ozone-initiated formation of indoor secondary organic aerosols with emissions from cleaning products. *J. Hazard. Mater.*, 192, 1787-1794.
- Hussein, T., Dada, L., Juwhari, H. and Faouri, D. (2015). Characterization, fate and re-suspension of aerosol particles (0.3-10 µm): The effects of occupancy and carpet use. *Aerosol Air. Qual. Res.* 15, 2367–2377.
- Hussein, T., Glytsos, T., Ondráček, J. et al. (2006). Particle size characterization and emission rates during indoor activities in a house. *Atmos. Environ.* 40, 4285- 4307.

- Hussein, T., Hruška, A., Dohányosová, P., Džumbová, L., Hemerka, J., Kulmala, M. and Smolík, J. (2009). Deposition rates on smooth surfaces and coagulation of aerosol particles inside a test chamber. *Atmos. Environ.* 43, 905–914.
- Ibrahim, A.H., Dunn, P.F. and Brach, R.M. (2003). Microparticle detachment from surfaces exposed to turbulent air flow: controlled experiments and modeling. *J. Aerosol Sci.* 34, 765-782.
- ICRP (2012). Occupational intakes of radionuclides. *Ann. ICRP*. Publication in advanced Drafting. http://www.icrp.org/docs/Occupational_Intakes_P1_for_consultation.pdf [Last accessed: 29 Apr 2017].
- Isaacs, K.K., Rosati, J.A. and Martonen, T.B. (2013). Modeling Deposition of Inhaled Particles, in *Aerosols Handbook: Measurement, Dosimetry, and Health Effects*, Second Edition, pp. 83–128 (eds. L.S. Ruzer and N.H. Harley), CRC Press, Taylor & Francis Group, FL, USA. ISBN: 978-1-4398-5510-2.
- Järvelä, M., Kauppi, P., Tuomi, T., Luukkonen, R., Lindholm, H., Nieminen, R., Moilanen, E. and Hannu, T. (2013). Inflammatory response to acute exposure to welding fumes during the working day. *Int. J. Occup. Med. Environ. Health* 26, 220-229.
- John, W. (2011). Size Distribution Characteristics of Aerosols, in *Aerosol Measurement: Principles, Techniques, and Applications*, Third Edition, pp. 41-53 (eds. P. Kulkarni, P. A. Baron and K. Willeke), John Wiley & Sons, Inc., Hoboken, NJ, USA. DOI: 10.1002/9781118001684.ch7
- Jones, R.M. and Brosseau, L.M. (2015). Aerosol transmission of infectious disease. *J. Occup. Environ. Med.* 57, 501-508.
- Jung, H., Kim, J., Lee, S., Lee, J., Kim, J., Tsai, P. and Yoon, C. (2014). Comparison of filtration efficiency and pressure drop in anti-yellow sandmasks, quarantine masks, medical masks, general masks, and handkerchiefs. *Aerosol Air Qual. Res.* 14, 991-1002.
- Kagi, N., Fujii, S., Horiba, Y., Namiki, N., Ohtani, Y., Emi, H., Tamura, H. and Kim, Y.S. (2007). Indoor air quality for chemical and ultrafine particle contaminants from printers. *Build. Environ.* 42, 1949–1954.
- Kalivitis, N., Birmili, W., Stock, M. et al. (2008). Particle size distribution in the Eastern Mediterranean troposphere. *Atmos. Chem. Phys.* 8, 6729-6738.

- Kao, H.M., Chang, T.J., Hsieh, Y.F., Wang, C.H. and Hsieh, C.I. (2009). Comparison of airflow and particulate matter transport in multi-room buildings for different natural ventilation patterns. *Energ. Buildings* 41, 966–974.
- Karanasiou, A.A., Siskos, P.A. and Eleftheriadis, K. (2009). Assessment of source apportionment by Positive Matrix Factorization analysis on fine and coarse urban aerosol size fractions. *Atmos. Environ.* 43, 3385-3395.
- Karrasch, S., Simon, M., Herbig, B. et al. (2017). Health effects of laser printer emissions: A controlled exposure study. *Indoor Air*, DOI: 10.1111/ina.12366.
- Kauppi, P., Järvelä, M., Tuomi, T. et al. (2015). Systemic inflammatory responses following welding inhalation challenge test. *Toxicol. Rep.* 2, 357-364.
- Khaleghi, A., Bartlett, K., and Hodgson, M. (2011). Factors affecting ventilation, indoor air quality, and acoustical quality in ‘green’ and non-“green” buildings: a pilot study. *J. Green Build.* 6, 168–180.
- Khatri, M., Bello, D., Gaines, P., Martin, J., Pal, A.K., Gore, R., and Woskie, S. (2013). Nanoparticles from photocopiers induce oxidative stress and upper respiratory tract inflammation in healthy volunteers. *Nanotoxicology*, 7, 1014-1027.
- Khatri, M., Bello, D., Martin, J. et al. (2017). Chronic upper airway inflammation and systemic oxidative stress from nanoparticles in photocopier operators: Mechanistic insights. *NanoImpact*, 5, 133-145.
- Kim, C.S. and Hu, S.C. (2006). Total respiratory tract deposition of fine micrometer-sized particles in healthy adults: Empirical equations for sex and breathing pattern. *J. Appl. Physiol.* 101, 401–412.
- Kim, Y., Gidwani, A., Wyslouzil, B.E. and Sohn, C.W. (2010). Source term models for fine particle resuspension from indoor surfaces. *Build. Environ.* 45, 1854-1865.
- Koblinger, L. (1985). Analysis of human lung morphometric data for stochastic aerosol deposition calculations. *Phys. Med. Biol.* 30, 541-556.
- Koçak, M., Theodosi, C., Zampas, P. et al. (2012). Influence of mineral dust transport on the chemical composition and physical properties of the Eastern Mediterranean aerosol. *Atmos. Environ.* 57, 266-277.
- Koivisto, A.J., Hussein, T., Niemelä, R., Tuomi, T. and Hämeri, K. (2010). Impact of particle emissions of new laser printers on modeled office room. *Atmos. Environ.* 44, 2140–2146.

- Kopanakis, I., Chatoutsidou, S.E., Torseth, K., Glytsos, T. and Lazaridis, M. (2013). Particle number size distribution in the Eastern Mediterranean: Formation and growth rates of ultrafine airborne atmospheric particles. *Atmos. Environ.* 77, 790–802.
- Kopanakis, I., Eleftheriadis, K., Mihalopoulos, N. et al. (2012). Physico-chemical characteristics of particulate matter in the Eastern Mediterranean. *Atmos. Res.* 106, 93-107.
- Korzhova, E.N., Stepanova, T.V., Lodousamba, S. and Smagunova, A.N. (2016). Monitoring of welding aerosol compositions (a review). *Inorganic Materials* 52, 1420-1430.
- Król, S., Namieśnik, J. and Zabiegała, B. (2014). α -Pinene, 3-carene and d-limonene in indoor air of Polish apartments: The impact on air quality and human exposure. *Sci. Total Environ.* 468-469, pp. 985-995.
- Kubota, Y. and Higuchi, H. (2013). Aerodynamic particle resuspension due to human foot and model foot motions. *Aerosol Sci. Tech.* 47, 208-217.
- Kulkarni, P., Baron, P. A. and Willeke, K. (2011). Introduction to Aerosol Characterization, in *Aerosol Measurement: Principles, Techniques, and Applications*, Third Edition, pp. 3-13 (eds. P. Kulkarni, P. A. Baron and K. Willeke), John Wiley & Sons, Inc., Hoboken, NJ, USA. DOI: 10.1002/9781118001684.ch1
- Kulmala, M., Lazaridis, M., Laaksonen, A. and Vesala, T. (1991). Extended hydrates interaction model: Hydrate formation and the energetics of binary homogenous nucleation. *J. Chem. Phys.* 94, 7411-7413.
- Kulmala, M., Vehkamäki, H., Petäjä, T. et al. (2004). Formation and growth rates of ultrafine atmospheric particles: a review of observation. *J. Aerosol Sci.* 35, 143-176.
- Kuo, Y.-M., Lai, C.-Y., Chen, C.-C., Lu, B.-H., Huang, S.-H. and Chen, C.-W. (2005). Evaluation of exhalation valves. *Ann. Occup. Hyg.* 49, 563-568.
- Lai, A.C.K. (2002). Particle deposition indoors: A review. *Indoor Air* 12, 211-214.
- Lai, A.C.K. and Nazaroff, W.W. (2000). Modeling indoor particle deposition from turbulent flow onto smooth surfaces. *J. Aerosol Sci.* 31, 463-476.
- Lai, A.C.K., Fung, J.L.S. and Leung, K.Y. (2012). Penetration of fine particles through rough cracks. *Atmos. Environ.* 60, 436–443.
- Lamorenna, R.B., Jung, S.-G., Bae, G.-N. and Lee, W. (2007). The formation of ultra-fine particles during ozone-initiated oxidations with terpenes emitted from natural paint. *J. Hazard. Mater.* 141, 245-251.

- Lazaridis, M. (2001). New particle formation of ternary droplets in the atmosphere – a steady state nucleation kinetics approach. *Atmos. Environ.* 35, 599-607.
- Lazaridis, M. and Colbeck, I. (2013). Introduction, in *Aerosol Science: Technology and Applications*, pp. 1-14 (eds I. Colbeck and M. Lazaridis), John Wiley & Sons, Ltd, Chichester, UK. ISBN: 978-1-1199-7792-6.
- Lazaridis, M. and Drossinos, Y. (2013). Aerosol Dynamics, in *Aerosol Science: Technology and Applications*, pp. 15-43 (eds I. Colbeck and M. Lazaridis), John Wiley & Sons, Ltd, Chichester, UK. ISBN: 978-1-1199-7792-6.
- Lazaridis, M., Drossinos, Y. and Georgopoulos, P.G. (1998). Turbulent resuspension of small nondeformable particles. *J. Colloid. Interf. Sci.* 204, 24-32.
- Lazaridis, M., Džumbová, L., Kopanakis, I., Ondracek, J., Glytsos, T., Alexandropoulou, V., Voulgarakis, A., Katsivela, E., Michalopoulos, N., Eleftheriadis, K. (2008). PM10 and PM2.5 levels in the Eastern Mediterranean (Akrotiri research station, Crete, Greece). *Water Air Soil Poll.* 189, 85–101.
- Lazaridis, M., Spyridaki, A., Solberg, S. et al. (2005). Mesoscale modeling of combined aerosol and photo-oxidant processes in the eastern Mediterranean. *Atmos. Chem. Phys.* 5, 927-940.
- Lee, C.W. and Hsu, D.J. (2007). Measurements of fine and ultrafine particles formation in photocopy centers in Taiwan. *Atmos. Environ.* 41, 6598–6609.
- Lee, E.-Y., Flynn, M.R., Du, G. et al. (2016). Lower fractional anisotropy in the globus pallidus of asymptomatic welders, a marker for long-term welding exposure. *Toxicol. Sci.* 153, 165-173.
- Lee, S. C., Lam, S., and Kin, F. H. (2001). Characterization of VOCs, ozone, and PM10 emissions from office equipment in an environmental chamber. *Build. Environ.* 36, 837–842.
- Lee, S.-A., Adhikari, A., Grinshpun, S.A., McKay, R., Shukla, R., Zeigler, H.L. and Reponen, T. (2005). Respiratory protection provided by N95 filtering facepiece respirators against airborne dust and microorganisms in agricultural farms. *J. Occup. Environ. Hyg.* 2, 577-585.
- Lee, S.-A., Grinshpun, S.A. and Reponen, T. (2008). Respiratory performance offered by N95 respirators and surgical masks: Human subject evaluation with NaCl aerosol representing bacterial and viral particle size range. *Ann. Occup. Hyg.* 52, 177-185.

- Lehnert, M., Pesch, B., Lotz, A. et al. (2012). Exposure to inhalable, respirable, and ultrafine particles in welding fume. *Ann. Occup. Hyg.* 56, 557-567.
- Leski, T.A., Malanoski, A.P., Gregory, M.J., Lin, B. and Stenger, D.A. (2011). Application of a broad-range resequencing array for detection of pathogens in desert dust samples from Kuwait and Iraq. *Appl. Environ. Microbiol.* 77, 4285-4292.
- Leung, C.C., Yu, I.T.S. and Chen, W. (2012). Silicosis. *Lancet* 379, 2008-2018.
- Liddament, M.W. (2000). A review of ventilation and the quality of ventilation air. *Indoor Air* 10, 193-199.
- Lin, C.-C., Chen, M.-R., Chang, S.-L., Liao, W.-H. and Chen, H.-L. (2015). Characterization of ambient particles size in workplace of manufacturing physical fitness equipments. *Ind. Health* 53, 78-84.
- Liu, D.L. and Nazaroff, W.W. (2001). Modeling pollutant penetration across building envelopes. *Atmos. Environ.* 35, 4451-4462.
- Long, Z., Jiang, Y.-M., Li, X.-R. et al. (2014). Vulnerability of welders to manganese exposure - A neuroimaging study. *Neurotoxicology* 45, 285-292.
- Lore, M.B., Sebastian, J.M., Brown, T.L., Viner, A.S., McCullough, N.V. and Hinrichs, S.H. (2012). Performance of conventional and antimicrobial-treated filtering facepiece respirators challenged with biological aerosols. *J. Occup. Environ. Hyg.* 9, 69-80.
- Martin, S.B. and Moyer, E.S. (2000). Electrostatic respirator filter media: Filter efficiency and most penetrating particle size effects. *App. Occup. Environ. Hyg.* 15, 609-617.
- Martinelli, N., Olivieri, O. and Girelli, D. (2013). Air particulate matter and cardiovascular disease: A narrative review. *Eur. J. Intern. Med.* 24, 295-302.
- Martonen, T.B. (1993). Mathematical model for the selective deposition of inhaled pharmaceuticals. *J. Pharm. Sci.* 82, 1191-1199.
- Martonen, T.B. and Guan, X. (2001). Effects of tumors on inhaled pharmacologic drugs. I. Flow patterns. *Cell Biochem. Biophys.*, 35, 233-243.
- McCullough, N.V. and Brosseau, L.M. (1999). Selecting respirators for control of worker exposure to infectious aerosols. *Infect. Cont. Hosp. Ep.* 20, 135-144.
- McGarry, P., Morawska, L., He, C., Jayaratne, R., Falk, M., Tran, Q. and Wang, H. (2011). Exposure to particles from laser printers operating within office workplaces. *Environ. Sci. Technol.* 45, 6444-6452.

- McGrath, J.A., Byrne, M.A., Ashmore, M.R., Terry, A.C. and Dimitropoulou, C. (2014). Development of a probabilistic multi-zone multi-source computational model and demonstration of its applications in predicting PM concentrations indoors. *Sci. Total Environ.* 490, 798–806.
- Miettinen, M., Torvela, T. and Leskinen, J.T.T. (2016). Physicochemical Characterization of Aerosol Generated in the Gas Tungsten Arc Welding of Stainless Steel. *Ann. Occup. Hyg.* 60, 960–968.
- Miller, S.L. and Nazaroff, W.W. (2001). Environmental tobacco smoke particles in multizone indoor environments. *Atmos. Environ.* 35, 2053–2067.
- Mølgaard, B., Koivisto, A.J., Hussein, T., and Hämeri, K. (2014). A New Clean Air Delivery Rate Test Applied to Five Portable Indoor Air Cleaners. *Aerosol Sci. Technol.* 48, 409–417.
- Montgomery, J.F., Storey, S., and Bartlett, K. (2015). Comparison of the indoor air quality in an office operating with natural or mechanical ventilation using short-term intensive pollutant monitoring. *Indoor Built Environ.* 24, 777-787.
- Morawska, L., Asfari, A., Bae, G.N. et al. (2013). Review Article, Indoor aerosols: from personal exposure to risk assessment. *Indoor Air* 23, 462-487.
- Morawska, L., He, C.R., Johnson, G. et al. (2009). An Investigation into the characteristics and formation mechanisms of particles originating from the operation of laser printers. *Environ. Sci. Technol.* 43, 1015–1022.
- Morawska, L. and Salthammer, T. (2003). *Indoor environment, Airborne particles and settled dust.* Willey-VCH GmbH & Co. KGaA. ISBN: 978-3-527-30525-4.
- Moyer, E.S. (1986). Respirator Filtration Efficiency Testing. *Fluid Filtration: Gas, ASTM STP 975; 1*, 167-180.
- Moyer, E.S. and Stevens, G.A. (1989a). “Worst Case” Aerosol Testing Parameters: II. Efficiency Dependence of Commercial Respirator Filters on Humidity Pretreatment. *Am. Ind. Hyg. Assoc. J.* 50, 265-270.
- Moyer, E.S. and Stevens, G.A. (1989b). “Worst-Case” Aerosol Testing Parameters: III. Initial Penetration of Charged and Neutralized Lead Fume and Silica Dust Aerosols through Clean, Unloaded Respirator Filters. *Am. Ind. Hyg. Assoc. J.* 50, 271-274.
- Muller, J., Huaux, F., Moreau, N. et al. (2005). Respiratory toxicity of multi-wall carbon nanotubes. *Toxicol. Appl. Pharm.* 207, 221-231.

- Myojo, T. and Sugimoto, M. (1997). Comparative study of challenge aerosols for performance test for dust respirators. *Ind. Health* 35, 502-507.
- Nazaroff, W.W. (2004). Indoor particle dynamics. *Indoor Air* 14, 175-183.
- Nazaroff, W.W. and Weschler, C.J. (2004). Cleaning products and air fresheners: Exposure to primary and secondary air pollutants. *Atmos. Environ.* 38, 2841–2865.
- Ng, L.C., Musser, A., Persily, A.K. and Emmerich, S.J. (2013). Multizone airflow models for calculating infiltration rates in commercial reference buildings. *Energ. Buildings* 58, 11-18.
- Nicholson, K.W. (1988). A review of particle resuspension. *Atmos. Environ.* 22, 2639-2651.
- NIOSH (1997). 42 CFR 84 Respiratory protective devices; Final rules and notice. *Federal Register* 60:110. US Centers for Disease Control and Prevention, National Institute for Occupational Safety and Health.
- Niu, J., Tung, T.C.W., and Burnett, J. (2001). Ozone emission rate testing and ranking method using environmental chamber. *Atmos. Environ.*, 35, 2143-2151.
- Niu, X., Ho, S.S.H., Ho, K.F. et al. (2017). Indoor secondary organic aerosols formation from ozonolysis of monoterpene: An example of D-limonene with ammonia and potential impacts on pulmonary inflammations. *Sci. Total. Environ.* 579, 212-220.
- Nørgaard, A.W., Kudal, A.W., Kofoed-Sørensen, V., Koponen, I.K. and Wolkoff, P. (2014). Ozone-initiated VOC and particle emissions from a cleaning agent and an air freshener: Risk assessment of acute airway effects. *Environ. Int.*, 68, 209-218.
- Oberdörster, G., Oberdörster, E. and Oberdörster, J. (2005). Nanotoxicology: an emerging discipline evolving from studies of ultrafine particles. *Environ. Health Perspec.* 113, 823–39.
- Oberoi, R.C., Choi, J., Edwards, J.R., Rosati, J.A., Thornburg, J., Rodes, C.E. (2010). Human-induced particle re-suspension in a room. *Aerosol Sci. Tech.* 45, 216-229.
- Oprya, M., Kiro, S., Worobiec, A. et al. (2012). Size distribution and chemical properties of welding fumes of inhalable particles. *J. Aero Sci.* 45, 50-57.
- Pagels, J., Wierzbicka, A., Nilsson, E. et al. (2009). Chemical composition and mass emission factors of candle smoke particles. *J. Aerosol Sci.* 40, 193-208.
- Park, J.S., Jee, N.-Y. and Jeong, J.-W. (2014). Effects of types of ventilation system on indoor particle concentrations in residential buildings. *Indoor Air*. doi, 10.1111/ina.12117.

- Penconek, A., Drayk, P. and Moskal, A. (2013). Penetration of diesel exhaust particles through commercially available dust half masks. *Ann. Occup. Hyg.* 57, 360-373.
- Pirela, S.V., Miousse, I.R., Lu, X. et al. (2016). Effects of laser printer-emitted engineered nanoparticles on cytotoxicity, chemokine expression, reactive oxygen species, DNA methylation, and DNA damage: A comprehensive in vitro analysis in human small airway epithelial cells, macrophages, and lymphoblasts. *Environ. Health Persp.*, 124, 210-219.
- Plebani, C., Listrani, S. and Di Luigi, M. (2010). Filtering facepieces: Effect of oily aerosol load on penetration through the filtering material. *Med. Lav.* 101, 293-302.
- Plebani, C., Listrani, S., Tranfo, G. and Tombolini, F. (2012). Variation in penetration of submicrometric particles through electrostatic filtering facepieces during exposure to paraffin oil aerosol. *J. Occup. Environ. Hyg.* 9, 556-561.
- Poland, C.A., Duffin, R., Kinloch, I. et al. (2008). Carbon nanotubes introduced into the abdominal cavity of mice show asbestos-like pathogenicity in a pilot study. *Nat. Nanotechnol.* 3, 423-428.
- Pope, C.A. III. and Dockery, W.D. (2006). Health effects of fine particulate air pollution: Lines that connect. *J. Air Waste Manag.* 56, 709:742.
- Pöschl, U. (2005). Atmospheric Aerosols: Composition, transformation, climate and health effects. *Angew Chem. Int. Ed.* 44, 7520-7540.
- Pouzou, J.G., Warner, C., Neitzel, R.L., Croteau, G.A., Yost, M.G. and Seixas, N.S. (2015). Confined space ventilation by shipyard welders: Observed use and effectiveness. *Ann. Occup. Hyg.* 59, 116-121.
- Présumé, M., Attoui, M., Maisser, A., Petit, G. and Lanone, S. (2015). Design and Characterization of an Inhalation System of Iron and Manganese Oxide Nanoparticles for Rodent Exposure. *Aerosol Sci. Tech.* 49, 580-588.
- Présumé, M., Simon-Deckers, A., Tomkiewicz-Raulet, C. et al. (2016). Exposure to metal oxide nanoparticles administered at occupationally relevant doses induces pulmonary effects in mice. *Nanotoxicology* 10, 1535-1544.
- Qian, J. and Ferro, R. (2008). Resuspension of dust particles in a chamber and associated environmental factors. *Aerosol Sci. Tech.* 42, 566-578.
- Qian, J., Ferro, A.R. and Fowler, K.R. (2008). Estimating the resuspension rate and residence time of indoor particles. *J. Air Waste Manag.* 58, 502-516.

- Qian, J., Peccia, J. and Ferro, A.R. (2014). Review: Walking-induced particle resuspension in indoor environments. *Atmos. Environ.* 89, 464-481.
- Qian, J., Tavakoli, B., Goldasteh, I., Ahmandi, G. and Ferro, A.R. (2014). Building removal of particulate pollutant plume during outdoor resuspension event. *Build. Environ.* 75, 161-169.
- Quang, T.N., He, C., Morawska, L. and Knibbs, L.D. (2013). Influence of ventilation and filtration on indoor particle concentrations in urban office buildings. *Atmos. Environ.* 79, 41-52.
- Quémerais, B., Mino, J., Amin, M.R., Golshahi, H. and Izadi, H. (2015). Detailed characterization of welding fumes in personal exposure samples. *J. Phys. Conf. Ser.* 617, Art. no. 012011.
- Racette, B.A., Nielsen, S.S., Criswell, S.R. et al. (2017). Dose-dependent progression of parkinsonism in manganese-exposed welders. *Neurology* 88, 344-351.
- Raynor, P. C., Leith, D., Lee, K. W. and Mukund, R. (2011). Sampling and Analysis Using Filters, in *Aerosol Measurement: Principles, Techniques, and Applications*, Third Edition, pp. 107-128 (eds. P. Kulkarni, P. A. Baron and K. Willeke), John Wiley & Sons, Inc., Hoboken, NJ, USA. DOI: 10.1002/9781118001684.ch7
- Reeks, M.D. and Hall, D. (2001). Kinetic models for particle resuspension in turbulent flows: theory and measurement. *J. Aerosol Sci.* 32, 1-31.
- Rengasamy, S. and Eimer, B.C. (2012). Nanoparticle penetration through filter media and leakage through face seal interface of n95 filtering facepiece respirators. *Ann. Occup. Hyg.*, 56, 568-580.
- Rengasamy, S., Eimer, B.C. and Shaffer, R.E. (2009). Comparison of nanoparticle filtration performance of NIOSH-approved and CE-marked particulate filtering facepiece respirators. *Ann. Occup. Hyg.* 53, 117-128.
- Rengasamy, S., Eimer, B.C. and Szalajda, J. (2014a). A quantitative assessment of the total inward leakage of nacl aerosol representing submicron-size bioaerosol through N95 filtering facepiece respirators and surgical masks. *J. Occup. Environ. Hyg.* 11, 388-396.
- Rengasamy, S., Fisher, E. and Shaffer, R.E. (2010). Evaluation of the survivability of MS2 viral aerosols deposited on filtering face piece respirator samples incorporating antimicrobial technologies. *Am. J. Infect. Control* 38, 9-17.

- Rengasamy, S., King, W.P., Eimer, B.C. and Shaffer, R.E. (2008). Filtration performance of NIOSH-approved N95 and P100 filtering facepiece respirators against 4 to 30 nanometer-size nanoparticles. *J. Occup. Environ. Hyg.* 5, 556-564.
- Rengasamy, S., Walbert, G., Newcomb, W., Coffey, C.C., Wassell, J.T. and Szalajda, J. (2015). Protection factor for N95 filtering facepiece respirators exposed to laboratory aerosols containing different concentrations of nanoparticles. *Ann. Occup. Hyg.* 59, 373-381.
- Rengasamy, S., Walbert, G.F. Newcomb, W.E. et al. (2014b). Total inward leakage measurement of particulates for n95 filtering facepiece respirators - A comparison study. *Ann. Occup. Hyg.* 58, 206-216.
- Rim, D., Persily, A., Emmerich, S., Dols, W.S. and Wallace, L. (2013). Multi-zone modeling of size-resolved outdoor ultrafine particle entry into a test house. *Atmos. Environ.* 69, 219-230.
- Roberge, R.J. (2012). Are Exhalation valves on N95 filtering facepiece respirators beneficial at low-moderate work rates: An overview. *J. Occup. Environ. Hyg.* 9, 617-623.
- Robinson, J., Nelson, W.C. (1995). National Human Activity Pattern Survey Data Base. United States Environmental Protection Agency, Research Triangle Park, NC; 1995.
- Rohr, A.C., Weschler, C.J., Koutrakis, P. and Spengler, J.D. (2003). Generation and qualification of ultrafine particles through terpene/ozone reaction in a chamber setting. *Aerosol Sci. Tech.* 37, 65-78.
- Rosati, J.A, Isaacs, K.K. and Martonen, T.B. (2013). Mechanism of Particle Deposition, in *Aerosols Handbook: Measurement, Dosimetry, and Health Effects*, Second Edition, pp. 47-74 (eds. L.S. Ruzer and N.H. Harley), CRC Press, Taylor & Francis Group, FL, USA. ISBN: 978-1-4398-5510-2.
- Rosati, J.A., Thornburg, J. and Rodes, C. (2008). Resuspension of particulate matter from carpet due to human activity. *Aerosol Sci. Tech.* 42, 472-482.
- Rudolf, G., Gebhart, J., Heyder, J., Scheuch, G. and Stahlhofen, W. (1983). Modeling the deposition of aerosol-particles in the human respiratory-tract. *J. Aerosol Sci.* 14, 188-192.
- Rudolf, G., Gebhart, J., Heyder, J., Schiller, C. F. and Stahlhofen, W. (1986). An empirical-formula describing aerosol deposition in man for any particle size. *J. Aerosol Sci.* 17, 350-355.

- Rudolf, G., Gebhart, J., Heyder, J., Schiller, C. F. and Stahlhofen, W. (1988). Mass deposition from inspired polydisperse aerosols. *Ann. Occup. Hyg.* 32, 919-938.
- Rudolf, G., Kobrich, R. and Stahlhofen, W. (1990). Modeling and algebraic formulation of regional aerosol deposition in man. *J. Aerosol Sci.* 21, S403-S406.
- Ruzer, L.S, Apte, M.G. and Sextro, R.G. (2013). Aerosol Dose, in *Aerosols Handbook: Measurement, Dosimetry, and Health Effects, Second Edition*, pp. 75–82 (eds. L.S. Ruzer and N.H. Harley), CRC Press, Taylor & Francis Group, FL, USA. ISBN: 978-1-4398-5510-2.
- Ruzer, L.S., Nero, A.V. and Harley, N.H. (1995). Assessment of lung deposition and breathing rate of underground miners in Tadjikistan. *Radiat. Prot. Dosim.* 58, 261-268.
- Sangiorgi, G., Ferrero, L., Ferrini, B.S. et al. (2013). Indoor airborne particle sources and semi-volatile partitioning effect of outdoor fine PM in offices. *Atmos. Environ.* 65, 205–214.
- Sarigiannis, D.A., Karakitsios, S.P., Gotti, A., Liakos, I.L. and Katsoyiannis, A. (2011). Exposure to major volatile organic compounds and carbonyls in European indoor environments and associated health risk. *Environ. Int.* 37, 743-765.
- Sarwar, G. and Corsi, R. (2007). The effects of ozone/limonene reactions on indoor secondary organic aerosols. *Atmos. Environ.* 41, 959-973.
- Sarwar, G., Olson, D.A., Corsi, R.L. and Weschler, C.J. (2004). Indoor fine particles: The role of terpene emissions from consumer products. *J. Air Waste Manag. Assoc.* 54, 367-377.
- Schripp, T., Wensing, M., Uhde, E., Salthammer, T., He, C., and Morawska, L. (2008). Evaluation of ultrafine particle emissions from laser printers using emission test chambers. *Environ. Sci. Technol.*, 42, 4338–4343.
- Seinfeld, J.H. and Pandis, S.N. (2006). *Atmospheric Chemistry and Physics: from Air Pollution to Climate Change*. John Wiley, New York. ISBN 978-0-471-72017-1.
- Semple, S., Garden, C., Coggins, M. et al. (2012). Contribution of solid fuel, gas combustion, or tobacco smoke to indoor air pollutant concentrations in Irish and Scottish homes. *Indoor Air* 22, 212-223.
- Sen, S., Mitra, R., Mukherjee, S., Das, P.K. and Moitra, S. (2016). Silicosis in current scenario: A review of literature. *Curr. Respir. Med. Rev.* 12, 56-64.
- Serfozo, N., Chatoutsidou, S.E. and Lazaridis, M. (2014). The effect of particle resuspension during walking activity to PM10 mass and number concentrations in an indoor microenvironment. *Build. Environ.* 82, 180–189.

- Serfozo, N., Ondráček, J., Zíková, N., Lazaridis, M. and Ždímal, V. (2017). Size-Resolved Penetrations of Filtering Materials from CE-marked Filtering Facepiece Respirators. *Aerosol Air Qual. Res.* 17, 1305-1315.
- Shaughnessy, R. and Vu, H. (2012). Particle loadings and resuspension related to floor coverings in chamber and in occupied school environments. *Atmos. Environ.* 55, 515-524.
- Shi, X., Chen, R., Huo, L. et al. (2015). Evaluation of nanoparticles emitted from printers in a clean chamber, a copy center and office rooms: Health risks of Indoor air quality. *J. Nanosci, Nanotechnol.*, 15, 9554-9564.
- Singer, B.C., Coleman, B.K., Destailats, H. et al. (2006). Indoor secondary pollutants from cleaning product and air freshener use in the presence of ozone. *Atmos. Environ.* 40, 6696-6710.
- Sisler, J.D., Pirela, S.V., Friend, S. et al. (2015). Small airway epithelial cells exposure to printer-emitted engineered nanoparticles induces cellular effects on human microvascular endothelial cells in an alveolar-capillary co-culture model. *Nanotoxicology*, 9 (6), 769-779.
- Slezakova, K., Pereira, M.C., and Alvim-Ferraz, M.C. (2009). Influence of tobacco smoke on the elemental composition of indoor particles of different sizes. *Atmos. Environ.* 43, 486-493.
- Smolík, J., Lazaridis, M., Moravec, P., Schwarz, J., Zaripov, S. K. and Ždímal, V. (2005). Indoor aerosol particle deposition in an empty office. *Water Air Soil Poll.* 165, 301-312.
- Soltani, M. and Ahmadi G. (1995). Particle detachment from rough surfaces in turbulent flows. *J. Adhesion* 51, 105-123.
- Spilak, M.P., Boor, B.E., Novoselac, A. and Corsi, R.L. (2014). Impact of bedding arrangements, pillows, and blankets on particle resuspension in the sleep microenvironment. *Build. Environ.* 81, 60-68.
- Srivastava, A. and Jain, V.K. (2007). A study to characterize the suspended particulate matter in an indoor environment in Delhi, India. *Build. Environ.* 42, 2046-2052.
- Steenland, K. and Ward, E. (2014). Silica: A lung carcinogen. *CA Cancer J. Clin.* 64, 63-69.
- Stevens, G.A. and Moyer, E.S. (1989). "Worst Case" Aerosol Testing Parameters: I. Sodium Chloride and Dioctyl Phthalate Aerosol Filter Efficiency as a Function of Particle Size and Flow Rate. *Am. Ind. Hyg. Assoc. J.* 50, 257-264.

- Sultan, Z.M. (2007). Estimates of associated outdoor particulate matter health risk and costs reductions from alternative building, ventilation and filtration scenarios. *Sci. Total Environ.*, 377, 1–11.
- Talbot, N., Kubelová, L., Makeš, O. et al. (2017). Transformations of aerosol particles from an outdoor to indoor environment. *Aerosol Air Qual. Res.* 17, 653-665.
- Tang, T., Hurraß, J., Gminski, R., and Mersch-Sundermann, V. (2012). Fine and ultrafine particles emitted from laser printers as indoor air contaminants in German offices. *Environ. Sci. Pollut. Res.*, 19, 3840-3849.
- Taylor, B.J., Webster, R. and Imbabi, M.S. (1999). The building envelope as an air filter. *Build. Environ.* 34, 353–361.
- Thatcher, T.L., Lunden, M.M., Revzan, K.L., Sextro, R.G. and Brown, N.J. (2003). A concentration rebound method for measuring particle penetration and deposition in the indoor environment. *Aerosol Sci. Technol.* 37, 847–864.
- Tian, L., Inthavong, K., Lidé, G., Shang, Y. and Tu, J. (2016). Transport and Deposition of Welding Fume Agglomerates in a Realistic Human Nasal Airway. *Ann. Occup. Hyg.* 60, 731-747.
- Tian, L., Zhang, G., Jinghua, T., Zhou, J. and Zhang, Q. (2009). Mathematical model of particle penetration through smooth/rough building envelop leakages. *Build. Environ.* 44, 1144-1149.
- Tian, Y., Sul, K., Qian, J., Mondal, S. and Ferro, A.R. (2014). A comparative study of walking-induced dust resuspension using a consistent test mechanism. *Indoor Air* 24, 592-603.
- Torkmahalleh, M.A., Goldasteh, I., Zhao, Y. et al. (2012). PM_{2.5} and ultrafine particles emitted during heating of commercial cooking oils. *Indoor Air* 22, 483-491.
- Uhde, E. and Salthammer, T. (2007). Impact of reaction products from building materials and furnishing on indoor air quality-A review of recent advantages. *Atmos. Environ.* 41, 3111-3128.
- Vartiainen, E., Kulmala, M., Ruuskanen, T.M., Taipale, R., Rinne, J., Vehkamäki, H. (2006). Formation and growth of indoor air aerosol particles as a result of d-limonene oxidation. *Atmos. Environ.* 40, 7882-7892.
- Vicente, E.D., Ribeiro, J.P., Custódio, D. and Alves, C.A. (2017). Assessment of the indoor air quality in copy centres at Aveiro, Portugal. *Air Qual. Atmos Health* 10, 117-127.

- Vishnyakov, V.I., Kiro, S.A., and Ennan, A.A. (2014b). Multicomponent condensation in the plasma of welding fumes. *J. Aero Sci.* 74, 1-10.
- Vishnyakov, V.I., Kiro, S.A., Oprya, M.V. and Ennan, A.A. (2014a). Coagulation of charged particles in self-organizing thermal plasmas of welding fumes. *J. Aero Sci.* 76, 138-147.
- Vo, E., Zhuang, Z., Horvatin, M., Liu, Y., He, X. and Rengasamy, S. (2015). Respirator Performance against Nanoparticles under Simulated Workplace Activities. *Ann. Occup. Hyg.* 59, 1012-1021.
- Wallace, L. (2006). Indoor sources of ultrafine and accumulation mode particles: Size distributions, size-resolved concentrations, and source strengths. *Aerosol Sci. Tech.* 40, 348-360.
- Wang, H., He, C., Morawska, L., McGarry, P., and Johnson, G. (2012b). Ozone-Initiated Particle Formation, Particle Aging, and Precursors in a Laser Printer. *Environ. Sci. Technol.* 46, 704-712.
- Wang, J., Kim, S.C. and Pui, D.Y.H. (2011b). Measurement of multi-wall carbon nanotube penetration through a screen filter and single-fiber analysis. *J. Nanopart. Research* 13, 4565-4573.
- Wang, S., Zhao, B., Zhou, B. and Tan, Z. (2012a). An experimental study on short-time particle resuspension from inner surfaces of straight ventilation ducts. *Build. Environ.* 53, 119-127.
- Wang, Z.-M., Wagner, J., and Wall, S. (2011a). Characterization of Laser Printer Nanoparticle and VOC Emissions, Formation Mechanisms, and Strategies to Reduce Airborne Exposures. *Aerosol Sci. Tech.*, 45, 1060-1068.
- Waring M.S., Siegel, J.A. and Corsi, R.L. (2008). Ultrafine particle removal and generation by portable air cleaners. *Atmos. Environ.* 42, 5003-5014.
- Waring, M.S., Wells, J.R. and Siegel, J. (2011). Secondary organic aerosol formation from ozone reactions with single terpenoids and terpenoid mixtures. *Atmos. Environ.* 45, 4235-4242.
- Weber, A., Willeke, K., Marchlioni, R. et al. (1993). Aerosol penetration and leakage characteristics of masks used in the health care industry. *Am. J. Infect. Control* 21, 167-173.
- Wensing, M., Schripp, T., Uhde, E. and Salthammer, T. (2008). Ultra-fine particles release from hardcopy devices: Sources, real-room measurements and efficiency of filter accessories. *Sci. Total Environ.* 407, 418-427.

- Weschler, C. (2009). Changes in indoor pollutants since the 1950s. *Atmos. Environ.* 43, 153-169.
- Weschler, C. and Shields, H. (1999). Indoor ozone/terpene reactions as a source of indoor particles. *Atmos. Environ.* 33, 2301-2312.
- Weschler, C.J. (2001). Reactions among indoor pollutants. *ScientificWorldJournal.* 1, 443-457.
- Wittczak, T., Dudek, W., Walusiak-Skorupa, J. et al. (2012). Metal-induced asthma and chest X-ray changes in welders. *Int. J. Occup. Med. Environ. Health* 25, 242-250.
- Wolkoff, P., Cornelius, K. W., Clausen, P. A., Larsen, K. (1993). Comparison of volatile organic compounds from processed paper and toners from office copiers and printers: Methods, emission rates, and modeled concentration. *Indoor Air* 3, 113–123.
- Wu, X.M., Apte, G.M. and Bennett, D.H. (2012). Indoor particle levels in small- and medium-sized commercial buildings in California. *Environ. Sci. Technol.* 46, 12355-12363.
- Yang, X., Chen, Q., Zeng, J., Zhang, J.S. and Shaw, C.Y. (2001). A mass transfer model for simulating volatile organic compound emissions from wet coating materials applied to absorptive substrates. *Int. J. Heat Mass Transfer* 44, 1803-1815.
- Zhang, H., Wang, S., Hao, J. et al. (2012). Chemical and size characterization of particles emitted from the burning of coal and wood in rural households in Guizhou, China. *Atmos. Environ.* 51, 94-99.
- Zhang, L.Z. and Niu, J.L. (2003). Mass transfer of volatile organic compounds from painting material in a standard field and laboratory emission cell. *Int. J. Heat Mass Transfer* 46, 2415-2423.
- Zhang, X., Ahmadi, G., Qian, J. and Ferro, A.R. (2008). Particle detachment, resuspension and transport due to human waling in indoor environments. *J. Adhes. Sci. Technol.* 22, 591-621.
- Zíková, N., Ondráček, J. and Ždímal, V. (2015). Size-resolved penetration through high-efficiency filter media typically used for aerosol sampling. *Aerosol Sci. Technol.* 49, 239-249.
- Ziskind, G., Fichman, M. and Gutfinger, C. (1995). Resuspension of particulates from surfaces to turbulent flows - Review and analysis. *J. Aerosol Sci.* 26, 613-644.
- Zuo, Z., Kuehn, T.H., Pui and D.Y.H. (2013). Performance evaluation of filtering facepiece respirators using virus aerosols. *Am. J. Infect. Control* 41, 80-82.

APPENDIX A.

A.1. Publications in International Peer-Reviewed Scientific Journals

Serfozo, N., Chatoutsidou, S.E. and Lazaridis, M. (2014). The effect of particle resuspension during walking activity to PM10 mass and number concentrations in an indoor microenvironment. *Building and Environment* 82, 180-189.

Lazaridis, M., **Serfozo, N.**, Chatoutsidou, S.E. and Glytsos, T. (2015). New particle formation events arising from painting materials in an indoor microenvironment. *Atmospheric Environment* 102, 86-95.

Serfozo, N., Ondráček, J., Zíková, N., Lazaridis, M. and Ždímal, V. (2017). Size-Resolved Penetration of Filtering Materials from CE-marked Filtering Facepiece Respirators. *Aerosol and Air Quality Research* 17, 1305-1315.

Chatoutsidou, S.E., **Serfozo, N.**, Glytsos T. and Lazaridis, M. (2017). Multi-zone measurement of particle concentrations in a HVAC building with massive printer emissions: influence of human occupation and particle transport indoors. *Article in Press, Air Quality, Atmosphere & Health*, DOI: 10.1007/s11869-017-0461-4.

Serfozo, N., Ondráček, J., Otáhal, P. Lazaridis, M. and Ždímal, V. (2017). Manikin-Based Size-Resolved Penetrations of CE-marked Filtering Facepiece Respirators. *Submitted manuscript in Journal of Occupational and Environmental Health*.

Serfozo, N., Ondráček, J., Glytsos, T. and Lazaridis, M. (2017). Evaluation of Nanoparticle Emissions from a Laser Printer in an Experimental Chamber and Estimation of the Human Particle Dose. *Submitted Manuscript in Environmental Science and Pollution Research*.

Serfozo, N. and Lazaridis, M. (2017). Estimation of Emission Rates and Calculation of Human Dose from Arc Welding and Cutting of Stainless Steel in a Simulated Confined Workspace. *Manuscript Prepared for submission in Metals*.

A.2. International Scientific Conferences

Serfozo, N., Chatoutsidou, S.E., Glytsos, T. and Lazaridis, M. Measurements of particulate matter of mass and number concentrations during controlled indoor activities and measurements of resuspension in working environment. *Poster presentation, European Aerosol Conference*, 1-6 September 2013, Prague, Czech Republic.

Serfozo, N., Chatoutsidou, S.E. and Lazaridis, M. The effect of particle resuspension during walking activity to PM10 mass and number concentrations in an indoor microenvironment. *Oral presentation, 15th Annual Conference of Czech Aerosol Society*, 30–31 October 2014, Valtice, Czech Republic.

Serfozo, N., Ondráček, J., Lazaridis, M. and Ždímal, V. Size-Resolved penetration of filters from respirator masks. *Poster presentation, European Aerosol Conference*, 6-11 September 2015, Milan, Italy.

[This page has been intentionally left blank]